UNIVERSIDAD DE GRANADA

PROGRAMA DE DOCTORADO EN QUÍMICA

FACULTAD DE CIENCIAS

Departamento de Química Inorgánica

TESIS DOCTORAL

Desarrollo de filtros basados en materiales de carbón nanoestructurados para la separación o purificación de gases

Development of filters based on nanostructured carbon materials for gas separation and purification

Jose Francisco Vivo Vilches

Granada, Febrero 2017

Editor: Universidad de Granada. Tesis Doctorales
Autor: José Francisco Vivo Vílches
ISBN: 978-84-9163-129-3
URI: http://hdl.handle.net/10481/45129

Desarrollo de filtros basados en materiales de carbón nanoestructurados para la separación o purificación de gases

Por

JOSE FRANCISCO VIVO VILCHES

Memoria presentada para aspirar al grado de Doctor
por la Universidad de Granada

Fdo.: Jose Francisco Vivo Vilches
Licenciado en Química

Los Directores de la Tesis

Prof. Dr. Francisco J. Maldonado Hódar
Catedrático del Departamento de Química Inorgánica, Universidad de Granada

Prof. Dr. Francisco Carrasco Marín
Catedrático del Departamento de Química Inorgánica, Universidad de Granada

DESARROLLO DE FILTROS BASADOS EN MATERIALES DE CARBÓN NANOESTRUCTURADOS PARA LA SEPARACIÓN O PURIFICACIÓN DE GASES

Tesis presentada para aspirar al grado de Doctor en Química por

JOSE FRANCISCO VIVO VILCHES

Realizada bajo la dirección del Catedrático de Química Inorgánica Prof. Dr. Francisco José Maldonado Hódar y del Catedrático de Química Inorgánica Prof. Dr. Francisco Carrasco Marín, en la Facultad de Ciencias de la Universidad de Granada, y juzgada el día 24 de Febrero de 2017, en dicha Facultad, por el siguiente Tribunal:

PRESIDENTE:

Prof. Dr. Carlos Moreno Castilla, Catedrático de Química Inorgánica, Universidad de Granada.

VOCALES:

Prof. Dr. Isabel Suelves Laiglesia, Investigadora Científica, Instituto de Carboquímica, CSIC, Zaragoza.
Prof. Dra. Vanessa Fierro Pastor, Research Director, Centre National de la Recherche Scientifique, Université de Lorraine, Francia.
Prof. Dr. Miguel Ángel Álvarez Merino, Profesor titular de Química Inorgánica, Universidad de Jaen.

SECRETARIO:

Prof. Dra. María Angeles Ferro García, Catedrática de Química Inorgánica, Universidad de Granada.

Francisco José Maldonado Hódar y Francisco Carrasco Marín como directores de la presente Tesis Doctoral y el doctorando Jose Francisco Vivo Vilches

GARANTIZAN QUE

el trabajo ha sido realizado por el doctorando respetando los derechos de otros autores a ser citados cuando se han utilizado sus resultados o publicaciones.

Y para que conste a los efectos oportunos, en el cumplimiento de la legislación vigente, firmamos el presente certificado en Granada a 2 de Febrero del 2017.

Fdo.: Francisco J. Maldonado Hódar
Catedrático de Química Inorgánica de la Universidad de Granada

Fdo.: Francisco Carrasco Marín
Catedrático de Química Inorgánica de la Universidad de Granada

Fdo.: Doctorando Jose F. Vivo Vilches
Licenciado en Química

"Caminante, son tus huellas
el camino y nada más;
caminante, no hay camino,
se hace camino al andar.
(…)
Caminante no hay camino
sino estelas en la mar…"

Antonio Machado, *Cantares*

"God made the bulk;
surfaces were invented by the devil."

Wolfgang Pauli

Agradecimientos:

No puedo comenzar de otra forma, sino agradeciendo a mis Directores de Tesis, Prof. Dr. Francisco José Maldonado Hódar y Prof. Dr. Francisco Carrasco Marín, por su dirección durante este arduo y laborioso camino que supone la realización de una tesis doctoral. Gracias por vuestros sabios consejos, por vuestra ayuda y por todo lo que he aprendido y disfrutado compartiendo momentos inolvidables con vosotros.

Agradecer también al Prof. Dr. Agustín Francisco Pérez Cadenas por su incondicional ayuda siempre que la he necesitado. Gracias también por darme la oportunidad de asistir a diversos cursos, congresos y reuniones científicas a nivel tanto nacional como internacional, que me han permitido conocer a algunos de los grandes científicos en el campo de la adsorción y de los materiales de carbón.

Al Prof. Dr. Carlos Moreno Castilla por darme la oportunidad de realizar esta Tesis en el Grupo de Investigación en Materiales de Carbón de la Universidad de Granada y por la formación adquirida al compartir con él docencia en la asignatura Química Inorgánica III del Grado en Química. También a los profesores José Rivera, Isidora Bautista y María Ángeles Ferro por su cariño, aprecio e inestimable ayuda.

Han sido muchos años en el laboratorio, en los que ha pasado mucha gente por el mismo, a la que quiero agradecer su amistad y apoyo en momentos difíciles. A los que se fueron Zula, Esther, David, Hakim, María Helena, Carmen, Fran y Abdallah, y a los que se quedan Jesica, Hesham muchas gracias y mucha suerte en vuestro futuro. También a los que, aunque en otros laboratorios, han compartido grupo y grandes momentos como Mahmoud, Raúl, Valente, Jacob, Iván, Ricardo, Ana e Inma. Y por supuesto, a todos los que pasaron por aquí en algún momento: Adrián, Camilo, Amra, Damarys, Luis, Adriana, Estefania, Karol, Amra y Tatiana.

Agradecer al Prof. Em. Alirio Rodrigues por permitirme trabajar en el LSRE de la Facultad de Ingeniería de la Universidad de Oporto, ciudad en la que pasé tres meses inolvidables de la mano de los compañeros de laboratorio de allí Mariana, Rui, Maria João, Patricia, Christoph, Miguel y de los que no fueron compañeros pero con los que pasé muy buenos momentos, María, Marina, Raquel y, en especial, Sergio y Luisa que

hicieron las veces de padres adoptivos. Por supuesto, no me puedo olvidar de Alexandre y Ana Mafalda, que estuvieron desde el minuto uno ayudándome en todo lo que necesité y dirigiendo mi trabajo durante mi estancia allí.

Quiero agradecer también al Grupo de Carbones de la Universidad de Jaén: Vicky, Miguel Ángel, María, y Paco, por sus consejos y amistad.

A los miembros del Centro de Investigación Científica de la Universidad de Granada, especialmente a Alicia e Isabel Sánchez (Técnicos especialistas en SEM) y a Miguel Ángel Salas (Técnico especialista en Análisis Termogravimétrico).

A mis padres y a mi hermano en particular y a mi familia en general, por apoyarme en todo momento y ser mi sustento en los momentos difíciles. A mis amigos y compañeros de piso durante estos años, por todo lo que han hecho por mí. Y por supuesto, a Rocío, mi compañera en los buenos y malos momentos, mi guía y mi ánimo para seguir caminando juntos.

Este trabajo no habría sido posible sin todos vosotros, por ello, otra vez GRACIAS.

Este Trabajo de Investigación ha sido financiado por el Ministerio de Educación, Cultura y Deportes, dentro del programa de Formación del Profesorado Universitario. El doctorando y los directores también quieren agradecer la financiación recibida por parte de distintas entidades: Ministerio de Ciencia e Innovación, proyecto CTM2010-18889; Junta de Andalucía, proyecto P12-RNM-2892; y Ministerio de Economía y Competitividad, proyecto CTQ2013-44789-R.

a Inmaculada y Jose Francisco, mis padres

a Carlos, mi hermano

a Rocío, mi compañera en este viaje

Contenidos y estructura de la Tesis


UNIVERSITAS GRANATENSIS
1531

CONTENIDOS Y ESTRUCTURA DE LA TESIS

En la presente Tesis se describe el uso de materiales de carbón para la adsorción de compuestos orgánicos volátiles presentes en biocombustibles, la separación de isómeros de octano y la adsorción selectiva de dióxido de carbono presente en el biogás. Para ello, se han sintetizado carbones activados a partir de residuos lignocelulósicos (hueso de aceituna y pelets de madera) y geles de carbón obtenidos a partir de aerogeles y xerogeles de resorcinol y formaldehído. Los materiales han sido caracterizados tanto a nivel textural como químico y la adsorción de los distintos contaminantes se ha ensayado en régimen dinámico y estático.

El **capítulo I** trata sobre la obtención de materiales de carbón y su uso en el tratamiento de emisiones contaminantes procedentes de biocombustibles, así como en el refinado de dichos biocombustibles y de biogás. Comienza con un resumen de la situación energética global y del papel de los materiales de carbón en lo referente al uso de biocombustibles y biogás. Posteriormente se describe la obtención de carbones activados a partir de diversas materias primas, diferentes métodos de activación y de funcionalización de la superficie. También se trata en profundidad la versatilidad que ofrece el proceso sol-gel para obtener materiales nanoestructurados con diferentes propiedades texturales y químicas a partir de geles derivados de la polimerización del resorcinol y el formaldehído. Por último se concretan las razones para usar este tipo de materiales tanto en la prevención de emisiones contaminantes durante el repostaje en dispositivos tipo canister de vehículos a motor, como en el refinado de biocombustibles y biogás.

En el **capítulo II** se describen la síntesis de los distintos materiales de carbón obtenidos, las técnicas empleadas para su caracterización a nivel textural y químico y los distintos métodos usados para probar los adsorción de los distintos contaminantes en régimen estático y dinámico. Además, se muestran las ecuaciones y modelos matemáticos aplicados para analizar los resultados.

El **capítulo III** versa sobre la preparación y caracterización de carbones activados con hidróxido potásico a partir de hueso de aceituna con distinto contenido en oxígeno. La caracterización química y textural de las muestras se llevó a cabo mediante diversas técnicas, con las que se pudo obtener información acerca de la naturaleza y distribución de los distintos grupos oxigenados generados.

En el **capítulo IV** se emplean los materiales obtenidos en el capítulo anterior en la adsorción monocomponente tanto en régimen estático como dinámico de n-octano y etanol, ambos componentes mayoritarios de biocombustibles y elegidos por su distinta naturaleza química. La capacidad de adsorción de las distintas muestras para los dos compuestos se relaciona con sus propiedades físico-químicas.

En el **capítulo V** se analizan la adsorción competitiva de etanol y n-octano en los carbones activados con distinto grado de oxidación y la influencia de la humedad. Los cambios producidos en las curvas de rotura respecto a la adsorción monocomponente se relacionan con el carácter hidrofóbico/hidrofílico de la superficie del adsorbente y con la naturaleza del compuesto a adsorber. Finalmente, se ajusta la composición del lecho adsorbente para optimizar la adsorción simultánea de ambos compuestos.

Estos tres capítulos demuestran la versatilidad del carbón activado derivada de la posibilidad de modificar la química superficial presente en la estructura carbonosa. De esta forma, mediante tratamientos de oxidación y eliminación selectiva de grupos oxigenados podemos modular el comportamiento adsorbente de los materiales en función de la naturaleza del compuesto que quiere ser adsorbido.

El **capítulo VI** recoge los resultados para la separación de n-octano y 2,2',4-trimetilpentano (TMP) mediante aerogeles y xerogeles de carbón obtenidos por catálisis ácida. También se analizan los cambios en la microporosidad del xerogel al ser activado físicamente con dióxido de carbono a

distintos grados de activación. Finalmente, se analiza la influencia del tipo de secado y del grado de activación de la serie de xerogeles en la adsorción y separación de ambos isómeros. El capítulo pone de manifiesto la utilidad del proceso sol-gel para obtener materiales de carbón nanoestructurados en los cuales podemos ajustar el tamaño de la porosidad para obtener tamices moleculares de carbón que son capaces de separar moléculas pequeñas.

En el **capítulo VII** se estudia el uso de carbón activado obtenido por activación física con dióxido de carbono de pelets de madera de pino como adsorbente selectivo de CO_2 en biogás. Para ello el material es caracterizado y se obtienen y analizan tanto las isotermas a alta presión de dióxido de carbono y metano, como la adsorción en dinámico de ambos compuestos (monocomponente y binaria). Los resultados obtenidos se relacionan con las propiedades texturales de la muestra.

Por último, en el **capítulo VIII** se desarrolla la síntesis y caracterización de un xerogel de carbón obtenido mediante catálisis básica y su empleo en la adsorción selectiva de CO_2 frente a CH_4. El comportamiento adsorbente se investiga mediante el análisis de las isotermas a alta presión y las curvas de rotura a distintas concentraciones para ambos gases. Al igual que en el caso del carbón activado obtenido a partir de madera de pino el comportamiento adsorbente del xerogel se relaciona con sus propiedades texturales.

Estos dos últimos capítulos ponen de manifiesto la utilidad de los materiales de carbón tanto tradicionales (obtenidos a partir de residuos lignocelulósicos) como más novedosos (geles de carbón nanoestructurados) en procesos de adsorción y separación de gases y, concretamente, en el refinado de biogás por adsorción selectiva de dióxido de carbono.

La mayor parte de los resultados de esta Tesis Doctoral han sido publicados en revistas científicas especializadas de alto índice de impacto y difusión internacional:

- J.F. Vivo-Vilches, E. Bailón-García, A.F. Pérez-Cadenas, F. Carrasco-Marín, and F.J. Maldonado-Hódar, Tailoring the surface chemistry and porosity of activated carbons: Evidence of reorganization and mobility of oxygenated surface groups, *Carbon*, **68** (2014) 520-530.

- J.F. Vivo-Vilches, E. Bailón-García, A.F. Pérez-Cadenas, F. Carrasco-Marín, and F.J. Maldonado-Hódar, Tailoring activated carbons for the development of specific adsorbents of gasoline vapors, *Journal of Hazardous Materials*, **263, Part 2** (2013) 533-540.

- J.F. Vivo-Vilches, A.F. Pérez-Cadenas, F. Carrasco-Marín, and F.J. Maldonado-Hódar, About the control of VOCs emissions from blended fuels by developing specific adsorbents using agricultural residues, *Journal of Environmental Chemical Engineering*, **3** (2015) 2662-2669.

- J.F. Vivo-Vilches, F. Carrasco-Marín, A.F. Pérez-Cadenas, and F.J. Maldonado-Hódar, Fitting the porosity of carbon xerogel by CO_2 activation to improve the TMP/n-octane separation, *Microporous and Mesoporous Materials*, **209** (2015) 10-17.

- J.F. Vivo-Vilches, A.F. Pérez-Cadenas, F.J. Maldonado-Hódar, F. Carrasco-Marín, R.P.V. Faria, A.M. Ribeiro, A.F.P. Ferreira, and A.E. Rodrigues, Biogas upgrading by selective adsorption onto CO_2 activated carbon from wood pellets, Submitted to *Journal of Environmental Chemical Engineering*.

- J.F. Vivo-Vilches, A.F. Pérez-Cadenas, F.J. Maldonado-Hódar, F. Carrasco-Marín, M.J. Regufe, A.M. Ribeiro, A.F.P. Ferreira, and A.E. Rodrigues, Resorcinol-formaldehyde carbon xerogel as selective adsorbent of carbon dioxide present on biogas. In progress.

- J.F. Vivo-Vilches, A.F. Pérez-Cadenas, F.J. Maldonado-Hódar, F. Carrasco-Marín, C. Siquet, A.M. Ribeiro, A.F.P. Ferreira, and A.E.

Rodrigues, Hexane isomers adsorption and separation onto carbon gels. In progress.

- J.F. Vivo-Vilches, A.F. Pérez-Cadenas, F. Carrasco-Marín, and F.J. Maldonado-Hódar, Carbon materials for VOCs adsorption, biofuel and biogas refining. In progress.

Los resultados obtenidos en el transcurso de la tesis han sido presentados en congresos tanto nacionales como internacionales:

- XXXIV Reunión Bienal Real Sociedad Española de Química (RSEQ). Santander, España, Septiembre 2013.

- XII Reunión del Grupo Español del Carbón (GEC). Madrid, España, Octubre 2013.

- 10th International Symposium on the Characterization of Porous Solids (COPS-X). Granada, Spain, May 2014.

- XXXIX Reunión Ibérica de Adsorción (39RIA). Baeza, España, Septiembre 2014.

- XIII Reunión del Grupo Español del Carbón (GEC). Alicante, España, Octubre 2015.

- 7th International Symposium on Carbon for Catalysis (Carbocat-VII). Strasbourg, France, June 2016.

- The Annual World Conference on Carbon (CARBON). State Collegue, Pennsylvania, United States, July 2016.

- XXXX Reunión Ibérica de Adsorción (40RIA). Évora, Portugal, Septiembre 2016.

Índice

Capítulo I

INTRODUCCIÓN

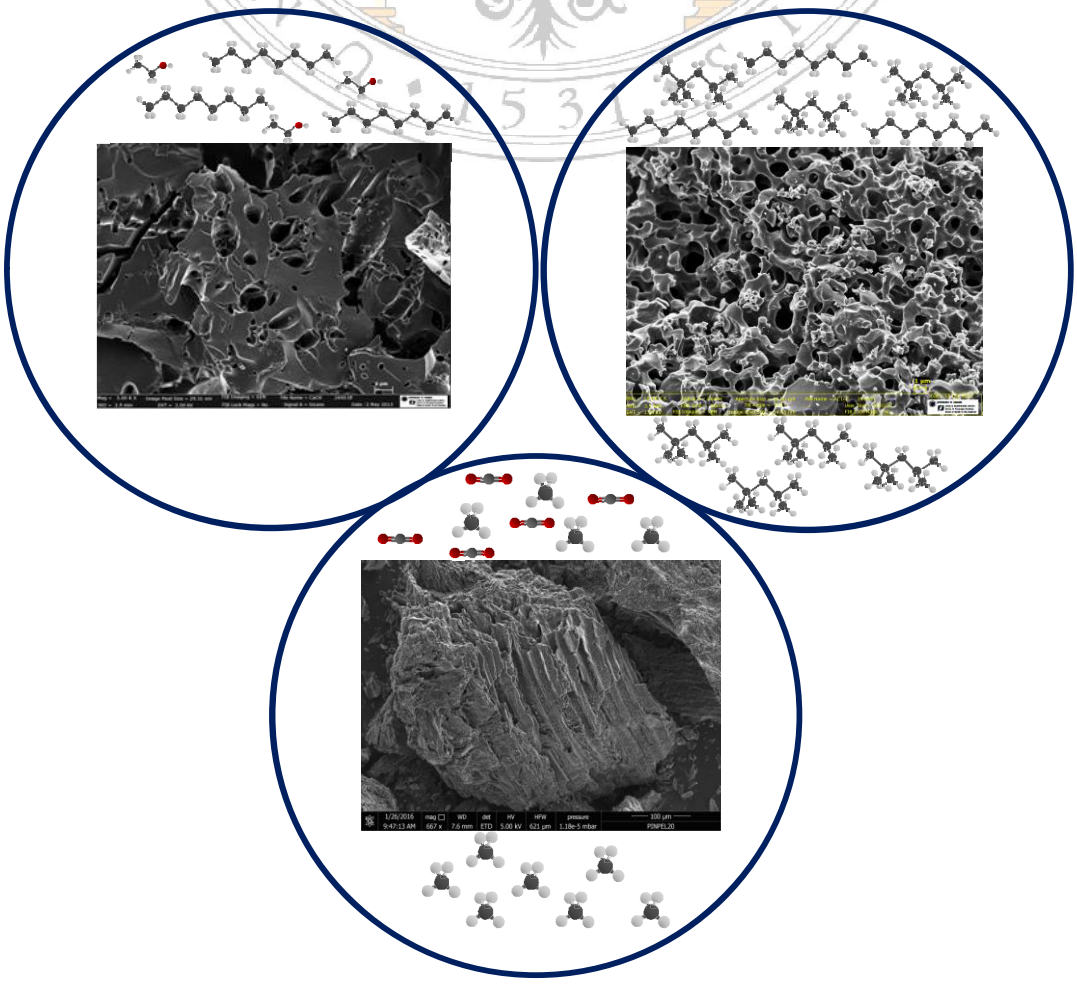

El carbón ha sido utilizado a lo largo de la historia principalmente en dos tipos de aplicaciones: la obtención de energía y los procesos descontaminación. En cuanto a la primera, el carbón es todavía una de las fuentes de energía más utilizadas, por lo que se siguen investigando nuevas formas de llevar a cabo su combustión reduciendo el impacto medioambiental[1-4]. Sin embargo, es en los procesos medioambientales[5-17] (tratamiento de efluentes tanto en fase líquida como en fase gaseosa) y en otras aplicaciones relacionadas con la textura porosa del carbón, por ejemplo, como soporte de catalizadores[18-20] o como dispositivos para almacenamiento de energía eléctrica[21-23], donde el desarrollo de los materiales de carbón resulta más marcado en las últimas décadas.

De esta forma, junto a los tradicionales carbones activados obtenidos a partir de carbones minerales o de desechos agrícolas, ha surgido una nueva serie de nanoestructuras de carbono, entre las cuales son más conocidas los nanotubos, grafenos y fullerenos, pero en las que también cabe destacar los materiales de carbono nanoestructurados, es decir, aquellos materiales de carbono que, obtenidos por diversas rutas sintéticas, dan lugar a un retículo poroso en el que podemos controlar a escala nanométrica la composición y la distribución de tamaños de dicha porosidad[24-33]. Entre estas técnicas, unas de las más utilizadas son las basadas en el proceso sol-gel, en el que el precursor del material de carbón es sintetizado bajo condiciones controladas, dando lugar a una estructura ordenada que luego es preservada durante la carbonización. La principal ventaja de esta técnica es su alta reproducibilidad, que unida a su gran versatilidad, hace que se puedan obtener materiales basados en carbono con una porosidad a medida, salvando así uno de los mayores inconvenientes que han tenido los carbones activados respecto a otros materiales porosos como los óxidos inorgánicos o las zeolitas (materiales que, al ser cristalinos, llevan intrínseca esta propiedad en su naturaleza).

Dentro de estos materiales de carbono nanoestructurados, unos de los más desarrollados han sido los que provienen de geles obtenidos por polimerización de compuestos fenólicos con aldehídos, y concretamente, los sintetizados a partir de la condensación resorcinol-formaldehido[29-33]. Entre finales de los años 80 y principios de los 90, el profesor Richard W. Pekala desarrolló y patentó la síntesis de estos geles de

carbón[29,30]. A partir de estos primeros trabajos se ha realizado un gran esfuerzo para entender, desarrollar y controlar las variables del proceso en sus distintas etapas, con objeto de estudiar su influencia en el mismo y poder obtener materiales con distintas propiedades texturales y químicas[31-40]. Se trata, por tanto, de un tipo de materiales en el que se pueden modificar las condiciones de síntesis: el catalizador, la composición de la mezcla, el uso o no de surfactantes, la temperatura de gelificación, el tipo de curado, el secado o las condiciones de carbonización obteniéndose materiales totalmente diferentes, pero de forma que si la síntesis se repite reproduciendo estrictamente todo el proceso, se llegará al mismo material. Los geles de carbón están formados por un retículo tridimensional de partículas primarias de tamaño nanométrico interconectadas entre sí. La microporosidad se desarrolla en el interior de las partículas primarias y los meso y macroporosidad se forma en los espacios entre las partículas primarias inicialmente ocupados por el disolvente. Por tanto, se puede controlar independientemente la concentración de micro y mesoporos, lo que es una ventaja de los geles de carbón como materiales porosos. Además de estas grandes ventajas, los geles de carbón son susceptibles, al igual que los materiales de carbón tradicionales, de ser modificados por post-tratamientos como la activación o funcionalización[36-44]. Puesto que en el desarrollo de esta Tesis Doctoral se han preparado dos tipos de materiales, a saber, carbones activados a partir de residuos agrícolas y geles de carbón, éstos serán analizados en mayor medida.

La demanda energética crece en todo el mundo, especialmente en países en pleno desarrollo y muy poblados como China e India, pero también en Europa[45,46]. Aunque lo ideal sería que la humanidad fuera capaz de generar toda la energía para cubrir dicha demanda por medio de energías renovables, la realidad es que, probablemente durante muchos años, estas fuentes de energía tengan que seguir conviviendo con las tradicionales (Figura 1.1). No obstante, se deben adoptar medidas para que el uso de combustibles fósiles no traiga consigo un impacto medioambiental a nivel de contaminación y de calentamiento global. Aunque en la reducción de emisiones contaminantes y peligrosas derivado del uso de vehículos se ha avanzado mucho, reduciéndose la emisión de óxidos de azufre y de nitrógeno, la gran preocupación en la actualidad la constituyen los gases de efecto invernadero, en particular el dióxido de carbono[47-50].

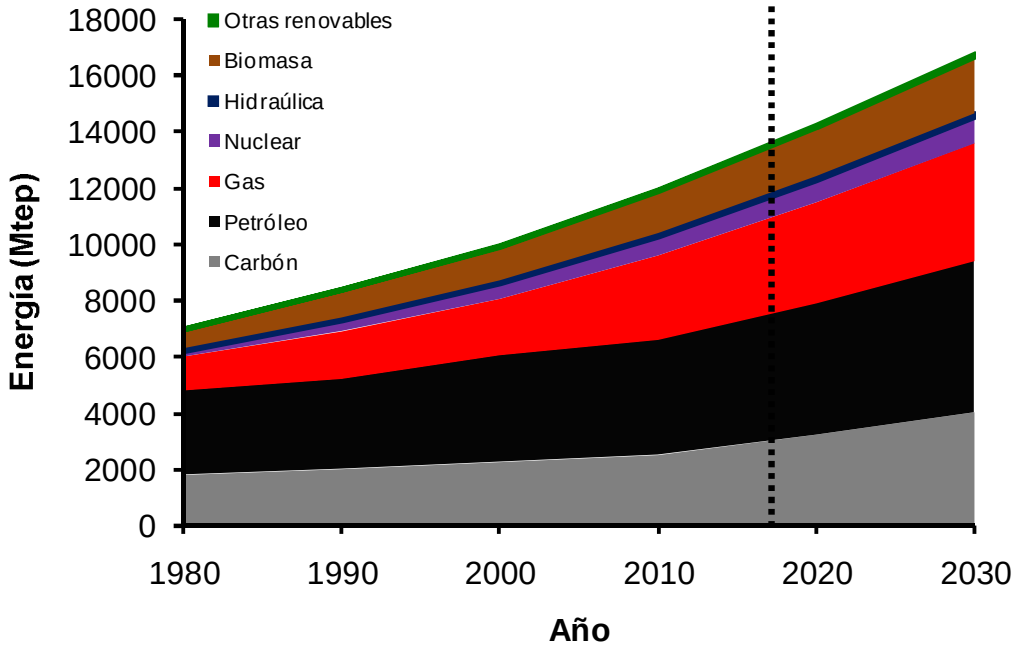

Figura 1.1. Previsión de consumo energético mundial hasta 2030[45,46].

Especial interés se ha mostrado por parte de la comunidad científica y de la sociedad en general en solucionar el problema del calentamiento global[1,3,4,47-52]. Una de las principales causas del mismo lo constituyen las emisiones de dióxido de carbono, ya que aunque es cierto que otros gases contribuyen en mayor medida a dicho efecto, sus emisiones han sido más controladas que las de CO_2, que sólo han empezado a considerarse un problema en años recientes[47-49]. Esta creciente preocupación por el incremento de la temperatura global del planeta producido por la elevada concentración de dióxido de carbono en la atmósfera ha llevado a invertir dinero y esfuerzo en el desarrollo de metodologías para captura de CO_2[1-4,50-59]. Uno de los problemas que se plantea es que en los procesos de combustión junto con el CO_2 se generan otros gases, y por tanto, para conseguir tratar las emisiones, se están desarrollando dos tipos de tecnologías: las llamadas de pre-combustión[1-4,57-59], que consisten en tratar el combustible previo a ser quemado para que su combustión sea más limpia y genere bien sólo agua o agua y dióxido de carbono y las de post-combustión[51-56,60,61] en las cuales los gases resultantes de la combustión son tratados para evitar que el CO_2 y otros contaminantes se emitan a la atmósfera.

Otro de los campos de investigación relacionados con la obtención de energía lo constituye el desarrollo de los biocombustibles, combustibles obtenidos a partir de desechos de la industria agroalimentaria o de biomasa[62-68]. Dentro de ellos, destacan los biocombustibles basados en etanol[62-64] y el biometano obtenido a partir de biogás[65-68]. Tanto el refinado como el control de las emisiones asociadas a estos dos últimos son objeto del trabajo de esta Tesis Doctoral y serán tratados en mayor profundidad en otras secciones. No obstante, cabe señalar que los materiales de carbono pueden y deben tener un papel fundamental en aplicaciones relacionadas con el uso de biocombustibles, ya sea en la adsorción de compuestos orgánicos volátiles (COVs) para prevenir las emisiones de los mismos y mejorar el aprovechamiento de los hidrocarburos presentes en el combustible a través de dispositivos tipo canister[11,17,69-72], como en los tratamientos previos al uso de estos combustibles para mejorar su rendimiento (refinamiento)[43,73-80].

Por ello, se plantea el uso de materiales basados en carbono como adsorbentes específicos de COVs presentes en biocombustibles y como adsorbentes selectivos de CO_2 en mezclas CH_4/CO_2. Para llevarlo a cabo, se han obtenido tanto carbones activados a partir de desechos agrícolas, como geles de carbón cuyas propiedades químicas y texturales han sido ajustadas mediante procesos de activación y oxidación, con objeto de mejorar su comportamiento en el tratamiento de mezclas de gases contenidos en biocombustibles o en biogás.

1.1. CARBONES ACTIVADOS

El carbón activado es uno de los materiales más usados para el tratamiento de efluentes tanto en fase gaseosa como en fase líquida[5,6,12,16,71,81-83]. Aunque su principal inconveniente resulte la baja reproducibilidad en el ajuste del tamaño del poro del material, debido a la gran dependencia de la materia prima, la investigación de los procesos de activación de carbones de fuentes muy diversas ha hecho posible la modelización de estos procesos, teniendo cada vez más conocimiento a priori del procedimiento sintético necesario para obtener un carbón activado con las propiedades deseadas, eligiéndose el proceso de activación en función de la aplicación, de la materia prima y de la bibliografía disponible sobre ella. Este hecho, sumado a su competitivo

precio, así como la versatilidad derivada de la posibilidad de llevar a cabo tratamientos de funcionalización química de la superficie del carbón activado, hace que estos materiales sigan siendo hoy en día fundamentales en el desarrollo de adsorbentes específicos tanto de metales y compuestos orgánicos en aguas, como de compuestos orgánicos volátiles (COVs) en aire[5,6,12,16,71,81-83].

Las posibilidades son, por tanto, muy diversas, pudiéndose preparar materiales con propiedades muy diferentes, incluso partiendo de la misma materia prima, simplemente modificando el proceso de activación[84-87]. Las principales materias primas de las que se obtienen carbones activados son: desechos agrícolas[77,84,85,88-94], carbones minerales[13,87,95-99] y derivados de la industria petroquímica (desechos de petróleo, plásticos o neumáticos)[100-111]. En cuanto a los métodos de activación se pueden dividir principalmente en dos: la activación física, que consiste en la gasificación del carbón a alta temperatura y la activación química, en la que el precursor se mezcla con un agente químico y se somete a un proceso de activación a alta temperatura[6,81-86]. Las dos vías implican reacciones químicas del agente activante con el material de carbón para desarrollar su porosidad, sin embargo se suele utilizar esta distinción histórica. Por último, el carbón activado puede ser tratado con distintos compuestos para introducir heteroátomos en su estructura (oxígeno, nitrógeno, azufre, boro, fósforo y halógenos)[88,112-114].

En esta sección se resumirán algunos de los resultados obtenidos con carbones activados, llevándose a cabo una clasificación de los mismos en función de los tres aspectos mencionados anteriormente, a saber: la materia de partida, el proceso de activación y los procesos de funcionalización química de la superficie.

1.1.1. Carbones activados a partir de residuos lignocelulósicos

Los carbones activados obtenidos usando como materia prima distintos desechos agrícolas, como huesos y cascaras de distintas frutas o restos de poda, constituyen uno de los grupos más importantes. De hecho, se calcula que en torno a un 50% de los carbones activados comerciales se obtienen a partir de ellos[6,81,82]. El principal inconveniente de este tipo de materiales es su bajo rendimiento en carbón,

debido a que alrededor del 75% del material de partida lo constituye materia volátil que se pierde durante la carbonización. Sin embargo, el precio de las materias primas usadas para obtenerlos es muy bajo, con lo que este inconveniente no supone un gran problema para la comercialización de carbones activados a partir de este tipo de residuos. En esta Tesis Doctoral se han obtenido carbones activados a partir de hueso de aceituna y de pellets de madera de pino usados en calefacción doméstica, por lo que éstos serán analizados en mayor profundidad.

En la región mediterránea, la industria del aceite de oliva tiene especial importancia. Esta industria genera desechos en forma de hueso de aceituna o en residuos sólidos contenidos en un subproducto resultante de la molienda de aceituna, el alperujo. Tanto el hueso de aceituna[17,88,115-120], como este residuo sólido (compuesto por hueso, pulpa, piel y restos grasos)[84,113,121] resultan excelentes candidatos para obtener carbones activados con un alto desarrollo de la porosidad, debido a su estructura natural, constituida por una red de canales que actúan como matriz del material de carbono. Así, existen numerosos trabajos en las que se analizan las distintas variables del proceso de activación de estos materiales para la obtención de carbones activados tanto en forma granular, como en polvo y con un retículo poroso que puede ir desde un gran desarrollo de la microporosidad, hasta materiales micro-mesoporosos, dependiendo del agente activante, de la cantidad usada del mismo en relación a la cantidad de materia prima o precarbonizado a tratar, o de la temperatura a la que se lleve a cabo la activación[5,84,85,116-121].

Otro residuo muy utilizado en la obtención de carbones activados lo constituyen las maderas[77,85,91-94,122-124]. En los últimos años, existe una creciente preocupación por la cantidad de biomasa generada derivada de procesos de poda y tala, ya que muchas veces estos restos son quemados al no poder ser usados, con el consiguiente riesgo de incendio. Por ello, y con el objetivo de poder aprovechar sus propiedades, se han investigado en los últimos años numerosos usos para esta biomasa. Cabe destacar su posible uso en la obtención de biocombustibles, ya sea por su conversión en biooil o bioetanol mediante distintos procesos[63,64,125-127], o por consolidación de astillados de madera (principalmente de pino) para la obtención de pellets que pueden sustituir, y de hecho ya lo están haciendo, a otros combustibles

tradicionales menos eficientes (cascara de almendra o hueso de aceituna) en calderas y estufas domésticas[128,129]. Estos materiales, los pellets de madera, constituyen un precursor válido y económico para la obtención de carbones activados, con la ventaja de que ya se encuentran peletizados, con lo que no es necesario llevar a cabo un proceso de consolidación del material que conlleva una reducción de su área superficial, siempre y cuando la estructura del material no sea destruida durante el proceso de activación.

1.1.2. Carbones activados a partir de carbones minerales

Los carbones minerales han sido ampliamente utilizados desde la Revolución Industrial, principalmente para su combustión y para la obtención de energía eléctrica en centrales térmicas[2,4,130,131]. En el norte de España, existió durante muchos años una gran tradición minera, siendo una de las industrias más importantes de esta zona[58,87,96,97,130,131]. Sin embargo, la tendencia a obtener la energía eléctrica por otras vías más limpias debido a los compromisos en lo que se refiere a reducción de emisiones de CO_2, junto con la baja competitividad del sector, ha llevado a la Unión Europea a tomar medidas drásticas, exigiendo el cierre en los próximos años de los pocos yacimientos que aún quedan en explotación en la zona septentrional de la península[130,131].

No obstante, todavía quedan grandes reservorios de carbón mineral, por lo que resulta necesario darle un uso. A este efecto, desde hace años, existe un gran desarrollo científico en cuanto a la producción de carbones activados a partir de este tipo de materiales[13,87,95-99]. La gran ventaja de este tipo de carbón es que tienen una estructura más consolidada que los materiales lignocelulósicos, puesto que ya están constituidos por una matriz carbonosa, con bajo contenido en materia volátil. Esto hace que se puedan obtener materiales de carbón con una porosidad muy desarrollada, sin que el rendimiento del proceso resulte bajo. Como inconveniente de este tipo de materiales cabe destacar el alto contenido en cenizas, que puede suponer un problema para algunas de las aplicaciones, por lo que muchas veces es necesario llevar a cabo un proceso de desmineralización[13,87,95-99]. Entre estos materiales, cabe destacar los carbones activados

obtenidos a partir de antracita, un carbón mineral muy usado debido principalmente a su alto contenido en carbono, su abundancia y su bajo coste[13,87,96,97].

1.1.3. Carbones activados a partir de otros desechos

Aunque tradicionalmente los dos principales grupos de materias primas utilizadas en la obtención de carbones activados han sido los anteriormente descritos, existen otros desechos que, cada vez con más frecuencia, se usan a este fin. Así, en los últimos años se pueden encontrar numerosos trabajos en bibliografía en el que se preparan carbones activados a partir de neumáticos usados[102-104,109], plásticos[100,101,109-111] o fracciones pesadas del petróleo[105-107].

Los neumáticos usados y su acumulación constituyen un problema medioambiental de primera magnitud, conllevando un riesgo de accidente en forma de incendio, como el ocurrido recientemente en el municipio toledano de Seseña[132]. Sumado al impacto medioambiental, la combustión del neumático produce una serie de compuestos tóxicos por inhalación, con lo que a los costes medioambientales, en caso de incendio de un vertedero de neumáticos, hay que sumar el posible impacto sobre la salud de las personas que habitan en zonas cercanas. Por tanto, buscar nuevas aplicaciones para la utilización de estos desechos, puede ser una buena vía, no sólo desde el punto de vista medioambiental, sino también de prevención ante estos posibles accidentes. Algunos grupos de investigación están trabajando en esta rama[102-104,109], con algunos resultados destacables, si bien uno de los principales inconvenientes es que los neumáticos contienen una gran cantidad de azufre, lo que puede resultar un problema a la hora de llevar a cabo los tratamientos necesarios para obtener el material de carbón.

Otra de las grandes preocupaciones ambientales que existe a nivel global está relacionada con el consumo creciente de materiales plásticos. Muchos de estos materiales son reciclables, pero no son biodegradables, por lo que aunque la concienciación sobre el reciclado y la recogida selectiva de basuras es cada vez mayor, la gran cantidad de desechos generados, especialmente de plásticos utilizados en la industria alimentaria (como el polietilenterftalato, PET), es inasumible en su totalidad por las plantas de reciclaje que sólo pueden tratar una parte de los mismos[100,101]. Por

tanto, resulta necesario dar otros usos a estos residuos, y la obtención de carbón activado a partir de ellos está demostrando ser una buena alternativa para evitar que estos desechos sean almacenados o incinerados. Existen también otros polímeros a partir de los cuales se puede obtener carbón activado como el polietileno (PE) y el polipropileno (PP). Resultan interesantes los trabajos en los que estos plásticos son sometidos a un proceso de descomposición para, añadiendo un catalizador metálico, utilizarlos como precursores en la obtención de nanofibras de carbono (CNF)[108,110,111].

Por último, una de las industrias en la que más se ha hecho por valorizar todos y cada uno de los subproductos generados seguramente es la industria del petróleo. Gracias a ello, se ha producido un gran crecimiento en el uso de polímeros en las últimas décadas. Sin embargo aunque de las distintas fracciones del petróleo casi todas se pueden utilizar para generar combustibles, asfaltos o monómeros para la industria petroquímica, sigue habiendo fracciones muy pesadas que generalmente constituyen un desecho. Así, las breas de petróleo, ricas en hidrocarburos aromáticos policíclicos, son utilizadas como precursores de grafito o nanofibras de carbono (cuando son grafitizables) o de carbón activado (cuando no pueden ser grafitizadas)[105-107].

1.1.4. Métodos de activación: activación física frente a activación química

El desarrollo de la porosidad de los carbones activados se puede llevar a cabo mediante dos vías, activación física o activación química, como se ha comentado anteriormente. El que se elija llevar a cabo una u otra dependerá principalmente de la aplicación en la que se quieren emplear los materiales y del tipo de precursor[84-86].

1.1.4.1. Activación física

En lo que se refiere a la activación física, ésta consiste en llevar a cabo la oxidación del material mediante un gas para que, tras descomponer los grupos oxigenados generados, se produzca un incremento de la porosidad por lo que se conoce como gasificación[81-83,98,101,115,116,121,133-136]. Este proceso suele constar de dos etapas: una carbonización del material en atmósfera inerte y un posterior tratamiento a alta temperatura en presencia del agente activante. Sin embargo, ambas etapas pueden

llevarse a cabo de forma simultánea, especialmente en materiales con bajo contenido en materia volátil, llevándose a cabo un calentamiento en atmósfera inerte, manteniendo una temperatura durante un tiempo, cambiando el gas inerte por el agente activante y cambiando otra vez al inerte durante el enfriamiento. Son las partes más reactivas del carbón, los bordes de grano y zonas más desordenadas, las primeras en reaccionar en los procesos de gasificación, y, por tanto, las más afectadas por los mismos. El grado de gasificación del material se conoce normalmente como grado de activación o de quemado y se suele expresar en porcentaje. Los gases más usados para la activación de carbones son el vapor de agua[98,121,133] y el dióxido de carbono, aunque algunas veces se lleva a cabo la combustión parcial del material de carbón mediante aire[115,134-136].

La activación con vapor de agua se produce mediante las reacciones descritas en las ecuaciones 1.1 y 1.2, mientras que las 1.3 y 1.4 corresponden a la activación con dióxido de carbono[6,81-83,85].

$$C + H_2O \rightarrow CO_2 + H_2$$ Ecuación 1.1

$$2C + H_2 \rightarrow 2C(H)$$ Ecuación 1.2

$$C + CO_2 \rightarrow C(O) + CO$$ Ecuación 1.3

$$C(O) \rightarrow CO$$ Ecuación 1.4

Según las ecuaciones anteriormente expuestas, el dióxido de carbono reacciona con la superficie del carbón para dar lugar a complejos oxigenados que descomponen dando CO a alta temperatura. El vapor de agua, sin embargo, reacciona dando lugar a hidrógeno que se quimisorbe en la matriz carbonosa estabilizando los electrones que quedan no enlazados al salir átomos de C como CO_2 de la estructura del carbón. Este CO_2 generado puede reaccionar con la superficie del carbón por las ecuaciones 1.3 y 1.4 dando lugar al desarrollo de la microporosidad[6,81-83,85].

Cuando los resultados de usar cada uno de los gases son comparados se observa que para el caso del CO_2 se incrementa en mayor medida el volumen de microporos, a través de la creación de nueva microporosidad o del ensanchamiento de la ya existente en el material a activar, mientras que con el H_2O se produce un mayor volumen de

mesoporos y un ensanchamiento de la macroporosidad[83-86,98,116]. En cualquiera de los casos se produce un alto desarrollo de la microporosidad, que aumenta a medida que aumenta el grado de quemado, hasta que el ensanchamiento de estos microporos resulta tan grande que comienza a aumentar significativamente la mesoporosidad. Sea cual sea el agente activante, los procesos de activación física suelen generar distribuciones del tamaño de poro muy anchas cuando se intenta desarrollar mucho la porosidad. Por ello, si se quiere obtener un carbón activado con un alto volumen de poros y una distribución de tamaños estrecha, se debe recurrir a la activación química[6,84-87,96,137]. No obstante, la activación física con dióxido de carbono a bajos grados de activación puede ser un buen método para aplicaciones relacionadas con la separación de gases, ya que consigue desarrollar un alto volumen de microporos estrechos en los que se pueden adsorber selectivamente moléculas más pequeñas frente a otras más voluminosas (como es el caso de la separación de isómeros lineales y ramificados). También se puede utilizar para el desarrollo de adsorbentes selectivos de CO_2 en biogás, ya que la interacción del CH_4 con la superficie del carbón es mucho más débil en estos microporos estrechos que la correspondiente al CO_2.

1.1.4.2. Activación química

Otro método para desarrollar la porosidad de un carbón activado es el conocido como activación química[6,21,81,82,84-89,96,97,113,118-120,124,137,138]. En este proceso se lleva a cabo la impregnación del material de partida con el agente químico activante y se trata a temperaturas moderadas en atmósfera inerte. Si el agente activante presenta carácter ácido o básico, se lleva a cabo finalmente una etapa de neutralización. En cualquier caso, es necesario un lavado y, generalmente, una desmineralización del carbón activado resultante para eliminar subproductos de la reacción y el agente activante que quede sin reaccionar[21,84-86,88,113]. Los reactivos más utilizados en la activación química de carbones son el ácido fosfórico[120,124,139], el cloruro de cinc[119,138,140] y los hidróxidos alcalinos[17,21,87,88,96,97,100,103,113,117,118,137,141,142].

En cuanto a las ventajas con respecto a la activación física se suelen destacar las cinéticas más favorables (lo que conlleva menores tiempos y temperaturas de tratamiento), rendimientos más altos para el mismo desarrollo de porosidad, un mayor

control del tipo de porosidad generada y el hecho de que se realice en una única etapa[84-86]. Sin embargo, esta última no es del todo cierta para todos los materiales de carbón, ya que es necesario que la estructura del material sea ya una estructura carbonosa estable para llevar a cabo el proceso de activación, como es el caso de los carbones minerales[87,96,97]. Por tanto, para llevar a cabo la activación química de un material lignocelulósico preservando su estructura intrínseca, es necesario realizar un precarbonizado a temperatura relativamente baja (entre 300 y 400°C) para obtener una estructura carbonosa estable que no se desmorone con el tratamiento, lo que permite un mayor desarrollo del volumen de poros[17,21,88,113]. En cuanto a los inconvenientes, los principales son la necesidad de la etapa de lavado y/o neutralización y que se trata de un proceso que emplea reactivos corrosivos. El que se opte por un agente activante u otro dependerá principalmente de la aplicación y del tipo de material usado como precursor[6,81,82,84-86].

El ácido fosfórico (H_3PO_4)[120,124,139] y el cloruro de cinc ($ZnCl_2$)[119,138,140] fueron los primeros en usarse a tal efecto. Ambos suelen utilizarse con materiales lignocelulósicos, ya que actúan deshidratando la celulosa, la hemicelulosa y la lignina. En cuanto al primero, se suele utilizar en materiales lignocelulósicos cuando se requiere un adsorbente con porosidad ancha (mesoporos anchos y macroporos), bien para tratamiento de aguas o bien para adsorción de compuestos grandes como pueden ser los hidrocarburos aromáticos policíclicos (PAHs) presentes en combustibles[120,124,139]. El cloruro de zinc cada vez se usa menos debido al impacto medioambiental del Zn, pero su principal ventaja es que desarrolla un gran volumen de microporos con una distribución de tamaños estrecha a bajas proporciones de agente activante. Cuando se incrementa la proporción de $ZnCl_2$ respecto al material a activar, se producen también mesoporos, dando lugar a materiales micro-mesoporosos[119,138,140].

Los hidróxidos alcalinos, principalmente el de sodio y el de potasio, permiten preparar carbones activados con un tamaño de microporos homogéneo y con alto volumen de microporos[17,21,87,88,96,97,102,103,113,142,143]. El mecanismo por el cual transcurre la activación de los hidróxidos ha sido ampliamente estudiado, demostrándose que estos hidróxidos reaccionan con la superficie del carbón dando lugar a carbonatos. Estos carbonatos descomponen a alta temperatura, formándose dióxido de carbono

responsable del desarrollo de la microporosidad, mientras que la intercalación del óxido del metal entre las capas grafíticas y, a temperaturas más altas, del propio metal, da lugar a un aumento de la distancia interlaminar, aumentando así la mesoporosidad[87,90,96,97,141]. El hidróxido de sodio precisa de temperaturas más altas de tratamiento que el de potasio, por lo que generalmente se opta por este último[87]. Ubago-Pérez y col.[118] estudiaron diversos factores que afectan a las propiedades texturales del material resultante, destacando la proporción de agente activante y la temperatura. En cuanto a la primera, para diversos materiales se ha demostrado que a bajas proporciones KOH:C los materiales que se obtienen son principalmente microporosos, mientras que a proporciones mayores de agente activante (KOH:C por encima de 4:1) se comienzan a generar también mesoporos (Tabla 1.1). En lo que respecta a la temperatura, a mayores temperaturas se produce una mayor cantidad de K metálico que queda intercalado entre las capas grafénicas, aumentando por tanto la distancia entre ellas y el volumen de mesoporos[90,142,143].

Tabla 1.1. Propiedades texturales de carbones activados con KOH.

Precursor	Muestra	KOH/C	T °C	S_{BET} $m^2 \cdot g^{-1}$	W_0 (N_2) $cm^3 \cdot g^{-1}$	V_T $cm^3 \cdot g^{-1}$	Ref.
Hueso de aceituna carbonizado	A1	1	800	460	0.19	0.21	118
	A2	2		957	0.38	0.38	
	A4	4		1059	0.40	0.42	
	A5	5		1062	0.41	0.44	
Hueso de jobo	CAK5	1	500	1384	0.50	0.63	90
	CAK7		700	2290	0.92	1.19	
Paja de arroz	SK4T50	4	500	370	0.12	0.25	143
	SK4T60		600	760	0.24	0.39	
	SK4T70		700	770	0.25	0.41	
	SK4T80		800	900	0.30	0.46	
Precarbonizada a 700 °C	C7K4T60		600	490	0.19	0.28	
	C7K4T70		700	1250	0.44	0.65	
	C7K4T80		800	2200	0.54	1.15	
	C7K4T90		900	2410	0.48	1.39	

1.1.5. Modificación química superficial

Además de los tratamientos de activación existentes para el desarrollo de la porosidad, existen diversos procesos aplicables a materiales de carbono para la modificación de su química superficial. Estos procesos, desarrollados para carbones activados, se pueden también llevar a cabo sobre otros materiales como nanoestructuras o geles de carbón. Entre los heteroátomos que se pueden introducir en la superficie del carbón activado destacan el oxígeno[112,144-149] y el nitrógeno[114,122,150,151], por ser los más utilizados, aunque también está creciendo el interés en la funcionalización con otros grupos superficiales que contienen azufre[113,152,153], fosforo[154,155], halógenos[156-159] o boro[28,160] para diversas aplicaciones. Puesto que en esta Tesis Doctoral se ha llevado a cabo la oxidación de un carbón activado, este proceso será descrito en mayor profundidad.

1.1.5.1. Oxidación

Los tratamientos de oxidación constituyen uno de los procesos más usados para modificar la superficie de los materiales carbonosos. Son usados, entre otras aplicaciones, para mejorar la dispersión de un catalizador[161], para crear centros ácidos que pueden convertir al material de carbón en catalizador para distintas reacciones[145-149] o para generar grupos que dan lugar a procesos redox produciendo un incremento de la capacidad de un dispositivo de almacenamiento de energía eléctrica por pseudocapacitancia[162]. En lo que se refiere a la adsorción, se utilizan sobre todo para crear interacciones específicas con moléculas polares o con metales pesados en disolución y para modular el balance hidrofílico/hidrofóbico del adsorbente[16,17,88,163-165]. La introducción de grupos oxigenados destaca sobre el resto debido a la multitud de posibilidades derivadas de las diferentes vías para llevarla a cabo, la accesibilidad de los reactivos empleados y la posibilidad de llevar a cabo los procesos en disolución a temperatura ambiente[16,112,145].

En cuanto a los métodos para la oxidación de materiales de carbono, se dividen principalmente en dos tipos: la oxidación por vía seca, en la que el carbón se somete a

temperaturas moderadas en presencia de un gas oxidante (aire, oxígeno u ozono) y por vía húmeda, que es un proceso en disolución en el que el material de carbón se pone en contacto con una disolución acuosa del oxidante[16,112,145].

Para la oxidación por vía seca, los gases más utilizados son aire y ozono, ambos generan principalmente grupos de carácter básico (carbonílicos) o ligeramente ácido (fenólicos), aunque también se pueden generar algunos grupos carboxílicos y anhídridos[144,145,166-169]. Debido a que la estabilidad de los grupos oxigenados depende de la temperatura, el tipo de grupos va a depender también de la que se utilice para llevar a cabo el tratamiento[147,168-170]. En este sentido, las oxidaciones con ozono tienen la ventaja de ser llevadas a cabo a menor temperatura[166,167].

No obstante, los métodos de oxidación en vía seca son cada vez menos comunes y se están sustituyendo por procesos en disolución. Entre los oxidantes usados para la reacción por vía húmeda destacan tres: el ácido nítrico (HNO_3)[7,112,145-147,168,171,172], el peróxido de hidrógeno (H_2O_2)[7,112,145,146,148,173] y el peroxidisulfato amónico ($(NH_4)_2S_2O_8$)[7,17,88,112,146,161,163]. Cada uno tiene una serie de ventajas e inconvenientes y existen diversos trabajos en los que se comparan las consecuencias de utilizar uno u otro[7,16,112,145,146,148,163]. Al igual que en los procesos de activación, las características del material final dependerán no sólo del oxidante elegido, sino también de la estructura del material (porosidad, tamaño de partícula, contenido en cenizas).

Los mayores contenidos en oxígeno se consiguen con la oxidación mediante el uso de ácido nítrico. Esto se debe a que el HNO_3 reacciona tanto con la superficie más externa del carbón como dentro del retículo poroso del mismo[7,112,145,147,168,171,172]. Además, es el oxidante que más grupos de tipo ácido carboxílico genera, aunque también da lugar a la formación de grupos carbonílicos y fenólicos en menor medida. Su principal inconveniente es que, al reaccionar también en el interior de la porosidad del carbón, el tratamiento con ácido nítrico suele reducir notablemente el área superficial del material, reduciendo su capacidad adsorbente[7,112,145,147,168]. Este oxidante también se ha usado en procesos de funcionalización hidrotermal, generándose una mayor proporción de grupos de tipo fenólico que en la oxidación convencional a presión atmosférica[171,172].

El peróxido de hidrógeno es otro oxidante usado en la oxidación de carbones activados[7,112,145,146,148,173]. Éste se puede utilizar a diversos pH (los nitratos no presentan carácter oxidante en medio básico) aunque su potencial es menor a pH básico, por lo que el tipo de grupos generados y la cantidad de los mismos va a depender de que este parámetro se ajuste o no[173]. Dadas las características ácidas del peróxido de hidrógeno se suele emplear directamente, generando principalmente grupos de tipo fenólico y carbónilico siendo el oxidante que más proporción de grupos estables que desorben como CO a altas temperaturas genera[7,112,145,146,148,173]. Sin embargo, si el pH se modifica aumentando la acidez de la mezcla, se suelen obtener mayores proporciones de grupos carboxílicos, en detrimento de los fenólicos, mientras que a pH básico se generan mayores cantidades de grupos carbonílicos y éteres, reduciéndose también la proporción de grupos fenólicos[173]. El peróxido de hidrógeno reacciona principalmente con la superficie más externa del carbón, con lo que no afecta significativamente a las propiedades texturales del mismo[7,112,145,146].

Por último, el peróxidisulfato amónico es un oxidante muy particular, cuya característica es la creación de centros ácidos muy fuertes, a pesar de fijar un menor número de grupos carboxílico que la oxidación con HNO_3[7,17,88,112,146,161,163]. Esto se debe a que el $(NH_4)_2S_2O_8$ genera grupos carboxílicos de los cuales muchos se hallan en posiciones contiguas o adyacentes de la superficie carbonosa[161]. Es conocido que la presencia de grupos electrón-atrayentes en posición α respecto al carboxilo aumenta la fortaleza ácida del mismo por efecto inductivo, mientras que los grupos electrón-donantes la disminuyen. Por ello, aunque la proporción de grupos ácidos es menor en carbones tratados con este oxidante que en el caso del ácido nítrico, el pH del punto cero de carga (pH_{ZPC}) de los mismos suele ser menor[146,161]. Aunque en general no afecta significativamente a las propiedades texturales del carbón activado, para carbones con un alto volumen de mesoporos y conformados por partículas muy finas, puede destruir parte de esta porosidad, reduciendo considerablemente la mesoporosidad[17,88].

En todos los casos, los carbones oxidados por los distintos métodos pueden ser tratados a distintas temperaturas, para eliminar parte de los grupos oxigenados generados o producir una reestructuración de los mismos[17,43,95,147,168-170]. Para llevar a

cabo este proceso tenemos que tener en cuenta el tipo de grupos que pueden existir en la superficie del carbón y su estabilidad térmica relativa (Tabla 1.2)[95,145,147,168,170].

Tabla 1.2. Grupos superficiales oxigenados y estabilidad térmica.

#	Grupo	CO/CO_2	T (°C)
1	Ác. Carboxílico	CO_2	200-300
2	Lactona	CO_2	350-400
3	Pirona	CO	≈ 1000
4	Anhídrido	CO_2 + CO	400-600
5	Fenol	CO	600-700
6	Éter	CO	≈ 700
7	Carbonilo	CO	800-900
8	Cromeno	CO	≈ 1000

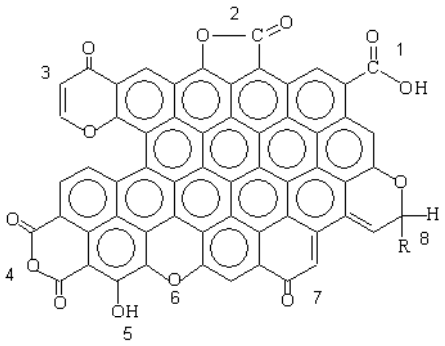

1.1.5.2. Nitrógeno

El nitrógeno es otro de los heteroátomos que se usa en mayor medida, sobre todo en aplicaciones relacionadas con el almacenamiento de energía (por dar también lugar a especies con actividad redox)[23,114,174,175] y en la electrorreducción tanto de O_2 en pilas de combustible, como de CO_2 para su conversión en hidrocarburos de bajo peso molecular[176-178]. Especial importancia tienen también los tratamientos de inmovilización con poliaminas o poliiminas para crear estructuras dendríticas que dotan al adsorbente de una capacidad de captura de CO_2 muy alta, debido a la interacción química de los grupos nitrogenados con el dióxido de carbono[122,150,151,179]. La adsorción de algunos metales también se puede ver favorecida por la presencia de grupos nitrogenados capaces de dar lugar a interacciones específicas con el ion metálico a adsorber[16].

También cabe destacar que la introducción de funcionalidades de nitrógeno se puede llevar a cabo no durante un post-tratamiento del carbón, sino directamente en la síntesis del precursor polimérico. Así la carbonización de polímeros de monómeros nitrogenados (melamina-formaldehido o hidroxipiridina-formaldehido) da lugar a

estructuras carbonosas con un contenido en nitrógeno que dependerá de la temperatura de carbonización y las condiciones de síntesis del polímero precursor[23,162,174,176,179,180].

En la funcionalización con agentes químicos posterior a la carbonización destacan los tratamientos con amoniaco, cianuro de hidrógeno, urea o la propia melamina[122,123,175,177,181]. En este caso, es necesario aplicar temperaturas relativamente altas, ya sea para facilitar la reacción gas-sólido (en el caso del amoniaco y el cianuro) o para producir la descomposición del reactivo usado para introducir el nitrógeno (urea y melamina). Esto limita las posibles funcionalidades que pueden ser introducidas en el carbón por esta vía, en función de la estabilidad térmica de los mismos.

1.1.5.3. Azufre

Una de las aplicaciones más importantes del azufre en estos momentos la constituye su incorporación a las baterías de ión litio para incrementar su capacidad[182]. También se han utilizado carbones azufrados en la electrorreducción de O_2[113,183], a veces combinado con funcionalidades de nitrógeno[178]. La generación de centros de una acidez muy fuerte, puede ser utilizada con fines catalíticos. En lo que respecta a la adsorción, destaca el uso de carbones funcionalizados con azufre para la adsorción de mercurio tanto en disolución como en fase gas[152,184] y para la adsorción en disolución de otros metales pesados con afinidad por el azufre como el cadmio o el plomo[16,153,185].

Tradicionalmente, para introducir grupos azufrados en la matriz carbonosa se utilizaban gases como el sulfuro de hidrógeno (H_2S), de carbono (CS_2) o el dióxido de azufre (SO_2)[152,153,184,185]. Estas reacciones requieren altas temperaturas, que pueden ser menores si se lleva a cabo una oxidación previa del material de carbono, lo que muchas veces modifica significativamente la estructura carbonosa obtenida. Sin embargo, en los últimos años se vienen desarrollando métodos en disolución ya sea a presión atmosférica o en reactores a presión (solvotermal o hidrotermal), en los que pequeñas moléculas que contienen azufre (tiourea, mercaptoetanol o ácido tioglicólico, por ejemplo) se hacen reaccionar con el carbón, lo que permite una funcionalización en condiciones menos severas de temperatura y que da lugar a carbones activados con una química superficial más controlada, en la que se generan funcionalidades concretas

según el reactivo utilizado y la química superficial ya existente en el material de partida[113,178,183].

1.1.5.4. Halogenación

Cuando se realiza un análisis bibliográfico sobre la funcionalización de materiales de carbono con halógenos, se observa que el cloro es, con diferencia, el más utilizado[156,157]. Esto se debe a que el carácter oxidante de los halógenos disminuye al bajar en el grupo, por lo que mientras que el bromo y el yodo tienen una reactividad muy baja y es difícil que reaccionen con la superficie del carbón, el flúor presenta el inconveniente contrario, es decir, una reactividad excesivamente alta que hace difícil el control del proceso. No obstante, el flúor se ha utilizado principalmente para modular la selectividad de membranas en separación CO_2/CH_4 ya que da lugar a interacciones específicas con el dióxido de carbono, siendo capaz de retenerlo[158,159]. El bromo se utiliza comúnmente en disolución, siendo este proceso un ensayo clásico usado en la determinación del grado de insaturación de un carbón. La reacción del yodo con el carbón genera grupos funcionales muy lábiles y con un alto grado de reversibilidad, por lo que prácticamente no se usa.

Como se ha mencionado en el párrafo anterior, el elemento del grupo de los halógenos más usado en funcionalización de materiales de carbono es el cloro. La inserción de cloro en la matriz carbonosa se produce a partir de los 200°C y aumenta con la temperatura[156,157]. En nuestro grupo, carbones clorados han sido utilizados para crear carbones con grupos superficiales de carácter ácido de Lewis que, al usarse como soportes de catalizadores, influyen en la dispersión del metal y en su comportamiento catalítico[156]. Sin embargo, la acidez de Brönsted de los carbones resultantes tiende a disminuir, y en mayor medida cuanto mayor es la temperatura de tratamiento, ya que los grupos clorados sustituyen a los grupos carboxílicos que se eliminan a temperaturas relativamente bajas (Tabla 1.2)[156].

1.1.5.5. Otros heteroátomos

Además de los heteroátomos descritos, se pueden introducir en la superficie del carbón otros, como son el fósforo y el boro. En cuanto al primero, la activación con fosfórico es la principal vía para generar grupos de P, que suelen usarse como retardantes de la combustión o para preservar electrodos de grafito de la oxidación[154,155]. En cuanto al boro, se suele introducir por deposición química en fase vapor (CVD) generando defectos en las láminas grafénicas, lo que da lugar a la curvatura de las mismas. Además, se utiliza para dopar con carácter p los materiales de carbono, ya que tiene un electrón menos que el C[160] y para prevenir la oxidación del carbón.

1.2. GELES DE CARBÓN

La aplicación de las técnicas sol-gel a la obtención de materiales de carbono ha sido una de las grandes aportaciones de las últimas décadas a este campo. El control en la forma del polímero precursor asociado a esta técnica ha llevado a poder crear estructuras de todo tipo[23-33]. La utilización de surfactantes y moléculas plantilla permite también modificar las propiedades texturales del gel y, como consecuencia, del material de carbono resultante[186-188]. Esta técnica permite además la inclusión de precursores de óxidos metálicos para los que también se aplica, pudiéndose obtener materiales compuestos con silica, titania, óxido de manganeso o de zinc, y cualquier óxido metálico que también pueda sintetizarse vía sol-gel[189-191].

La técnica consiste en la formación de un polímero en un disolvente, generalmente acuoso, de manera que las partículas primarias coloidales se van uniendo unas con otras, en lo que se conoce como gelificación, dejando huecos en los que el disolvente (y las micelas del surfactante en los casos en los que se use) queda atrapado[31-33,35]. De esta manera se forma un hidrogel que posteriormente deberá ser secado, pudiendo realizarse esta etapa mediante el empleo de fluidos supercríticos, obteniéndose un aerogel; con un secado térmico, con lo que se llegaría a un xerogel; o por congelación del disolvente, lo que se conoce como criogel[31-33,35]. Una vez secado el

gel se procede, en el caso de los geles de carbón, a un proceso de carbonización a alta temperatura.

La principal ventaja de esta técnica es que los materiales a los que da lugar son nanoestructurados, es decir, tienen un retículo poroso ordenado que viene determinado por las condiciones de síntesis. Además, la cantidad de variables en juego hace que sea posible modificar muchos parámetros para llegar a tener un material con una distribución de tamaño de poros prácticamente a medida, pudiendo fijar las condiciones de síntesis en función de las propiedades deseadas[31-33]. Al ser obtenidos de forma sintética este proceso da lugar a materiales de carbono de alta pureza. Los geles de carbón obtenidos a partir de la polimerización de resorcinol y formaldehido[29,30,32,33,43] son unos de los más estudiados y, al constituir uno de los materiales empleados en esta Tesis Doctoral, serán descritos en mayor profundidad.

Existen numerosos trabajos en los que se pone de manifiesto la versatilidad del proceso sol-gel en la obtención de geles de carbón a partir de mezclas resorcinol-formaldehido[29,30,32,33]. El estudio de las diversas variables que intervienen en el proceso es fundamental para poder optimizar la síntesis, sabiendo a priori que se debe hacer y que no para llegar al material que se busca para una determinada aplicación. Entre las condiciones estudiadas destacan las relativas a la síntesis y el gelificado[34,35,38-41,162,188], el tipo de secado[36,37,43,192,193], la carbonización y los posibles post-tratamientos, principalmente de activación[43,194-198].

Las opciones son tan amplias que los geles de carbón han sido utilizados para un sin fin de aplicaciones relacionadas con la adsorción[14,43,197,199,200], catálisis[15,18,42,191,201], separación de gases[43,202], almacenamiento de energía[44,162,195,196,203], liberación de fármacos[204], y prácticamente cualquier aplicación para la que se han desarrollado materiales inorgánicos porosos. Además, el hecho de que el proceso (Figura 1.2) transcurra a partir de una disolución precursora, permite obtener el material de carbón en multitud de formas que van desde membranas, a polvo o pelets[37].

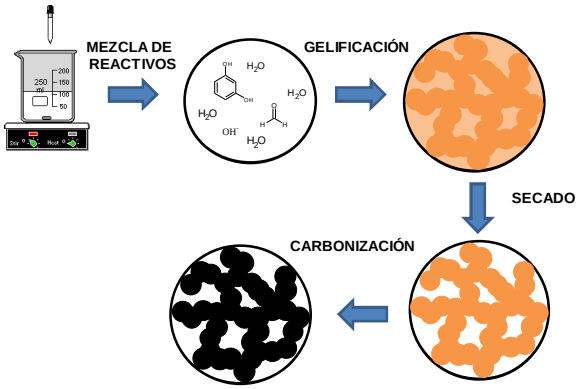

Figura 1.2. Etapas para obtener un gel de carbón Resorcinol-Formaldehído.

1.2.1. Síntesis y gelificación

Es, probablemente, en la etapa de síntesis donde más variables intervienen en el proceso de obtención de un gel de carbón. Por ello, es en esta etapa donde las posibilidades se multiplican, ya que podemos variar desde el disolvente, la proporción entre reactivos, el grado de dilución, el catalizador, la inclusión o no de surfactantes y moléculas plantillas[32,33,192]. Una vez mezclados los reactivos, la disolución precursora se introduce en moldes sellados, que pueden ser de distinta forma, y se someten a un tratamiento térmico para que tenga lugar el gelificado y curado del gel, pudiendo también variarse la temperatura y condiciones de la misma. Las reacciones que rigen el proceso (Figura 1.3) son dos: la adición del formaldehido al resorcinol en posiciones 2 y 4 (la 6 es equivalente a la 4) y la posterior condensación entre las especies formadas en la primera, dando lugar a moléculas cada vez más grandes[29,30,32,33]. Estas moléculas a su vez siguen reaccionando entre ellas para dar lugar a clusters que siguen reaccionando y uniéndose unos con otros formando una estructura de collar típica del gel (Figura 1.4).

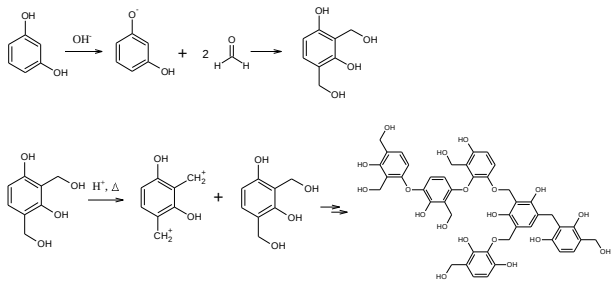

Figura 1.3. Mecanismo de la polimerización del Resorcinol y el Formaldehído.

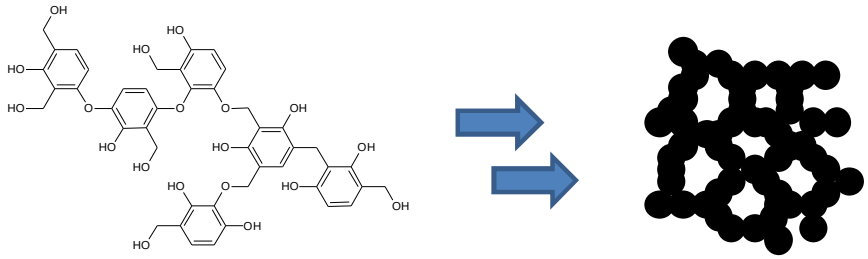

Figura 1.4. Condensación de clusters para formar el gel.

1.2.1.1. Disolvente y grado de dilución.

Puesto que el disolvente juega un papel activo en el ensamblaje de unas moléculas con otras, determinando gran parte del proceso de gelificación, es uno de los factores más importantes[32,33,205-207]. Generalmente se utiliza agua, aunque se han utilizado otros, principalmente alcoholes, por distintos motivos: por ejemplo, para obtener criogeles resulta conveniente el uso de tertbutanol u otro disolvente que no presente cambios de densidad (y por tanto de volumen) tan bruscos al pasar a estado sólido[205,207]; en el caso de aerogeles, la utilización de disolventes orgánicos evita la necesidad de realizar una etapa de intercambio con acetona del mismo, ya que éstos son solubles en CO_2. No obstante, las velocidades de polimerización en disolventes alcohólicos son menores, por lo que suelen usarse solamente cuando resulta necesario, esto es, cuando el resorcinol se sustituye por otros monómeros con una menor solubilidad en agua[206].

En cuanto al grado de dilución, este puede definirse como la cantidad de disolvente por cantidad total de resorcinol y de formaldehido presentes en la mezcla. No obstante, puesto que la proporción estequiométrica resorcinol:formaldehido suele ser 1:2 (la 1:1 da lugar a bajo grado de entrecruzamiento, mientras que la 1:3 produce un efecto de dilución debido a que gran parte del formaldehido no reacciona), la proporción de disolvente se suele dar como relación molar entre el resorcinol y el agua o cualquier otro disolvente empleado (R/W)[32,33]. Su influencia depende del pH al que se ajusta la mezcla para obtener el gel[32,33,40,192,208,209]: a pH ácido y grados de dilución intermedios, se obtienen geles con partículas muy interconectadas entre sí, dando lugar a geles

macroporosos, cuyo tamaño aumenta al aumentar el grado de dilución, mientras que a grados de dilución bajos se obtienen materiales eminentemente microporosos[33,40,208,209]; a pH ligeramente básico, se obtienen geles poliméricos con un gran volumen de microporos y mesoporos a altas concentraciones de reactivos, mientras que a medida que crece el grado de dilución se pasa de un gel polimérico a un gel coloidal formado por partículas grandes interconectadas por cuellos estrechos, lo que produce materiales con baja resistencia mecánica y un volumen de poros reducido[33,40,208,209]. No obstante, hay que tener en cuenta también la forma en la que se va a obtener el gel, ya que, por ejemplo, a la hora de obtener un gel en polvo en un reactor batch con agitación se deben usar mayores proporciones de disolvente que en el caso de los geles en forma de pellets obtenidos en moldes cilíndricos de vidrio sellados[18].

1.2.1.2. Catalizador

Como hemos visto anteriormente, las distintas reacciones de adición y condensación están catalizadas por iones hidroxilo o por protones respectivamente. Esto provoca, en consecuencia, que el hecho de que se opte por usar un catalizador de naturaleza básica o de naturaleza ácida va a modificar significativamente las propiedades del gel final (Tabla 1.3)[38-40,43,194,208,209]. En general, para proporciones de solvente comúnmente usadas en la síntesis de estos geles, los catalizadores ácidos dan lugar a la formación de partículas pequeñas con un alto grado de entrecruzamiento, de forma que se forman redes de macroporos en una estructura tipo nido[43,194]; cuando se usa un catalizador básico, se forman materiales micro-mesoporosos con una porosidad más desarrollada y formado por partículas esféricas más grandes que se unen unas con otras pero sin dar lugar a la formación de estos canales (Figura 1.5)[38-40].

No obstante, la naturaleza ácido-base del catalizador no es el único parámetro que influye en el proceso. Morales-Torres y col.[38] analizaron las variaciones morfológicas y en propiedades texturales de los geles de carbón cuando la polimerización es catalizada por distintos carbonatos alcalinos. Los autores concluyeron que a medida que aumenta el tamaño del catión alcalino, las partículas primarias que se obtienen son de tamaños similares, pero la aglomeración de éstas para formar partículas más grandes va creciendo. Esto hace también que tanto el tamaño de los mesoporos

como el volumen de los mismos vaya aumentando en este sentido, hasta el punto que cuando se usa carbonato de cesio, se obtiene un gel macroporoso (Tabla 1.3).

Tabla 1.3. Propiedades texturales de aerogeles en función del catalizador de polimerización utilizado.

Catalizador	Muestra	R:C	S_{BET} $m^2 \cdot g^{-1}$	W_0 (N_2) $cm^3 \cdot g^{-1}$	V_{meso} $cm^3 \cdot g^{-1}$	V_{Hg} $cm^3 \cdot g^{-1}$	Ref.
Ácido acético	CA	16	463	0.19	0.00	-	194
Ác. p-toluensulfónico	E	8000	751	0.28	0.00	0.33	39
Ác. oxálico	I	800	740	0.30	0.00	0.70	
Li_2CO_3	ALi900		902	0.37	1.06	1.06	
Na_2CO_3	ANa900		1071	0.44	1.23	1.23	
K_2CO_3	AK900	300	1345	0.55	1.32	1.31	38
Rb_2CO_3	ARb900		859	0.35	1.29	1.67	
Cs_2CO_3	ACs900		758	0.30	0.00	1.27	

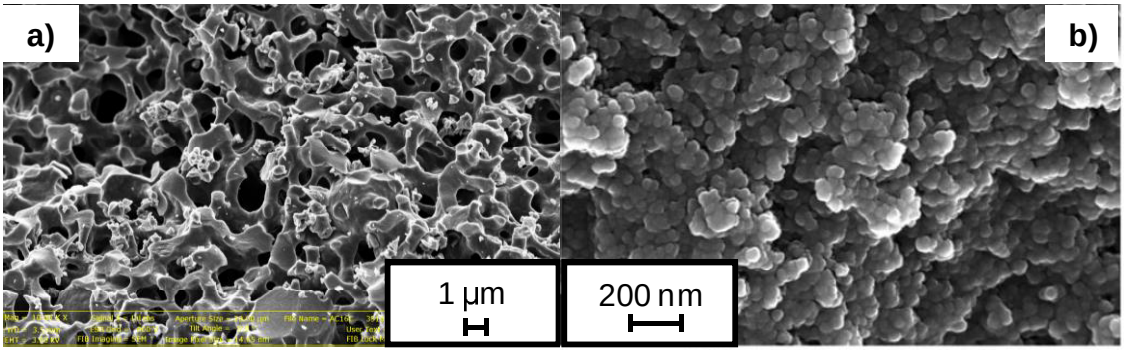

Figura 1.5. Microfotografías de SEM de aerogeles. a) Catalizador ácido acético[43]; b) Catalizador Li_2CO_3[38].

En cuanto a los geles de carbón obtenidos mediante catálisis ácida, estos poseen una microporosidad muy estrecha, que disminuye a medida que aumenta la proporción de catalizador[32,33,40,208,209]. Esto hace que estos materiales sean excelentes candidatos para ser utilizados como tamices moleculares de carbón, especialmente en la separación de isómeros lineales y ramificados, ya que por una parte la microporosidad es accesible

al isómero lineal y no al ramificado y, por otro, la red de macroporos que se forma en estas estructuras, presente siempre que se mantenga durante el secado y la carbonización (que no colapse), facilitará la difusión del compuesto no adsorbido[43].

1.2.1.3. Otras variables

Además de la proporción de reactivos, el grado de dilución y el catalizador, existen otra serie de factores que pueden condicionar las propiedades del material final. Uno de los más utilizados es el uso de surfactantes o moléculas plantilla[31-33,187,188,192,210-212], que permite mediante la formación de micelas, tener un control de la morfología de las partículas y del tamaño de las mismas en función del surfactante empleado y de su concentración, de manera que, por ejemplo, se pueden obtener microesferas aisladas homogéneas en tamaños que pueden ser muy útiles en diversas aplicaciones[210-212].

Otra de las variaciones posibles es la forma en la que se lleva a cabo el gelificado y curado. El proceso de gelificación típico para los geles resorcinol-formaldehido consta de un programa térmico en el cual la mezcla contenida en moldes sellados se mantiene a 25°C durante 24 horas, se calienta a 50°C durante 24 horas más para alcanzar el punto de gel (a partir del cual la disolución pierde su capacidad de fluir) y luego a 80°C durante varios días para producir el curado (aumentando el entrecruzamiento de las partículas formadas)[29,30,32,33,37,43]. Se puede también añadir medio ácido para acelerar esta última etapa. En los últimos años se está desarrollando el empleo de microondas en el proceso de gelificación, cuya principal ventaja está en el menor tiempo necesario para llevar a cabo esta etapa (pasamos de varios días a unas horas para obtener el gel)[203,213]. También se ha estudiado el empleo de monómeros presentes en la naturaleza (como taninos o el ácido gálico), lo que podría abaratar los costes de producción de este tipo de materiales[199,213-215].

1.2.2. Secado

La forma en la que se seca un gel de carbón es tan importante, que es este proceso el que condiciona el nombre que se le da al tipo de material obtenido. De esta manera podemos distinguir tres tipos de geles en función del tipo de secado: aerogeles,

cuando el secado lleva a cabo mediante el empleo de fluidos supercríticos[14,29,30,35,36,38,39]; xerogeles, en los que el secado se lleva a cabo en condiciones por debajo del punto crítico[18,34,36,37,43,180,208,211]; y criogeles en los que se evita el paso de líquido a gas pasando el disolvente a estado sólido y sublimando el mismo[193,205,207]. Los xerogeles y aerogeles son lo que se han aplicado en mayor medida en procesos de adsorción, por lo que en esta Tesis Doctoral se han preparado materiales de estos dos tipos y serán los que se describan en mayor medida.

El secado supercrítico, en el que normalmente se emplea CO_2 (punto crítico T_c = 31°C y P_c = 75atm), es el que da lugar a materiales con mayor porosidad[32,33,36-39]. Esto se debe a la ausencia de tensiones superficiales entre las paredes del sólido y el fluido en condiciones supercríticas, lo que hace que cuando se produce el paso de líquido a fluido supercrítico no haya un colapso de la porosidad. Por ello los aerogeles son réplicas del hidrogel o liogel correspondiente, en el que al final lo único que se ha hecho es eliminar el disolvente del interior de los poros, pero sin que esto produzca un encogimiento de la estructura, lo que daría lugar a poros de menor tamaño y con un volumen total menor. Los principales inconvenientes de los aerogeles son: la necesidad, en el caso de hidrogeles, de llevar a cabo un paso intermedio en el que el agua (no soluble en CO_2 por ser este apolar) debe ser sustituida por un disolvente orgánico (soluble); las altas presiones requeridas para alcanzar el punto crítico hacen difícil implementar el secado supercrítico a nivel industrial, además el CO_2 debe ser introducido a temperaturas bajas para que se mantenga en fase líquida antes de aumentar la presión y la temperatura necesarias para alcanzar el punto crítico[32,33].

En el caso de los xerogeles, su principal inconveniente lo constituye el colapso de la porosidad, resultante del paso de estado líquido a gaseoso del disolvente[32-34,36,37,43]. Este efecto es mayor cuanto mayor es la tensión superficial del líquido a secar. Es por ello que en los últimos años se han desarrollado técnicas de secado que, sin ser tan difíciles de implementar como el secado supercrítico, sean capaces de mantener la estructura porosa del gel en el mayor grado posible. Así, Gallegos-Suárez y col.[36] demostraron que un intercambio del agua por un disolvente con una menor tensión superficial, como puede ser la acetona, reduce el fenómeno del colapso, siendo el volumen y tamaño de mesoporos del xerogel intercambiado con acetona intermedio

entre el del aerogel y el xerogel obtenido por secado directo. Además estos autores demostraron que los tiempos de secado se pueden disminuir mediante el uso de microondas o plasma sin que ello afecte a las propiedades texturales del xerogel resultante.

1.1.3. Carbonización

Una vez secos, los geles deben ser sometidos a un tratamiento en atmosfera inerte para dar lugar a geles de carbón[33,35,40,216]. El tratamiento térmico ha sido estudiado por algunos investigadores mediante ensayos termogravimétricos en atmósfera inerte[35,40,216] en los que se observan las pérdidas de peso a medida que aumenta la temperatura, determinándose que, independientemente de la morfología del gel, hasta 250°C descomponen subproductos de la reacción, a partir de los 300°C los grupos oxigenados comienzan a descomponer, y cuando se aumenta la temperatura hasta 550°C se comienzan a romper también enlaces C-H, produciéndose una reestructuración de los enlaces C-C. Los rendimientos de carbonización de los geles de carbón suelen ser de un 50% aproximadamente, liberándose H_2, H_2O, CO, CO_2 e hidrocarburos de bajo peso molecular durante el proceso. El calentamiento se debe hacer con rampas bajas (1-2 $°C \cdot min^{-1}$) para que la descomposición de los grupos oxigenados y puentes metileno no se produzca de forma abrupta y los gases producto de dicha descomposición puedan salir lentamente[32,33]. La carbonización produce una contracción de la estructura que reduce el tamaño y el volumen de los mesoporos y macroporos, mientras que es durante este proceso cuando se forma la microporosidad, debido a la perdida de los grupos lábiles descrita anteriormente.

1.1.4. Post-tratamientos

Al igual que los materiales obtenidos a partir de desechos o de minerales, los geles de carbón son susceptibles de ser modificados tanto a nivel textural como químico. No obstante, la introducción de heteroátomos se suele llevar a cabo durante el proceso de síntesis, por ejemplo, sustituyendo el resorcinol por monómeros nitrogenados[23,162,180,200]. Sin embargo, es relativamente común que geles con porosidad no muy desarrollada, sean sometidos a procesos de activación para modificar,

principalmente su microporosidad, ya que carece de sentido emplear un método que permita el ajuste de los poros más grandes, para luego modificar esta estructura por un proceso de activación[43,44,172,195-198,203,211].

Para desarrollar la microporosidad de los geles de carbón, se han utilizado principalmente la activación física, tanto con vapor de agua como con dióxido de carbono[43,172,195-198,211], y la activación química con hidróxido de potasio[44,172,197,198,203]. Estos métodos permiten aumentar el volumen de microporos de los geles de carbón, que suele ser reducido, bien por la creación de nuevos microporos o por el ensanchamiento de los microporos ya existentes. En el capítulo VI de esta Tesis, se demuestra como la activación con CO_2 puede servir para ajustar la microporosidad de un xerogel, pasando de un material poco poroso, a uno con propiedades de tamiz molecular para grados de activación bajos, hasta a un filtro de hidrocarburos totales al aumentar el grado de activación.

1.3. ADSORCIÓN DE COMPUESTOS ORGÁNICOS VOLÁTILES (COVs) PRESENTES EN BIOCOMBUSTIBLES Y REFINADO

Como ya se ha comentado, una de las principales aplicaciones de los materiales de carbono en general y del carbón activado en particular es su uso en el control de emisiones contaminantes[12,15,201,217,218]. Esto implica optimizar tanto la textura porosa del carbón como su química superficial, para adaptar sus propiedades al adsorbato concreto, mejorando la interacción con el mismo[9,10,16,17,219-221]. Mediante los procedimientos anteriormente descritos (activación, funcionalización y control sobre el tipo de porosidad) podremos obtener materiales con una serie de propiedades específicas que nos permitan adsorber selectivamente algunos de los compuestos presentes en la mezcla[17,43,73,74,163,220,221].

Una de estas aplicaciones la constituyen los dispositivos tipo canister[17,69,70,222]. Los vehículos a motor llevan instalado entre el depósito y el motor un dispositivo que contiene un adsorbente, generalmente carbón activado (Figura 1.6). El canister retiene los gases resultantes de la evaporación del combustible almacenado en el depósito cuando el motor está parado y al arrancar, se produce el arrastre de estos gases al motor

donde son quemados[69-71,222]. Esto permite prevenir la emisión de contaminantes desde el depósito del coche al aire y, al mismo tiempo, un mejor aprovechamiento del combustible, con el consecuente beneficio medioambiental. Aunque los canister están implantados en los vehículos comerciales desde hace años, sus propiedades no han sido modificadas significativamente ante la aparición de los nuevos biocombustibles[222-227].

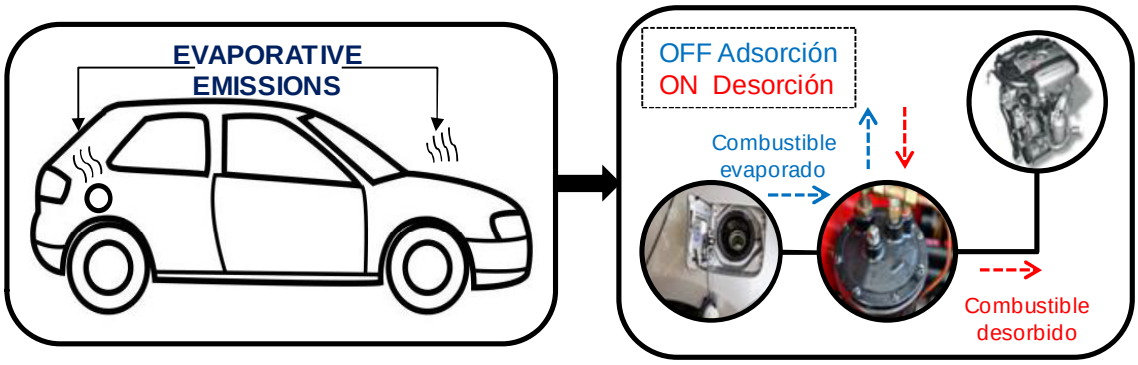

Figura 1.6. Funcionamiento de un canister de vehículos a motor.

Los biocombustibles basados en etanol son atractivos para países que no tienen reservas de combustibles fósiles y que no quieren depender energéticamente de otros. El etanol se comenzó a usar como antidenonante en combustibles, al igual que otros compuestos oxigenados (MTBE, ETBE o TAME) cuando se prohibió el uso del tetraetilplomo[125,226-230]. La introducción de etanol en combustibles para automóviles ha crecido hasta el punto que ya hay muchos biocombustibles cuyo contenido en etanol supera el 50% de la mezcla. El bioetanol de hecho se usa propiamente como un biocombustible[125,228-232].

Sin embargo, aunque el uso de etanol en biocombustibles tiene una serie de ventajas[228,229], como el no depender de los países productores de petróleo, muchos de ellos con un contexto sociopolítico inestable, también plantea una serie de inconvenientes a los que hay que hacer frente. Uno de ellos ha sido estudiado por varios autores, que han llegado a la conclusión de que la adición de etanol a combustibles provoca mayores pérdidas por evaporación, generándose concentraciones de hidrocarburos, tanto alifáticos como aromáticos, mayores[72,225-227,231]. Esto, sumado a que los vapores generados contendrán compuestos polares, hace que las propiedades de los lechos de carbón activado que van a ser usados en los canister deban ser ajustadas

tanto a nivel textural como químico, para que éstos sean capaces de retener tanto los compuestos polares como los apolares[17,71,72,233].

El estudio del comportamiento de un sistema canister es complicado, debido a que la mezcla de sustancias que deben ser adsorbidas es compleja, con lo que son muchos factores los que deben ser analizados. No obstante, existen algunos trabajos que mediante modelos empíricos tratan de estimar las pérdidas por evaporación en vehículos equipados con este tipo de sistemas[69-72,222-225]. En función del diseño del vehículo el canister puede localizarse en la parte trasera junto al depósito o en la parte delantera junto al motor. El propio diseño del coche, la temperatura o el combustible empleado, son algunos de los factores que afectan a las emisiones del vehículo cuando se encuentra parado[71,72,225].

Para mejorar la adsorción de compuestos polares como el etanol, debemos introducir funcionalidades en la superficie del carbón mediante los protocolos de oxidación descritos previamente[17,164,234,235]. Sin embargo, hay que tener en cuenta que, mientras que para la adsorción de etanol a concentraciones bajas la variable crítica va a ser el contenido y la forma de los grupos superficiales oxigenados, a altas concentraciones (próximas a condiciones de saturación) la porosidad total del adsorbente va a ser fundamental para la adsorción de este compuesto[17,164,234]. Además, en los casos en los que el vapor de agua también está presente, la presencia de algunos de estos grupos puede ser contraproducente, ya que puede ser que el agua presente una mayor interacción con estas funcionalidades que el propio contaminante[233,235-237]. Por ello, será necesario ajustar la química superficial del material, pero teniendo en cuenta que una reducción significativa de las propiedades texturales viene acompañada por una menor adsorción de hidrocarburos y de una menor adsorción de etanol si éste se halla a altas concentraciones.

El índice de octanos de un combustible es una propiedad que se determina experimentalmente y que está relacionada con la capacidad de compresión de esa mezcla en un cilindro del motor antes de producirse la detonación de la misma[43,73,74,78,228,229]. Este índice está basado en una escala arbitraria en el que el 0 está asignado al n-heptano (comúnmente empleado como disolvente de la mezcla) y el 100

al 2,2',4-trimetilpentano (TMP). A partir de ellos, se determinan el resto de índices (Tabla 1.4) basándose en la capacidad de cada compuesto para ser comprimido en el cilindro sin llegar a producirse su detonación, y para determinar el número de octanos de una mezcla, se comparará la capacidad antidenonante de la misma con la del TMP puro y la del n-heptano puro.

Tabla 1.4. Índice de octanos de hidrocarburos presentes en biocombustibles[74].

Compuesto	**Índice de octanos**
n-heptano	0
2,2',4-trimetilpentano	100
n-octano	-17
2-metilheptano	22
n-hexano	25
2-metilpentano	44
2,2-dimetilbutano	93

Los antidetonantes oxigenados anteriormente mencionados (alcoholes y éteres) tienen un índice de octanos que en muchos de ellos supera el valor 100 del TMP[228,229]. No obstante, conllevan otra serie de problemas medioambientales como es su alta solubilidad en agua, que los convierte en un contaminante importante de acuíferos[72,220,221,232]. Pero la adición de antidetonantes no es la única forma de mejorar el comportamiento de los combustibles. El índice de octanos también puede ser elevado mediante diversos procesos de refinamiento del combustible[43,73,74,78,238]. Hay que tener en cuenta que los combustibles tal y como se obtienen del petróleo no cumplen las especificaciones necesarias para ningún tipo de combustible comercial. Por ello, para evitar los problemas asociados al uso de combustibles de bajo octanaje en motores de alto régimen de compresión (deterioro de los pistones y las bielas por la detonación prematura de la mezcla) los combustibles deben ser sometidos a diferentes procesos.

Por ejemplo, los hidrocarburos de entre 6 y 8 átomos de carbono son parcialmente convertidos en Benceno, Tolueno y Xilenos (BTX) que tienen índices de

octano muy alto mediante un proceso de aromatización llevado a cabo por un lecho catalítico que a la vez produce la deshidrogenación y la ciclación de estos compuestos[238]. Los hidrocarburos ligeros que son gases a condiciones ambientales se transforman en hidrocarburos más grandes[239] y los más pesados se someten a un proceso de crackeo (generalmente mediante zeolitas) para dar lugar a hidrocarburos de menor peso molecular[240].

Una tendencia que se observa cuando se analizan los índices de octano de distintos hidrocarburos saturados es que este es mayor en el caso de las parafinas ramificadas que en el de las lineales (Tabla 1.4). Por ello, los combustibles suelen ser tratados mediante un tamiz molecular para llevar a cabo una separación de los productos, pudiendo obtenerse un mayor contenido en compuestos ramificados, con lo que el índice de octanos de la mezcla combustible aumentará[43,73,74,78].

La adsorción selectiva de hidrocarburos lineales frente a ramificados ha sido estudiada en distintos adsorbentes como tamices moleculares de carbón[43,73,74,78], zeolitas[241-245] y MOFs[246,247]. Aunque las zeolitas han sido las más usadas debido a que se puede controlar fácilmente el tamaño de sus poros[241-245], en los últimos años, gracias al avance en los procesos para controlar la porosidad de los materiales de carbono, se han desarrollado una serie de tamices moleculares de carbón que son capaces de llevar a cabo este tipo de procesos[43,73,74,78].

1.4. OBTENCIÓN Y REFINADO DE BIOGÁS

El biogás se obtiene mediante digestión anaeróbica de biomasa de distintos orígenes como abonos, restos de la industria alimentaria o cereales[65-68,126,248-250]. Ya existen en algunas ciudades proyectos que pretenden implementar un sistema de transporte público movido por biogás generado a partir de residuos urbanos, por ejemplo, Londres[251]. La composición del biogás (Tabla 1.5) varía dependiendo del origen y del proceso de digestión, pero está compuesto normalmente por metano (alrededor de un 60%), dióxido de carbono (cerca de un 40%) y el resto de componentes

son minoritarios, pero algunos de ellos muy perjudiciales como el sulfuro de hidrógeno o los siloxanos[66,67,126,250,252].

Tabla 1.5. Composición típica del biogás.

Gas	**%**
CH_4	40-75
CO_2	15-60
H_2O	5-10
N_2	0-2
H_2S	0.005-2
Siloxanos	0-0.02
CO	0-0.6

Para que el biogás pueda ser usado en cualquier aplicación es necesario eliminar tanto los siloxanos (ya que pueden dar lugar a SiO_2 que daña las turbinas de los motores)[252,253] como el sulfuro de hidrógeno (corrosivo)[252,254]. Una vez eliminados estos compuestos, se obtiene un biogás que puede ser utilizado, por ejemplo, para obtener la energía eléctrica necesaria para mantener la refinería de biogás en funcionamiento (Figura 1.7)[249,252]. Sin embargo, si el biogás necesita ser licuado para su transporte o va a ser utilizado como combustible, necesita ser convertido en lo que se conoce como biometano, que no es más que metano obtenido a partir de biogás. Para ello es necesario llevar a cabo una etapa en la que el CO_2 presente en la mezcla es separado del CH_4[75,76,255-261].

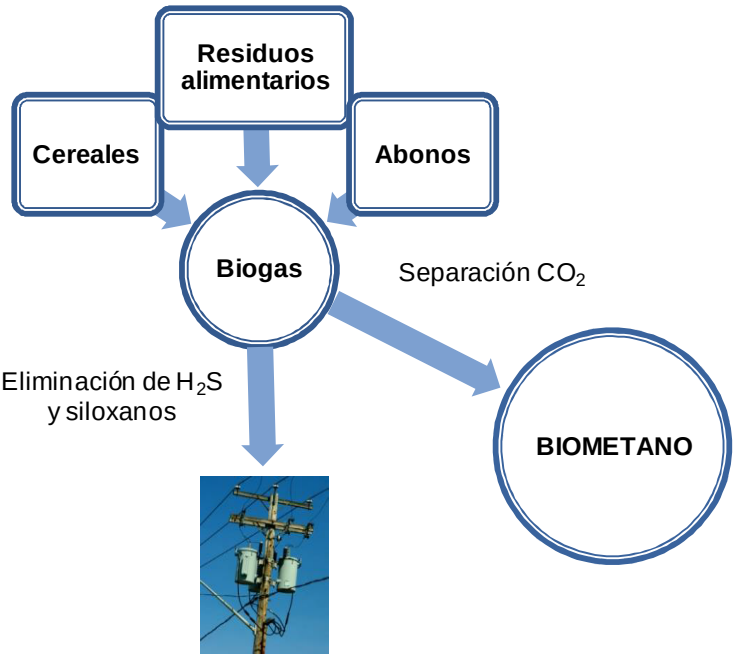

Figura 1.7. Producción y refinamiento de biogás.

En aras de separar el CO_2 presente en el biogás del CH_4 existen diversas tecnologías como la destilación criogénica[262,263], la separación en membranas[264-266] o la absorción en aminas líquidas[60,61,259]. La última es la que se utiliza a nivel industrial (Figura 1.8), sin embargo, plantea una serie de problemas como son la perdida de absorbente por evaporación y, sobre todo, la gran cantidad de energía necesaria para regenerar la amina[77,80,260,267,268]. Con objeto de salvar este inconveniente, se han estudiado tecnologías basadas en la adsorción, de manera que la mezcla se hace pasar por un lecho adsorbente que retiene selectivamente el dióxido de carbono, dejando pasar metano limpio[79,80,255,257,258,260,261,267-275]. Este adsorbente luego es regenerado para ser utilizado nuevamente y en función de cómo se lleva a cabo esta regeneración tenemos diversas técnicas: Temperature Swing-Adsorption (TSA)[274,275], en la que el adsorbente se regenera mediante calentamiento; Pressure Swing-Adsorption (PSA)[79,255,267], en la que se varía la presión para producir la desorción del gas; o Vacuum Pressure Swing-Adsorption (VPSA)[261,275] en la que el compuesto adsorbido se desorbe al hacer vacío en el lecho adsorbente. Las últimas son las más utilizadas ya que requieren de un menor gasto energético y variar la temperatura puede repercutir en las propiedades del material.

Figura 1.8. Planta de refinamiento de biogás por aminas líquidas en Könnern (Alemania).

En cuanto a los adsorbentes utilizados, se han probado MOFs con un alto contenido en nitrógeno[269-271], zeolitas y materiales zeolíticos de tipo red de imidazol (ZIFs)[79,256,257,261,273,276] y carbones activados[77,79,80,93,165,260,267,272]. Los tres primeros son adsorbentes de un precio elevado, lo que limita su aplicabilidad debido a que su precio no es competitivo con el que supone la absorción con aminas líquidas. Sin embargo, el uso de carbones activados que sean capaces de llevar a cabo el proceso, que puedan ser obtenidos a partir de materiales de desecho y por procedimientos sintéticos relativamente sencillos y baratos, puede ser una buena alternativa.

En este sentido, se han preparado materiales de carbón de distintos orígenes, pero principalmente a partir de materiales lignocelulósicos y, concretamente, de madera, para llevar a cabo el refinamiento de biogás, obteniéndose resultados que igualan o incluso mejoran a los obtenidos mediante zeolitas[77,79,80,93,165,260,272,276]. Las propiedades del carbón pueden ser modificadas mediante procesos de activación, para ajustar la porosidad del adsorbente y por introducción de heteroátomos, principalmente nitrógeno, para aumentar la capacidad de adsorción de CO_2[75,76,272]. No obstante, a la hora de llevar a cabo dichos procedimientos hay que tener en cuenta que: el coste final del material no ha de ser elevado para que pueda ser competitivo; la modulación de la selectividad a partir de la introducción de funcionalidades químicas debe ser controlada, de manera que la interacción del adsorbente con la molécula de CO_2 no sea tan fuerte que dificulte

significativamente luego la desorción del gas, lo que llevaría a problemas similares en cuanto a la regeneración de la fase activa a los que encontramos cuando se usan directamente aminas en fase líquida.

1.5. OBJETIVOS

El objetivo principal de la presente Tesis Doctoral es el desarrollo de adsorbentes específicos de COVs presentes en biocombustibles basados en carbono, tanto carbones activados como geles de carbón. También se plantea el refinamiento de biogás mediante separación de mezclas CO_2 y CH_4 por procesos de adsorción selectiva.

De este modo, para la preparación de los adsorbentes se han tenido en cuenta tanto las propiedades del adsorbato concreto (polaridad, tamaño, forma) como las características del proceso de adsorción (concentración, régimen estático o dinámico), con el fin de obtener materiales que sean capaces de adsorber selectiva o específicamente uno o varios gases de una mezcla concreta.

En los primeros capítulos de esta Tesis se detalla el desarrollo de carbones activados a partir de hueso de aceituna para la adsorción específica de etanol y n-octano, ambos COVs presentes en biocombustibles. La porosidad del material se incrementó mediante un proceso de activación química para generar un alto volumen de microporos (para favorecer la adsorción) y de mesoporos (que actúan como alimentadores y mejoran la desorción de los compuestos). El carbón activado fue sometido a un proceso de oxidación para crear una serie de grupos superficiales oxigenados, y luego a tratamientos térmicos a distintas temperaturas para eliminar parte de estos grupos. De esta forma, se pudo estudiar la influencia de los distintos grupos oxigenados en el proceso de adsorción de etanol a bajas concentraciones. Además, puesto que el tratamiento generó modificaciones en la textura porosa de los distintos carbones activados, se pudo estudiar la influencia de la microporosidad en la adsorción de n-octano. Los estudios fueron llevados a cabo en régimen tanto dinámico como estático, se estudió la influencia del vapor de agua en los procesos de adsorción de ambos COVs y la adsorción competitiva de etanol y n-octano. También se intentaron optimizar las

propiedades del lecho mediante la mezcla física de dos de los adsorbentes, para así poder llevar a cabo la adsorción simultánea de ambos contaminantes.

En el capítulo VI de esta Tesis, se plantea el diseño de adsorbentes específicos de hidrocarburos lineales de ramificados. Para ello se sintetizó un aerogel y un xerogel de carbón mediante catálisis ácida, de manera que se obtuvieron materiales con un tamaño medio de microporos por debajo de los 0.7 nm (tamaño menor que el de la molécula de 2,2',4-trimetilpentano, TMP). La porosidad del xerogel fue modificada mediante activación física con CO_2 para estudiar la relación entre la microporosidad del adsorbente y la capacidad para adsorber tanto n-octano (lineal) como TMP (ramificado). Los estudios se llevaron a cabo en régimen dinámico, tanto para la adsorción de cada hidrocarburo individualmente, como para la adsorción competitiva.

Los dos últimos capítulos se refieren a la preparación de carbones para la adsorción selectiva de CO_2 en el refinado de biogás. Este proceso está gobernado principalmente por el tamaño de los microporos y por la presencia de funcionalidades químicas (principalmente grupos de tipo amina) en la superficie del carbón. En este trabajo se han empleado dos materiales: un carbón activado obtenido por activación física con CO_2 de pellets de madera de pino y un xerogel de carbón. En ambos casos se procuró que los materiales tuvieran un volumen de microporos elevado pero cuya anchura fuera pequeña, ya que es en los microporos estrechos donde las diferencias entre la interacción de la superficie del carbón con la molécula de dióxido de carbono y con la de metano son más acentuadas. También se optó por materiales mesoporosos que facilitaran la desorción del CO_2 para regenerar el lecho adsorbente. Ambos materiales fueron caracterizados y utilizados como adsorbentes de ambos gases en condiciones de equilibrio (isotermas a alta presión de cada gas) y en régimen dinámico (tanto de un componente como competitiva), analizándose su comportamiento como adsorbentes selectivos de CO_2.

1.6. BIBLIOGRAFÍA

[1] W.L. Theo, J.S. Lim, H. Hashim, A.A. Mustaffa, and W.S. Ho, Review of pre-combustion capture and ionic liquid in carbon capture and storage, *Applied Energy*, **183** (2016) 1633-1663.

[2] X. Jiang, D. Chen, Z. Ma, and J. Yan, Models for the combustion of single solid fuel particles in fluidized beds: A review, *Renewable and Sustainable Energy Reviews*, **68, Part 1** (2017) 410-431.

[3] P. Babu, P. Linga, R. Kumar, and P. Englezos, A review of the hydrate based gas separation (HBGS) process for carbon dioxide pre-combustion capture, *Energy*, **85** (2015) 261-279.

[4] A. Nandy, C. Loha, S. Gu, P. Sarkar, M.K. Karmakar, and P.K. Chatterjee, Present status and overview of Chemical Looping Combustion technology, *Renewable and Sustainable Energy Reviews*, **59** (2016) 597-619.

[5] A. Baçaoui, A. Dahbi, A. Yaacoubi, C. Bennouna, F.J. Maldonado-Hódar, J. Rivera-Utrilla, F. Carrasco-Marín, and C. Moreno-Castilla, Experimental Design To Optimize Preparation of Activated Carbons for Use in Water Treatment, *Environ. Sci. Technol.*, **36** (2002) 3844-3849.

[6] R.G. Bansal, J.B. Donnet, and F. Stoeckli, *Activated Carbon*, Marcel Dekker, New York and Basel, 1988.

[7] M.I. Bautista-Toledo, J. Rivera-Utrilla, J.D. Méndez-Díaz, M. Sánchez-Polo, and F. Carrasco-Marín, Removal of the surfactant sodium dodecylbenzenesulfonate from water by processes based on adsorption/bioadsorption and biodegradation, *Journal of Colloid and Interface Science*, **418** (2014) 113-119.

[8] A. Derylo-Marczewska, M. Blachnio, A.W. Marczewski, A. Swiatkowski, and B. Buczek, Adsorption of chlorophenoxy pesticides on activated carbon with

gradually removed external particle layers, *Chemical Engineering Journal*, **308** (2017) 408-418.

[9] R.R. Gil, B. Ruiz, M.S. Lozano, M.J. Martín, and E. Fuente, VOCs removal by adsorption onto activated carbons from biocollagenic wastes of vegetable tanning, *Chemical Engineering Journal*, **245** (2014) 80-88.

[10] F. Gironi and V. Piemonte, VOCs removal from dilute vapour streams by adsorption onto activated carbon, *Chemical Engineering Journal*, **172** (2011) 671-677.

[11] C. Ji, P. Xu, S. Wang, Y. Feng, T. Su, M. Yu, and X. Cong, Reducing HC emissions from a gasoline engine at the starting conditions through activated carbon adsorption, *Applied Thermal Engineering*, **112** (2017) 124-132.

[12] F.I. Khan and A. Ghoshal, Removal of Volatile Organic Compounds from polluted air, *Journal of Loss Prevention in the Process Industries*, **13** (2000) 527-545.

[13] J. Lladó, M. Solé-Sardans, C. Lao-Luque, E. Fuente, and B. Ruiz, Removal of pharmaceutical industry pollutants by coal-based activated carbons, *Process Safety and Environmental Protection*, **104, Part A** (2016) 294-303.

[14] F.J. Maldonado-Hódar, C. Moreno-Castilla, F. Carrasco-Marín, and A.F. Pérez-Cadenas, Reversible toluene adsorption on monolithic carbon aerogels, *Journal of Hazardous Materials*, **148** (2007) 548-552.

[15] F.J. Maldonado-Hódar, Removing aromatic and oxygenated VOCs from polluted air stream using Pt–carbon aerogels: Assessment of their performance as adsorbents and combustion catalysts, *Journal of Hazardous Materials*, **194** (2011) 216-222.

[16] J. Rivera-Utrilla, M. Sánchez-Polo, V. Gómez-Serrano, P.M. Álvarez, M.C.M. Alvim-Ferraz, and J.M. Dias, Activated carbon modifications to enhance its

water treatment applications. An overview, *Journal of Hazardous Materials*, **187** (2011) 1-23.

[17] J.F. Vivo-Vilches, E. Bailón-García, A.F. Pérez-Cadenas, F. Carrasco-Marín, and F.J. Maldonado-Hódar, Tailoring activated carbons for the development of specific adsorbents of gasoline vapors, *Journal of Hazardous Materials*, **263, Part 2** (2013) 533-540.

[18] E. Bailón-García, F. Carrasco-Marín, A.F. Pérez-Cadenas, and F.J. Maldonado-Hódar, Development of carbon xerogels as alternative Pt-supports for the selective hydrogenation of citral, *Catalysis Communications*, **58** (2015) 64-69.

[19] B. Meryemoglu, S. Irmak, and A. Hasanoglu, Production of activated carbon materials from kenaf biomass to be used as catalyst support in aqueous-phase reforming process, *Fuel Processing Technology*, **151** (2016) 59-63.

[20] R.M. Mironenko, O.B. Belskaya, T.I. Gulyaeva, M.V. Trenikhin, A.I. Nizovskii, A.V. Kalinkin, V.I. Bukhtiyarov, A.V. Lavrenov, and V.A. Likholobov, Liquid-phase hydrogenation of benzaldehyde over Pd-Ru/C catalysts: Synergistic effect between supported metals, *Catalysis Today*, **279, Part 1** (2017) 2-9.

[21] A. Elmouwahidi, Z. Zapata-Benabithe, F. Carrasco-Marín, and C. Moreno-Castilla, Activated carbons from KOH-activation of argan (Argania spinosa) seed shells as supercapacitor electrodes, *Bioresource Technology*, **111** (2012) 185-190.

[22] M. Olivares-Marín, J.A. Fernández, M.J. Lázaro, C. Fernández-González, A. Macías-García, V. Gómez-Serrano, F. Stoeckli, and T.A. Centeno, Cherry stones as precursor of activated carbons for supercapacitors, *Materials Chemistry and Physics*, **114** (2009) 323-327.

[23] M.J. Mostazo-López, R. Ruiz-Rosas, E. Morallón, and D. Cazorla-Amorós, Nitrogen doped superporous carbon prepared by a mild method. Enhancement

of supercapacitor performance, *International Journal of Hydrogen Energy*, **41** (2016) 19691-19701.

[24] X. Ren, M. Xia, Q. Yan, and C. Ge, Controllable modification of nanostructured carbon with hollow macroporous core/mesoporous shell and its application as templates in aqueous solution, *Chemical Physics Letters*, **662** (2016) 286-290.

[25] P. Jana, V. Fierro, and A. Celzard, Sucrose-based carbon foams with enhanced thermal conductivity, *Industrial Crops and Products*, **89** (2016) 498-506.

[26] X. He, Z. Liu, H. Ma, N. Zhang, M. Yu, and M. Wu, Shell-like hierarchical porous carbons for high-rate performance supercapacitors, *Microporous and Mesoporous Materials*, **236** (2016) 134-140.

[27] Y. Kido, K. Nakanishi, N. Okumura, and K. Kanamori, Hierarchically porous nickel/carbon composite monoliths prepared by sol–gel method from an ionic precursor, *Microporous and Mesoporous Materials*, **176** (2013) 64-70.

[28] J. Gao, X. Wang, Y. Zhang, J. Liu, Q. Lu, and M. Liu, Boron-doped ordered mesoporous carbons for the application of supercapacitors, *Electrochimica Acta*, **207** (2016) 266-274.

[29] R.W. Pekala, Low density, resorcinol-formaldehyde aerogels, US Patent, *US4873218 A*, 1989.

[30] R.W. Pekala, Organic aerogels from the polycondensation of resorcinol with formaldehyde, *Journal of Materials Science*, **24** (1989) 3221-3227.

[31] M. Enterría and J.L. Figueiredo, Nanostructured mesoporous carbons: Tuning texture and surface chemistry, *Carbon*, **108** (2016) 79-102.

[32] F.J. Maldonado-Hódar, Advances in the development of nanostructured catalysts based on carbon gels, *Catalysis Today*, **218–219** (2013) 43-50.

[33] S.A. Al-Muhtaseb and J.A. Ritter, Preparation and Properties of Resorcinol−Formaldehyde Organic and Carbon Gels, *Advanced Materials*, **15** (2003) 101-114.

[34] E.G. Calvo, J.A. Menéndez, and A. Arenillas, Influence of alkaline compounds on the porosity of resorcinol-formaldehyde xerogels, *Journal of Non-Crystalline Solids*, **452** (2016) 286-290.

[35] F.J. Maldonado-Hódar, M.A. Ferro-García, J. Rivera-Utrilla, and C. Moreno-Castilla, Synthesis and textural characteristics of organic aerogels, transition-metal-containing organic aerogels and their carbonized derivatives, *Carbon*, **37** (1999) 1199-1205.

[36] E. Gallegos-Suárez, A.F. Pérez-Cadenas, F.J. Maldonado-Hódar, and F. Carrasco-Marín, On the micro- and mesoporosity of carbon aerogels and xerogels. The role of the drying conditions during the synthesis processes, *Chemical Engineering Journal*, **181–182** (2012) 851-855.

[37] S. Morales-Torres, F.J. Maldonado-Hódar, A.F. Pérez-Cadenas, and F. Carrasco-Marín, Structural characterization of carbon xerogels: From film to monolith, *Microporous and Mesoporous Materials*, **153** (2012) 24-29.

[38] S. Morales-Torres, F.J. Maldonado-Hódar, A.F. Pérez-Cadenas, and F. Carrasco-Marín, Textural and mechanical characteristics of carbon aerogels synthesized by polymerization of resorcinol and formaldehyde using alkali carbonates as basification agents, *Phys. Chem. Chem. Phys.*, **12** (2010) 10365-10372.

[39] D. Fairén-Jiménez, F. Carrasco-Marín, and C. Moreno-Castilla, Porosity and surface area of monolithic carbon aerogels prepared using alkaline carbonates and organic acids as polymerization catalysts, *Carbon*, **44** (2006) 2301-2307.

[40] C. Lin and J.A. Ritter, Effect of synthesis pH on the structure of carbon xerogels, *Carbon*, **35** (1997) 1271-1278.

[41] L. Zhang, W. Dong, and W.C. Li, Nitrogen-doped porous carbon with a 3D network structure produced from resorcinol-gelatin-formaldehyde co-polymers and its use as an electrode material for supercapacitors, *Carbon*, **110** (2016) 521.

[42] C. Alegre, D. Sebastián, M.E. Gálvez, R. Moliner, and M.J. Lázaro, Sulfurized carbon xerogels as Pt support with enhanced activity for fuel cell applications, *Applied Catalysis B: Environmental*, **192** (2016) 260-267.

[43] J.F. Vivo-Vilches, F. Carrasco-Marín, A.F. Pérez-Cadenas, and F.J. Maldonado-Hódar, Fitting the porosity of carbon xerogel by CO2 activation to improve the TMP/n-octane separation, *Microporous and Mesoporous Materials*, **209** (2015) 10-17.

[44] G. Wang, Z. Ling, C. Li, Q. Dong, B. Qian, and J. Qiu, Ionic liquid as template to synthesize carbon xerogels by coupling with KOH activation for supercapacitors, *Electrochemistry Communications*, **31** (2013) 31-34.

[45] X. Cao, X. Dai, and J. Liu, Building energy-consumption status worldwide and the state-of-the-art technologies for zero-energy buildings during the past decade, *Energy and Buildings*, **128** (2016) 198-213.

[46] E. Panos, M. Densing, and K. Volkart, Access to electricity in the World Energy Council's global energy scenarios: An outlook for developing regions until 2030, *Energy Strategy Reviews*, **9** (2016) 28-49.

[47] E. Dace and D. Blumberga, How do 28 European Union Member States perform in agricultural greenhouse gas emissions? It depends on what we look at: Application of the multi-criteria analysis, *Ecological Indicators*, **71** (2016) 352-358.

[48] A.C. Christiansen and J. Wettestad, The EU as a frontrunner on greenhouse gas emissions trading: how did it happen and will the EU succeed?, *Climate Policy*, **3** (2003) 3-18.

[49] M. Meinshausen, N. Meinshausen, W. Hare, S.C.B. Raper, K. Frieler, R. Knutti, D.J. Frame, and M.R. Allen, Greenhouse-gas emission targets for limiting global warming to 2 °C, *Nature*, **458** (2009) 1158-1162.

[50] A. Burnham, J. Han, C.E. Clark, M. Wang, J.B. Dunn, and I. Palou-Rivera, Life-Cycle Greenhouse Gas Emissions of Shale Gas, Natural Gas, Coal, and Petroleum, *Environmental Science & Technology*, **46** (2012) 619-627.

[51] D. Moreira and J.C.M. Pires, Atmospheric CO2 capture by algae: Negative carbon dioxide emission path, *Bioresource Technology*, **215** (2016) 371-379.

[52] D. Archer, M. Eby, V. Brovkin, A. Ridgwell, L. Cao, U. Mikolajewicz, K. Caldeira, K. Matsumoto, G. Munhoven, A. Montenegro, and K. Tokos, Atmospheric Lifetime of Fossil Fuel Carbon Dioxide, *Annual Review of Earth and Planetary Sciences*, **37** (2009) 117-134.

[53] H. Chen, F. Wang, C. Zhao, and N. Khalili, The effect of fly ash on reactivity of calcium based sorbents for CO2 capture, *Chemical Engineering Journal*, **309** (2017) 725-737.

[54] Y. Du, Y. Wang, and G.T. Rochelle, Piperazine/4-hydroxy-1-methylpiperidine for CO2 capture, *Chemical Engineering Journal*, **307** (2017) 258-263.

[55] Y. Hu, G. Xu, C. Xu, and Y. Yang, Thermodynamic analysis and techno-economic evaluation of an integrated natural gas combined cycle (NGCC) power plant with post-combustion CO2 capture, *Applied Thermal Engineering*, **111** (2017) 308-316.

[56] P. Luis, T. Van Gerven, and B. Van der Bruggen, Recent developments in membrane-based technologies for CO2 capture, *Progress in Energy and Combustion Science*, **38** (2012) 419-448.

[57] D. Schweitzer, M. Beirow, A. Gredinger, N. Armbrust, G. Waizmann, H. Dieter, and G. Scheffknecht, Pilot-Scale Demonstration of Oxy-SER steam

Gasification: Production of Syngas with Pre-Combustion CO2 Capture, *Energy Procedia*, **86** (2016) 56-68.

[58] R. Pérez-Vega, A. Abad, F. García-Labiano, P. Gayán, L.F. de Diego, and J. Adánez, Coal combustion in a 50 kWth Chemical Looping Combustion unit: Seeking operating conditions to maximize CO2 capture and combustion efficiency, *International Journal of Greenhouse Gas Control*, **50** (2016) 80-92.

[59] S. Mukherjee, P. Kumar, A. Yang, and P. Fennell, Energy and exergy analysis of chemical looping combustion technology and comparison with pre-combustion and oxy-fuel combustion technologies for CO2 capture, *Journal of Environmental Chemical Engineering*, **3** (2015) 2104-2114.

[60] J. Kim, D.A. Pham, and Y.I. Lim, Gas–liquid multiphase computational fluid dynamics (CFD) of amine absorption column with structured-packing for CO2 capture, *Computers & Chemical Engineering*, **88** (2016) 39-49.

[61] J. Zhang, D.W. Agar, X. Zhang, and F. Geuzebroek, CO2 absorption in biphasic solvents with enhanced low temperature solvent regeneration, *Energy Procedia*, **4** (2011) 67-74.

[62] L.Y. Batan, G.D. Graff, and T.H. Bradley, Techno-economic and Monte Carlo probabilistic analysis of microalgae biofuel production system, *Bioresource Technology*, **219** (2016) 45-52.

[63] R.A. Voloshin, M.V. Rodionova, S.K. Zharmukhamedov, T. Nejat Veziroglu, and S.I. Allakhverdiev, Review: Biofuel production from plant and algal biomass, *International Journal of Hydrogen Energy*, **41** (2016) 17257-17273.

[64] H.B. Aditiya, T.M.I. Mahlia, W.T. Chong, H. Nur, and A.H. Sebayang, Second generation bioethanol production: A critical review, *Renewable and Sustainable Energy Reviews*, **66** (2016) 631-653.

[65] C. Chen, W. Guo, H.H. Ngo, D.J. Lee, K.L. Tung, P. Jin, J. Wang, and Y. Wu, Challenges in biogas production from anaerobic membrane bioreactors, *Renewable Energy*, **98** (2016) 120-134.

[66] H. Chen, J. Wan, K. Chen, G. Luo, J. Fan, J. Clark, and S. Zhang, Biogas production from hydrothermal liquefaction wastewater (HTLWW): Focusing on the microbial communities as revealed by high-throughput sequencing of full-length 16S rRNA genes, *Water Research*, **106** (2016) 98-107.

[67] F.A. Lattieff, A study of biogas production from date palm fruit wastes, *Journal of Cleaner Production*, **139** (2016) 1191-1195.

[68] C. Liu, H. Li, Y. Zhang, and C. Liu, Improve biogas production from low-organic-content sludge through high-solids anaerobic co-digestion with food waste, *Bioresource Technology*, **219** (2016) 252-260.

[69] U. Mohr, Activated carbon canisters for automobiles, *Filtration & Separation*, **34** (1997) 1016-1018.

[70] K. Sato and N. Kobayashi, Adsorption and Desorption Simulation of Carbon Canister Using n-Butane as Model Compound of Gasoline, *Journal of the Japan Petroleum Institute*, **54** (2011) 136-145.

[71] W.M.T.M. Reimerink, J.D. MacDowall, and D. Kleut, New developments of activated carbons for evaporative loss control devices (ELCD), in: *Studies in Surface Science and Catalysis Adsorption and its Applications in Industry and Environmental ProtectionVol II: Applications in Environmental Protection*, Elsevier, 1999, pp. 821-831.

[72] M. De Gennaro, E. Paffumi, and G. Martini, Data-driven analysis of the effectiveness of evaporative emissions control systems of passenger cars in real world use condition: Time and spatial mapping, *Atmospheric Environment*, **129** (2016) 277-293.

[73] G.C. Laredo, J. Castillo, and J.O. Marroquin, Gas-phase diffusion of linear and multi-branched alkanes on a carbon molecular sieve by the ZLC method, *Separation and Purification Technology*, **103** (2013) 36-42.

[74] G.C. Laredo, J.L. Cano, J. Castillo, J.A. Hernandez, and J.O. Marroquin, Octane enhancement by the selective separation of branched and linear paraffins in naphthas using a PVDC-PVC carbon molecular sieve, *Fuel*, **117, Part A** (2014) 660-666.

[75] D.J. Seo, Z. Gou, H. Fujita, T. Fujii, and A. Sakoda, Simple fabrication of molecular sieving carbon for biogas upgrading via a temperature controlled carbonization of Phyllostachys pubescens, *Renewable Energy*, **86** (2016) 693-702.

[76] L. Pino, C. Italiano, A. Vita, C. Fabiano, and V. Recupero, Sorbents with high efficiency for CO2 capture based on amines-supported carbon for biogas upgrading, *Journal of Environmental Sciences*, **48** (2016) 138-150.

[77] N. Álvarez-Gutiérrez, M.V. Gil, F. Rubiera, and C. Pevida, Adsorption performance indicators for the CO2/CH4 separation: Application to biomass-based activated carbons, *Fuel Processing Technology*, **142** (2016) 361-369.

[78] A. Bassam, R.A. Conde-Gutierrez, J. Castillo, G. Laredo, and J.A. Hernandez, Direct neural network modeling for separation of linear and branched paraffins by adsorption process for gasoline octane number improvement, *Fuel*, **124** (2014) 158-167.

[79] M. Kacem, M. Pellerano, and A. Delebarre, Pressure swing adsorption for CO2/N2 and CO2/CH4 separation: Comparison between activated carbons and zeolites performances, *Fuel Processing Technology*, **138** (2015) 271-283.

[80] C.A. Grande, R. Blom, A. Möller, and J. Möllmer, High-pressure separation of CH4/CO2 using activated carbon, *Chemical Engineering Science*, **89** (2013) 10-20.

[81] F. Rodríguez-Reinoso, Activated Carbon and Adsorption A2 - Buschow, K.H. Jürgen, in: *Encyclopedia of Materials: Science and Technology (Second Edition)*, Elsevier, Oxford, 2001, pp. 22-34.

[82] F. Rodriguez-Reinoso and J. Silvestre-Albero, Activated Carbon and Adsorption, *Reference Module in Materials Science and Materials Engineering*, Elsevier, 2016.

[83] H. Marsh and F. Rodríguez-Reinoso, CHAPTER 5 - Activation Processes (Thermal or Physical), in: *Activated Carbon*, Elsevier, Oxford, 2006, pp. 243-321.

[84] C. Moreno-Castilla, F. Carrasco-Marín, M.V. López-Ramón, and M.A. Alvarez-Merino, Chemical and physical activation of olive-mill waste water to produce activated carbons, *Carbon*, **39** (2001) 1415-1420.

[85] F. Rodríguez-Reinoso and M. Molina-Sabio, Activated carbons from lignocellulosic materials by chemical and/or physical activation: an overview, *Carbon*, **30** (1992) 1111-1118.

[86] P. Nowicki, J. Kazmierczak, and R. Pietrzak, Comparison of physicochemical and sorption properties of activated carbons prepared by physical and chemical activation of cherry stones, *Powder Technology*, **269** (2015) 312-319.

[87] M.A. Lillo-Ródenas, D. Cazorla-Amorós, and A. Linares-Solano, Understanding chemical reactions between carbons and NaOH and KOH: An insight into the chemical activation mechanism, *Carbon*, **41** (2003) 267-275.

[88] J.F. Vivo-Vilches, E. Bailón-García, A.F. Pérez-Cadenas, F. Carrasco-Marín, and F.J. Maldonado-Hódar, Tailoring the surface chemistry and porosity of activated carbons: Evidence of reorganization and mobility of oxygenated surface groups, *Carbon*, **68** (2014) 520-530.

[89] A. Ahmadpour and D.D. Do, The preparation of activated carbon from macadamia nutshell by chemical activation, *Carbon*, **35** (1997) 1723-1732.

[90] G.H. Oh and C.R. Park, Preparation and characteristics of rice-straw-based porous carbons with high adsorption capacity, *Fuel*, **81** (2002) 327-336.

[91] P.S. Thue, M.A. Adebayo, E.C. Lima, J.M. Sieliechi, F.M. Machado, G.L. Dotto, J.C.P. Vaghetti, and S.L.P. Dias, Preparation, characterization and application of microwave-assisted activated carbons from wood chips for removal of phenol from aqueous solution, *Journal of Molecular Liquids*, **223** (2016) 1067-1080.

[92] A.R. Mohamed, M. Mohammadi, and G.N. Darzi, Preparation of carbon molecular sieve from lignocellulosic biomass: A review, *Renewable and Sustainable Energy Reviews*, **14** (2010) 1591-1599.

[93] M.G. Plaza, I. Durán, F. Rubiera, and C. Pevida, CO2 adsorbent pellets produced from pine sawdust: Effect of coal tar pitch addition, *Applied Energy*, **144** (2015) 182-192.

[94] A. Amaya, N. Medero, N. Tancredi, H. Silva, and C. Deiana, Activated carbon briquettes from biomass materials, *Bioresource Technology*, **98** (2007) 1635-1641.

[95] F. Carrasco-Marin, J. Rivera-Utrilla, J.P. Joly, and C. Moreno-Castilla, Effects of ageing on the oxygen surface complexes of an oxidized activated carbon, *Journal of the Chemical Society, Faraday Transactions*, **92** (1996) 2779-2782.

[96] D. Lozano-Castelló, M.A. Lillo-Ródenas, D. Cazorla-Amorós, and A. Linares-Solano, Preparation of activated carbons from Spanish anthracite: I. Activation by KOH, *Carbon*, **39** (2001) 741-749.

[97] M.A. Lillo-Ródenas, D. Lozano-Castelló, D. Cazorla-Amorós, and A. Linares-Solano, Preparation of activated carbons from Spanish anthracite: II. Activation by NaOH, *Carbon*, **39** (2001) 751-759.

[98] J. McCarthy, An investigation of the design variables for producing activated carbons from victorian brown coals by reaction with steam, *Carbon*, **15** (1977) 95-101.

[99] A. Khelifi, M.C. Almazán-Almazán, M. Pérez-Mendoza, M. Domingo-García, F.J. López-Domingo, L. Temdrara, F.J. López-Garzón, and A. Addoun, Influence of nitric acid concentration on the characteristics of active carbons obtained from a mineral coal, *Fuel Processing Technology*, **91** (2010) 1338-1344.

[100] R. Mendoza-Carrasco, E.M. Cuerda-Correa, M.F. Alexandre-Franco, C. Fernández-González, and V. Gómez-Serrano, Preparation of high-quality activated carbon from polyethyleneterephthalate (PET) bottle waste. Its use in the removal of pollutants in aqueous solution, *Journal of Environmental Management*, **181** (2016) 522-535.

[101] A. Esfandiari, T. Kaghazchi, and M. Soleimani, Preparation and evaluation of activated carbons obtained by physical activation of polyethyleneterephthalate (PET) wastes, *Journal of the Taiwan Institute of Chemical Engineers*, **43** (2012) 631-637.

[102] A.S. Al-Rahbi and P.T. Williams, Production of activated carbons from waste tyres for low temperature NOx control, *Waste Management*, **49** (2016) 188-195.

[103] R. Acosta, V. Fierro, A. Martinez de Yuso, D. Nabarlatz, and A. Celzard, Tetracycline adsorption onto activated carbons produced by KOH activation of tyre pyrolysis char, *Chemosphere*, **149** (2016) 168-176.

[104] Y. Li, M.P. Paranthaman, K. Akato, A.K. Naskar, A.M. Levine, R.J. Lee, S.O. Kim, J. Zhang, S. Dai, and A. Manthiram, Tire-derived carbon composite

anodes for sodium-ion batteries, *Journal of Power Sources*, **316** (2016) 232-238.

[105] X. He, N. Zhang, X. Shao, M. Wu, M. Yu, and J. Qiu, A layered-template-nanospace-confinement strategy for production of corrugated graphene nanosheets from petroleum pitch for supercapacitors, *Chemical Engineering Journal*, **297** (2016) 121-127.

[106] N.G. Asenjo, C. Botas, C. Blanco, R. Santamaría, M. Granda, R. Menéndez, and P. Alvarez, Synthesis of activated carbons by chemical activation of new anthracene oil-based pitches and their optimization by response surface methodology, *Fuel Processing Technology*, **92** (2011) 1987-1992.

[107] N. Díez, P. Álvarez, R. Santamaría, C. Blanco, R. Menéndez, and M. Granda, Optimisation of the melt-spinning of anthracene oil-based pitch for isotropic carbon fibre preparation, *Fuel Processing Technology*, **93** (2012) 99-104.

[108] M.H. Al-Saleh and U. Sundararaj, A review of vapor grown carbon nanofiber/polymer conductive composites, *Carbon*, **47** (2009) 2-22.

[109] F. Paradela, F. Pinto, A.M. Ramos, I. Gulyurtlu, and I. Cabrita, Study of the slow batch pyrolysis of mixtures of plastics, tyres and forestry biomass wastes, *Journal of Analytical and Applied Pyrolysis*, **85** (2009) 392-398.

[110] A. Bazargan and G. McKay, A review – Synthesis of carbon nanotubes from plastic wastes, *Chemical Engineering Journal*, **195–196** (2012) 377-391.

[111] N.A. Kiselev, J. Sloan, D.N. Zakharov, E.F. Kukovitskii, J.L. Hutchison, J. Hammer, and A.S. Kotosonov, Carbon nanotubes from polyethylene precursors: Structure and structural changes caused by thermal and chemical treatment revealed by HREM, *Carbon*, **36** (1998) 1149-1157.

[112] C. Moreno-Castilla, M.A. Ferro-García, J.P. Joly, I. Bautista-Toledo, F. Carrasco-Marín, and J. Rivera-Utrilla, Activated Carbon Surface Modifications

by Nitric Acid, Hydrogen Peroxide, and Ammonium Peroxydisulfate Treatments, *Langmuir*, **11** (1995) 4386-4392.

[113] A. Elmouwahidi, J.F. Vivo-Vilches, A.F. Pérez-Cadenas, F.J. Maldonado-Hódar, and F. Carrasco-Marín, Free metal oxygen-reduction electro-catalysts obtained from biomass residue of the olive oil industry, *Chemical Engineering Journal*, **306** (2016) 1109-1115.

[114] F. Gao, J. Qu, Z. Zhao, Z. Wang, and J. Qiu, Nitrogen-doped activated carbon derived from prawn shells for high-performance supercapacitors, *Electrochimica Acta*, **190** (2016) 1134-1141.

[115] I. Ghouma, M. Jeguirim, S. Dorge, L. Limousy, C. Matei Ghimbeu, and A. Ouederni, Activated carbon prepared by physical activation of olive stones for the removal of NO2 at ambient temperature, *Comptes Rendus Chimie*, **18** (2015) 63-74.

[116] S. Román, J.F. González, C.M. González-García, and F. Zamora, Control of pore development during CO2 and steam activation of olive stones, *Fuel Processing Technology*, **89** (2008) 715-720.

[117] G.G. Stavropoulos and A.A. Zabaniotou, Production and characterization of activated carbons from olive-seed waste residue, *Microporous and Mesoporous Materials*, **82** (2005) 79-85.

[118] R. Ubago-Pérez, F. Carrasco-Marín, D. Fairén-Jiménez, and C. Moreno-Castilla, Granular and monolithic activated carbons from KOH-activation of olive stones, *Microporous and Mesoporous Materials*, **92** (2006) 64-70.

[119] M. Ugurlu, A. Gürses, and M. Açikyildiz, Comparison of textile dyeing effluent adsorption on commercial activated carbon and activated carbon prepared from olive stone by ZnCl2 activation, *Microporous and Mesoporous Materials*, **111** (2008) 228-235.

[120] R. Yavuz, H. Akyildiz, N. Karatepe, and E. Çetinkaya, Influence of preparation conditions on porous structures of olive stone activated by H3PO4, *Fuel Processing Technology*, **91** (2010) 80-87.

[121] H. Demiral, Î. Demiral, B. Karabacakoglu, and F. Tümsek, Production of activated carbon from olive bagasse by physical activation, *Chemical Engineering Research and Design*, **89** (2011) 206-213.

[122] A. Heidari, H. Younesi, A. Rashidi, and A.A. Ghoreyshi, Evaluation of CO2 adsorption with eucalyptus wood based activated carbon modified by ammonia solution through heat treatment, *Chemical Engineering Journal*, **254** (2014) 503-513.

[123] S. Bashkova and T.J. Bandosz, The effects of urea modification and heat treatment on the process of NO2 removal by wood-based activated carbon, *Journal of Colloid and Interface Science*, **333** (2009) 97-103.

[124] A.J. Romero-Anaya, M.A. Lillo-Ródenas, C. Salinas-Martínez de Lecea, and A. Linares-Solano, Hydrothermal and conventional H3PO4 activation of two natural bio-fibers, *Carbon*, **50** (2012) 3158-3169.

[125] C.A. Cardona and Ó.J. Sánchez, Fuel ethanol production: Process design trends and integration opportunities, *Bioresource Technology*, **98** (2007) 2415-2457.

[126] R. Borja, 2.55 - Biogas Production, in: *Comprehensive Biotechnology (Second Edition)*, Academic Press, Burlington, 2011, pp. 785-798.

[127] A.J. Ward, P.J. Hobbs, P.J. Holliman, and D.L. Jones, Optimisation of the anaerobic digestion of agricultural resources, *Bioresource Technology*, **99** (2008) 7928-7940.

[128] I. García-Maroto, A. García-Maraver, F. Muñoz-Leiva, and M. Zamorano, Consumer knowledge, information sources used and predisposition towards the

adoption of wood pellets in domestic heating systems, *Renewable and Sustainable Energy Reviews*, **43** (2015) 207-215.

[129] H. Thomson and C. Liddell, The suitability of wood pellet heating for domestic households: A review of literature, *Renewable and Sustainable Energy Reviews*, **42** (2015) 1362-1369.

[130] European Council, Council Decision of 10 December 2010 on State aid to facilitate the closure of uncompetitive coal mines, *Official Journal of the European Union*, **336** (2010) 24-29.

[131] J.E. Zafrilla, The mining industry under the thumb of politicians: the environmental consequences of the Spanish Coal Decree, *Journal of Cleaner Production*, **84** (2014) 715-722.

[132] M. Nadal, J. Rovira, J. Díaz-Ferrero, M. Schuhmacher, and J.L. Domingo, Human exposure to environmental pollutants after a tire landfill fire in Spain: Health risks, *Environment International*, **97** (2016) 37-44.

[133] T. Shim, J. Yoo, C. Ryu, Y.K. Park, and J. Jung, Effect of steam activation of biochar produced from a giant Miscanthus on copper sorption and toxicity, *Bioresource Technology*, **197** (2015) 85-90.

[134] J. Alvarez, G. Lopez, M. Amutio, J. Bilbao, and M. Olazar, Preparation of adsorbents from sewage sludge pyrolytic char by carbon dioxide activation, *Process Safety and Environmental Protection*, **103, Part A** (2016) 76-86.

[135] X. Gao, Y. Zhang, B. Li, Y. Zhao, and B. Jiang, Determination of the intrinsic reactivities for carbon dioxide gasification of rice husk chars through using random pore model, *Bioresource Technology*, **218** (2016) 1073-1081.

[136] M.L. Sekirifa, M. Hadj-Mahammed, S. Pallier, L. Baameur, D. Richard, and A.H. Al-Dujaili, Preparation and characterization of an activated carbon from a

date stones variety by physical activation with carbon dioxide, *Journal of Analytical and Applied Pyrolysis*, **99** (2013) 155-160.

[137] M. Molina-Sabio and F. Rodríguez-Reinoso, Role of chemical activation in the development of carbon porosity, *Colloids and Surfaces A: Physicochemical and Engineering Aspects*, **241** (2004) 15-25.

[138] F. Caturla, M. Molina-Sabio, and F. Rodríguez-Reinoso, Preparation of activated carbon by chemical activation with ZnCl2, *Carbon*, **29** (1991) 999-1007.

[139] G.O. El-Sayed, M.M. Yehia, and A.A. Asaad, Assessment of activated carbon prepared from corncob by chemical activation with phosphoric acid, *Water Resources and Industry*, **7–8** (2014) 66-75.

[140] A. Kumar and H. Mohan Jena, High surface area microporous activated carbons prepared from Fox nut (Euryale ferox) shell by zinc chloride activation, *Applied Surface Science*, **356** (2015) 753-761.

[141] J. Laine and A. Calafat, Factors affecting the preparation of activated carbons from coconut shell catalized by potassium, *Carbon*, **29** (1991) 949-953.

[142] R.A. Fiuza-Jr, R.C. Andrade, and H.M.C. Andrade, CO2 capture on KOH-activated carbons derived from yellow mombin fruit stones, *Journal of Environmental Chemical Engineering*, **4** (2016) 4229-4236.

[143] J. Fiuza, R. Medeiros de Jesus Neto, L.B. Correia, and H.M. Carvalho Andrade, Preparation of granular activated carbons from yellow mombin fruit stones for CO2 adsorption, *Journal of Environmental Management*, **161** (2015) 198-205.

[144] P.E. Fanning and M.A. Vannice, A DRIFTS study of the formation of surface groups on carbon by oxidation, *Carbon*, **31** (1993) 721-730.

[145] J.L. Figueiredo, M.F.R. Pereira, M.M.A. Freitas, and J.J.M. Órfão, Modification of the surface chemistry of activated carbons, *Carbon*, **37** (1999) 1379-1389.

[146] C. Moreno-Castilla, M.V. López-Ramón, and F. Carrasco-Marín, Changes in surface chemistry of activated carbons by wet oxidation, *Carbon*, **38** (2000) 1995-2001.

[147] G. de la Puente, J.J. Pis, J.A. Menéndez, and P. Grange, Thermal stability of oxygenated functions in activated carbons, *Journal of Analytical and Applied Pyrolysis*, **43** (1997) 125-138.

[148] A.B. Dongil, B. Bachiller-Baeza, A. Guerrero-Ruiz, I. Rodríguez-Ramos, A. Martínez-Alonso, and J.M.D. Tascón, Surface chemical modifications induced on high surface area graphite and carbon nanofibers using different oxidation and functionalization treatments, *Journal of Colloid and Interface Science*, **355** (2011) 179-189.

[149] E. Papirer, R. Lacroix, and J.B. Donnet, Chemical modifications and surface properties of carbon blacks, *Carbon*, **34** (1996) 1521-1529.

[150] M. Keramati and A.A. Ghoreyshi, Improving CO2 adsorption onto activated carbon through functionalization by chitosan and triethylenetetramine, *Physica E: Low-dimensional Systems and Nanostructures*, **57** (2014) 161-168.

[151] A. Kongnoo, P. Intharapat, P. Worathanakul, and C. Phalakornkule, Diethanolamine impregnated palm shell activated carbon for CO2 adsorption at elevated temperatures, *Journal of Environmental Chemical Engineering*, **4** (2016) 73-81.

[152] W. Feng, E. Borguet, and R.D. Vidic, Sulfurization of carbon surface for vapor phase mercury removal – I: Effect of temperature and sulfurization protocol, *Carbon*, **44** (2006) 2990-2997.

[153] A. Fouladi Tajar, T. Kaghazchi, and M. Soleimani, Adsorption of cadmium from aqueous solutions on sulfurized activated carbon prepared from nut shells, *Journal of Hazardous Materials*, **165** (2009) 1159-1164.

[154] J.M. Rosas, R. Ruiz-Rosas, J. Rodríguez-Mirasol, and T. Cordero, Kinetic study of the oxidation resistance of phosphorus-containing activated carbons, *Carbon*, **50** (2012) 1523-1537.

[155] R. Berenguer, R. Ruiz-Rosas, A. Gallardo, D. Cazorla-Amorós, E. Morallón, H. Nishihara, T. Kyotani, J. Rodríguez-Mirasol, and T. Cordero, Enhanced electro-oxidation resistance of carbon electrodes induced by phosphorus surface groups, *Carbon*, **95** (2015) 681-689.

[156] A.F. Pérez-Cadenas, F.J. Maldonado-Hódar, and C. Moreno-Castilla, On the nature of surface acid sites of chlorinated activated carbons, *Carbon*, **41** (2003) 473-478.

[157] J.A.F. MacDonald, M.J.B. Evans, S. Liang, S.E. Meech, P.R. Norman, and L. Pears, Chlorine and oxygen on the carbon surface, *Carbon*, **38** (2000) 1825-1830.

[158] S. Cho, H.R. Yu, K.D. Kim, K.B. Yi, and Y.S. Lee, Surface characteristics and carbon dioxide capture characteristics of oxyfluorinated carbon molecular sieves, *Chemical Engineering Journal*, **211–212** (2012) 89-96.

[159] H.R. Yu, S. Cho, B.C. Bai, K.B. Yi, and Y.S. Lee, Effects of fluorination on carbon molecular sieves for CH4/CO2 gas separation behavior, *International Journal of Greenhouse Gas Control*, **10** (2012) 278-284.

[160] A. Jafari, M. Ghoranneviss, and A. Salar Elahi, Growth and characterization of boron doped graphene by Hot Filament Chemical Vapor Deposition Technique (HFCVD), *Journal of Crystal Growth*, **438** (2016) 70-75.

[161] C. Moreno-Castilla, A.F. Pérez-Cadenas, F.J. Maldonado-Hódar, F. Carrasco-Marín, and J.L. Fierro, Influence of carbon–oxygen surface complexes on the surface acidity of tungsten oxide catalysts supported on activated carbons, *Carbon*, **41** (2003) 1157-1167.

[162] Z. Zapata-Benabithe, F. Carrasco-Marín, and C. Moreno-Castilla, Preparation, surface characteristics, and electrochemical double-layer capacitance of KOH-activated carbon aerogels and their O- and N-doped derivatives, *Journal of Power Sources*, **219** (2012) 80-88.

[163] F. Carrasco-Marín, A. Mueden, A. Centeno, F. Stoeckli, and C. Moreno-Castilla, Water adsorption on activated carbons with different degrees of oxidation, *Journal of the Chemical Society, Faraday Transactions*, **93** (1997) 2211-2215.

[164] A.J. Romero-Anaya, M.A. Lillo-Ródenas, and A. Linares-Solano, Factors governing the adsorption of ethanol on spherical activated carbons, *Carbon*, **83** (2015) 240-249.

[165] S. Furmaniak, P. Kowalczyk, A.P. Terzyk, P.A. Gauden, and P.J.F. Harris, Synergetic effect of carbon nanopore size and surface oxidation on CO2 capture from CO2/CH4 mixtures, *Journal of Colloid and Interface Science*, **397** (2013) 144-153.

[166] D.B. Mawhinney and J.T. Yates Jr, FTIR study of the oxidation of amorphous carbon by ozone at 300 K - Direct COOH formation, *Carbon*, **39** (2001) 1167-1173.

[167] Z.B. Wang, G.P. Yin, and P.F. Shi, Effects of ozone treatment of carbon support on Pt–Ru/C catalysts performance for direct methanol fuel cell, *Carbon*, **44** (2006) 133-140.

[168] Y. Otake and R.G. Jenkins, Characterization of oxygen-containing surface complexes created on a microporous carbon by air and nitric acid treatment, *Carbon*, **31** (1993) 109-121.

[169] J.H. Zhou, Z.J. Sui, J. Zhu, P. Li, D. Chen, Y.C. Dai, and W.K. Yuan, Characterization of surface oxygen complexes on carbon nanofibers by TPD, XPS and FT-IR, *Carbon*, **45** (2007) 785-796.

[170] B. Marchon, J. Carrazza, H. Heinemann, and G.A. Somorjai, TPD and XPS studies of O2, CO2, and H2O adsorption on clean polycrystalline graphite, *Carbon*, **26** (1988) 507-514.

[171] A.M.T. Silva, B.F. Machado, J.L. Figueiredo, and J.L. Faria, Controlling the surface chemistry of carbon xerogels using HNO3-hydrothermal oxidation, *Carbon*, **47** (2009) 1670-1679.

[172] N. Mahata, M.F.R. Pereira, F. Suárez-García, A. Martínez-Alonso, J.M.D. Tascón, and J.L. Figueiredo, Tuning of texture and surface chemistry of carbon xerogels, *Journal of Colloid and Interface Science*, **324** (2008) 150-155.

[173] V. Gómez-Serrano, M. Acedo-Ramos, A.J. López-Peinado, and C. Valenzuela-Calahorro, Oxidation of activated carbon by hydrogen peroxide. Study of surface functional groups by FT-i.r, *Fuel*, **73** (1994) 387-395.

[174] G. Sun, L. Ma, J. Ran, B. Li, X. Shen, and H. Tong, Templated synthesis and activation of highly nitrogen-doped worm-like carbon composites based on melamine-urea-formaldehyde resins for high performance supercapacitors, *Electrochimica Acta*, **194** (2016) 168-178.

[175] H. Peng, G. Ma, K. Sun, Z. Zhang, Q. Yang, and Z. Lei, Nitrogen-doped interconnected carbon nanosheets from pomelo mesocarps for high performance supercapacitors, *Electrochimica Acta*, **190** (2016) 862-871.

[176] J. Liu, B.V. Cunning, T. Daio, A. Mufundirwa, K. Sasaki, and S.M. Lyth, Nitrogen-Doped Carbon Foam as a Highly Durable Metal-Free Electrocatalyst for the Oxygen Reduction Reaction in Alkaline Solution, *Electrochimica Acta*, **220** (2016) 554-561.

[177] H. Huang, X. Wei, and S. Gao, Nitrogen-Doped Porous Carbon Derived from Malachium Aquaticum Biomass as a Highly Efficient Electrocatalyst for Oxygen Reduction Reaction, *Electrochimica Acta*, **220** (2016) 427-435.

[178] R. Nie, X. Bo, C. Luhana, A. Nsabimana, and L. Guo, Simultaneous formation of nitrogen and sulfur-doped carbon nanotubes-mesoporous carbon and its electrocatalytic activity for oxygen reduction reaction, *International Journal of Hydrogen Energy*, **39** (2014) 12597-12603.

[179] R.L. Tseng, F.C. Wu, and R.S. Juang, Adsorption of CO2 at atmospheric pressure on activated carbons prepared from melamine-modified phenol–formaldehyde resins, *Separation and Purification Technology*, **140** (2015) 53-60.

[180] M. Pérez-Cadenas, C. Moreno-Castilla, F. Carrasco-Marín, and A.F. Pérez-Cadenas, Surface Chemistry, Porous Texture, and Morphology of N-Doped Carbon Xerogels, *Langmuir*, **25** (2009) 466-470.

[181] Y. El-Sayed and T.J. Bandosz, Acetaldehyde Adsorption on Nitrogen-Containing Activated Carbons, *Langmuir*, **18** (2002) 3213-3218.

[182] A. Swiderska-Mocek and E. Rudnicka, Lithium−sulphur battery with activated carbon cloth-sulphur cathode and ionic liquid as electrolyte, *Journal of Power Sources*, **273** (2015) 162-167.

[183] Z. Yang, Z. Yao, G. Li, G. Fang, H. Nie, Z. Liu, X. Zhou, X. Chen, and S. Huang, Sulfur-Doped Graphene as an Efficient Metal-free Cathode Catalyst for Oxygen Reduction, *ACS Nano*, **6** (2012) 205-211.

[184] P. Hadi, M.H. To, C.W. Hui, C.S.K. Lin, and G. McKay, Aqueous mercury adsorption by activated carbons, *Water Research*, **73** (2015) 37-55.

[185] A. Macías-García, C. Valenzuela-Calahorro, A. Espinosa-Mansilla, A. Bernalte-García, and V. Gómez-Serrano, Adsorption of Pb2+ in aqueous solution by SO2-treated activated carbon, *Carbon*, **42** (2004) 1755-1764.

[186] M.M. Bruno, N.G. Cotella, M.C. Miras, T. Koch, S. Seidler, and C. Barbero, Characterization of monolithic porous carbon prepared from resorcinol/formaldehyde gels with cationic surfactant, *Colloids and Surfaces A: Physicochemical and Engineering Aspects*, **358** (2010) 13-20.

[187] J. Xu, A. Wang, and T. Zhang, A two-step synthesis of ordered mesoporous resorcinol–formaldehyde polymer and carbon, *Carbon*, **50** (2012) 1807-1816.

[188] N. Rey-Raap, S. Rodríguez-Sánchez, I.D. Alonso-Buenaposada, E.G. Calvo, J.A. Menéndez, and A. Arenillas, The enhancement of porosity of carbon xerogels by using additives, *Microporous and Mesoporous Materials*, **217** (2015) 39-45.

[189] V.M. Gun'ko, V.M. Bogatyrov, O.I. Oranska, I.V. Urubkov, R. Leboda, B. Charmas, and J. Skubiszewska-Zieba, Synthesis and characterization of resorcinol–formaldehyde resin chars doped by zinc oxide, *Applied Surface Science*, **303** (2014) 263-271.

[190] Y. Kong, Y. Zhong, X. Shen, S. Cui, M. Yang, K. Teng, and J. Zhang, Facile synthesis of resorcinol–formaldehyde/silica composite aerogels and their transformation to monolithic carbon/silica and carbon/silicon carbide composite aerogels, *Journal of Non-Crystalline Solids*, **358** (2012) 3150-3155.

[191] E. Bailón-García, A. Elmouwahidi, M.A. Álvarez, F. Carrasco-Marín, A.F. Pérez-Cadenas, and F.J. Maldonado-Hódar, New carbon xerogel-TiO2 composites with high performance as visible-light photocatalysts for dye mineralization, *Applied Catalysis B: Environmental*, **201** (2017) 29-40.

[192] J. Lee, J. Kim, and T. Hyeon, Recent Progress in the Synthesis of Porous Carbon Materials, *Advanced Materials*, **18** (2006) 2073-2094.

[193] H. Tamon, H. Ishizaka, T. Yamamoto, and T. Suzuki, Influence of freeze-drying conditions on the mesoporosity of organic gels as carbon precursors, *Carbon*, **38** (2000) 1099-1105.

[194] T.F. Baumann, M.A. Worsley, T.Y.-J. Han, and J. Satcher, High surface area carbon aerogel monoliths with hierarchical porosity, *Journal of Non-Crystalline Solids*, **354** (2008) 3513-3515.

[195] Y.M. Chang, C.Y. Wu, and P.W. Wu, Synthesis of large surface area carbon xerogels for electrochemical double layer capacitors, *Journal of Power Sources*, **223** (2013) 147-154.

[196] T. Tsuchiya, T. Mori, S. Iwamura, I. Ogino, and S.R. Mukai, Binderfree synthesis of high-surface-area carbon electrodes via CO2 activation of resorcinol–formaldehyde carbon xerogel disks: Analysis of activation process, *Carbon*, **76** (2014) 240-249.

[197] R.S. Ribeiro, N.A. Fathy, A.A. Attia, A.M.T. Silva, J.L. Faria, and H.T. Gomes, Activated carbon xerogels for the removal of the anionic azo dyes Orange II and Chromotrope 2R by adsorption and catalytic wet peroxide oxidation, *Chemical Engineering Journal*, **195ΓÇô196** (2012) 112-121.

[198] M.S. Contreras, C.A. Páez, L. Zubizarreta, A. Léonard, S. Blacher, C.G. Olivera-Fuentes, A. Arenillas, J.P. Pirard, and N. Job, A comparison of physical activation of carbon xerogels with carbon dioxide with chemical activation using hydroxides, *Carbon*, **48** (2010) 3157-3168.

[199] N.A. Fathy, M.S. Rizk, and R.M.S. Awad, Pore structure and adsorption properties of carbon xerogels derived from carbonization of tannic acid-resorcinol-formaldehyde resin, *Journal of Analytical and Applied Pyrolysis*, **119** (2016) 60-68.

[200] P. Veselá, V. Slovák, T. Zelenka, M. Kostejn, and M. Mucha, The influence of pyrolytic temperature on sorption ability of carbon xerogel based on 3-aminophenol-formaldehyde polymer for Cu(II) ions and phenol, *Journal of Analytical and Applied Pyrolysis*, **121** (2016) 29-40.

[201] R.A. Catalao, F.J. Maldonado-Hódar, A. Fernandes, C. Henriques, and M.F. Ribeiro, Reduction of NO with metal-doped carbon aerogels, *Applied Catalysis B: Environmental*, **88** (2009) 135-141.

[202] S.C. Rodrigues, R. Whitley, and A. Mendes, Preparation and characterization of carbon molecular sieve membranes based on resorcinol–formaldehyde resin, *Journal of Membrane Science*, **459** (2014) 207-216.

[203] E.G. Calvo, N. Ferrera-Lorenzo, J.A. Menéndez, and A. Arenillas, Microwave synthesis of micro-mesoporous activated carbon xerogels for high performance supercapacitors, *Microporous and Mesoporous Materials*, **168** (2013) 206-212.

[204] G.K. Eleftheriadis, M. Filippousi, V. Tsachouridou, M.A. Darda, L. Sygellou, I. Kontopoulou, N. Bouropoulos, T. Steriotis, G. Charalambopoulou, I.S. Vizirianakis, G. Van Tendeloo, and D.G. Fatouros, Evaluation of mesoporous carbon aerogels as carriers of the non-steroidal anti-inflammatory drug ibuprofen, *International Journal of Pharmaceutics*, **515** (2016) 262-270.

[205] A. Feaver and G. Cao, Activated carbon cryogels for low pressure methane storage, *Carbon*, **44** (2006) 590-593.

[206] H. Jirglová, A.F. Pérez-Cadenas, and F.J. Maldonado-Hódar, Synthesis and Properties of Phloroglucinol–Phenol–Formaldehyde Carbon Aerogels and Xerogels, *Langmuir*, **25** (2009) 2461-2466.

[207] B.B. García, D. Liu, S. Sepehri, S. Candelaria, D.M. Beckham, L.W. Savage, and G. Cao, Hexamethylenetetramine multiple catalysis as a porosity and pore size modifier in carbon cryogels, *Journal of Non-Crystalline Solids*, **356** (2010) 1620-1625.

[208] N. Rey-Raap, J. Angel Menéndez, and A. Arenillas, RF xerogels with tailored porosity over the entire nanoscale, *Microporous and Mesoporous Materials*, **195** (2014) 266-275.

[209] N. Rey-Raap, J. Angel Menéndez, and A. Arenillas, Simultaneous adjustment of the main chemical variables to fine-tune the porosity of carbon xerogels, *Carbon*, **78** (2014) 490-499.

[210] F. Awadallah and S.A. Al-Muhtaseb, Nanofeatures of resorcinol–formaldehyde carbon microspheres, *Materials Letters*, **87** (2012) 31-34.

[211] Z. Zapata-Benabithe, J. de Vicente, F. Carrasco-Marín, and C. Moreno-Castilla, Synthesis, surface characteristics, and electrochemical capacitance of Cu-doped carbon xerogel microspheres, *Carbon*, **55** (2013) 260-268.

[212] C. Moreno-Castilla, Colloidal and micro-carbon spheres derived from low-temperature polymerization reactions, *Advances in Colloid and Interface Science*, **236** (2016) 113-141.

[213] N. Rey-Raap, A. Szczurek, V. Fierro, J.A. Menéndez, A. Arenillas, and A. Celzard, Towards a feasible and scalable production of bio-xerogels, *Journal of Colloid and Interface Science*, **456** (2015) 138-144.

[214] N. Rey-Raap, A. Szczurek, V. Fierro, A. Celzard, J.A. Menéndez, and A. Arenillas, Advances in tailoring the porosity of tannin-based carbon xerogels, *Industrial Crops and Products*, **82** (2016) 100-106.

[215] F. Carrasco-Marín, D. Fairén-Jiménez, and C. Moreno-Castilla, Carbon aerogels from gallic acid–resorcinol mixtures as adsorbents of benzene, toluene and xylenes from dry and wet air under dynamic conditions, *Carbon*, **47** (2009) 463-469.

[216] D.W. Schaefer, R. Pekala, and G. Beaucage, Origin of porosity in resorcinol-formaldehyde aerogels, *Journal of Non-Crystalline Solids*, **186** (1995) 159-167.

[217] A. Martínez de Yuso, M.T. Izquierdo, R. Valenciano, and B. Rubio, Toluene and n-hexane adsorption and recovery behavior on activated carbons derived from almond shell wastes, *Fuel Processing Technology*, **110** (2013) 1-7.

[218] S. Morales-Torres, A.F. Pérez-Cadenas, F. Kapteijn, F. Carrasco-Marín, F.J. Maldonado-Hódar, and J.A. Moulijn, Palladium and platinum catalysts supported on carbon nanofiber coated monoliths for low-temperature combustion of BTX, *Applied Catalysis B: Environmental*, **89** (2009) 411-419.

[219] M.M. Abdel daiem, J. Rivera-Utrilla, M. Sánchez-Polo, and R. Ocampo-Pérez, Single, competitive, and dynamic adsorption on activated carbon of compounds used as plasticizers and herbicides, *Science of The Total Environment*, **537** (2015) 335-342.

[220] I. Levchuk, A. Bhatnagar, and M. Sillanpää, Overview of technologies for removal of methyl tert-butyl ether (MTBE) from water, *Science of The Total Environment*, **476–477** (2014) 415-433.

[221] A.M. Redding and F.S. Cannon, The role of mesopores in MTBE removal with granular activated carbon, *Water Research*, **56** (2014) 214-224.

[222] G. Mellios and Z. Samaras, An empirical model for estimating evaporative hydrocarbon emissions from canister-equipped vehicles, *Fuel*, **86** (2007) 2254-2261.

[223] J. Wang, L. Jin, J. Gao, J. Shi, Y. Zhao, S. Liu, T. Jin, Z. Bai, and C.Y. Wu, Investigation of speciated VOC in gasoline vehicular exhaust under ECE and EUDC test cycles, *Science of The Total Environment*, **445–446** (2013) 110-116.

[224] H. Yamada, Contribution of evaporative emissions from gasoline vehicles toward total VOC emissions in Japan, *Science of The Total Environment*, **449** (2013) 143-149.

[225] J.Y. Chin and S.A. Batterman, VOC composition of current motor vehicle fuels and vapors, and collinearity analyses for receptor modeling, *Chemosphere*, **86** (2012) 951-958.

[226] R.K. Niven, Ethanol in gasoline: environmental impacts and sustainability review article, *Renewable and Sustainable Energy Reviews*, **9** (2005) 535-555.

[227] M. Winther, F. Müller, and T.C. Jensen, Emission consequences of introducing bio ethanol as a fuel for gasoline cars, *Atmospheric Environment*, **55** (2012) 144-153.

[228] J.E. Anderson, D.M. DiCicco, J.M. Ginder, U. Kramer, T.G. Leone, H.E. Raney-Pablo, and T.J. Wallington, High octane number ethanol–gasoline blends: Quantifying the potential benefits in the United States, *Fuel*, **97** (2012) 585-594.

[229] T.M. Foong, K.J. Morganti, M.J. Brear, G. da Silva, Y. Yang, and F.L. Dryer, The octane numbers of ethanol blended with gasoline and its surrogates, *Fuel*, **115** (2014) 727-739.

[230] L.A. Graham, S.L. Belisle, and C.L. Baas, Emissions from light duty gasoline vehicles operating on low blend ethanol gasoline and E85, *Atmospheric Environment*, **42** (2008) 4498-4516.

[231] R. Magnusson and C. Nilsson, The influence of oxygenated fuels on emissions of aldehydes and ketones from a two-stroke spark ignition engine, *Fuel*, **90** (2011) 1145-1154.

[232] M.B. Gramajo de Doz, C.M. Bonatti, and H.N. Sólimo, Water Tolerance and Ethanol Concentration in Ethanol-Gasoline Fuels at Three Temperatures, *Energy Fuels*, **18** (2003) 334-337.

[233] J.F. Vivo-Vilches, A.F. Pérez-Cadenas, F. Carrasco-Marín, and F.J. Maldonado-Hódar, About the control of VOCs emissions from blended fuels by developing

specific adsorbents using agricultural residues, *Journal of Environmental Chemical Engineering*, **3** (2015) 2662-2669.

[234] K. Uddin, I.I. El-Sharkawy, T. Miyazaki, B.B. Saha, S. Koyama, H.S. Kil, J. Miyawaki, and S.H. Yoon, Adsorption characteristics of ethanol onto functional activated carbons with controlled oxygen content, *Applied Thermal Engineering*, **72** (2014) 211-218.

[235] L.M. Vane, Separation technologies for the recovery and dehydration of alcohols from fermentation broths, *Biofuels, Bioproducts & Biorefining*, **2** (2008) 553-588.

[236] A. Khazraei Vizhemehr, F. Haghighat, and C.S. Lee, Gas-phase filters breakthrough models at low concentration - Effect of relative humidity, *Building and Environment*, **75** (2014) 1-10.

[237] A.M. Slasli, M. Jorge, F. Stoeckli, and N.A. Seaton, Modelling of water adsorption by activated carbons: effects of microporous structure and oxygen content, *Carbon*, **42** (2004) 1947-1952.

[238] X. Su, G. Wang, X. Bai, W. Wu, L. Xiao, Y. Fang, and J. Zhang, Synthesis of nanosized HZSM-5 zeolites isomorphously substituted by gallium and their catalytic performance in the aromatization, *Chemical Engineering Journal*, **293** (2016) 365-375.

[239] A.G. Popov, V.S. Pavlov, and I.I. Ivanova, Effect of crystal size on butenes oligomerization over MFI catalysts, *Journal of Catalysis*, **335** (2016) 155-164.

[240] Y. Jiao, S. Li, B. Liu, Y. Du, J. Wang, J. Lu, and Y. Chen, Catalytic cracking of RP-3 jet fuel over wall-coated Pt/$Zr_xTi_{0.9-x}Al_{0.1}O_2$ mixed oxides catalysts, *Applied Thermal Engineering*, **91** (2015) 417-425.

[241] J.A.C. Silva and A.E. Rodrigues, Separation of n/iso-paraffins mixtures by pressure swing adsorption, *Separation and Purification Technology*, **13** (1998) 195-208.

[242] L.I. Devriese, J.A. Martens, J.W. Thybaut, G.B. Marin, G.V. Baron, and J.F.M. Denayer, A new methodology to probe Shape Selectivity in Porous Adsorbents, *Microporous and Mesoporous Materials*, **116** (2008) 607-613.

[243] J.F. Denayer, W. Souverijns, P.A. Jacobs, J.A. Martens, and G.V. Baron, High-Temperature Low-Pressure Adsorption of Branched C5−C8 Alkanes on Zeolite Beta, ZSM-5, ZSM-22, Zeolite Y, and Mordenite, *Journal of Physical Chemistry B*, **102** (1998) 4588-4597.

[244] A.F.P. Ferreira, M.C. Mittelmeijer-Hazeleger, M.A. Granato, V.F.D. Martins, A.E. Rodrigues, and G. Rothenberg, Sieving di-branched from mono-branched and linear alkanes using ZIF-8: experimental proof and theoretical explanation, *Physical Chemistry Chemical Physics*, **15** (2013) 8795-8804.

[245] A.F.P. Ferreira, M.C. Mittelmeijer-Hazeleger, J. Bergh, S. Aguado, J.C. Jansen, G. Rothenberg, A.E. Rodrigues, and F. Kapteijn, Adsorption of hexane isomers on MFI type zeolites at ambient temperature: Understanding the aluminium content effect, *Microporous and Mesoporous Materials*, **170** (2013) 26-35.

[246] J.H. Cavka, S. Jakobsen, U. Olsbye, N. Guillou, C. Lamberti, S. Bordiga, and K.P. Lillerud, A New Zirconium Inorganic Building Brick Forming Metal Organic Frameworks with Exceptional Stability, *Journal of the American Chemical Society*, **130** (2008) 13850-13851.

[247] P.A.P. Mendes, F. Ragon, A.E. Rodrigues, P. Horcajada, C. Serre, and J.A.C. Silva, Hexane isomers sorption on a functionalized metal–organic framework, *Microporous and Mesoporous Materials*, **170** (2013) 251-258.

[248] K. Bernat, A. Cydzik-Kwiatkowska, I. Wojnowska-Bary+éa, and M. Karczewska, Physicochemical properties and biogas productivity of aerobic

granular sludge and activated sludge, *Biochemical Engineering Journal*, **117, Part B** (2017) 43-51.

[249] S.E. Hosseini and M.A. Wahid, Utilization of biogas released from palm oil mill effluent for power generation using self-preheated reactor, *Energy Conversion and Management*, **105** (2015) 957-966.

[250] M. Balat and H. Balat, Biogas as a Renewable Energy Source–A Review, *Energy Sources, Part A: Recovery, Utilization, and Environmental Effects*, **31** (2009) 1280-1293.

[251] A. Velazquez Abad, T. Cherrett, and P. Holdsworth, Waste-to-fuel opportunities for British quick service restaurants: A case study, *Resources, Conservation and Recycling*, **104, Part A** (2015) 239-253.

[252] F. Bauer, T. Persson, C. Hulteberg, and D. Tamm, Biogas upgrading – technology overview, comparison and perspectives for the future, *Biofuels, Bioproducts & Biorefining*, **7** (2013) 499-511.

[253] A. Cabrera-Codony, A. Georgi, R. Gonzalez-Olmos, H. Valdés, and M.J. Martín, Zeolites as recyclable adsorbents/catalysts for biogas upgrading: Removal of octamethylcyclotetrasiloxane, *Chemical Engineering Journal*, **307** (2017) 820-827.

[254] L. Sigot, M. Fontseré Obis, H. Benbelkacem, P. Germain, and G. Ducom, Comparing the performance of a 13X zeolite and an impregnated activated carbon for H2S removal from biogas to fuel an SOFC: Influence of water, *International Journal of Hydrogen Energy*, **41** (2016) 18533-18541.

[255] R. Augelletti, M. Conti, and M.C. Annesini, Pressure swing adsorption for biogas upgrading. A new process configuration for the separation of biomethane and carbon dioxide, *Journal of Cleaner Production*, **140, Part 3** (2017) 1390-1398.

[256] S. Cavenati, C.A. Grande, and A.E. Rodrigues, Adsorption Equilibrium of Methane, Carbon Dioxide, and Nitrogen on Zeolite 13X at High Pressures, *Journal of Chemical Engineering Data*, **49** (2004) 1095-1101.

[257] Z. Bacsik, O. Cheung, P. Vasiliev, and N. Hedin, Selective separation of CO2 and CH4 for biogas upgrading on zeolite NaKA and SAPO-56, *Applied Energy*, **162** (2016) 613-621.

[258] M.J. Regufe, J. Tamajon, A.M. Ribeiro, A. Ferreira, U.H. Lee, Y.K. Hwang, J.S. Chang, C. Serre, J.M. Loureiro, and A.E. Rodrigues, Syngas Purification by Porous Amino-Functionalized Titanium Terephthalate MIL-125, *Energy Fuels*, **29** (2015) 4654-4664.

[259] Y. Liu, H. Li, G. Wei, H. Zhang, X. Li, and Y. Jia, Mass transfer performance of CO2 absorption by alkanolamine aqueous solution for biogas purification, *Separation and Purification Technology*, **133** (2014) 476-483.

[260] M.V. Gil, N. Álvarez-Gutiérrez, M. Martínez, F. Rubiera, C. Pevida, and A. Morán, Carbon adsorbents for CO2 capture from bio-hydrogen and biogas streams: Breakthrough adsorption study, *Chemical Engineering Journal*, **269** (2015) 148-158.

[261] M.C. Campo, A.M. Ribeiro, A.F.P. Ferreira, J.C. Santos, C. Lutz, J.M. Loureiro, and A.E. Rodrigues, Carbon dioxide removal for methane upgrade by a VSA process using an improved 13X zeolite, *Fuel Processing Technology*, **143** (2016) 185-194.

[262] A.M.I. Yousef, Y.A. Eldrainy, W.M. El-Maghlany, and A. Attia, Upgrading biogas by a low-temperature CO2 removal technique, *Alexandria Engineering Journal*, **55** (2016) 1143-1150.

[263] G. De Guido, S. Langè, and L.A. Pellegrini, Refrigeration cycles in low-temperature distillation processes for the purification of natural gas, *Journal of Natural Gas Science and Engineering*, **27, Part 2** (2015) 887-900.

[264] E. Favre, R. Bounaceur, and D. Roizard, Biogas, membranes and carbon dioxide capture, *Journal of Membrane Science*, **328** (2009) 11-14.

[265] A. Molino, M. Migliori, Y. Ding, B. Bikson, G. Giordano, and G. Braccio, Biogas upgrading via membrane process: Modelling of pilot plant scale and the end uses for the grid injection, *Fuel*, **107** (2013) 585-592.

[266] A. Makaruk, M. Miltner, and M. Harasek, Membrane biogas upgrading processes for the production of natural gas substitute, *Separation and Purification Technology*, **74** (2010) 83-92.

[267] Y.J. Kim, Y.S. Nam, and Y.T. Kang, Study on a numerical model and PSA (pressure swing adsorption) process experiment for CH4/CO2 separation from biogas, *Energy*, **91** (2015) 732-741.

[268] L. Yang, X. Ge, C. Wan, F. Yu, and Y. Li, Progress and perspectives in converting biogas to transportation fuels, *Renewable and Sustainable Energy Reviews*, **40** (2014) 1133-1152.

[269] P. Serra-Crespo, R. Berger, W. Yang, J. Gascon, and F. Kapteijn, Separation of CO2/CH4 mixtures over NH2-MIL-53–An experimental and modelling study, *Chemical Engineering Science*, **124** (2015) 96-108.

[270] A.F.P. Ferreira, A.M. Ribeiro, S. Kulaç, and A.E. Rodrigues, Methane purification by adsorptive processes on MIL-53(Al), *Chemical Engineering Science*, **124** (2015) 79-95.

[271] Z.H. Rada, H.R. Abid, J. Shang, Y. He, P. Webley, S. Liu, H. Sun, and S. Wang, Effects of amino functionality on uptake of CO2, CH4 and selectivity of CO2/CH4 on titanium based MOFs, *Fuel*, **160** (2015) 318-327.

[272] T. Dasgupta, S.N. Punnathanam, and K.G. Ayappa, Effect of functional groups on separating carbon dioxide from CO2/N2 gas mixtures using edge

functionalized graphene nanoribbons, *Chemical Engineering Science*, **121** (2015) 279-291.

[273] X. Wu, M. Niknam Shahrak, B. Yuan, and S. Deng, Synthesis and characterization of zeolitic imidazolate framework ZIF-7 for CO2 and CH4 separation, *Microporous and Mesoporous Materials*, **190** (2014) 189-196.

[274] M. Clausse, J. Bonjour, and F. Meunier, Adsorption of gas mixtures in TSA adsorbers under various heat removal conditions, *Chemical Engineering Science*, **59** (2004) 3657-3670.

[275] N. Tlili, G. Grévillot, and C. Vallières, Carbon dioxide capture and recovery by means of TSA and/or VSA, *International Journal of Greenhouse Gas Control*, **3** (2009) 519-527.

[276] J. McEwen, J.D. Hayman, and A. Ozgur Yazaydin, A comparative study of CO2, CH4 and N2 adsorption in ZIF-8, Zeolite-13X and BPL activated carbon, *Chemical Physics*, **412** (2013) 72-76.

Capítulo II

MATERIALES Y MÉTODOS

En este capítulo se detallan los procedimientos experimentales que se usaron para obtener los distintos materiales y las distintas técnicas utilizadas para caracterizar los adsorbentes tanto a nivel textural como químico. También se describe el diseño de las instalaciones en las que se han llevado a cabo las distintas experiencias que nos permiten testar los materiales como adsorbentes específicos de compuestos orgánicos volátiles (COVs) y de gases. Finalmente, se detallan las ecuaciones y modelos que permiten analizar los resultados obtenidos, incluyendo los fundamentos teóricos en los que se basan cada una de las técnicas usadas.

2.1. PREPARACIÓN DE MUESTRAS

2.1.1. Carbones activados obtenidos a partir de residuos de biomasa

2.1.1.1.Activación química de hueso de aceituna

La preparación de carbones activados a partir de hueso de aceituna tuvo como primera etapa la preparación del material de partida, el cual fue molturado y tamizado a tamaños de partícula entre 1.0 y 2.0 mm. Posteriormente, fue tratado con H_2SO_4 1M para eliminar restos de materia inorgánica presentes en el hueso y se lavó con agua destilada hasta ausencia de sulfatos.

Para llevar a cabo la activación química con hidróxido de potasio (KOH), se procedió a una etapa previa de carbonización en atmósfera inerte a baja temperatura (10 °C·min^{-1}, 400°C 2h, N_2 300 cm^3·min^{-1}) con objeto de tener una estructura carbonosa estable previa a la activación. Este carbonizado de hueso de aceituna se mezcló con KOH en una proporción másica 1:7 (C:KOH), sometiéndose la mezcla a un proceso de activación a alta temperatura en nitrógeno (10 °C·min^{-1}, 350 °C 2h, 850 °C 3h, N_2 300 cm^3·min^{-1}).

Una vez enfriado, el material se retiró del horno y se llevó a cabo un tratamiento con ácido clorhídrico HCl 0.1M para neutralizar el exceso de KOH. Con objeto de reducir el contenido en materia inorgánica se llevó a cabo un proceso de

desmineralización siguiendo el método desarrollado por Bishop-Ward[1]. Este proceso consiste en tratar el material de carbón con distintas cantidades de HCl y HF de manera que se puedan solubilizar los compuestos inorgánicos presentes en el carbón activado. Una vez realizados dichos tratamientos ácidos, el material de carbón ya desmineralizado es lavado con agua destilada hasta ausencia de cloruros. El material así obtenido se denominó CA y el rendimiento global del proceso fue de un 15%. En la Fig. 2.1 se representa el proceso de síntesis en forma de esquema.

Figura 2.1. Síntesis de la muestra CA obtenida por activación química de hueso de aceituna.

2.1.1.2. Oxidación y descomposición selectiva de grupos oxigenados

La muestra CA fue dividida en porciones, una de las cuales fue sometida a un proceso de oxidación con una disolución saturada de peroxidisulfatoamónico[2] (($(NH_4)_2S_2O_8$) en H_2SO_4 1M (600 $g \cdot L^{-1}$)y a temperatura ambiente. Para ello, la disolución se mezcló con el carbón activado en una proporción de 20 $mL \cdot g^{-1}$y se dejó reaccionar durante 24 h en agitación. Una vez transcurrida la reacción, el carbón activado se filtró y se lavó repetidamente con agua destilada hasta ausencia de sulfatos, secándose en una estufa a 110 °C. El material obtenido se denominó CAOX.

Como ya se vio en el Capítulo I, los distintos grupos oxigenados presentes en una estructura carbonosa presentan diferencias en cuanto su estabilidad térmica[3,4] (Tabla 1.2). Basándose en esto, el carbón activado CAOX fue también dividido en distintas porciones que, con objeto de eliminar selectivamente los distintos tipos de grupos superficiales oxigenados, se sometieron a tratamientos térmicos en atmósfera inerte y a temperatura creciente: 300 °C, 500 °C y 700 °C (10 min, 20 °C·min^{-1}, N_2 150 cm^3·min^{-1}). Los materiales así obtenidos fueron denominados CAOX300, CAOX500 y CAOX700 respectivamente, en función de la temperatura a la que fueron tratados. La obtención de muestras por oxidación y la eliminación térmica selectiva de grupos superficiales se resumen en la Fig. 2.2.

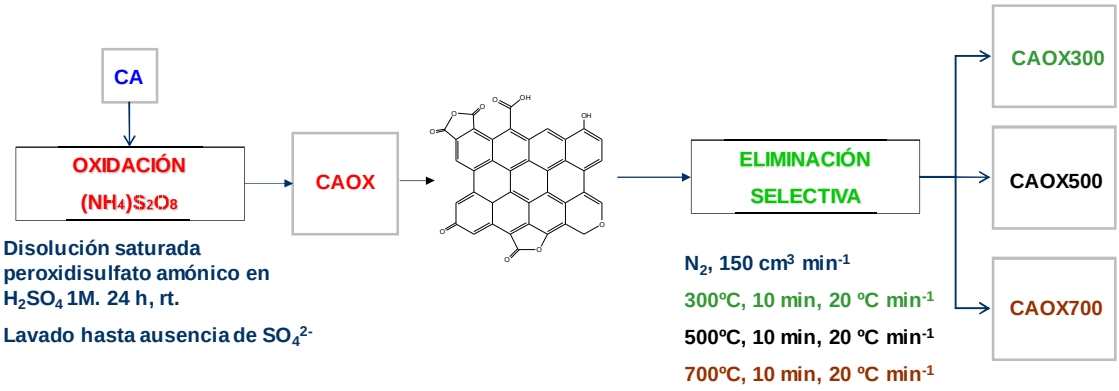

Figura 2.2. Oxidación del CA y tratamientos térmicos para descomposición selectiva de grupos superficiales oxigenados.

2.1.1.3. Activación física de pellets de madera de pino

Para la preparación de carbón activado a partir de pellets de madera se partió de un producto comercial suministrado por Los Reyes del Pellets C.B.. Este material, usado en calefacción doméstica, se obtiene por extrusión en caliente de astillas de madera provenientes principalmente de desechos de la industria maderera. La normativa europea prohíbe el uso de aditivos para la fabricación de pellets en este tipo de aplicaciones, por lo que la humedad tiene que ser controlada durante el proceso.

Una porción de estos pellets fue carbonizada en atmósfera inerte (10 °C·min^{-1}, 900 °C 2h, N_2 300 cm^3·min^{-1}). La muestra carbonizada se denominó PINPEL y el rendimiento del proceso fue 25%. Con una segunda porción, se preparó una muestra activada físicamente con CO_2. Para ello, el tratamiento comienza con una carbonización similar a la usada previamente, pero una vez alcanzados los 900 °C, el flujo de N_2se cambió por otro similar de CO_2 y se mantuvo la muestra en estas condiciones durante 5 h, tras este tiempo de activación, se retorna al flujo de N_2 para enfriar la muestra en el horno en atmósfera inerte. El grado de activación alcanzado fue del 20% respecto al carbonizado en nitrógeno, por lo quela muestra se nombró como PINPEL20. En la Fig. 2.4 se representa el proceso desde las astillas de pino hasta los materiales finales.

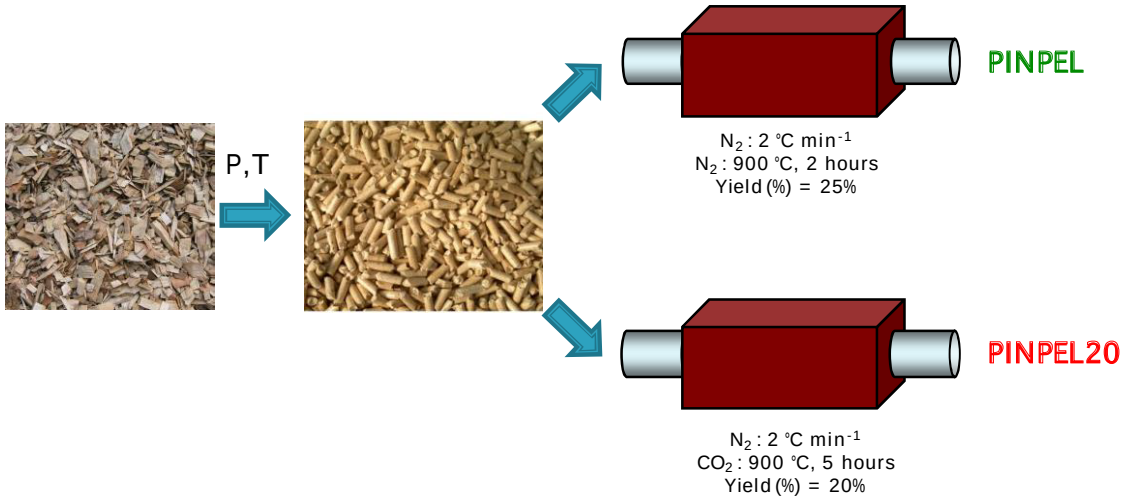

Figura 2.4. Síntesis de las muestras PINPEL y PINPEL20.

2.1.2. Aerogeles y xerogeles de carbón

2.1.2.1. Aerogel y Xerogel de carbón obtenidos por catálisis ácida

Para llevar a cabo el proceso sol-gel[5,6] se procedió a la solubilización en agua de los distintos reactivos: los monómeros resorcinol y formaldehído (en relación molar R/F = 0.5) y el ácido acético usado como catalizador de polimerización (en relación molar R/C = 16). La proporción molar R/W elegida fue 1/7.5 incluyendo el agua

presente en el formaldehido. Estas proporciones fueron ajustadas, acorde a la bibliografía disponible, para obtener un material con las propiedades texturales deseadas[7]. Los reactivos empleados fueron: resorcinol, 99% (Sigma-Aldrich); formaldehido, 37% (Sigma-Aldrich); y ácido acético glacial (Panreac).

La disolución preparada fue introducida en moldes cilíndricos de vidrio (diámetro interno 6 mm) que se sellaron por ambos extremos. El proceso de gelificación se llevó a cabo en el interior de una estufa mediante un programa de temperatura (25 °C 1 día, 50 °C 1 día, 80 °C 5 días). Transcurrido este tiempo el hidrogel fue sacado de los moldes, cortado en pellets de 2-3 cm y sumergidos en acetona durante tres días, cambiando el disolvente cada día, para intercambiar el agua por el disolvente orgánico. Esta etapa, como ya se comentó en el Capítulo I, es necesaria en el caso del secado supercrítico con CO_2, ya que el agua no es soluble en este; sin embargo, también es recomendable llevarla a cabo cuando se opta por un secado térmico, ya que presenta una menor tensión superficial, con lo que se reduce el colapso de la porosidad en esta etapa del proceso[8].

En aras de obtener el aerogel, parte del material se sometió a un proceso de secado con CO_2 supercrítico (41°C, 100 bar, 6h). El resto se secó en una estufa a vacío (50 °C, 65 mbar, 3 h) para obtener el xerogel. Una vez secas ambas muestras se carbonizaron en un horno tubular con flujo de nitrógeno (2 °C·min^{-1}, 900 °C 2 h, N_2 300 cm^3·min^{-1}). El aerogel se denominó AC16 y el xerogel AC16X.

2.1.2.2. Activación física con CO_2 del xerogel de carbón AC16X

Para ajustar la microporosidad del xerogel de carbón AC16X, la muestra se dividió en varias porciones que fueron activadas a 870 °C con mezclas de CO_2 y N_2 hasta distintos porcentajes: 5, 10, 20 y 40 %. Estos procesos generan nuevos microporos a bajos grados de activación y ensanchan los microporos ya generados a grados más altos. Las muestras se denominaron AC16X5, AC16X10, AC16X20 y AC16X40, de acuerdo con su grado de activación. En la Fig.2.3 se representa tanto la síntesis del aerogel y el xerogel, como la etapa de activación de este último.

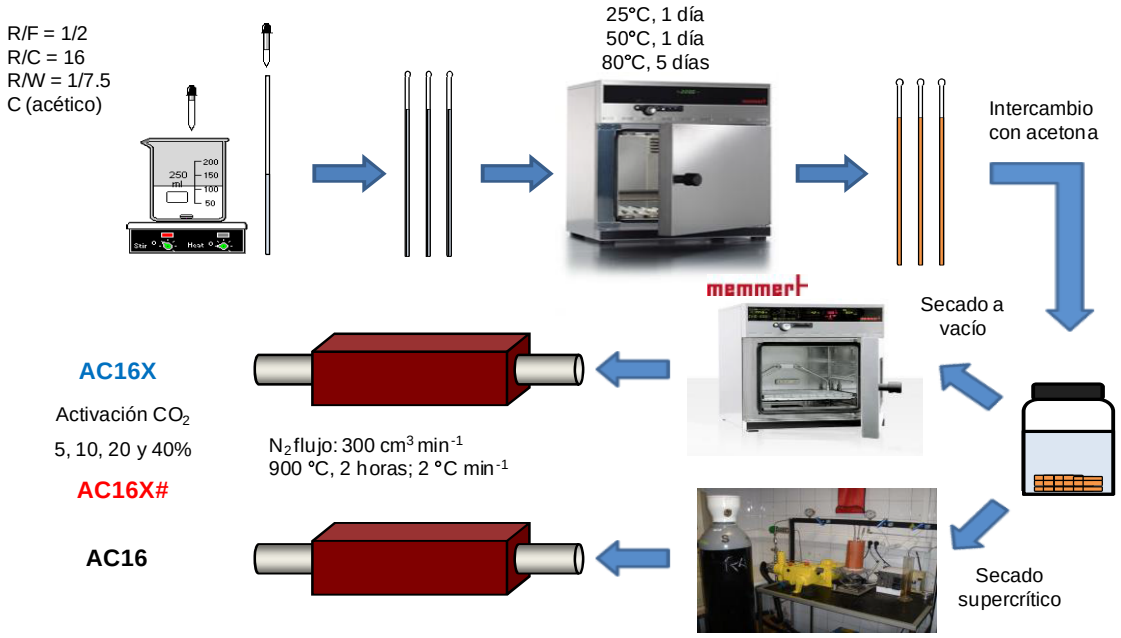

Figura 2.3. Síntesis, carbonización y activación de las muestras de la serie AC16 y AC16X.

2.1.2.3. Xerogel de carbón obtenido por catálisis básica

Para generar macroporos anchos similares a los encontrados en las muestras derivadas de la madera y un gran volumen de microporos estrechos, se optó por usar el Cs_2CO_3 como catalizador de polimerización, de acuerdo con trabajos previos desarrollados en esteGrupo[9]. Al igual que en el caso de las muestras sintetizadas por catálisis ácida, se preparó una disolución acuosa empleando como monómeros el resorcinol, 99% (Sigma-Aldrich) y el formaldehido, 37% (Sigma-Aldrich), y como catalizador Carbonato de Cesio, 99.9% (Sigma-Aldrich). Las relaciones molares usadas fueron R/F = 0.5, R/W = 0.07 y R/C = 300.

Una vez disueltos los reactivos, la mezcla se transfirió a moldes cilíndricos de vidrio que fueron sellados por ambos extremos. Ya en los moldes, la mezcla fue gelificada en condiciones controladas de temperatura con el siguiente programa: 25 °C 1 día, 50 °C 1 día, 80 °C 5 días. Concluida la gelificación, el gel fue sacado de los moldes y cortado en pellets de 2-3 cm que fueron secados en una estufa a 110 °C

durante 12 h. El xerogel orgánico ya seco fue carbonizado en atmósfera inerte (1.5 °C·min^{-1}, 900 °C 2 h, N_2 300 cm^3·min^{-1}). La muestra se denominó XCs300 y en la Fig. 2.5 se puede encontrar un resumen del proceso de preparación en forma de esquema.

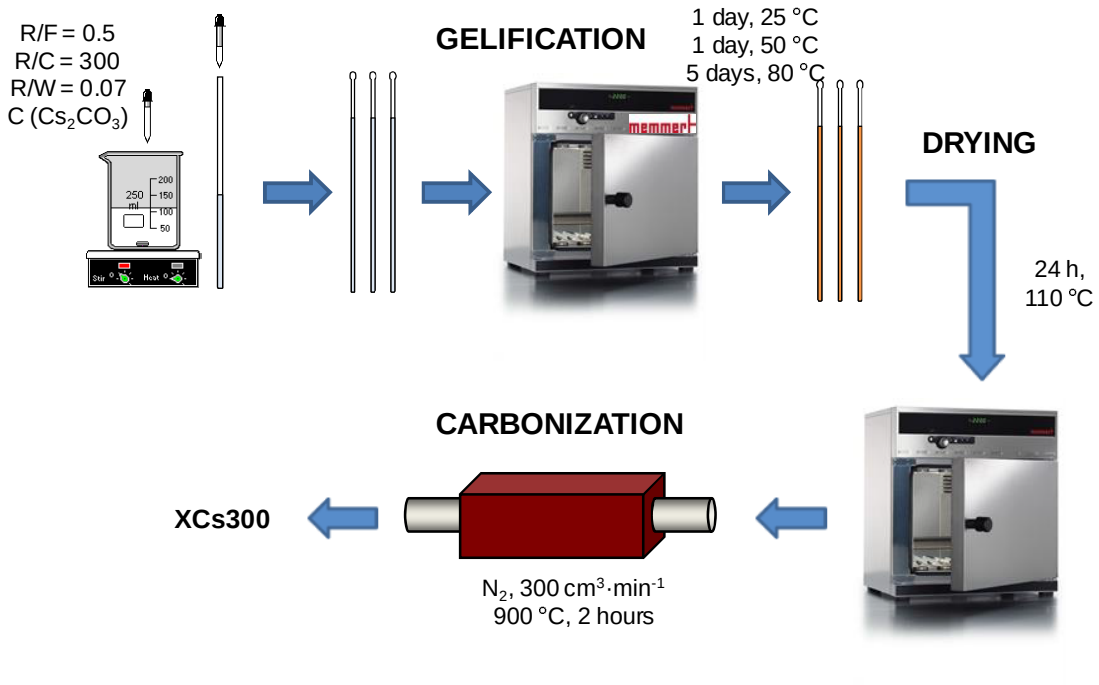

Figura 2.5. Síntesis de la muestra XCs300.

2.2. CARACTERIZACIÓN TEXTURAL

2.2.1. Adsorción física de gases

Las isotermas de adsorción de N_2 a -196 °C y de CO_2 a 0 °C fueron obtenidas en un equipo QUADRASORB-SI y en un AUTOSORB-1C ambos de la casa comercial Quantachrome Ins.. Para ello aproximadamente 0.1 g de muestra se introducen en un bulbo de 9 mm y se desgasifican a alto vacío (10^{-6} bar) a 110 °C durante 12 h. Los adsorbatos fueron nitrógeno (99.999 %) y dióxido de carbono (99.999 %) suministrados por Air Liquide.

A partir de las isotermas de N_2 se calcularon los siguientes parámetros: la superficie específica (S_{BET}) mediante el modelo propuesto por Brünauer, Emmett y Teller[10] (B.E.T.), el volumen de microporos (W_0) por el método de Dubinin-Radushkevich[11], la anchura media de microporos (L_0) a partir de la ecuación de Stoeckli[12] y el volumen de mesoporos (V_{meso}) aplicando el método de Barrett, Joyner y Halenda[13] (B.J.H.). En el caso de la isoterma de adsorción de CO_2 se obtuvieron también el volumen y la anchura media de los microporos más estrechos de la misma forma. Las ecuaciones y los distintos modelos empleados se describen a continuación.

2.2.1.1. Ecuación de B.E.T.

El modelo de Brünauer-Emmett-Teller[10] se basa en la formación de una monocapa a bajas presiones, de manera que sabiendo la cantidad de moléculas adsorbida y la superficie que ocupa cada una de estas moléculas, podemos calcular la superficie total del adsorbente. El cálculo de la S_{BET} se lleva a cabo aplicando las Ecuaciones 2.1 y 2.2.

$$\frac{P}{V_{ads}(P_0 - P)} = \frac{1}{V_m C} + \frac{C-1}{V_m C}\frac{P}{P_0} \qquad \text{Ecuación 2.1}$$

$$S_{BET}(m^2 g^{-1}) = V_m(cm^3 g^{-1}) \times \frac{1\,(mol)}{22400\,(cm^3)} \times N_A\left(\frac{molec}{mol}\right) \times 0.162\left(\frac{nm^2}{molec}\right) \times 10^{-18}\left(\frac{m^2}{nm^2}\right) \qquad \text{Ecuación2.2}$$

2.2.1.2. Ecuación de Dubinin-Radushkevich y ecuación de Stoeckli

El modelo de Dubinin-Radushkevich[11] es posterior y tiene en cuenta que la adsorción depende en gran medida del tamaño de poro, ya que para poros más pequeños la interacción adsorbato-adsorbente será más grande y, por lo tanto, a bajas presiones la adsorción se dará sólo en los microporos. Por ello en lugar de suponer la formación de monocapa y a partir de la misma, calcular la superficie, el modelo propuesto por Dubinin-Radushkevich (ecuaciones 2.3 y 2.4) se utiliza para calcular el volumen de microporos teniendo en cuenta que una vez adsorbido, el adsorbato va a pasar de estado gaseoso a líquido en el interior del poro.

$$W = W_0 exp\left[-\left(\frac{A}{\beta E_0}\right)^2\right]$$ Ecuación 2.3

$$A = RTln\left(\frac{P}{P_0}\right)$$ Ecuación 2.4

Para linealizar la ecuación se toman logaritmos de manera que a partir de la ordenada en el origen se obtiene el volumen de microporos (W_0) y de la pendiente se obtiene la energía de adsorción (E_0).La ecuación se aplica tanto a las isotermas de adsorción de nitrógeno a -196 °C como a las de dióxido de carbono a 0 °C, de manera que obtenemos dos valores $W_0(N_2)$ y $W_0(CO_2)$. Hay que tener en cuenta que a presión atmosférica el CO_2 sólo se puede adsorber en poros menores de 0.7 nm, por lo que el $W_0(CO_2)$ puede ser menor que el $W_0(N_2)$ para carbones con altos grados de activación en los que haya microporos más anchos. Por el contrario, cuando existen constricciones a la entrada de los microporos la adsorción de nitrógeno se ve impedida y en este caso $W_0(CO_2)$ será mayor que $W_0(N_2)$, lo que suele ocurrir en carbones con bajos grados de activación. La anchura media de los microporos se puede obtener a partir de la Ecuación de Stoeckli[12] (Ecuación 2.5) o de Dubinin[14] (Ecuación 2.6) cuando E_0 es menor de 20 $kJ \cdot mol^{-1}$.

$$L_0(nm) = \frac{10,8}{\left(E_0 - 11,4kJ/mol\right)}$$ Ecuación 2.5

$$L_0(nm) = \frac{24}{E_0(kJ/mol)}$$ Ecuación 2.6

2.2.1.3. Método de B. J. H.

Cuando se analizan muestras mesoporosas mediante adsorción de nitrógeno, las isotermas generalmente presentan ciclos de histéresis, es decir, la rama de adsorción y la de desorción no son coincidentes. Esto se debe a la forma en la que se produce adsorción y la desorción en poros cilíndricos abiertos, lo que hace que para una presión relativa dada haya una cantidad de gas adsorbida, mientras que la presión relativa

necesaria para desorber esta misma cantidad de gas será menor. El fenómeno de histéresis puede explicarse mediante la ecuación de Kelvin[15], que relaciona el radio de un poro con la presión relativa a la que es llenado en función de las características del sistema adsorbente-adsorbato. Basándose en esto se puede aplicar el modelo propuesto por Barrett, Joyner y Halenda[13] para calcular, generalmente a partir de la rama de desorción, tanto la distribución del tamaño de poros en la región correspondiente al llenado de mesoporos como el volumen total de mesoporos.

2.2.2. Porosimetría de Intrusión de Mercurio

La porosimetría de intrusión de mercurio permite obtener la curva de distribución de tamaño de poros para los macroporos y mesoporos más anchos, complementando así los resultados obtenidos por adsorción de gases. Esta técnica permite también calcular la densidad aparente del sólido. Puesto que el mercurio tiene una tensión superficial muy alta, no moja la superficie del sólido y debe ser introducido en los poros a presión. De esta forma, a presiones más bajas se llenaran los poros más anchos y a presiones más altas los más estrechos. La relación entre el radio de un poro y la presión a la que hay que introducir el Hg para que penetre en el mismo viene dada por la Ecuación de Washburn[16] (ecuación 2.7).

$$r = \frac{-2\sigma\cos\theta}{P}$$ Ecuación 2.7

De esta forma se puede saber a una presión dada que poros se están llenando y midiendo la cantidad de Hg que penetra en el sólido a cada presión podemos construir la curva de distribución de tamaño de poros (PSD). Las porosimetrías se llevaron a cabo en el Instituto Pedro Nunes de Coimbra (Portugal) con un equipo AUTOPORE IV 9500 (Micromeritics).

2.2.3. Microscopia Electrónica de Barrido (SEM)

Con objeto de visualizar la morfología de la superficie de los adsorbentes se tomaron microfotografías de la superficie por Microscopía Electrónica de Barrido

(SEM). Estas fueron realizadas en el Centro de Instrumentación Científica de la Universidad de Granada, con un microscopio electrónico de alta resolución modelo GEMINI-1430-VP de la casa comercial LEO Carl Zeiss.

2.3. CARACTERIZACIÓN QUIMICA

2.3.1. Análisis termogravimétrico (TGA)

El estudio termogravimétrico de los adsorbentes nos permite medir la estabilidad térmica de los mismos en diversas atmósferas. En el caso de carbones oxidados tratados térmicamente nos permite simular los procesos que se dan en el horno y dilucidar a que temperaturas se produce la eliminación de grupos superficiales de la muestra. Estos análisis son necesarios también cuando se lleva a cabo la adsorción en régimen estático de COVs ya que hay que tener en cuenta los procesos de descomposición de grupos superficiales de la superficie del carbón a la hora de analizar la desorción de los contaminantes.

En nuestro caso, los análisis termogravimétricos se llevaron a cabo en el Centro de Instrumentación de la Universidad de Granada con un instrumento TGA-50H de la casa Shimadzu. Los análisis se realizaron en flujo de nitrógeno hasta 950 °C y con una velocidad de calentamiento de 10 $°C \cdot min^{-1}$.

2.3.2. Calorimetría diferencial de barrido (DSC)

Además de las pérdidas de masa, en los procesos de descomposición y reoxidación por parte de los grupos superficiales de oxígeno y en los procesos de desorción de COVs, los intercambios de energía son importantes, ya que podemos calcular la energía de interacción adsorbato-adsorbente, así como analizar posibles procesos que pueden darse en la superficie del carbón. Los procesos de descomposición de grupos y de desorción de COVs serán ambos endotérmicos, por lo que a la hora de

analizar el proceso de desorción habrá que tener en cuenta que en la muestra también tienen lugar cambios químicos que pueden influir en la medida.

Los experimentos de DSC fueron llevados a cabo en el Centro de Instrumentación Científica de la Universidad de Granada, usando para ello un TGA/DSC1 de la casa Mettler-Toledo. En este caso el equipo sólo puede alcanzar los 500 °C por lo que los análisis se llevaron a cabo hasta esta temperatura, con una velocidad de calentamiento de 10 °C·min^{-1} y en flujo de nitrógeno.

2.3.3. Desorción térmica programada (TPD)

La técnica de desorción térmica programada (TPD) nos permite analizar la química superficial de los adsorbentes basándonos en la estabilidad térmica relativa de los grupos superficiales y en el compuesto químico que se genera al producirse su descomposición. En el caso de los grupos oxigenados, como ya se vio en el Capítulo I (Tabla 1.2) son bien conocidas las temperaturas a la que cada uno de ellos es eliminado, así como las especies químicas (CO o CO_2) a las que dan lugar[3,4]. Esta técnica permite caracterizar los grupos oxigenados presentes en toda la muestra, por lo que el %O obtenido por TPD ($\%O_{TPD}$) corresponde al de todo el sólido.

Las curvas de TPD se obtuvieron colocando aproximadamente 0.15 g de la muestra en un reactor de cuarzo en el que se coloca un termopar para medir la temperatura. La muestra se calienta hasta 1000 °C con una velocidad de calentamiento de 50 °C·min^{-1}, y los gases generados son arrastrados por un flujo de Helio (60 cm^3·min^{-1}) que pasa a través de la muestra y los lleva hasta el sistema de detección, un Espectrómetro de Masas PRISMA (Pfeiffer).

Las señales que se analizan son las de los fragmentos iónicos(m/z) correspondiente a los gases H_2, He, H_2O, CO y CO_2: 2, 4, 12, 14, 16, 17, 18, 22, 28 y 44. Previamente, los gases a analizar (CO, CO_2, H_2) fueron calibrados utilizando los gases diluidos en Helio (10 vol%) y el H_2O registrándose un TPD de sulfato de cobre pentahidratado ($CuSO_4 \cdot 5H_2O$).

2.3.4. Espectroscopía de fotoemisión de Rayos-X (XPS)

La espectroscopía de fotoemisión de Rayos-X (XPS) se utiliza para caracterizar la química superficial de la muestra en su superficie más externa. La conjunción de ambas técnicas (TPD y XPS) nos permite, por tanto, tener una idea, no sólo de la química superficial del sólido y de la composición química del mismo, sino también de como los distintos grupos superficiales están distribuidos en dicho sólido.

Los espectros fueron obtenidos en el Centro de Instrumentación de la Universidad de Granada, con un espectrómetro Kratos Axis Ultra-DLD usando como fuente la radiación de MgKα ($h\upsilon$ = 1253.6 eV) y un analizador hemiesférico de electrones operando a 12 kV y 10 mA. Las muestras analizadas se colocaron en un portamuestras de acero y fueron introducidas en la cámara de análisis siendo desgasificadas a una presión inferior a 10^{-8} Torr. Las regiones analizadas fueron las correspondientes a los elementos C y O (C_{1s} y O_{1s}). Ambas señales fueron deconvolucionadas usando funciones de tipo suma asimétricas Gaussianas-Lorentzianas para determinar el número de componentes, la energía de ligadura de los picos (B.E.) y las áreas de los mismos (análisis cuantitativo). La energía de ligadura del pico de la región C_{1s}, correspondiente a C=C (aromático-alifático) se tomó como pico de referencia para conocer la posición de los demás, asignándole el valor de 284,6 eV y la asignación de los distintos picos se llevó a cabo en función de la bibliografía disponible[17,18] (Tabla 2.1)

Tabla 2.1. Grupos funcionales asignados a las energías de ligadura de los picos obtenidos en la deconvolución de las regiones espectrales C_{1s} y O_{1s}.

Región espectral	C						O		
B.E. (eV)	284.6	286.1	287.3	289.1	290.6	291.6	531.6	533.0	534.7
Asignación	C=C	C–O	C=O	COO^-	CO_2	Plasmón	C=O	C–O	H_2O

2.3.5. pH del punto cero de carga (pH_{ZPC})

El pH del punto cero de carga (pH_{ZPC}) da una idea del carácter ácido-base de la superficie del material. Resulta muy útil en el caso de adsorción de especies iónicas (por ejemplo, iones metálicos en agua) ya que nos indica a que pH la superficie de nuestro adsorbente estará cargada (positiva o negativamente) o no. No obstante, puede ser utilizada como una herramienta más de caracterización en otro tipo de aplicaciones, corroborando, por ejemplo, que se han generado centros ácidos en un carbón activado por oxidación del mismo.

Para determinar este parámetro se ha empleado el método propuesto por Leon y col.[19] que es una variante del método de Schwarz y col.. Unos 0.250 g de muestra son suspendidos en 4 mL de agua destilada previamente desgasificada con objeto de eliminar el dióxido de carbono disuelto. La suspensión se mantiene en agitación a temperatura ambiente y se mide su pH periódicamente hasta un valor constante que es considerado como el pH_{ZPC} de la muestra.

2.4. ADSORCIÓN Y SEPARACIÓN DE COMPUESTOS ORGÁNICOS VOLÁTILES PRESENTES EN BIOCOMBUSTIBLES

Una vez caracterizados los materiales fueron utilizados en adsorción de compuestos orgánicos volátiles presentes en biocombustibles. Para estudiar los procesos de adsorción se llevaron a cabo experimentos en régimen estático y dinámico en el caso de adsorción de n-octano y etanol en carbones activados obtenidos a partir de hueso de aceituna y con distinto contenido en oxígeno. La adsorción de isómeros de n-octano y su separación en la serie de aerogel y xerogeles (AC16 y AC16X) sólo fue testeada en régimen dinámico.

2.4.1. Adsorción en estático de vapor saturado

Para llevar a cabo las experiencias de adsorción de COVs en régimen estático, las muestras se saturaron a T ambiente en un desecador que contenía etanol (absoluto,

Panreac), n-octano (>99% GC, Sigma-Aldrich) o agua. Se usaron aproximadamente 0.050 g de cada adsorbente seco que se introdujeron en el desecador. La muestra se pesó periódicamente hasta pesada constante, considerándose entonces el adsorbente saturado, con lo que la cantidad adsorbida se calculó por diferencia con el peso de muestra seca. La desorción se estudió entonces por TGA y DSC, calculando tanto la cantidad desorbida como la energía de desorción.

2.4.2. Adsorción en régimen dinámico. Curvas de rotura

Las curvas de rotura para la adsorción en dinámico de COVs presentes en biocombustibles (etanol, n-octano y 2,2',4-trimetilpentano) fueron obtenidas en el sistema experimental de la Fig. 2.6. Este sistema presentó ligeras variaciones en función del tipo de adsorbente, usándose cargas más grandes de adsorbente y por tanto reactores más grandes en el caso de muestras en pellets. Las peculiaridades del sistema para cada grupo de adsorbentes se especifican en cada uno de los siguientes capítulos, pero en general el sistema consta de un reactor de vidrio termostatizado que contiene el lecho del adsorbente y por el que se hace pasar el flujo de gases (He o aire (60 $cm^3 \cdot min^{-1}$)).Estos flujos se controlan mediante sus correspondientes controladores de flujo másico (MFC). Una de las líneas de gas de arrastre se hace burbujear en una ampolla que contiene el COVs líquido a 0 °C, obteniendo así un flujo saturado en el mismo. La concentración de contaminante en el flujo entrante en la columna se ajusta, pues, mediante dilución con la línea de gas puro. Dos válvulas de cuatro vías nos permiten seleccionar cual de las corrientes de gas entra en el reactor, a la salida del mismo, si esta pasa por el sistema de detección o va directamente al de purga (lo que permite hacer bypass para medir la concentración sin pasar por la columna). La concentración de contaminantes se determina mediante un cromatógrafo de gases VARIANT CP-3800 equipado con una columna Carbowax-20M y un detector de llama FID.

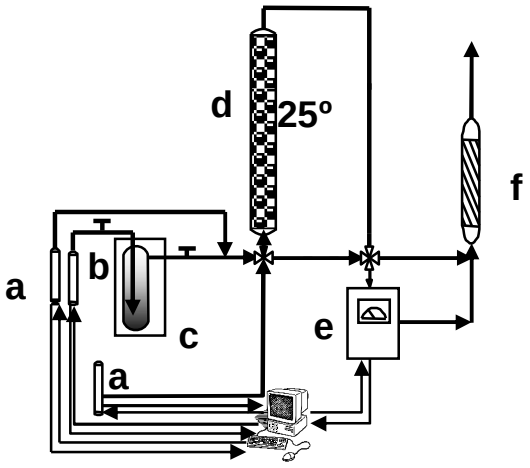

Figura 2.6. Sistema para obtención de curvas de rotura: a) MFCs, b) ampolla COV líquido, c) criostato, d) columna con lecho adsorbente, e) GC-FID, f) Trampa.

En cuanto al análisis de las curvas de rotura, este fue llevado a cabo mediante el concepto de la Zona de Transferencia de Masas (MTZ) descrito por Webber[20] y Luckchis[21]. Así, se considera la resistencia global al proceso de adsorción de un flujo continuo de efluente contaminado, de forma que existe un frente que avanza por la columna y se encuentra justo delante de la zona donde la columna se encuentra ya saturada. Este frente es conocido como la Zona de transferencia de masas (MTZ), y corresponde a la zona del lecho donde el contaminante está siendo adsorbido. En estas curvas se representa la relación entre la concentración del contaminante a la salida de la columna (C) y a la entrada (C_0) en función del tiempo, pudiéndose obtener, además de la altura y velocidad de avance de la MTZ, otros datos como los volúmenes, tiempos y cantidad de contaminante adsorbido tanto a rotura como a saturación. El cálculo de cada uno de ellos se lleva a cabo de la siguiente forma[22]:

- Volumen a rotura (V_B) y volumen a saturación (V_S): Son los volúmenes de aire contaminado que pasan por el reactor hasta alcanzar una concentración relativa del contaminante a la salida, respecto a la entrada, de 0.02 y 0.90 para rotura y saturación respectivamente. Se obtuvieron multiplicando los tiempos a los que se alcanzaron dichas concentraciones por el caudal del efluente.

- Cantidad adsorbida a rotura (X_B) y cantidad adsorbida a saturación (X_S): Se obtuvieron mediante la diferencia entre la concentración de entrada y la concentración a la salida del reactor ($C_0 - C$), teniendo en cuenta el volumen de elución, realizando la sumatoria hasta rotura y hasta saturación, respectivamente. Ambas se expresaron en mg de contaminante por g de carbón.

- Altura de la Zona de Transferencia de Masa (H_{MTZ}): El cálculo de este parámetro se llevó a cabo mediante las Ecuaciones 2.8 y 2.9 descritas en bibliografía.

$$H_{ZTM} = h\left(\frac{V_{0.90} - V_{0.02}}{V_{0.02} + \phi(V_{0.90} - V_{0.02})}\right) \qquad \text{Ecuación 2.8}$$

$$\phi = \frac{\int_{V_{0.02}}^{V_{0.90}} (C_0 - C)dV}{C_0 (V_{0.90} - V_{0.02})} \qquad \text{Ecuación 2.9}$$

Donde h es la altura del lecho, $V_{0.90}$ y $V_{0.02}$ son los volúmenes a rotura y a saturación tal y como se han definido anteriormente y ϕ es un parámetro que se conoce como la capacidad fraccional de la columna. La capacidad fraccional (ϕ) es la relación entre la cantidad de contaminante adsorbida por el lecho entre los volúmenes de rotura y saturación y la cantidad que ha entrado en la columna entre estos volúmenes y, por tanto, debe variar entre 0 y 1.

- Velocidad de avance de la ZTM (R_{ZTM}):Se calcula multiplicando la H_{ZTM} por el caudal y dividiendo el producto por la diferencia entre el volumen a rotura y el volumen a saturación.

- Grado de utilidad de la columna (Du(%)):Es la relación, en porcentaje, entre la cantidad adsorbida hasta el punto de rotura y la cantidad adsorbida hasta

el punto de saturación, de manera que cuanto más alto sea el Du(%) mayor es el tiempo que la columna está adsorbiendo todo el contaminante que pasa por ella con respecto al tiempo total del experimento. Se calcula mediante la Ecuación 2.10 como una relación de áreas sobre la curva de rotura, según la fórmula mostrada en la Fig. 2.7.

$$Du(\%)=\frac{(0.90-0.02)V_{0.02}}{(0.90-0.02)V_{0.02}+\int_{V_{0.02}}^{V_{0.9}}\left(0.9-\frac{C}{C_0}\right)dV} \qquad \text{Ecuación 2.10}$$

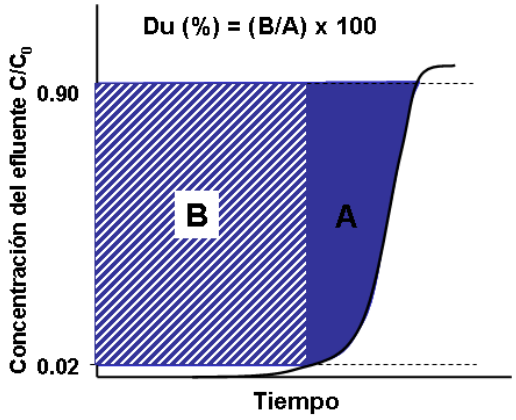

Figura 2.7. Cálculo del Du(%) a partir de una curva de rotura.

2.5. ADSORCIÓN SELECTIVA DE CO_2 EN REFINADO DE BIOGÁS

Las experiencias para el estudio de los adsorbente en refinado de biogás fueron realizadas durante la estancia pre-doctoral en el Laboratory of Separation and Reaction Engineering (LSRE) perteneciente a la Facultad de Ingeniería de la Universidad de Oporto. Las isotermas de alta presión fueron obtenidas en un equipo gravimétrico mientras que los estudios de adsorción en dinámico se llevaron a cabo con un equipamiento ligeramente diferente en diseño y de un tamaño mayor que el que utilizamos en el Laboratorio de Adsorción y Catálisis de la Universidad de Granada.

2.5.1. Isotermas de adsorción a alta presión.

Las isotermas de adsorción y desorción de CO_2 y CH_4 a altas presiones fueron obtenidas en una microbalanza de suspensión magnética Rubotherm. La principal ventaja de este equipo con respecto a equipos gravimétricos convencionales es que el compartimento de la muestra está separado físicamente de la parte electrónica de la balanza, lo que permite tener una mayor precisión y emplear condiciones de medida más drásticas. Además contiene un material de referencia que permite llevar a cabo medidas de densidad (Fig. 2.8).

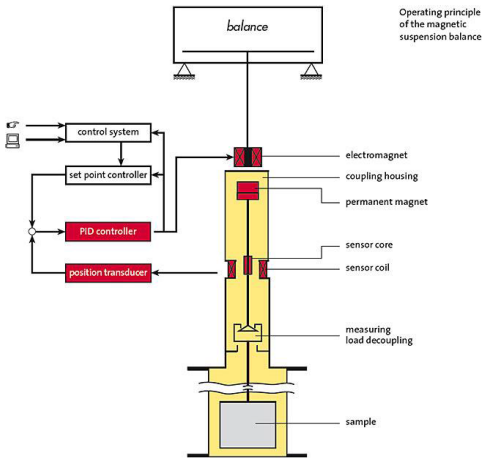

Figura 2.8. Esquema de la microbalanza de suspensión magnética (RUBOTHERM).

Para llevar a cabo la medida, lo primero que hubo que hacer fue desgasificar la muestra a vacío (P < 0.01 bar, T = 150 °C) durante 24 h. Es necesario llevar a cabo una picnometría de Helio del sistema vacío previamente y, una vez desgasificada la muestra, del sistema con la muestra dentro ya que se necesitan los valores de volumen muerto, volumen de muestra y densidad real para poder hacer corrección del efecto de empuje, fenómeno que será importante especialmente a altas presiones. Una vez realizada la picnometría se procedió a la obtención de las isotermas a 30, 50 y 70 °C y en un rango de presiones de 0 a 10 bar. Para ello, el gas se va introduciendo en dosis, fijando la presión a la que se requiere cada uno de los puntos y midiendo el cambio de masa producido a cada una de las presiones. Después el gas se va retirando haciendo vacío para registrar la desorción.

Una vez obtenidas, las isotermas fueron ajustadas al modelo de Langmuir/Toth (Ecuaciones 2.11 y 2.12), usándose el mismo ajuste para las tres isotermas (30, 50 y 70 °C). Finalmente, con objeto de determinar la curva característica del sistema adsorbato-adsorbente, se calculó la variación del calor isostérico de adsorción con la cantidad adsorbida. Para ello, fue necesario representar el mejor ajuste posible para cada una de las isotermas a 30 °C y a 50 °C de manera que se pudieran obtener por interpolación los valores de presión a los que la cantidad adsorbida coincidía con la de los puntos experimentales de la isoterma a 70 °C. Estos puntos se usaron para obtener las rectas de regresión (ln P vs. 1/T) de cuya pendiente podemos obtener el calor isostérico de adsorción (Ecuación 2.13).

$$q = q_{sat}\frac{bP}{(1+(bP)^n)^{1/n}} \qquad \text{Ecuación 2.11}$$

$$b = b_0 e^{\frac{-\Delta H_{ads}}{RT}} \qquad \text{Ecuación 2.12}$$

$$(\Delta H_{ads})_q = -R\left(\frac{\partial(lnP)}{\partial(1/T)}\right)_q \qquad \text{Ecuación 2.13}$$

Donde q, cantidad adsorbida y, q_{sat}, cantidad adsorbida a saturación (mol kg^{-1}); b, constante Langmuir/Toth (bar^{-1}); n, parámetro de heterogeneidad (n=1 para modelo Langmuir); P and T, presión y temperatura (bar, K); and ΔH_{ads}, calor de adsorción (kJ mol^{-1}).

2.5.2. Adsorción en régimen dinámico CO_2 y CH_4

Las curvas de rotura de CO_2 y CH_4 se obtuvieron en equipos distintos para el caso del xerogel (XCs300) y el carbón activado obtenido a partir de pellets de madera (PINPEL20). Los detalles experimentales en cuanto a carga de adsorbente, presión, temperatura y concentraciones de gases se recogen en los capítulos correspondientes a cada uno de los trabajos. En ambos casos el sistema es parecido, una serie de controladores de flujo másico (MFC) para regular la entrada de los gases, una columna termostatizada en la que se coloca el adsorbente con termopares para medir los cambios

de temperatura, un medidor de flujo másico (MFM) a la salida y un equipo para cuantificar de los gases.

Las principales diferencias entre una equipo y otro son que por un lado, la columna para la muestra PINPEL20 era mucho más alta (aproximadamente 80 cm) que la que se usó para la muestra XCs300 (de unos 10 cm), con lo que en este caso había tres termopares a distinta alturas para seguir la variación de temperatura en distintos puntos de la columna; por otro lado, el sistema de detección que en el caso de la muestra PINPEL20 fue un cromatógrafo de gases GC (DANI) con detectores FID y TCD y una columna capilar (HPPLOT U), mientras que en el caso de la muestra XCs300 se empleó un analizador de gases por infrarrojo GasDataLMSxiTypeG4.18 (GasDataLtd,UK).

En este caso no se utilizó el concepto de Zona de Transferencia de Masas para analizar las curvas de rotura y en lugar de trabajar con concentraciones de gas, se calcularon los flujos molares de cada uno de ellos a la salida, lo que permite la integración directa de las curvas de rotura. También se registró la desorción sin aumentar la temperatura, simplemente cambiando la corriente de entrada por He de manera que este arrastra a la fase adsorbida y comprobando que las cantidades desorbidas y adsorbidas, calculadas por integración de las curvas fueran similares.

2.6. BIBLIOGRAFÍA

[1] M. Bishop and D.L. Ward, The direct determination of mineral matter in coal, *Fuel*,**37** (1958) 191-199.

[2] C. Moreno-Castilla, M.A. Ferro-García, J.P. Joly, I. Bautista-Toledo, F. Carrasco-Marín, and J. Rivera-Utrilla, Activated Carbon Surface Modifications by Nitric Acid, Hydrogen Peroxide, and Ammonium Peroxydisulfate Treatments, *Langmuir*, **11** (1995) 4386-4392.

[3] J.L. Figueiredo, M.F.R. Pereira, M.M.A. Freitas, and J.J.M. Órfão, Modification of the surface chemistry of activated carbons, *Carbon*, **37** (1999) 1379-1389.

[4] G. de la Puente, J.J. Pis, J.A. Menéndez, and P. Grange, Thermal stability of oxygenated functions in activated carbons, *Journal of Analytical and Applied Pyrolysis*, **43** (1997) 125-138.

[5] R.W. Pekala, Low density, resorcinol-formaldehyde aerogels, US Patent, *US4873218 A*, 1989.

[6] R.W. Pekala, Organic aerogels from the polycondensation of resorcinol with formaldehyde, *Journal of Materials Science*, **24** (1989) 3221-3227.

[7] T.F. Baumann, M.A. Worsley, T.Y.-J. Han, and J. Satcher, High surface area carbon aerogel monoliths with hierarchical porosity, *Journal of Non-Crystalline Solids*, **354** (2008) 3513-3515.

[8] E. Gallegos-Suárez, A.F. Pérez-Cadenas, F.J. Maldonado-Hódar, and F. Carrasco-Marín, On the micro- and mesoporosity of carbon aerogels and xerogels. The role of the drying conditions during the synthesis processes, *Chemical Engineering Journal*, **181–182** (2012) 851-855.

[9] S. Morales-Torres, F.J. Maldonado-Hódar, A.F. Pérez-Cadenas, and F. Carrasco-Marín, Structural characterization of carbon xerogels: From film to monolith, *Microporous and Mesoporous Materials*, **153** (2012) 24-29.

[10] S. Brunauer, P.H. Emmett, and E. Teller, Adsorption of gases in multimolecular layers, *Journal of the American Chemical Society*, **60** (1938) 309-319.

[11] M.M. Dubinin, Inhomogeneous microporous structures of carbonaceous adsorbents, *Carbon*, **19** (1981) 321-324.

[12] F. Stoeckli, *Porosity in carbon. Characterization and applications*, Eds. Patrick J. Arnold, London, 1995.

[13] E.P. Barrett, L.G. Joyner, and P.P. Halenda, The Determination of Pore Volume and Area Distributions in Porous Substances. I. Computations from Nitrogen Isotherms, *Journal of the American Chemical Society*, **73** (1951) 373-380.

[14] M.M. Dubinin, Generalization of the theory of volume filling of micropores to nonhomogeneous microporous structures, *Carbon*, **23** (1985) 373-380.

[15] S.J. Gregg and K.S.W. Sing, *Adsorption, Surface Area & Porosity*, Academic Press, London, 1982.

[16] E.W. Washburn, Note on a method of determining the distribution of pore sizes in a porous material, *Proceedings of the National Academy of Sciences*, **7** (1921) 115-116.

[17] A.F. Pérez-Cadenas, F.J. Maldonado-Hódar, and C. Moreno-Castilla, On the nature of surface acid sites of chlorinated activated carbons, *Carbon*, **41** (2003) 473-478.

[18] E. Desimoni, G.I. Casella, and A.M. Salvi. XPS/XAES study of carbon fibres during thermal annealing under UHV conditions,*Carbon*,**30**(1992) 521-526.

[19] C.A. Leon, J.M. Solar, V. Calemma, and L.R. Radovic, Evidence for the protonation of basal plane sites on carbon,*Carbon*,**30**(1992)797-811.

[20] W.J.J. Webber, *Physiochemical Processes for Water Quality Control*, Wiley-Interscience ed., New Cork, 1972.

[21] G.M. Luckchis, Adsorption systems 1. Design by mass-transfer-zone concept, *Chemical Engineering*,**80** (1973) 111-116.

[22] P.N. Cheremisinoff and F. Ellerbusch, *Carbon Adsorption Handbook*, Ann Arbor Science Pub. ed., Michigan, 1978.

Capítulo III

TAILORING THE SURFACE CHEMISTRY AND POROSITY OF ACTIVATED CARBONS: EVIDENCE OF REORGANIZATION AND MOBILITY OF OXYGENATED SURFACE GROUPS

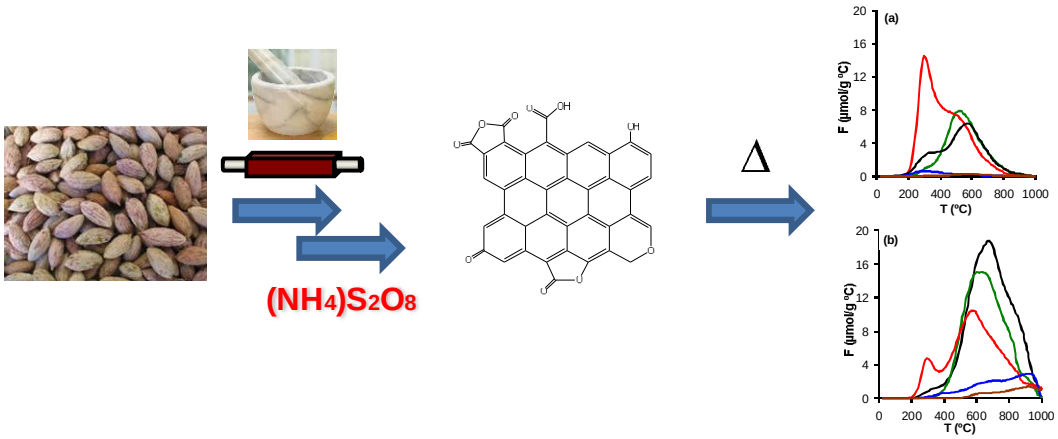

TAILORING THE SURFACE CHEMISTRY AND POROSITY OF ACTIVATED CARBONS: EVIDENCE OF REORGANIZATION AND MOBILITY OF OXYGENATED SURFACE GROUPS

Article published in Carbon, 68 (2014) 520-530, doi: 10.1016/j.carbon.2013.11.030

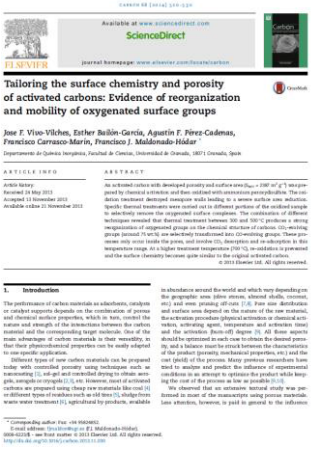
Available at www.sciencedirect.com
ScienceDirect
journal homepage: www.elsevier.com/locate/carbon
Tailoring the surface chemistry and porosity of activated carbons: Evidence of reorganization and mobility of oxygenated surface groups
José F. Vivo-Vilches, Esther Bailón-García, Agustín F. Pérez-Cadenas, Francisco Carrasco-Marín, Francisco J. Maldonado-Hódar *
Departamento de Química Inorgánica, Facultad de Ciencias, Universidad de Granada, 18071 Granada, Spain
ARTICLE INFO
ABSTRACT
1. Introduction

Highlights

- Activated carbon was prepared by chemical activation with KOH of olive stones.
- Oxidation lead to an activated carbon with different oxygenated surface groups.
- Thermal treatments at 300 °C and 500 °C produced a reorganization of OSGs.
- At 700°C almost all of the oxygen is eliminated from carbon surface.

Abstract

An activated carbon with developed porosity and surface area (S_{BET} = 2387 m^2g^{-1}) was prepared by chemical activation and then oxidized with ammonium peroxydisulfate. The oxidation treatment destroyed mesopore walls leading to a severe surface area reduction. Specific thermal treatments were carried out in different portions of the oxidized sample to selectively remove the oxygenated surface complexes. The combination of different techniques revealed that thermal treatment between 300 and 500 ºC produces a strong reorganization of oxygenated groups on the chemical structure of carbons. CO_2-evolving groups (around 75 wt.%) are selectively transformed into CO-evolving groups. These processes only occur inside the pores, and involve CO_2 desorption and re-adsorption in this temperature range. At a higher treatment temperature (700 ºC), re-oxidation is prevented and the surface chemistry becomes quite similar to the original activated carbon.

Keywords: Activated carbons, porosity, surface chemistry, mobile oxygenated complexes.

3.1. INTRODUCTION

The performance of carbon materials as adsorbents, catalysts or catalyst supports depends on the combination of porous and chemical surface properties, which in turn, control the nature and strength of the interactions between the carbon material and the corresponding target molecule. One of the main advantages of carbon materials is their versatility, in that their physicochemical properties can be easily adapted to one specific application.

Different types of new carbon materials can be prepared today with controlled porosity using techniques such as nanocasting[1], sol-gel and controlled drying to obtain aerogels, xerogels or cryogels[2,3], etc. However, most of activated carbons are prepared using cheap raw materials like coal[4] or different types of residues such as old tires[5], sludge from waste water treatment[6], agricultural by-products, available in abundance around the world and which vary depending on the geographic area (olive stones, almond shells, coconut, etc) and even pruning off-cuts[7,8]. Pore size distribution and surface area depend on the nature of the raw material, the activation procedure (physical activation or chemical activation, activating agent, temperature and activation time) and the activation (burn-off) degree[9]. All these aspects should be optimized in each case to obtain the desired porosity, and a balance must be struck between the characteristics of the product (porosity, mechanical properties, etc) and the cost (yield) of the process. Many previous researchers have tried to analyze and predict the influence of experimental conditions in an attempt to optimize the product while keeping the cost of the process as low as possible[9,10].

We observed that an extensive textural study was performed in most of the manuscripts using porous materials. Less attention, however, is paid in general to the influence of chemical properties, although surface groups based on different heteroatoms (O, N, S, halogens, etc) are specifically generated by the treatment of carbon materials both in gas and liquid phase[11]. The control of surface chemistry is a powerful tool for developing specific adsorbents and catalysts. It is well known that surface chemistry strongly influences the behavior of carbon materials in the adsorption of organic molecules from solutions, controlling electrostatic/non-electrostatic

interactions[12]. Specific chemical groups, like sulfur surface groups, were introduced to increase the mercury adsorption[13,14], and oxygenated surface groups (OSG) were used to favor the separation/capture of CO_2 from mixtures of gases[15].

OSG are the most extensively studied of the various types of surface chemical groups[16-18]. In the activation process, OSG are the intermediate species before they are evolved as gaseous CO or CO_2[9]. In catalytic applications, acid carbons were produced by oxidation processes for fine chemistry applications[16]. OSG influence the metal dispersion of supported catalysts[17] and have been used to anchor active metal-complexes[18]. Some OSG are acidic (carboxylic, lactones, anhydrides, phenol) while other such as chromene or pyrone groups are classified as basic centers[11,19]. Parameters such as hydrophobicity or the acid/base nature of the carbon surface can therefore be modified by the oxidation process and a controlled removal of the groups generated[20]. All these processes involving the generation and removal of OSG imply the mobility and transformation of these chemical species. Theoretical studies of this question have been made using different approaches (density functional theories or computational chemistry calculations)[21,22], but in general, there is a lack of information and experimental proof. In previous studies[20], we observed that oxygenated surface groups can be removed selectively by heating oxidized samples in an inert atmosphere: the oxygen content decreases linearly as the treatment temperature increases. After these thermal treatments, both CO-evolving groups and to a lesser extent CO_2-evolving groups show some degree of mobility on the carbon surface, and a significant amount of CO is evolved below the treatment temperature, when the sample is heated again from room temperature without air exposure. This shows that the thermal stability of some of these groups decreases because they move to previously generated free sites.

In this work, a highly porous activated carbon was obtained by chemical activation of carbonized olive stones and deeply oxidized by treatment with $(NH_4)_2S_2O_8$. Textural and chemical transformations induced by the formation/elimination of OSG after oxidation, thermal treatments and storage in air were analyzed using different techniques. We present experimental evidence of the mobility of oxygenated surface groups and the transformation of acidic CO_2-evolving groups into CO-evolving groups.

3.2. MATERIALS AND METHODS

3.2.1. Preparation of carbon materials

Olive stones were milled and sieved to 1.0 – 2.0 mm, treated with sulfuric acid (1N) to remove the rest of pulp and washed until all sulfates had been removed. An initial carbonization was carried out by heating at 10 ºC min^{-1} to 400 ºC and a soak time of two hours under a nitrogen flow of 300 cm^3 min^{-1} using a tubular furnace (from Heraeus) equipped with a stainless steel tube (180 cm long x 8 cm diameter x 0.8 cm wall) with reduction made by steel welding and graphite joints between the taps.

The purity of the N_2 flow was 99.999 % (H_2O, CO and O_2 contents below 3 ppm), and air leaks were prevented by placing a Gas Purifier MDL III from Supelco (Ref. 23800-U) at the entry to the furnace, which removed the possible residues of H_2O, O_2, CO and CO_2. The composition of the N_2 flow was identical at the entry and the exit of the furnace tube (analyzed by MS), the leak absence was carefully checked before any sample preparation and the system was purged for 1 h before heating. After thermal treatments, samples were cooled in the same N_2 flow to room temperature and finally stored in a desiccator.

The carbon yield was 30%. Chemical activation was carried out using a mixture of this carbonized material and KOH in a 1:7 mass ratio. This mixture was treated under nitrogen flow (300 cm^3 min^{-1}) for two hours at 350 ºC followed by three hours at 850 ºC (heating rate of 10 ºC min^{-1}). Cooling to ambient temperature was performed by keeping the sample under nitrogen atmosphere. Finally, the sample was demineralized with HCl and HF, which also removed the excess base (KOH), washed with distilled water until chlorides had been removed and dried in an oven at 110 ºC for 24 hours before storage. This sample was labeled as CA.

3.2.2. Chemical Surface Modifications

Ammonium peroxydisulfate ($(NH_4)_2S_2O_8$) was chosen as an oxidizing agent. CA was mixed with a saturated solution of this salt on H_2SO_4 1 M. After 24 hours

under stirring at room temperature, oxidized carbon was filtered and washed with distilled water until sulfates had been removed[17,23,24]. This material was dried at 110 ºC and labeled as CAOX. Thermal treatments under nitrogen atmosphere (150 cm^3 min^{-1}) at 300 ºC, 500 ºC and 700 ºC (10 min, 20 ºC min^{-1}) were carried out on different portions of CAOX, following the same experimental procedure described previously, in order to remove some of the oxygenated surface groups (OSG) selectively, thus obtaining three samples CAOX300, CAOX500 and CAOX700.

3.2.3. Textural Characterization

The morphology of carbons was analyzed using a scanning electron microscope (Leo, Carl Zeiss, Geminy-153). Images were obtained at excitation energy of 20 kV. Textural properties of ACs were determined by adsorption isotherms of N_2 (-196 °C) and CO_2 (0 °C) using an Autosorb 1 from Quantachrome after outgassing samples overnight at 110 °C under high vacuum (10^{-6} mbar). Parameters such as BET surface area, micropore volume (W_0) and micropore mean width (L_0) were calculated by applying BET, Dubinin-Radushkevich and Stoeckli equations respectively to the corresponding isotherms[25,26]. The pore size distributions (PSD) were determined by applying Quenched Solid Density Functional Theory (QSDFT), assuming slit-shaped pores and BJH derived methods[27,28] to the N_2 adsorption isotherms. Mesopore volume (V_{meso}) was estimated according to Gurvitch's rule, therefore considering the total pore volume as the volume of adsorbed nitrogen at a relative pressure of $P/P_0 = 0.95$ ($V_{0.95}$). Mesopore volume, V_{meso}, was obtained consequently from the difference[29] between $V_{0.95}$ and W_0 (N_2).

3.2.4. Chemical Characterization

Thermal treatments of samples were simulated by thermogravimetric analysis using a SHIMADZU mod. TGA-50H and a METTLER-TOLEDO mod. TGA/DSC1 for TG-DTG and DSC experiments respectively. The weight loss (W.L.) and the associated heat flow (TG – DSC) were recorded. Experiments were carried out in N_2 flow and a heating ramp of 10 ºC min^{-1} up to 950 ºC (TG-DTG experiments) or 500 ºC (DSC-experiments).

Thermal Programmed Desorption (TPD) curves of carbon monoxide, carbon dioxide, water and hydrogen were recorded. The integration of CO and CO_2-TPD profiles enabled us to determine quantitatively the total oxygen content and the different oxygenated groups. The identification and quantification of these groups were based on assignments in the bibliography[20,30]. Experiments were carried out by heating 150 mg of sample at 50 ºC min^{-1} up to 1000 °C using He as the carrier gas (60 cm^3 min^{-1}). The analysis of desorbed gases was performed with a Mass Spectometer model Prisma (Pfeiffer). The calibrations for CO and CO_2 were carried out by analyzing these gases diluted in He (10 vol%) and the calibration for H_2O was performed by means of a TPD of $CuSO_4 \cdot 5H_2O$. The masses (uma) analyzed for these gases were: H_2O - 16, 17, 18; CO -12, 16, 28; and CO_2, 12, 16, 28, 44. Consecutive TPD experiments were carried out in order to check that samples had not been oxidized by He impurities and the reproducibility of the results. The estimated error in the determination of these gases was less than 5%, and this was obtained by repeating the TPD runs on each sample at least twice.

X-ray photo emission spectra (XPS) were recorded using a Kratos Axis Ultra-DLD spectrometer. This instrument uses MgKα ($h\nu$ = 1253.6 eV) as the radiation source and a hemispheric electron analyzer operating at 12 kV and 10 mA. Survey and multi-region spectra were recorded at C_{1s} and O_{1s} photoelectron peaks. Each spectral region of interest was scanned several times to obtain good signal-to-noise ratios. The spectra obtained after background signal correction were fitted to Lorentzian and Gaussian curves in order to obtain the number of components, the position of each peak and peak areas. Peak assignments were carried out according to the bibliography[31,32].

Zero-point charge pH (pH_{ZPC}) of samples was determined according to the method proposed by Leon et al.[33]. Approximately 250 mg of each sample were suspended on 4 mL of previously degasified distilled water. Suspensions were stirred and thermostated at 25 ºC measuring the pH periodically until the reading was constant. The final pH obtained this way was considered as the pH_{ZPC} for each sample.

3.3. RESULTS AND DISCUSSION

3.3.1. Textural Characterization

In a previous study[34] the preparation of activated carbons from KOH activation demonstrated the influence of parameters such as the initial particle size of the olive stone, the raw material/KOH ratio and the effect of a previous carbonization before activation. Without a previous carbonization, i.e. the direct chemical activation of the olive stone, KOH activation destroyed olive stone grains producing a very fine activated carbon. By carbonizing the olive stones first at 840 ºC, the raw grains are preserved and only microporous materials are obtained. This difference is due to the weaker interaction of the activating agent with carbonized materials than with cellulosic raw materials[35]. Microporosity and S_{BET} values increase strongly when the carbon:KOH ratio is increased from 1 to 2, but only slowly at higher ratios. In this case, we changed the experimental activation conditions: a lower carbonization temperature (400 ºC) was used to try to improve the shape stability of the raw material, but the carbonized:KOH ratio was increased to 1:7 in search of a developed porosity. During carbonization the degree of pyrolysis is 70% and the activation produces an additional W.L. of 44%, thus after neutralizing and washing, the CA sample is also a very fine material.

The morphology of the CA sample (Fig. 3.1, top) is similar to those previously observed; however, flat surfaces from cellulosic fibers are clearly less interconnected[34] . Microphotographs show highly porous particles, with large macropores at the micrometer scale denoting the strong effect of the activation procedure. After oxidation (Figures, bottom), sample morphology is quite similar, as the carbon particles also present large macropores with a wide range of diameters. Nevertheless, the carbon surface shows the effects of oxidation, becoming more heterogeneous and corrugated (Fig. 3.1, bottom-right).

Textural characteristics of samples were determined by the analysis of N_2 and CO_2 adsorption isotherms. The N_2-adsorption isotherms we measured are shown in Fig. 3.2. Adsorption parameters obtained from N_2 and CO_2 adsorption isotherms are summarized in Table 3.1.

N_2 adsorption isotherms are mixtures of Type I and Type IV. Thus an important amount of N_2 is adsorbed at low relative pressure but the slope of the isotherms at intermediate P/P_0 values and the formation of the hysteresis loop in the CA sample denotes a strong influence of mesoporosity on the isotherm profile. As regards the microporosity (Table 3.1), it is noteworthy that in all cases $W_0(N_2) > W_0(CO_2)$, which also indicates the contribution of large micropores and mesopores to the N_2-adsorption capacity. The presence of large micropores is also corroborated by the L_0 (CO_2) values, because although CO_2 adsorption is used to determine the porosity below 0.7 nm[36], in this case L_0 values are, in general, greater than 1.0 nm.

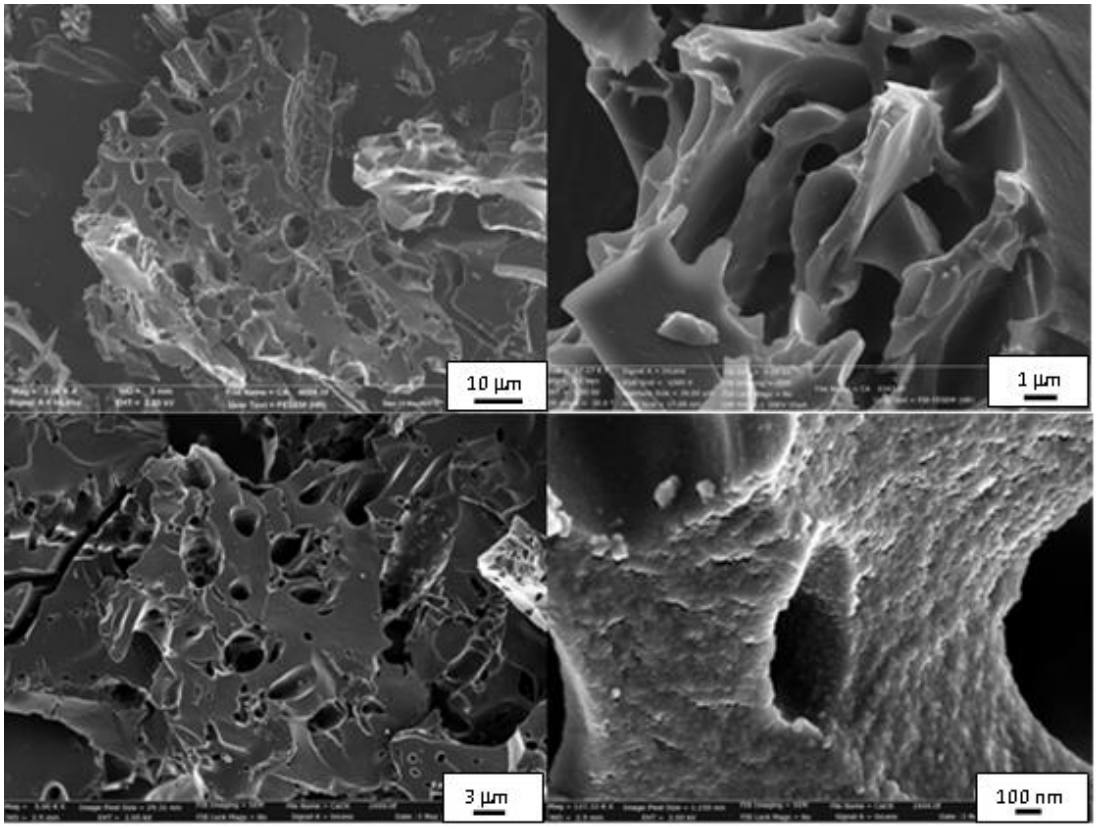

Figure 3.1. Morphology (SEM pictures) of CA (top) and CAOX (bottom).

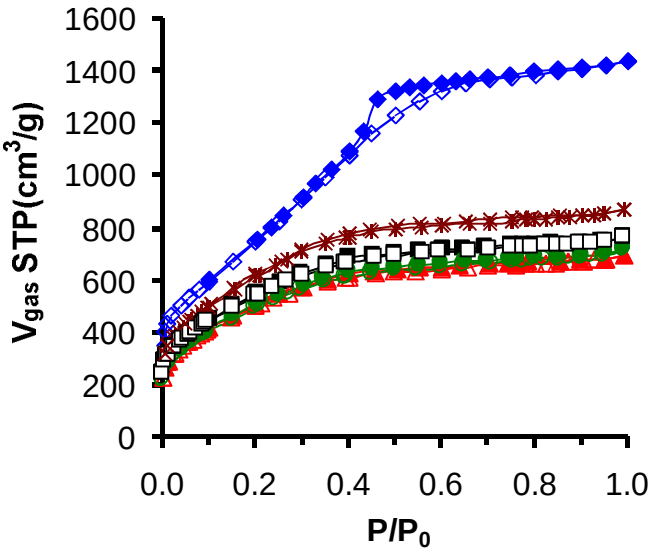

Figure 3.2. N_2 adsorption-desorption isotherms. CA (◊), CAOX (△), CAOX300 (○), CAOX500 (□), CAOX700 (×).

Table 3.1. Textural properties of samples

Sample	S_{BET} $m^2 \cdot g^{-1}$	W_0 (N_2) $cm^3 \cdot g^{-1}$	W_0 (CO_2) $cm^3 \cdot g^{-1}$	L_0 (CO_2) nm	$V_{0.95}$ $cm^3 \cdot g^{-1}$	V_{meso} $cm^3 \cdot g^{-1}$
CA	2387	0.92	0.39	1.1	2.23	1.31
CAOX	1661	0.63	0.43	0.9	1.07	0.44
CAOX300	1686	0.63	0.44	1.0	1.10	0.47
CAOX500	1696	0.68	0.48	1.1	1.18	0.50
CAOX700	1972	0.78	0.48	1.2	1.34	0.56

When we analyzed the textural transformation produced by the oxidation we observed that the shape of the N_2 adsorption isotherm changes dramatically, denoting transformations mainly at the mesopore range: the hysteresis loop disappears and the slope of isotherms decreases significantly, as does the total amount of N_2 adsorbed. Thus, W_0 (N_2) decreases 32% and V_{meso} 60% while the volume of the narrowest micropores determined by CO_2 adsorption[36], W_0 (CO_2), increases by only about 10%. These transformations lead to a drastic reduction of S_{BET} from 2387 to 1661 $m^2 \cdot g^{-1}$ due to a destruction of pore walls of activated carbon CA during oxidation treatments that

affect the mesopores and the largest micropores and/or due to pore blockage by the oxygenated surface groups formed. Two mechanisms, acting at the same time, have been proposed to explain the breaking of pore walls[20,37] after treatments with strong oxidants: the first is gasification, i.e. the release of oxygenated terminal groups generated by the oxidation treatment and the second is the mechanical destruction of pores by the surface tension of the oxidizing solution.

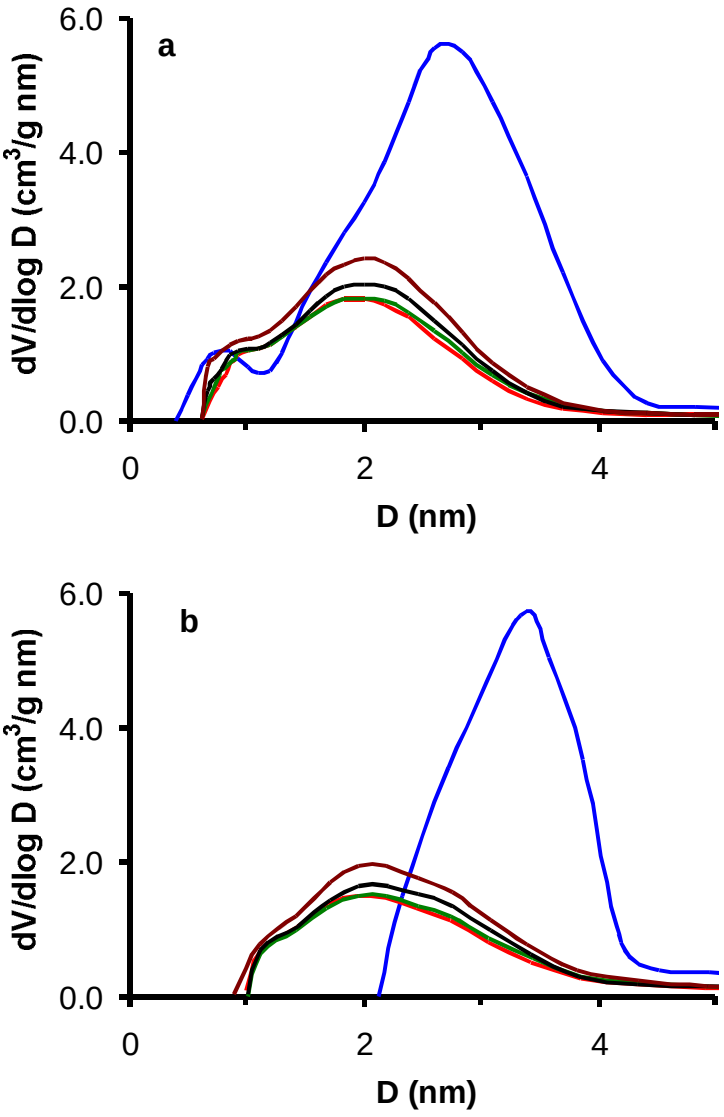

Figure 3.3. Pore size distributions of activated carbons by application of QSDFT, a, and BJH, b, methods to N_2 adsorption isotherms at −196 °C (Blue (CA), red (CAOX), green (CAOX300), black (CAOX500) and brown (CAOX700).

After progressive thermal treatments at 300, 500, 700 ºC the main increases were in V_{meso} and W_0 (N_2), and consequently S_{BET} values also increase. These transformations showed that oxidation mainly produces the gasification of original mesopore walls and that oxygenated surface groups are blocking micropores that when gasified produce a pore widening, leading to large micropores and mesopores, as summarized in Table 3.1.

Fig. 3.3 depicts the pore size distribution obtained by applying the QSDFT and BJH methods to the N_2 adsorption. Similar mesopore PSD profiles were obtained with both methods. The PSD of the original CA sample presents a maximum for mesopores with diameters between 2.8-3.0 nm. PSD determined by QSDFT method shows a bimodal distribution around pores with widths of 0.8 nm and 2.0 nm. Original mesopores are destroyed and partially blocked by OSG with the oxidation process in such a way that the mesopore volume of CAOX and their derivative samples is always smaller than the original volume in CA. Their PSD shifted to small mesopores compared to CA, which are progressively favored by the micropore widening after subsequent thermal treatments. However, the mesoporosity in the original pore range was never recovered.

4.3.2. Chemical characterization

The interest in the study and tailoring of the surface chemistry of ACs by introduction and/or elimination of different kinds of surface groups is clear from the large number of research papers on these subjects[11-22]. Nevertheless this is a matter under continuous discussion due to their inherent complexity. Results are influenced by a large number of factors (porosity, activating agent, heating rate, secondary reactions, energetic heterogeneity of the surface, etc)[38]. It is therefore always desirable to use different experimental techniques that can provide complementary information about the samples and the processes that take place in the different experimental conditions. In our case, the surface chemistry of the ACs was extensively analyzed by XPS, TPD and pH_{ZPC} experiments. The results we obtained are summarized in Table 3.2. The sharp increase in the oxygen content of CA after oxidation to CAOX is particularly noteworthy. This also causes a strong acidification of the carbon surface as denoted by

the variation in the pH_{ZPC} values. This is the typical behavior previously observed for other oxidized carbon materials[17,20,23]. The nature and distribution of OSG generated on carbon materials depend on the physical and chemical characteristics of ACs and the oxidizing agent. As an example, treatment with $(NH_4)_2S_2O_8$ produces stronger acid sites than those generated after treatment with H_2O_2 or HNO_3[23]. In a previous manuscript[17] we oxidized meso and macroporous carbon aerogels with H_2O_2 and $(NH_4)_2S_2O_8$. The oxidation treatment with $(NH_4)_2S_2O_8$ is stronger than that with H_2O_2 in both support series and the nature of OSG depends on the textural properties, thus, the formation of anhydrides from neighboring carboxylic acid groups is favored in the case of macroporous samples. These OSG had a strong influence on Pt-dispersion when oxidized materials were used as catalysts supports. Similarly, experimental conditions for the synthesis and characteristics of carbon xerogels strongly influence their behavior during activation with O_2[39,40]. Highly oxidized samples (14 and 16 % wt of oxygen content) were obtained after activation at 400 ºC in a 5% O_2 (in N_2) flow (B.O. 14 and 18% wt, respectively)[40]. The CO/CO_2 ratio determined by TPD increases from 3.3 for untreated samples to 6.6 for the sample with 14% of B.O. and then decreases to 5.9 for the sample with 18% wt B.O.

Gomez-Serrano et al.[41] showed that the amount and nature of OSG generated during activation with air strongly depends on the activation temperature. At low activation temperature (250 ºC) the formation of lactonic structures are favored, while at 750 or 900 ºC activation takes place without the formation of permanent OSG on the carbon surface[40]. On this question, Otake and Jenkins[42] described four types of OSG for air and HNO_3 oxidized microporous carbons studied by TPD: lower- and higher-temperature CO or CO_2-yielding surface complexes. They concluded that the oxidation temperature is a very important factor in determining the type of CO_2-evolving complexes that will be formed on a carbon surface. The highest temperature CO_2 surface complexes found in chars that had been air-oxidized above 325 ºC are in the form of carboxyl anhydrides, although a small amount of carboxylic acid is measurable. As in the case of Samant et al.[40], they found a high CO/CO_2 ratio (around 6) for all samples.

In our samples, OSG are mainly located inside the pores (namely large micropores and small mesopores, as previously commented) and thus $\%O_{TPD} > \%O_{XPS}$. Note also that this difference can be greater, because while $\%O_{XPS}$ was calculated from the complete O_{1s} signal in the corresponding spectra, $\%O_{TPD}$ values shown in Table 3.2 are calculated only on the basis of the amount of CO and CO_2 desorbed. This calculation avoids interferences of adsorbed water but leads to oxygen contents that can be underestimated, because oxygen evolved as water from the dehydration of groups such as carboxylic acids or phenols is not evaluated. By weighing the sample before and after thermal treatments, we observed a significant total weight loss of 40% after treatment at 700 ºC. This was due to a release of gases and caused the surface development and the pore widening described above. This value is in agreement with the WL detected by TG (Figure 3.4). The TG profile shows higher content and smaller thermal stability of groups evolved from CAOX with respect to CA.

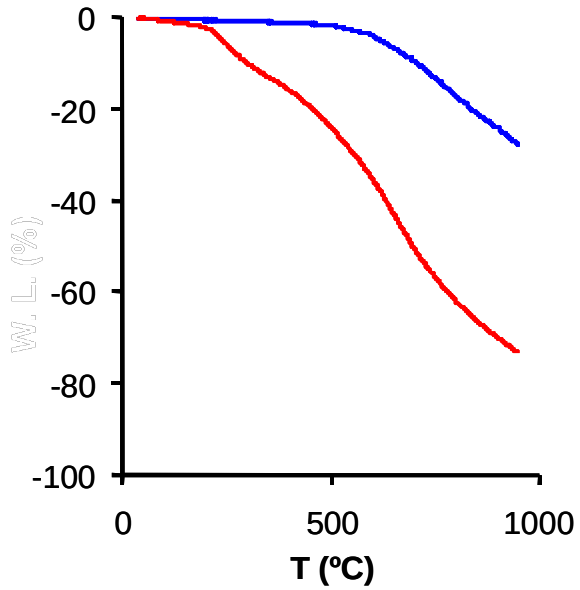

Figure 3.4. TG experiments of CA (blue) and CAOX (red) samples carried out in N_2 flow up to 950 ºC.

Information about the chemical nature of oxygenated surface groups present in each sample is obtained by analyzing XPS and TPD profiles. The highest peak in the CO_2 profile of sample CAOX (Fig. 3.5) is located at 278 ºC and is assigned to carboxylic acids release. The strong shoulder at 450 ºC and the large tail of the CO_2-

profile indicate the presence of different CO_2-evolving groups such as anhydrides or lactones. Anhydrides can be formed from the dehydration of two neighboring carboxylic groups, and decomposed generating simultaneously CO + CO_2. This process seems to be confirmed by the coincidence at 278 ºC of CO, CO_2 and H_2O peaks (Fig. 3.5). Besides this, the first peak of water desorption at 140 ºC corresponds mainly to the physisorbed water, while water desorption at high temperature (600 ºC) confirms the dehydration of more stable oxygenated groups like phenols. The maximum CO-desorption takes place at 555 ºC, but the peak is very wide and shows a large tail. Thus, different CO-evolving groups can also be present. The coincidence of the maximum CO-desorption rate with the last peak of the H_2O-profile indicates a large proportion of phenol groups. According to previous research, phenols[17,20,30,43] evolve between 600-700 ºC, ether groups at around 700 ºC, carbonyls between 800-900 ºC and more stable chromenes at around 1000 ºC. However, Marchon[43] tentatively assigned different peaks of the CO-profile to semiquinone functional groups on energetically different sites. There is also an important H_2 release from 600 ºC mainly as a consequence of C-H breaking and C-C reorganization. Carboxylic acid groups are thermally more unstable than very stable basic groups such as ether, carbonyl or chromene groups, which can remain in the sample up to high temperature as observed in Figs. 3.5 and 3.6. Consequently, the pH_{ZPC} of samples increases progressively with the treatment temperature (Table 3.2).

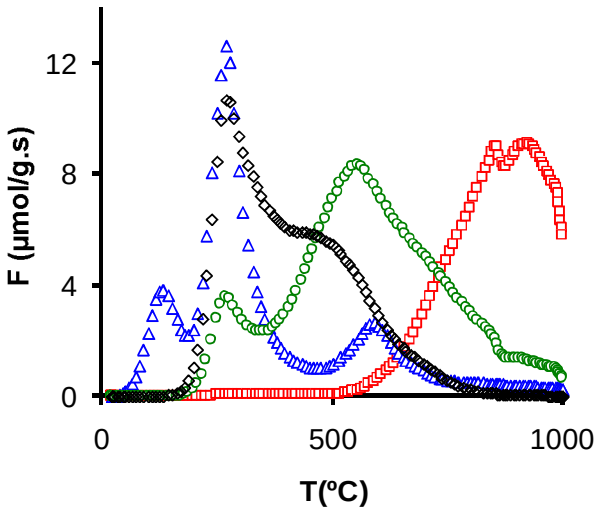

Figure 3.5. Profiles of TPD for CO (○), CO_2 (◇), H_2 (□) and H_2O (△) in sample CAOX.

Table 3.2. Chemical characteristics of samples from TPD, XPS and pH_{ZPC} determinations.

Sample	WL %	CO μmol g^{-1}	CO_2 μmol g^{-1}	O_{TPD} %	O_{XPS} %	pH_{ZPC}
CA	-	1160	150	2.3	1.8	7.5
CAOX	-	3680	3010	15.5	10.0	2.4
CAOX300	20	5070	2110	14.9	7.6	2.9
CAOX500	24	6030	1370	14.0	6.0	3.0
CAOX700	40	680	110	1.4	1.6	7.8

The selective removal of OSG from the oxidized sample (CAOX) was carried out by thermal treatments in an inert atmosphere, according to their thermal stability previously determined by TPD. These thermal treatments, including the treatment at lower temperature (300 ºC), are strong enough to completely eliminate carboxylic acid groups present in the CAOX sample (Fig. 3.6). Nevertheless, CO_2-desorption starts in all heat-treated samples at around 230 ºC (Fig. 3.6a), i.e. some CO_2-evolving groups occupy the free sites again after the corresponding heat treatment, as previously described[20]. This process seems to be favored at 500 ºC compared with treatments carried out at 300 ºC (Fig. 3.6a). The main peak in the CO_2-profile appears at 500 ºC and 570 ºC for CAOX300 and CAOX500 respectively, i.e. this profile is also shifted towards higher temperatures in line with increases in the treatment temperature. Thus after treatments, thermally weaker and stronger CO_2-evolving groups are generated by the reorganization of oxygenated surface groups. In the case of the CO-profile (Fig. 3.6b), the CO-peak also shifted to higher temperatures but, simultaneously, strongly increases with increasing treatment temperature from 300 to 500 ºC. During the preparation of both CAOX-300 and CAOX-500 around 75% of the oxygen released as CO_2 is again reincorporated into the sample as CO-evolving groups (Table 3.2).

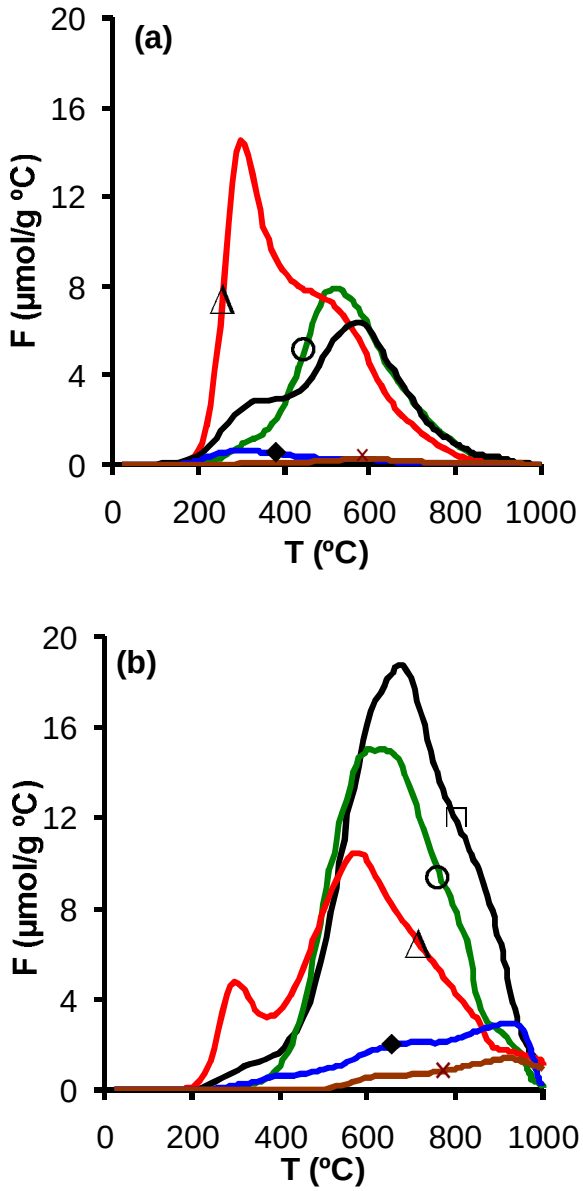

Figure 3.6. TPD curves for CO_2 (a) and CO (b). CA (◆), CAOX (Δ), CAOX300 (○), CAOX500 (□), CAOX700 (×).

XPS patterns of C_{1s} and O_{1s} regions for the sample series are depicted in Fig. 3.7, which also shows their different components. Fitting the C_{1s} spectrum, different functions were considered and assigned according to the bibliography[31,32]: aromatic and aliphatic carbon (284.6 eV), single C-O bonds (286.0 eV), double C=O bonds (287.5 eV), carboxyl -COO- groups (289.1 eV), carbonate groups (290.6 eV) and plasmon

(291.3 eV). The O_{1s} spectra was fitted using two components, assigned as C=O at 531.3 eV and C-O at 533.2 eV.

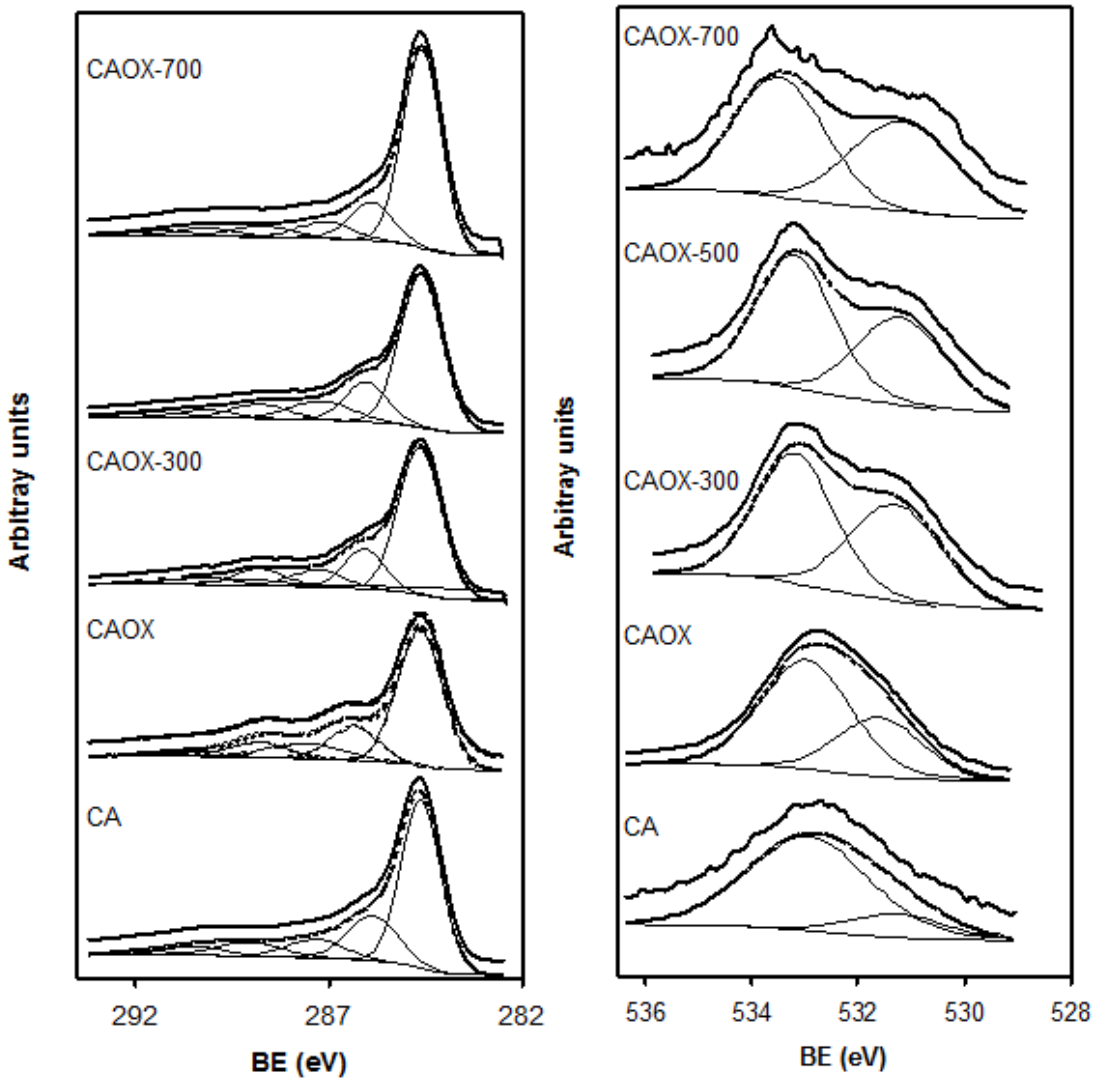

Figure 3.7. Curve-fitted C_{1s} (left), O_{1s} (right) core-level spectra for samples series (from top to bottom: CA, CAOX, CAOX300, CAOX500, CAOX700).

The formation of OSG after oxidation is observed by the appearance of clear maxima on the large tail of the C_{1s} peak of the CAOX spectrum. Thus, the contribution of the peak at 284.6 eV decreases, while also showing an increase in the FWHM and mainly favoring the increase of the peak at 287 eV (C=O bonds). These relative maxima on the tail disappear progressively from the C_{1s} spectra (the FWHM of the peak at 284.6 eV decreases) with increasing treatment temperature and according to the

decrease in $\%O_{XPS}$ (Table 3.2). Thus, finally, CA and CAOX700 show similar C_{1s} spectra. If we analyze the O_{1s} region, the same conclusion is obtained by comparing the CA and CAOX spectra, i.e. oxidation favors the formation of C=O bonds. In spite of the fact that C=O bonds are present in different types of OSG, such as quinone or lactone groups, according to the TPD results they are due mainly to carboxylic groups and their anhydride derivatives. After heat treatment, the expected decrease due to the release of carboxylic acid of the O_{1s} peak at 531.6 eV with respect to that at 533.0 eV does not occur (Fig. 3.7). On the contrary, the proportion of C=O/C-O seems to bear no relation to treatment temperature.

Sample CAOX therefore behaves in a very particular manner during treatments between 300-500 ºC. As observed in Table 3.2, the $\%O_{XPS}$ progressively decreases as expected, however, $\%O_{TPD}$ remains practically unmodified in this temperature range. Moreover, TPD showed that the formation of CO-evolving groups is favored, whereas XPS showed that CO_2-evolving groups are formed. The external and internal carbon surfaces therefore behave differently. There is a strong reorganization of oxygenated surface groups inside the pores according to TPD results, in such a way that CO_2-evolving groups decrease as treatment temperature increases, although this results simultaneously in a spectacular increase in CO-evolving groups, which maintain the oxygen content practically constant. By contrast, on the external carbon surface, the oxygen content decreases and the C=O bonds seem to be favored compared to the C-O bonds, according to XPS results.

Different hypotheses must be examined in order to explain the behavior described. The first option is that new OSG (basically CO-desorbing groups) were generated during heat treatments by the presence of residual O_2 in the N_2 flow. However, as explained in the experimental section, we used a high purity N_2 flow and air leaks were successfully prevented in such a way that no difference was observed between the flow composition at the entry and exit of the tube oven. Therefore, the only oxygen source inside the oven during the thermal treatment of CAOX sample must be COx evolved from the corresponding OSG.

Moreover, according to previous results[40-42] air activation favors the formation of CO-evolving groups compared to CO_2-evolving ones only at a low activation degree. However in our case, the CO/CO_2 ratio progressively increases in the direction CAOX (1.2) < CAOX300 (2.4) < CAOX500 (4.4) < CAOX700 (6.2) in spite of the fact that during the preparation at 700 °C of this last sample CAOX undergoes a weight loss of 40%, associated with the gasification process inside the pores as previously described.

The second option is that TPD experiments were carried out under experimental conditions that could mask the true oxygen content or chemical nature of the OSG. For this reason, consecutive TPD runs were performed in order to ensure that there were no oxygenated impurities on He and that every evolved OSG was transported by the carrier to the MS and analyzed. The results can be seen in Fig. 3.8. As observed, the amount of oxygen evolved after the first heating cycle up to 1000 ºC became negligible (O (% W) = 0.6 for the second run). Only residual CO-evolving groups were detected at high temperature during the second run. CO-evolving groups are highly stable thermally, thus, some of them remain in the sample after a first heating cycle and because these species are mobile they again occupy free sites generated by the evolved OSG[20]. A small amount of CO is detected in the second run.

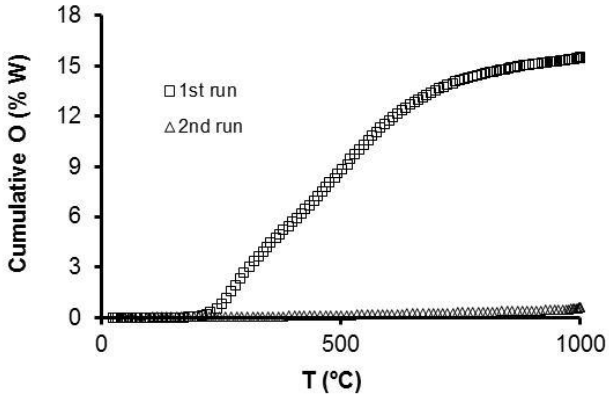

Figure 3.8. Cumulative oxygen content evolved from the CAOX sample during two consecutive TPD experiments.

These results showed that there was no reoxidation of the carbon surface by He impurities or even by the OSG evolved in the first run, in the experimental conditions used for TPD experiments. The reproducibility of the TPD results was also checked, and we found that the difference of COx desorbed in duplicate experiments was always less than 5%, which is within the experimental error limits. Therefore, sample contamination does not occur and OSG are properly evolved, transported and analyzed under the TPD experimental conditions used.

Alternatively, these new groups could be generated after the exposure and storage of heat treated samples in air. Nevertheless it is also well known that the higher the previous outgassing temperature the higher the extent of the regeneration of the OSG by air oxidation during storage[44]. However, after treatments at 700 ºC, the oxygen content and the pH_{ZPC} of CAOX700 and CA become quite similar, i.e. the re-oxidation of this sample is negligible, even taking into account the higher concentration of free sites, highly reactive and susceptible to being reoxidized either during the longer cooling period needed (once again demonstrating the absence of air leaks) or during air storage. Because all the samples were manipulated in a similar way, the oxidation by air during transfer or storage of samples CAOX300 and CAOX500 should be even smaller, and this cannot therefore be the reason for the high oxygen content of these samples. According to XPS results, oxidation by air can be favored on the external surface of heat treated samples.

Thus, the most plausible option to explain the results described above seems to be the re-oxidation of the surface by CO_2 desorbed at low treatment temperature or the reorganization of OSG on the chemical structure by atomic diffusion during the heat treatment. The thermally weaker carboxylic groups are certainly desorbed as CO_2 even with the treatment at 300 ºC. This CO_2 should therefore be re-adsorbed, oxidizing the carbon surface with the formation of new CO groups inside the pores in such a way that the total oxygen content remains practically unchanged in sample CAOX300 compared to sample CAOX (Table 3.2). This is observed even for treatment at 500 ºC. In the case of CAOX700 it is very likely that readsorption and oxidation occur as previous steps within the gasification process[9], but then many of these complexes are decomposed as they are not stable at 700 ºC (Figs. 3.4, 3.5 and 3.8), leading to a widening of porosity

in this sample (Table 3.1). These new CO-evolving groups are stable inside the pores after exposure to the air and storage of samples. However, at the most external surface, free sites generated by the heat treatment seem to be reoxidized by air to CO_2-evolving groups, although the total amount of these groups is low (Table 3.2).

DSC experiments (Figure 3.9) confirm the re-adsorption (re-oxidation) of the carbon surface during the thermal treatment of sample CAOX in N_2. In the case of the original CA sample, the DSC profile practically matched the base line up to around 350 ºC. Above this temperature, endothermic processes occur, related with the C-O bond breakage and CO release according to the TPD results (Fig. 3.5). The bond breakage and desorption processes are clearly endothermic. The small deviations observed are due to the small amount of oxygen desorbed up to 500 ºC.

However, when we analyzed the DSC of the CAOX sample, we initially observed a strong endothermic peak, associated with a dehydration process. Physisorbed water and probably water formed from neighboring carboxylic acid groups forming anhydrides were evolved at low temperature. However, between 200 – 350 ºC, the temperature range within which the carboxylic groups are evolved as CO_2, there is a clear and significant exothermic peak. The bond breakage and the CO_2 relay are endothermic processes; therefore, the exothermic peak corresponds to the chemisorption of the CO_2 on highly energetic free carbon sites (C_f) and the adsorption energy is enough to favor the formation of CO-evolving groups. The reaction $CO\ (g) + C(O)\ (s) = CO_2\ (g) + C_f$ is exothermic[9], but is improbable in this case taking into account the low CO concentration in this temperature range and because, in fact, the amount of CO_2 detected decreases while that of CO increased (Table 3.2). At higher temperature, the DSC profile again decreases with respect to the base line, indicating the endothermic release of surface groups. The re-oxidation of the carbon surface is associated only with the release of carboxylic groups, so, in the DSC of thermally treated CAOX (even at 300 ºC), this exothermic peak disappears because a great proportion of carboxylic groups were previously evolved (Fig. 3.6). The release of CO_2 from more stable groups such as anhydrides or lactones does not provide this effect, probably because they decompose at higher temperatures so preventing CO_2 chemisorption. It is also noteworthy that this process only occurs inside micropores and

is favored in this sample due to the high micropore volume. The influence of porosity in these processes was noted by previous authors[9], who established that "porosity enhanced dispersion forces, creating quasi-high pressure effects and a quasi-lowering of temperature". Porosity also strongly influences the evolved CO/CO_2 ratio (and consequently the intermediate OSG formed), which decreases with increasing burn-off (porosity) of PFA-carbons[45]. This fact can also favor the ratio of C=O bonds found on the surface by XPS analysis.

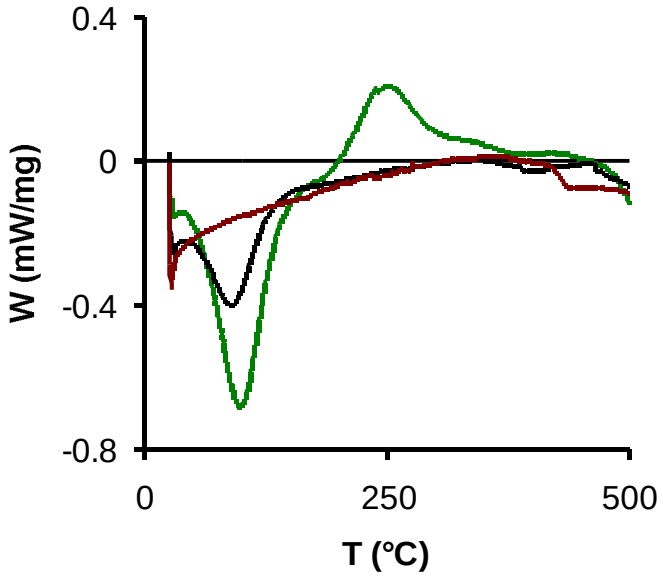

Figure 3.9. DSC-profiles obtained by heating samples at 10 ºC.min^{-1} in N_2 up to 500 ºC. CA (brown), CAOX (green) and CAOX300 (black).

These experimental results confirm the hypothesis in the theoretical study by Montoya et al.[21] who proposed that the formation of semiquinone (CO-evolving groups) from chemisorbed CO_2 is thermodynamically possible due to the energy (heat of adsorption) liberated by the formation of the CO_2–surface complex (intermediate lactones). More recently, Radovic[22] performed a computational chemistry study which confirmed that dissociative CO_2-chemisorption is favored, mainly on zigzag active sites (which are abundant in the CAOX sample once contiguous carboxylic acid groups are decomposed). In a classic paper[46] Hall and Calo also advised about the influence of a large number of variables on the TPD profiles due to secondary interactions upon thermal desorption. They concluded that "CO can be strongly chemisorbed on coal

chars and/or formed by secondary reaction of CO_2 with free active sites" which is in agreement with our results and with the discussion provided.

3.4. CONCLUSIONS

Highly porous activated carbons are produced by chemical activation of carbonized olive stones. In this case, the high activation degree caused pore walls to become weak and to be gasified during oxidation treatment carried out in order to functionalize the carbon surface. Oxidation destroyed the mesoporosity of the sample obtaining acid activated carbons. Oxygen surface groups (OSG) were removed by thermal treatments. We observed a strong reorganization of OSG inside pores when samples were heated up to 300 or 500 ºC, where 75% of the OSG evolved as CO_2 (carboxylic acids) are fixed again as a CO-evolving group (semiquinone). The exothermic chemisorption of CO_2 previously released was detected by DSC. Treatment at 700 ºC prevents re-oxidation of the surface and leads to a strong degree of gasification (40% w), which favors pore widening, and the decrease of the oxygen content, which in turn favors an increase in the pH_{pzc}. However, XPS showed that at the external carbon surface the oxygen content decreases as treatment temperature increases and the formation of C=O bonds is favored by open porosity.

3.5. REFERENCES

[1] J. Lee, J. Kim, and T. Hyeon, Recent Progress in the Synthesis of Porous Carbon Materials, *Advanced Materials,* **18** (2016) 2073-2094.

[2] R.W. Pekala, Low density, resorcinol-formaldehyde aerogels, US Patent, *US4997804 A*, 1991.

[3] S.A. Al-Muhtaseb and J.A. Ritter, Preparation and Properties of Resorcinol–Formaldehyde Organic and Carbon Gels, *Advanced Materials*, **15** (2003) 101-114.

[4] G. Gong, Q. Xie, Y. Zheng, S. Ye, and Y. Chen, Regulation of pore size distribution in coal-based activated carbon, *New Carbon Materials* **24** (2009) 141-146.

[5] A. Aranda, R. Murillo, T. García, A.M. Mastral, Simulation and optimization of tyre-based steam activated carbons production for gas-phase polycyclic aromatic hydrocarbons abatement, *Chemical Engineering Journal*, **187** (2012) 123-132.

[6] V.M. Monsalvo, A.F. Mohedano, and J.J. Rodriguez, Activated carbons from sewage sludge: Application to aqueous-phase adsorption of 4-chlorophenol, *Desalination*, **277** (2011) 377-382.

[7] S. Morales-Torres, A.M.T. Silva, A.F. Pérez-Cadenas, J.L. Faria, F.J. Maldonado-Hódar, J.L. Figueiredo, and F. Carrasco-Marín, Wet air oxidation of trinitrophenol with activated carbon catalysts: Effect of textural properties on the mechanism of degradation, *Applied Catalysis B: Environmental*, **100** (2010) 310-317.

[8] Y. Tang, Q. Liu, and F. Chen, Preparation and characterization of activated carbon from waste ramulus mori, *Chemical Engineering Journal*, **203** (2012) 19-24.

[9] H. Marsh and F. Rodríguez-Reinoso, *Activated Carbon*, Elsevier, Oxford, 2006.

[10] A. Baçaoui, A. Dahbi, A. Yaacoubi, C. Bennouna, F.J. Maldonado-Hódar, J. Rivera-Utrilla, F. Carrasco-Marín, and C. Moreno-Castilla, Experimental Design To Optimize Preparation of Activated Carbons for Use in Water Treatment, *Environmental Science & Technology*, **36** (2002) 3844-3849.

[11] T.J. Bandosz, Chapter 2: Surface Chemistry of Carbon Materials, in: *Carbon Materials for Catalysis*, John Wiley & Sons, Inc. New Jersey, 2009, pp. 45-93.

[12] C. Moreno-Castilla, Adsorption of organic molecules from aqueous solutions on carbon materials, *Carbon*, **42** (2004) 83-94.

[13] T. Wajima and K. Sugawara, Adsorption behaviors of mercury from aqueous solution using sulfur-impregnated adsorbent developed from coal, *Fuel Processing Technology*, **92** (2011) 1322-1327.

[14] M. Mullett, P. Pendleton, and A. Badalyan, Removal of elemental mercury from Bayer stack gases using sulfur-impregnated activated carbons, *Chemical Engineering Journal*, **211-212** (2012) 133-142.

[15] S. Furmaniak, P. Kowalczyk, A.P. Terzyk, P.A. Gauden, and P.J.F. Harris, Synergetic effect of carbon nanopore size and surface oxidation on CO2 capture from CO2/CH4 mixtures, *Journal of Colloid and Interface Science*, **397** (2013) 144-153.

[16] I. Matos, P.D. Neves, J.E. Castanheiro, E. Perez-Mayoral, R. Martin-Aranda, C. Duran-Valle, J. Vital, A.M. Botelho do Rego, and I.M. Fonseca, Mesoporous carbon as an efficient catalyst for alcoholysis and aminolysis of epoxides, *Applied Catalysis A: General*, **439-440** (2012) 24-30.

[17] S. Morales-Torres, F.J. Maldonado-Hódar, A.F. Pérez-Cadenas, and F. Carrasco-Marín, Design of low-temperature Pt-carbon combustion catalysts for VOC's treatments, *Journal of Hazardous Materials*, **183** (2010) 814-822.

[18] A.R. Silva, C. Freire, B. de Castro, M.M.A. Freitas, and J.L. Figueiredo, Anchoring of a nickel(II) Schiff base complex onto activated carbon mediated by cyanuric chloride, *Microporous & Mesoporous Materials*, **46** (2001) 211-221.

[19] M.A. Montes-Morán, D. Suárez, J.A. Menéndez, and E. Fuente, On the nature of basic sites on carbon surfaces: an overview, *Carbon*, **42** (2004) 1219-1225.

[20] C. Moreno-Castilla, F. Carrasco-Marín, F.J. Maldonado-Hódar, and J. Rivera-Utrilla, Effects of non-oxidant and oxidant acid treatments on the surface properties of an activated carbon with very low ash content, *Carbon*, **36** (1998) 145-151.

[21] A. Montoya, F. Mondragón, and T.N. Truong, Formation of CO precursors during char gasification with O_2, CO_2 and H_2O, *Fuel Processing Technology*, **77-78** (2002) 125-130.

[22] L.R. Radovic L R, The mechanism of CO_2 chemisorption on zigzag carbon active sites: A computational chemistry study, *Carbon*, **43** (2005) 907-915.

[23] C. Moreno-Castilla, M.A. Ferro-Garcia, J.P. Joly, I. Bautista-Toledo, F. Carrasco-Marin, and J. Rivera-Utrilla, Activated Carbon Surface Modifications by Nitric Acid, Hydrogen Peroxide, and Ammonium Peroxydisulfate Treatments, *Langmuir*, **11** (1995) 4386-4392.

[24] C. Moreno-Castilla, M.V. López-Ramón, and F. Carrasco-Marín, Changes in surface chemistry of activated carbons by wet oxidation, *Carbon*, **38** (2000) 1995-2001.

[25] R.G. Bansal, J.B. Donnet, and F. Stoeckli, *Activated Carbon*, Marcel Dekker, New York and Basel, 1988.

[26] F. Stoeckli, *Porosity in carbon. Characterization and applications*. Eds. Patrick J. Arnold, London, 1995.

[27] E.P. Barrett, L.G. Joyner, and P.P. Halenda, The Determination of Pore Volume and Area Distributions in Porous Substances. I. Computations from Nitrogen Isotherms, *Journal of the American Chemical Society*, **73** (1951) 373-380.

[28] A.V. Neimark, Y. Lina, I. Peter, P.I. Ravikovitchb, and M. Thommes, Quenched solid density functional theory and pore size analysis of micro-mesoporous carbons, *Carbon* **47** (2009) 1617–1628.

[29] F. Duarte, F.J. Maldonado-Hodar, and L.M. Madeira, Influence of the characteristics of carbon materials on their behaviour as heterogeneous Fenton catalysts for the elimination of the azo dye Orange II from aqueous solutions, *Applied Catalysis B: Environmental*, **103** (2011) 109–115.

[30] J.L. Figueiredo, M.F.R. Pereira, M.M.A. Freitas, and J.J.M. Órfão, Modification of the surface chemistry of activated carbons, *Carbon*, **37** (1999) 1379-1389.

[31] A.F. Pérez-Cadenas, F.J. Maldonado-Hódar, and C. Moreno-Castilla, On the nature of surface acid sites of chlorinated activated carbons, *Carbon*, **41** (2003) 473-478.

[32] E. Desimoni, G.I. Casella, and A.M. Salvi. XPS/XAES study of carbon fibres during thermal annealing under UHV conditions, *Carbon*, **30** (1992) 521-526.

[33] C.A. Leon, J.M. Solar, V. Calemma, and L.R. Radovic, Evidence for the protonation of basal plane sites on carbon, *Carbon*, **30** (1992) 797-811.

[34] R. Ubago-Pérez, F. Carrasco-Marín, D. Fairén-Jiménez, and C. Moreno-Castilla, Granular and monolithic activated carbons from KOH-activation of olive stones, *Microporous and Mesoporous Materials*, **92** (2006) 64-70.

[35] M. Molina-Sabio and F. Rodríguez-Reinoso, Role of chemical activation in the development of carbon porosity, *Colloids and Surfaces A: Physicochemical and Engineering Aspects*, **241** (2004) 15-25.

[36] D. Cazorla-Amorós, J. Alcañiz-Monge, M.A. Casa-Lillo, and A. Linares-Solano, CO2 as an Adsorptive To Characterize Carbon Molecular Sieves and Activated Carbons, *Langmuir*, **14** (1998) 4589-4596.

[37] Y. Matsumura, Production of acidified active carbon by wet oxidation and its carbon structure, *Journal of Applied Chemistry & Biotechnology*, **25** (1975) 39-56.

[38] Z. Du, A.F. Sarofim, and J.P. Longwell, Activation energy distribution in temperature-programmed desorption: modeling and application to the soot oxygen system, *Energy & Fuels*, **4** (1990) 296-302.

[39] X. Xu, J. Zhu, J.L. Faria, J. Li, and J.L. Figueiredo, Tuning the textural and surface properties of carbon xerogels to be used as supports for gold catalysts, *Central European Journal of Chemistry*, **10** (2012) 1867-1874.

[40] P.V. Samant, F. Goncalves, M.M.A. Freitas, M.F.R. Pereira, and J.L. Figueiredo, Surface activation of a polymer based carbon, *Carbon*, **42** (2004) 1321–1325

[41] V. Gómez-Serrano, F. Piriz-Almeida, C.J. Durán-Valle, and J. Pastor-Villegas, Formation of oxygen structures by air activation. A study by FT-IR spectroscopy, *Carbon*, **37** (1999) 1517–1528.

[42] Y. Otake and R.G. Jenkins, Characterization of oxygen-containing surface complexes created on a microporous carbon by air and nitric acid treatment, *Carbon*, **31** (1993) 109-121.

[43] B. Marchon, J. Carrazza, H. Heinemann, and G.A. Somorjai, TPD and XPS studies of O2, CO2, and H2O adsorption on clean polycrystalline graphite, *Carbon*, **26** (1988) 507-514.

[44] F. Carrasco-Marin, J. Rivera-Utrilla, J.P. Joly, and C. Moreno-Castilla, Effects of ageing on the oxygen surface complexes of an oxidized activated carbon, *Journal of the Chemical Society, Faraday Transactions*, **92** (1996) 2779-2782.

[45] H. Marsh, D.A. Taylor, and J.R. Lander, Kinetic study of gasification by oxygen and carbon dioxide of pure and doped graphitizable carbons of increasing heat treatment temperatures, *Carbon*, **19** (1981) 375-381.

[46] P.J. Hall and J.M. Calo, Secondary Interactions upon Thermal Desorption of Surface Oxides from Coal Chars, *Energy & Fuels*, **3** (1989) 370-376.

Capítulo IV

TAILORING ACTIVATED CARBONS FOR THE DEVELOPMENT OF SPECIFIC ADSORBENTS OF GASOLINE VAPORS

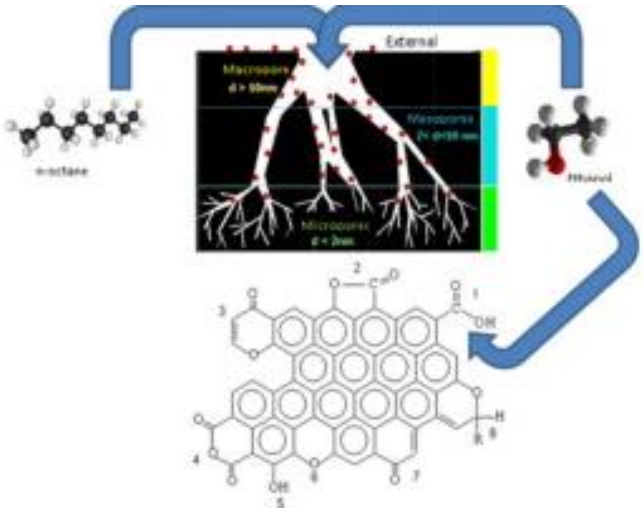

TAILORING ACTIVATED CARBONS FOR THE DEVELOPMENT OF SPECIFIC ADSORBENTS OF GASOLINE VAPORS

Article published in J. of Hazardous Materials, 263, Part 2, (2013) 533-540, doi: 10.1016/j.jhazmat.2013.10.012

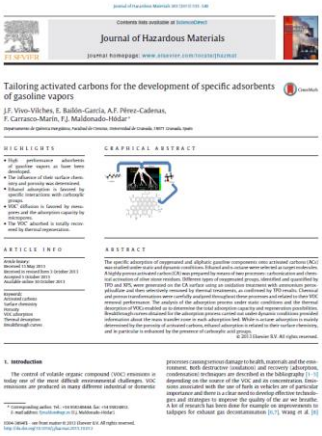
Journal of Hazardous Materials

Tailoring activated carbons for the development of specific adsorbents of gasoline vapors

J.F. Vivo-Vilches, E. Bailón-García, A.F. Pérez-Cadenas, F. Carrasco-Marín, F.J. Maldonado-Hódar*

Highlights

- High performance adsorbents of gasoline vapors as have been developed.
- The influence of their surface chemistry and porosity was determined.
- Ethanol adsorption is favored by specific interactions with carboxylic groups.
- VOC' diffusion is favored by mesopores and the adsorption capacity by micropores.
- The VOC' adsorbed is totally recovered by thermal regeneration.

Abstract

The specific adsorption of oxygenated and aliphatic gasoline components onto activated carbons (ACs) was studied under static and dynamic conditions. Ethanol and n-octane were selected as target molecules. A highly porous activated carbon (CA) was prepared by means of two processes: carbonization and chemical activation of olive stone residues. Different types of oxygenated groups, identified and quantified by TPD and XPS, were generated on the CA surface using an oxidation treatment with ammonium peroxydisulfate and then selectively removed by thermal treatments, as confirmed by TPD results. Chemical and porous transformations were carefully analyzed throughout these processes and related to their VOC removal performance. The analysis of the adsorption process under static conditions and the thermal desorption of VOCs enabled us to determine the total adsorption capacity and regeneration possibilities. Breakthrough curves obtained for the adsorption process carried out under dynamic conditions provided information about the mass transfer zone in each adsorption bed. While n-octane adsorption is mainly determined by the porosity of activated carbons, ethanol adsorption is related to their surface chemistry, and in particular is enhanced by the presence of carboxylic acid groups.

Keywords: Activated carbons, surface chemistry, porosity, VOC adsorption, thermal desorption, breakthrough curves. complexes.

4.1. INTRODUCTION

The control of volatile organic compound (VOC) emissions is today one of the most difficult environmental challenges. VOC emissions are produced in many different industrial or domestic processes causing serious damage to health, materials and the environment. Both destructive (oxidation) and recovery (adsorption, condensation) techniques are described in the bibliography[1-5] depending on the source of the VOC and its concentration. Emissions associated with the use of fuels in vehicles are of particular importance and there is a clear need to develop effective technologies and strategies to improve the quality of the air we breathe. A lot of research has been done for example on improvements to tailpipes for exhaust gas decontamination[6,7]. Wang et al.[8] identified a total of 57 individual VOCs in the exhaust gas of gasoline vehicles.

Historically, less attention has been paid to evaporative emissions produced during fuel storage and/or transfer. Nevertheless, a number of papers have been published also on this topic[9,10]. For example, Yamada quantified evaporative emissions as the sixth highest source of VOC in Japan, with 4.6 % of total VOC emissions[9]. Specific devices (canisters) for adsorbing VOCs have been developed, which mainly use activated carbons as the adsorbent[11-13]. Furthermore, the American Petroleum Institute (API) has continuously pointed out the effects of these vapors on the environment, health and safety[14], analyzing tank and pipeline regulations to ensure the safe transport, storage and disposal of gasoline.

In recent years there has also been increasing interest in ethanol-based fuels all over the world. The addition of ethanol to gasoline is interesting from an environmental and economic point of view since it can be produced from biomass. Moreover, ethanol is added to gasoline as an anti-knock agent because it is less harmful than MTBE and ETBE. However, the presence of ethanol in fuels is the subject of controversy, since some studies have proved that ethanol-based fuels produce larger quantities of evaporative emissions[15,16].

Some empirical models have been developed in order to estimate evaporative emissions from canister-equipped vehicles[9-12]. These models considered several factors such as vehicle design (tanks), ambient temperature, driving conditions, or gasoline volatility[13] but there is a lack of experimental confirmation of the relationship between canister performance, gasoline composition and the characteristics of the adsorbent, as indicated by Yamada[9]. Activated carbons (ACs) are the most widely used adsorbent due to the fact that both their porous and chemical nature can be easily tailored. Moreover, cheap ACs can be produced from raw materials such as agricultural residues[2,5,17,18]. In comparison, zeolites are about ten times more expensive[19].

In this work, we prepared a series of ACs from olive stones. We developed the porous texture by chemical activation and modified the surface chemistry by means of a severe oxidation process. After that, a selective removal of oxygenated surface groups was performed in order to find out more about specific VOC-AC interactions, which may affect the adsorption and regeneration capacities. Ethanol and n-octane were selected as target VOCs because they are the main components of gasoline and have different chemical natures (ethanol is hydrophilic and n-octane is hydrophobic). Finally we correlated the evolution of porosity and chemical surface characteristics for these activated carbons with their ethanol and n-octane adsorption performance under static and dynamic conditions.

4.2. MATERIALS AND METHODS

4.2.1. Activated carbon synthesis by KOH activation

Olive stones were milled and sieved to 1.0 – 2.0 mm, treated with sulfuric acid (1 N) in order to remove any remains of the pulp and then washed until all sulfates had been removed. A two-stage activation procedure was designed: initially, olive stones were carbonized at 400 ºC for two hours under a nitrogen flow (300 $cm^3\ min^{-1}$) and then the char obtained was chemically activated using a mixture of char and KOH in a 1:7 mass ratio. This mixture was treated under nitrogen flow (300 $cm^3\ min^{-1}$) for 2 h at 350

ºC followed by 3 h at 850 ºC (heating rate 10 ºC min^{-1}). The sample was kept under nitrogen atmosphere while it was cooled to room temperature. Finally, it was treated with HCl and HF, which also removed the excess base (KOH), washed with distilled water till all chlorides had been removed and dried in an oven at 110 ºC for 24 h before storage. This sample was called CA.

4.2.2. Chemical surface modifications

Ammonium peroxydisulfate ($(NH_4)_2S_2O_8$) was chosen as the oxidizing agent[20]. CA was mixed with a saturated solution of this salt on H_2SO_4 1 M. After 24 h under stirring at room temperature, oxidized carbon was filtered and washed with distilled water several times until all sulfates had been removed. This material was dried at 110 ºC and labeled as CAOX. Thermal treatments under nitrogen atmosphere (150 cm^3 min^{-1}) at 300 ºC, 500 ºC and 700 ºC (10 min, 20 ºC min^{-1}) were carried out on different portions of CAOX in order to selectively remove oxygenated surface groups (OSG). These samples were labeled as CAOX300, CAOX500 and CAOX700.

4.2.3. Textural Characterization

The corresponding N_2 and CO_2 adsorption isotherms at -196 ºC and 0 ºC were obtained using an AUTOSORB 1 (QUANTACHROME Ins.) instrument. Parameters such as BET surface area, micropore volume (W_0) and micropore mean width (L_0) were calculated by applying BET, Dubinin-Radushkevich and Stoeckli equations to isotherms[21,22]. Pore size distribution (PSD) curves were obtained by DFT or BJH derived methods[23,24]. Mesopore volume (V_{meso}) was estimated considering the total pore volume as the volume of nitrogen adsorbed at a relative pressure P/P_0 = 0.95 ($V_{0.95}$). Therefore, V_{meso} was obtained from the difference between $V_{0.95}$ and W_0 (N_2). Mercury pycnometry was carried out in order to determine the apparent density of samples. In preparation for this procedure, samples were previously degasified at 110 ºC under dynamic vacuum (10^{-3} Torr).

4.2.4. Chemical Characterization

Thermal Programmed Desorption (TPD) curves of carbon monoxide and carbon dioxide were recorded. The analysis of TPD profiles enabled us to quantitatively determine the total oxygen content and the number of different oxygenated groups. The assignment of these groups was based on the bibliography[25-28]. Experiments were carried out by heating around 150 mg of sample at 50 K min^{-1} up to 1273 K using He as the carrier gas (60 cm^3 min^{-1}). The analysis of desorbed gases was performed with a Mass Spectrometer model Prisma (Pfeiffer).

X-ray photo emission spectra (XPS) were recorded using a Kratos Axis Ultra-DLD spectrometer. As a radiation source this instrument uses MgKα (hν = 1253.6 eV) and a hemispheric electron analyzer operating at 12 kV and 10 mA. Since we wanted to quantify total oxygen content, we analyzed regions for C_{1s} and O_{1s}. The deconvolution of spectra and the assignment of bands were also performed according to the bibliography[28,29].

Zero-point charge pH (pH_{ZPC}) of samples was determined with the method proposed by Leon et al.[30]. Approximately 250 mg of each sample were suspended on 4 mL of distilled water previously degasified. Suspensions were stirred and thermostated at 25 ºC measuring the pH periodically until readings were constant. The final pH obtained this way was considered as the pH_{ZPC} for each sample.

4.2.5. VOC adsorption

4.2.5.1. Static adsorption

Ethanol and n-octane static adsorption experiments were carried out by exposing 0.050 g of each sample, previously dried at 110 ºC, in a desiccator containing ethanol (absolute ethanol, Panreac) or n-octane (octane ≥99% GC, Sigma-Aldrich) at room temperature (≈ 25 ºC) (P_0 = 57 and 16 Torr respectively). In these experiments, samples were placed in a saturated atmosphere of the organic vapor until equilibrium was reached, and then the total adsorption capacity of the samples was determined[3,4].

Samples were weighed daily till constant weight by using a Denver Instruments SI-234 balance with an accuracy of 0.1 mg. VOC desorption was studied by DSC and TG with a METTLER-TOLEDO TGA/DSC1, heating VOC-saturated samples under N_2 flow (60 cm^3 min^{-1}) to 500 and 950 ºC respectively (10 ºC min^{-1}). Desorbed amounts of VOC and desorption energies were determined and correlated with the textural and chemical characteristics of the samples.

4.2.5.2. Dynamic adsorption

Breakthrough curves were determined by using the instrumental set-up described in Fig. 1. Breakthrough columns consist of a U-shaped reactor (0.4 cm inner diameter) containing 0.1 g of adsorbent fixed bed. ACs were pretreated at 200 ºC under He flow (60 cm^3 min^{-1}) for one hour, and then, breakthrough adsorption curves were obtained at controlled temperature by changing from a He flow to an air/VOC flow (60 cm^3 min^{-1}, 480 ppm n-octane or 560 ppm ethanol). VOC concentration was fitted by bubbling the air flow through liquid VOC at 0 ºC and diluting with pure air in the appropriate proportion. VOC concentration was determined by a Gas Chromatograph CP-3800 (VARIAN) equipped with a Carbowax-20M column and FID detection.

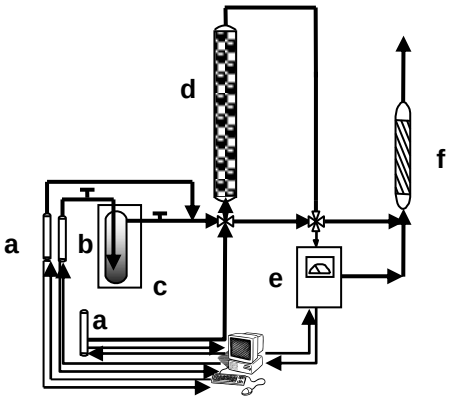

Figure 4.1. a) Mass flux controllers for He and air flows b) VOC reservoir c) Cryostat d) AC column e) Gas chromatograph f) Waste trap.

The analysis of breakthrough curves was performed using the mass transfer zone (MTZ) concept[31,32]. Different parameters may be determined from the analysis of breakthrough curves: breakthrough ($V_{0.02}$) and saturation ($V_{0.90}$) points that are defined

as eluted volumes when the VOC concentration at the column exit reached values of 2 and 90% of the initial VOC concentration (expressed as time on stream or volume treated), the amount adsorbed at these points $X_{0.02}$ and $X_{0.90}$, the mass transfer zone height (H_{MTZ}) and the rate at which MTZ moved forward (R_{MTZ}).

The mass transfer zone (MTZ) and the mass transfer zone height (H_{MTZ}) are defined as the region of the bed within which the adsorption process is taking place. MTZ is therefore located between the saturated part of the bed and the clean part. This means that there is a VOC concentration gradient which moves with the MTZ along the adsorbent bed to the end column. Diffusion and adsorption are happening at the same time. Therefore, values of H_{MTZ} are smaller for rapid adsorption than for slow adsorption. The calculation of this parameter was carried out by applying the following equation described in the bibliography[33]:

$$H_{ZTM} = h\left(\frac{V_{0.90} - V_{0.02}}{V_{0.02} + \phi(V_{0.90} - V_{0.02})}\right) \qquad \phi = \frac{\int_{V_{0.02}}^{V_{0.90}} (C_0 - C)dV}{C_0 (V_{0.90} - V_{0.02})}$$

Where $V_{0.02}$ and $V_{0.90}$ have been already defined, h is the height of the adsorption bed and ϕ is the fractional capacity which is related to the efficiency of the adsorption process within the MTZ and is calculated using the equation shown above on the right.

As adsorption occurs, part of the adsorbent is saturated and the MTZ moves forward, so enabling us to calculate the mass transfer zone displacement rate (R_{MTZ}). This is done by multiplying H_{MTZ} by the flow rate and then dividing by the difference between breakthrough and saturation volumes.

4.3. RESULTS AND DISCUSSION

4.3.1. Textural Characterization

The textural characteristics of the samples were determined by analyzing N_2 and CO_2 adsorption isotherms. The results are summarized in Table 4.1 and the PSD

obtained from N_2 adsorption isotherms (QSDFT analysis) is shown in Fig. 4.2. The high KOH:carbon ratio led to a high activation degree (44 % wt.). The original CA therefore showed a high micro/mesopore volume and surface area values (Table 4.1). CA oxidation led to the destruction of about 50 % of porosity ($V_{0.95}$). This explains the big difference in apparent density between the two samples (CA, 0.20 g cm^{-3} and CAOX, 0.41 g cm^{-3}). After thermal treatments this parameter slowly decreased.

Textural transformations clearly took place above all within the mesopore range (Fig. 4.2 and Table 4.1). The original PSD of the CA sample presents a maximum for mesopores with diameters between 2.8 - 3.0 nm and a maximum for micropores of around 0.8 nm in diameter, indicated in the latter case by the small peak of the PSD curve.

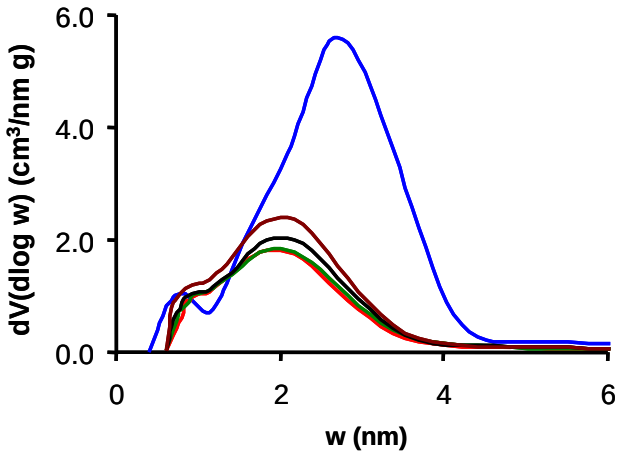

Figure 4.2. Pore size distributions obtained by applying the QSDFT method to the corresponding N_2 adsorption isotherm. CA (blue), CAOX (red), CAOX300 (green), CAOX500 (black), CAOX700 (brown).

Original mesopores were destroyed by the oxidation process and transformed into macropores (not detected by N_2 adsorption). The pore destruction becomes progressively smaller as pore size decreases: V_{meso} decreases by 52 % and, at the micropore range, W_0 (N_2) decreases by 32 % while the narrowest micropores, W_0 (CO_2), determined by CO_2 adsorption[34], increase by around 10 %. This pore volume reduction also leads to a drastic reduction of S_{BET} from 2387 to 1661 m^2 g^{-1}.

Nevertheless, not only pore destruction occurred. Oxygen surface groups (OSG) were also partially blocking the porosity in the same range (large micropores and mesopores), thus after progressive thermal treatments at 300, 500, and 700 ºC, carried out to selectively remove these OSG, as will be described below, W_0 (N_2), W_0 (CO_2) and V_{meso} increased, leading also to a simultaneous increase in S_{BET}. Thus there is a pore widening associated with the release of the OSG favoring large micropores and mesopores, which again shifts the PSD to the mesopore range. However, mesoporosity in the original pore range was never recovered (Fig. 4.2).

Table 4.1. Textural properties of samples obtained by gas (N_2 and CO_2) adsorption.

Sample	S_{BET} $m^2\ g^{-1}$	W_0 (N_2) $cm^3\ g^{-1}$	W_0 (CO_2) $cm^3\ g^{-1}$	$V_{0.95}$ $cm^3\ g^{-1}$	V_{meso} $cm^3\ g^{-1}$
CA	2387	0.92	0.39	2.23	1.31
CAOX	1661	0.63	0.43	1.07	0.44
CAOX300	1686	0.63	0.44	1.10	0.47
CAOX500	1696	0.68	0.48	1.18	0.50
CAOX700	1972	0.78	0.48	1.34	0.56

4.3.2. Chemical characterization

In addition to porous texture, surface chemistry will also determine the nature and extent of interactions with target VOCs. We therefore extensively analyzed the surface chemistry of ACs using XPS, TPD and pH_{ZPC} experiments. The results are summarized in Table 4.2. Particularly noteworthy is the sharp increase in CA oxygen content after oxidation to CAOX, which also produced a strong acidification of the carbon surface as denoted by the variation in pH_{ZPC} values. Oxygenated surface groups are located inside pores (mainly large micropores and small mesopores, as previously commented) and thus $\%O_{TPD} > \%O_{XPS}$. By weighing each sample before and after thermal treatments, we observed a significant total weight loss due to the release of gases, reaching as high as 40% at 700 ºC , responsible for the surface development and pore widening described above.

Table 4.2. Chemical characteristics of samples from TPD, XPS and pH_{ZPC} analyses.

Sample	WL %	CO μmol g^{-1}	CO_2 μmol g^{-1}	O_{TPD} %	O_{XPS} %	pH_{ZPC}
CA	-	1160	150	2.3	1.7	7.5
CAOX	-	3680	3010	15.5	9.3	2.4
CAOX300	20	5070	2110	14.9	7.0	2.9
CAOX500	24	6030	1370	14.0	5.6	3.0
CAOX700	40	680	110	1.4	1.4	7.8

Information about the chemical nature of the OSG present in each sample was obtained by analyzing TPD profiles (Fig. 4.3). This is because OSG are evolved at different temperature ranges and can therefore be identified and quantified (Table 4.2). The highest peak in the CO_2 profile of sample CAOX is located at 278 ºC and is attributed to the release of carboxylic acid groups. The strong shoulder at 450 ºC and the long tail of the CO_2-profile indicate that other CO_2-evolving groups, such as anhydrides and lactones, are present. Anhydrides may be formed from the dehydration of two neighboring carboxylic groups. Maximum CO-desorption takes place at 555 ºC, but this peak is very wide and has a long tail. This means that different CO-evolving groups may also be present. According to previous studies, phenols[25-27] evolve between 600-700 ºC, ether groups at around 700 ºC, carbonyls between 800-900 ºC and more stable chromenes at around 1000 ºC. However, Marchon[35] tentatively assigned different peaks and the CO-profile shoulder to semiquinone functional groups on energetically different sites.

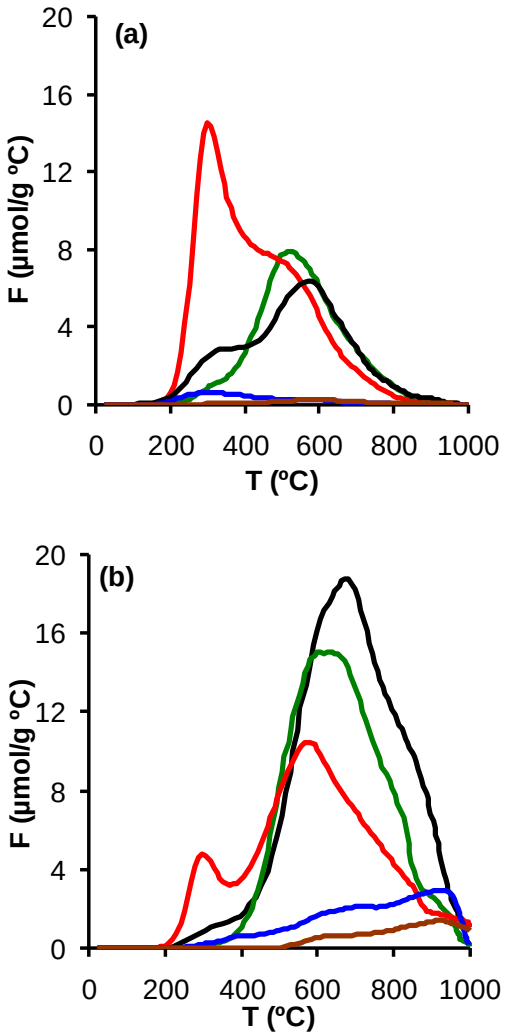

Figure 4.3. TPD curves for CO_2 (a) and CO (b). CA (blue), CAOX (red), CAOX300 (green), CAOX500 (black), CAOX700 (brown).

As published in a previous paper[27] oxygenated surface groups are selectively removed at different temperature ranges, and the oxygen content decreases linearly as the treatment temperature increases. Nevertheless, it is important to note the exceptional behavior of CAOX after treatments between 300 ºC and 500 ºC. Thus, as can be seen in Table 4.2, $\%O_{XPS}$ progressively decreases in contrast to $\%O_{TPD}$, which remains practically unchanged at this temperature range. After treatments at 700 ºC, the oxygen content fell sharply and CAOX700 showed a similar surface chemistry to the original CA. Therefore, there is a dramatic reorganization of OSG inside the pores in the 300 – 500 ºC range. It is remarkable that even at the lower temperature (300 ºC), the

treatment is strong enough to completely eliminate the carboxylic acid groups present in the CAOX sample (Fig. 4.3). CO_2 evolved in this process from both CAOX300 and CAOX500 is mainly reincorporated forming CO-evolving groups (semiquinone) that are also progressively more stable, as indicated by the CO-peak shifting to higher temperatures.

4.3.3. Adsorption of n-octane and ethanol

4.3.3.1. Static adsorption

The objective of this study was to develop specific traps for VOCs. Adsorption capacities determined under static conditions at 25 ºC are summarized in Table 4.3. Results are expressed as liquid volume, considering n-octane and ethanol density values as 0.703 and 0.791 g cm^{-3} respectively, to facilitate correlations with pore volumes. It is interesting to note that these adsorption values are a very good match for the total pore volume ($V_{0.95}$) of the samples. It is also noteworthy that the adsorption values for our samples are significantly higher than for other adsorbents[36], including activated carbons[37]. Thus, for example, BASF activated carbon with a micropore volume of 0.39 cm^3 g^{-1} and a macropore volume of 0.31 cm^3 g^{-1} has an ethanol adsorption capacity of 0.43 cm^3 g^{-1} at a relative pressure of 0.9 and 25 ºC[37]. In our case, the ethanol adsorption capacity of CA was enhanced by the presence of mesopores (instead of macroporosity on BASF carbon), in agreement with previously observed results[3] for toluene adsorption. The developed porosity of the CA sample favors both the higher adsorption capacities and the desorption energies (E_d), determined from DSC-experiments, of the samples series (Table 4.3). n-octane adsorption seems to be favored compared to ethanol adsorption by the mainly hydrophobic character of the carbon surface, which means that E_d is smaller.

The adsorption capacity decreases for both ethanol and octane after oxidation due to the huge porosity destruction mentioned earlier. The hydrophilic surface of CAOX now favors ethanol adsorption relative to n-octane, E_d takes the maximum value of the samples series for ethanol adsorption, and the minimum value for n-octane adsorption. Curiously, sample CAOX presents a higher adsorption capacity (for both

ethanol and octane) than CAOX300. Given that they have similar textural properties (Table 4.1), the decrease in adsorption capacity must therefore be associated with chemical transformations (i.e. the release of carboxylic acid groups). Simultaneously, there is a sharp fall in the ethanol desorption energy (E_d), while the contrary effect is observed for octane. Thus carboxylic acids clearly favor interactions with ethanol and make those with n-octane more difficult. The CAOX300 and CAOX500 samples showed quite similar adsorption/desorption characteristics based on a similar total oxygen content ($\%O_{TPD}$) and pH_{ZPC}. This means that despite the substantial reorganization of OSG that takes place in these samples (decomposition of labile CO_2-evolving groups and formation of more stable CO-evolving groups, Table 4.2), interactions between adsorbates and these new OSG are less specific than those previously commented for carboxylic acid groups. When the treatment temperature is increased to 700 ºC, the pore opening and the increase in surface area again enhance the adsorption capacity of the samples.

There is also a good match between the adsorbed and desorbed amounts. This shows that the thermal regeneration of samples is effective and consequently that they can be reused in subsequent adsorption-desorption cycles. VOC desorption was carried out by heating during TG-experiments, and as a result OSG were simultaneously evolved, which could influence these results. In order to avoid these interferences, we also analyzed fresh samples, and the VOCs desorbed in the temperature range in fresh samples were shown to be thermally stable in terms of weight loss. Fig. 4.4 shows some of the TG profiles for VOC desorption including the corresponding fresh samples.

As can be observed in Fig. 4.4, the CA samples saturated with ethanol (Fig. 4.4a) and with n-octane (Fig. 4.4e) both suffer a severe weight loss (WL) at low temperature, followed by a large plateau. Fresh CA shows good thermal stability up to around 550 ºC. The amount of CO_2 released is low and the observed WL above this temperature is due mainly to the release of CO-evolving groups (Fig. 4.3), with the two curves more or less parallel. VOC desorption is therefore associated exclusively with the first part of the TG profile, where the WL is not influenced by OSG release. Consequently, the saturated sample can be regenerated at low temperature. It should also be pointed out however that the CAOX sample has the weakest OSG and the

strongest interactions with ethanol. This sample is only stable up to around 200 ºC, from which the WL observed for the fresh sample (Fig. 4.4) is primarily due to the elimination of carboxylic groups (Fig. 4.3). Nevertheless, ethanol desorption clearly finished before the carboxylic groups were eliminated (Fig. 4.4b), and the TG profile of the saturated sample shows a small plateau between 150 – 200 ºC. The amount of ethanol desorbed from the CAOX sample decreases compared to that from CA, as mentioned above. Nevertheless, desorption occurs within a large temperature range, as a consequence of interactions between EtOH-carboxylic acid groups. In this case, the sample regeneration should be carried out carefully at temperatures of less than 200 ºC in order to preserve carboxylic groups which, as previously described, enhance the EtOH adsorption capacity. The small plateau detected for saturated CAOX becomes progressively larger when the pretreatment temperature increases (Fig. 4.4 c and d), and in all cases, the WL curves associated to the OSG run quite parallel to each other in fresh and saturated samples. DSC profiles for the ethanol desorption from certain selected samples are also included in Fig. 4. The desorption process is obviously endothermic, the DSC-peak of CAOX saturated samples shows a long tail at higher temperatures, due to the interaction of ethanol with carboxylic groups, which falls significantly after the treatment at 300 ºC (CAOX300).

Table 4.3. Adsorbed amounts of ethanol and n-octane at saturation under static conditions and the amounts desorbed by thermal treatments.

	ethanol			n-octane		
Sample	Adsorbed (cm^3g^{-1})	Desorbed (cm^3g^{-1})	Ed (kJ mol^{-1})	Adsorbed (cm^3g^{-1})	Desorbed (cm^3g^{-1})	Ed (kJ mol^{-1})
CA	2.35	2.04	61.1	2.60	1.99	23.5
CAOX	1.61	1.37	62.3	1.22	1.18	7.5
CAOX300	1.07	1.05	48.2	0.86	0.85	18.8
CAOX500	1.11	1.18	49.2	0.85	0.81	19.9
CAOX700	1.28	1.31	38.1	1.12	1.11	12.5

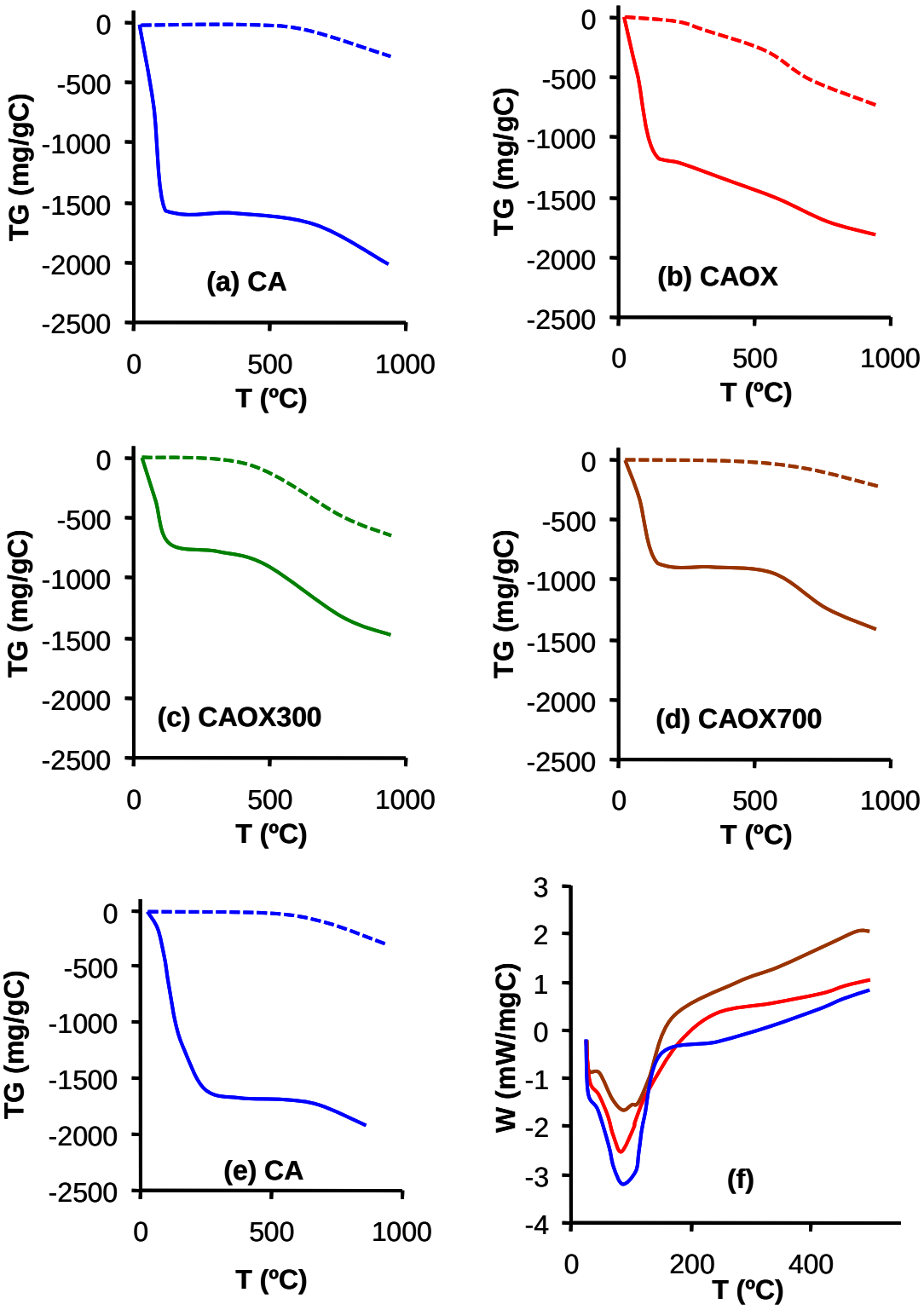

Figure 4.4. TG profiles of fresh (dash line) and VOC-saturated (a,b,c,d – ethanol, e - octane) samples (solid line). (f) DSC curves for ethanol desorption.

4.3.3.2. Dynamic adsorption

In Fig. 4.5, the behavior of samples as n-octane (Fig. 4.5a) and ethanol (Fig. 4.5b) adsorbents under dynamic experimental conditions is presented by the corresponding breakthrough curves. The parameters obtained from the analysis of these curves are summarized in Tables 4.4 and 4.5 for n-octane and ethanol respectively. The contrasting behavior of these samples when adsorbing the alkane or the alcohol is easy to observe. This behavior is related to the evolution of the textural and chemical properties discussed earlier and coincides with results obtained under static conditions. Previous studies of ACs and carbon fiber ethanol adsorption showed that the adsorption rate is determined by diffusion processes[38] and that the adsorption kinetics could be fitted to empirical correlations showing the influence of adsorption temperature and VOC concentration[39,40]. In a previous article[3] we pointed out the strong influence of mesoporosity in carbon aerogels used as toluene adsorbents under static and dynamic conditions.

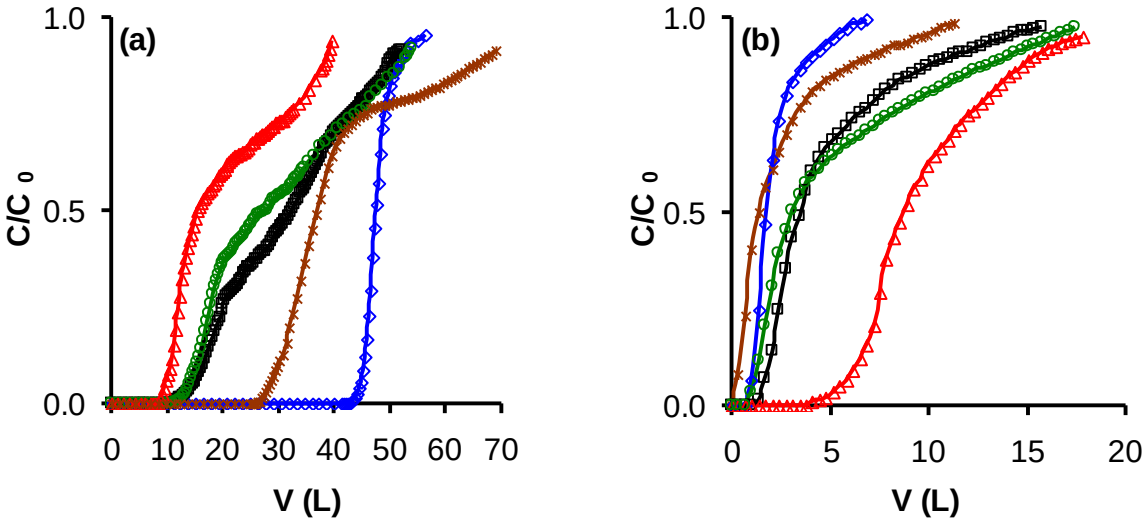

Figure 4.5. Breakthrough curves in dry air (a) n-octane (b) ethanol. CA (◆), CAOX (Δ), CAOX300 (○), CAOX500 (□), CAOX700 (×).

Clearly, within these experimental conditions the series of samples prepared is more specific for the adsorption of n-octane than of ethanol. Thus, in the worst case 43.7 mg g^{-1} of n-octane are adsorbed as compared to the 26.5 mg g^{-1} of ethanol

adsorbed in the best case at the breakthrough point. Under these experimental conditions, the porosity involved in the adsorption processes is different than under static conditions, because of the smaller P/P_0, thus the volume of n-octane adsorbed approximately matches $W_0(CO_2)$ for CA and CAOX700 samples. These results agree with those observed by other authors[2]. The adsorption capacity strongly decreases for CAOX and gradually recovers after thermal treatments (Table 4.4). In the case of ethanol adsorption, the volume of ethanol adsorbed is significantly smaller than the micropore volume in all cases. The fact that more ethanol was adsorbed in the CAOX sample despite it having the smallest pore volume denotes that in this case adsorption is enhanced by chemical interactions.

After oxidation, the hydrophilic character of the CAOX surface increases[40,41], which favors ethanol adsorption but makes n-octane adsorption more difficult. Thus, the corresponding breakthrough curves appear before and after the original CA adsorption curve for n-octane and ethanol respectively. There is also an important change in terms of the curve shapes. For both pollutants the difference between breakthrough and saturation points increased compared to CA, and the curves showed important slope changes indicating changes in the accessibility of the pores and/or interactions with the carbon surface. After removing the OSG, breakthrough curves tended to return to the shape and position of the original CA curves.

The BET surface area drops by 32 % from CA to CAOX, however, n-octane adsorption capacity decreases by about 78 % at the breakthrough point and 56% at the saturation point, which shows the influence of surface chemistry. The smaller n-octane - adsorbent interaction after oxidation is also indicated by an increase in the R_{MTZ}, which leads to an increase in the H_{MTZ} of 500 % with regard to the CA sample. Opposite effects are observed for ethanol adsorption: the increase of the adsorption capacity by a factor of four and the six-fold decrease of the R_{MTZ} are indicative of stronger ethanol - adsorbent interactions. These results are also in line with those previously obtained in static conditions and related with E_d variations (Table 4.3).

Table 4.4. Parameters obtained from the analysis of n-octane breakthrough curves.

Sample	Bed Height cm	$V_{0.02}$ L	$X_{0.02}$ mg g^{-1}	$V_{0.90}$ L	$X_{0.90}$ mg g^{-1}	H_{MTZ} cm	R_{MTZ} cm h^{-1}
CA	6.7	43.9	206.3	52.0	223.8	0.34	0.15
CAOX	4.2	9.0	43.7	38.8	99.0	1.73	0.21
CAOX300	4.2	13.1	62.5	53.2	146.6	1.57	0.14
CAOX500	4.1	13.9	66.9	51.9	158.5	1.37	0.13
CAOX700	4.1	27.1	130.0	67.6	198.7	1.17	0.10

Table 4.5. Parameters obtained from the analysis of ethanol breakthrough curves.

Sample	$V_{0.02}$ L	$X_{0.02}$ mg g^{-1}	$V_{0.90}$ L	$X_{0.90}$ mg g^{-1}	H_{MTZ} cm	R_{MTZ} cm h^{-1}
CA	1.2	5.0	4.1	10.7	2.80	3.48
CAOX	4.6	26.5	15.6	53.4	1.72	0.56
CAOX300	0.9	5.2	14.0	28.4	3.02	0.83
CAOX500	1.5	8.0	11.1	25.5	2.53	0.95
CAOX700	0.2	1.2	7.0	12.0	3.80	3.80

After treatment at 300 ºC, the release of carboxylic groups strongly decreases the adsorption of ethanol while enhancing that of n-octane. The specificity of these groups for ethanol adsorption is pointed out by the variation of the breakthrough point, $X_{0.02}$, which decreases about fivefold (Table 4.5). It is also important to note that at this point ethanol adsorption is favored in the case of CAOX500 compared to CAOX300. This is probably due to the stronger regeneration capacity at this temperature of the carboxylic acid groups evolving at 280 ºC (Fig. 4.3a). Smaller differences were observed at the saturation point, $X_{0.90}$ decreases by a half after treatment at 300 ºC, and only drops slightly after treatment at 500 ºC, in spite of the OSG reorganization mentioned earlier. This fact also highlights the unspecific character of CO-evolving

groups, in contrast to that of carboxylic groups. For CAOX700 both $X_{0.02}$ and $X_{0.90}$ decrease in spite of the higher S_{BET}. The low affinity of the CAOX700 surface for ethanol is highlighted by the sharp increase in R_{MTZ}.

n-octane adsorption is progressively enhanced with the elimination of oxygenated surface groups, although the n-octane adsorption capacity of CA is not recovered. The adsorption of n-octane is mainly determined by textural characteristics (Fig. 4.6) while ethanol adsorption is more influenced by surface chemistry (Fig. 4.7a), namely, by the presence of carboxylic acid groups (Fig. 4.7b). The stronger the interaction, the smaller the R_{MTZ} and H_{MTZ} in the corresponding fixed bed columns. Therefore, because the performance of the trap will depend on the nature and concentration of the VOCs and on the activated carbon porosity and surface chemistry, the preparation of traps for gasoline vapors based on mixtures of adsorbents could be an appropriate approach. We are currently studying this question in our laboratory, along with those of competitive adsorption and the influence of humidity in the stream.

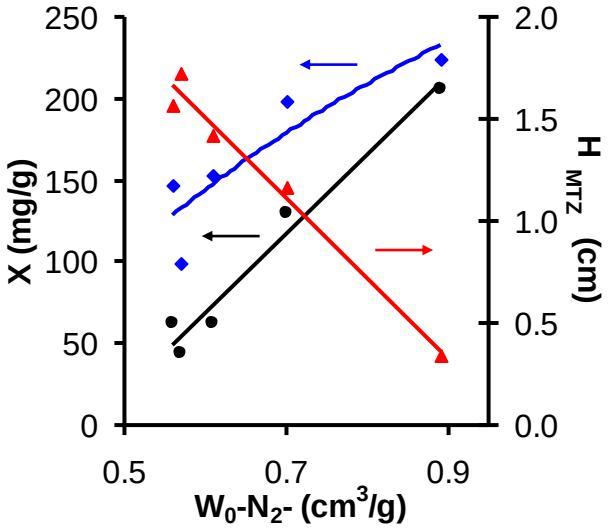

Figure 4.6. Variation of n-octane adsorption capacity, $X_{0.02}$(•), $X_{0.90}$(♦) and H_{MTZ} (▲) with the micropore volume of samples $W_0(N_2)$.

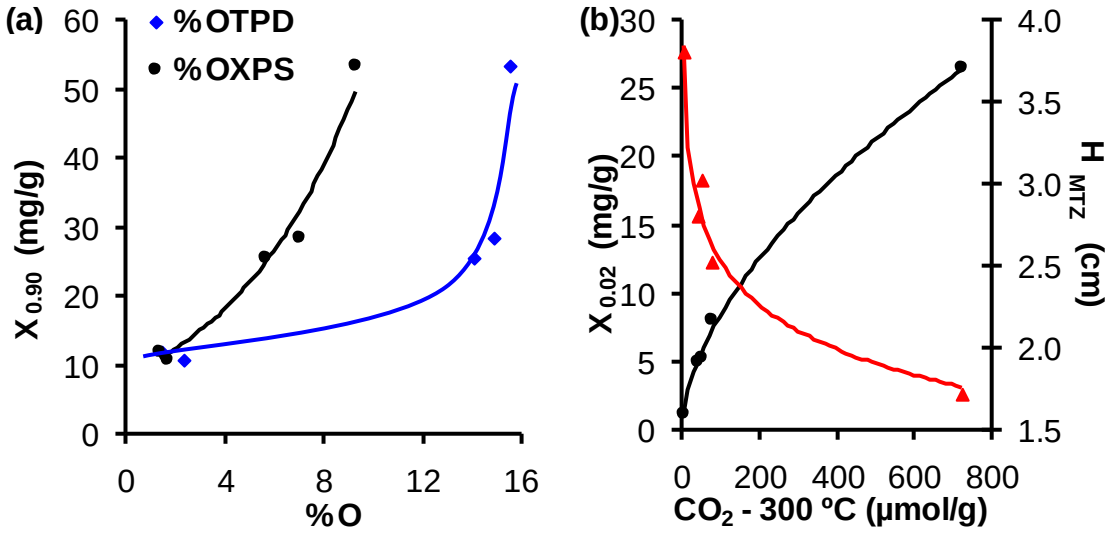

Figure 4.7. Variation of ethanol adsorption capacity. (a) Saturation point with oxygen content and (b) Breakthrough point $X_{0,02}$(•) and H_{MTZ} (▲) with CO_2 desorbed by samples up to 300ºC.

4.4. CONCLUSIONS

A highly porous activated carbon (CA) was obtained by means of chemical activation of carbonized olive stones. The surface chemistry was modified with an oxidation treatment (CAOX) reaching an oxygen content of 16% wt. Different types of oxygenated surface groups were identified by TPD and selectively removed by heating CAOX sample proportions at different temperatures. Treatments up to 500 ºC did not produce any significant changes in the oxygen content (determined by TPD) but OSG varied from CO_2 to CO-evolving groups. Treatment at 700 ºC prevented this OSG reorganization, since these groups are no longer stable at this temperature, and as a result the oxygen content fell sharply and pH_{ZPC} returned to basic values for CAOX700.

All samples performed well as ethanol and n-octane adsorbents, under both static and dynamic conditions. Nevertheless, the two compounds have different requirements. ACs working at a high relative pressure of VOCs under static conditions (such as in a canister connected to the car tank) can be saturated at room temperature using the complete porosity. Under these conditions, in spite of the fact that surface chemistry (carboxylic groups) enhances the interactions with ethanol, the main factor is

clearly its highly developed meso-microporosity. TG experiments showed that spent adsorbents can be regenerated with oxygenated or aliphatic VOCs for these kind of samples below 200 ºC.

The development of traps working in a stream of polluted VOCs at low concentration (ppm) requires only highly microporous samples. The surface functionalization favors ethanol adsorption, but makes octane adsorption more difficult. Of the different OSG analyzed by TPD, carboxylic acid groups were shown to produce a specific effect on ethanol adsorption, although adsorption capacity depends on the total oxygen content (hydrophobicity) of the carbon surface. The stronger the interaction, the smaller the R_{MTZ} and H_{MTZ} in the corresponding fixed bed columns.

4.5. REFERENCES

[1] F.I. Khan and A. Ghoshal, Removal of Volatile Organic Compounds from polluted air, *Journal of Loss Prevention in the Process Industries*, **13** (2000) 527-545.

[2] J. Carratalá-Abril, M.A. Lillo-Ródenas, A. Linares-Solano, and D. Cazorla-Amorós, Activated Carbons for the Removal of Low-Concentration Gaseous Toluene at the Semipilot Scale, *Industrial & Engineering Chemistry Research*, **48** (2009) 2066-2075.

[3] F.J. Maldonado-Hódar, C. Moreno-Castilla, F. Carrasco-Marín, and A.F. Pérez-Cadenas, Reversible toluene adsorption on monolithic carbon aerogels, *Journal of Hazardous Materials*, **148** (2007) 548-552.

[4] F.J. Maldonado-Hódar, Removing aromatic and oxygenated VOCs from polluted air stream using Pt-carbon aerogels: Assessment of their performance as adsorbents and combustion catalysts, *Journal of Hazardous Materials*, **194** (2011) 216-222.

[5] A. Martínez de Yuso, M.T. Izquierdo, R. Valenciano, and B. Rubio, Toluene and n-hexane adsorption and recovery behavior on activated carbons derived from almond shell wastes, *Fuel Processing Technology*, **110** (2013) 1-7.

[6] S. Morales-Torres, A.F. Pérez-Cadenas, F. Kapteijn, F. Carrasco-Marín, F.J. Maldonado-Hódar, and J.A. Moulijn, Palladium and platinum catalysts supported on carbon nanofiber coated monoliths for low-temperature combustion of BTX, *Applied Catalysis B: Environmental*, **89** (2009) 411-419.

[7] R.A. Catalao, F.J. Maldonado-Hódar, A. Fernandes, C. Henriques, and M.F. Ribeiro, Reduction of NO with metal-doped carbon aerogels, *Applied Catalysis B: Environmental*, **88** (2009) 135-141.

[8] J. Wang, L. Jin, J. Gao, J. Shi, Y. Zhao, S. Liu, T. Jin, Z. Bai, and C.Y. Wu, Investigation of speciated VOC in gasoline vehicular exhaust under ECE and EUDC test cycles, *Science of The Total Environment*, **445-446** (2013) 110-116.

[9] H. Yamada, Contribution of evaporative emissions from gasoline vehicles toward total VOC emissions in Japan, *Science of The Total Environment*, **449** (2013) 143-149.

[10] W.Q. Huang, J. Bai, S.H. Zhao, and A.H. Lv, Investigation of oil vapor emission and its evaluation methods, *Journal of Loss Prevention in the Process Industries*, **24** (2011) 178-186.

[11] G. Mellios and Z. Samaras, An empirical model for estimating evaporative hydrocarbon emissions from canister-equipped vehicles, *Fuel*, **86** (2007) 2254-2261.

[12] K. Sato and N. Kobayashi, Adsorption and Desorption Simulation of Carbon Canister Using n-Butane as Model Compound of Gasoline, *Journal of the Japan Petroleum Institute*, **54** (2011) 136-145.

[13] J.Y. Chin and S.A. Batterman, VOC composition of current motor vehicle fuels and vapors, and collinearity analyses for receptor modeling, *Chemosphere*, **86** (2012) 951-958.

[14] http://www.api.org/environment-health-and-safety/environmental-performance/innovation/recovered-gas-vapors-add-value-cut-emissions.

http://www.api.org/environment-health-and-safety/health-safety/product-safety-home/safe-storage-and-disposal-of-gasoline

[15] R.K. Niven, Ethanol in gasoline: environmental impacts and sustainability review article, *Renewable and Sustainable Energy Reviews*, **9** (2005) 535-555.

[16] M. Winther, F. Müller, and T.C. Jensen, Emission consequences of introducing bio ethanol as a fuel for gasoline cars, *Atmospheric Environment*, **55** (2012) 144-153.

[17] A. Baçaoui, A. Dahbi, A. Yaacoubi, C. Bennouna, F.J. Maldonado-Hódar, J. Rivera-Utrilla, F. Carrasco-Marín, and C. Moreno-Castilla, Experimental Design To Optimize Preparation of Activated Carbons for Use in Water Treatment, *Environmental Science & Technology*, **36** (2002) 3844-3849.

[18] A.S. Mestre, A.S. Bexiga, M. Proença, M. Andrade, M.L. Pinto, I. Matos, I.M. Fonseca, and A.P. Carvalho, Activated carbons from sisal waste by chemical activation with K2CO3: Kinetics of paracetamol and ibuprofen removal from aqueous solution, *Bioresource Technology*, **102** (2011) 8253-8260.

[19] H. Zaitan, D. Bianchi, O. Achak, and T. Chafik, A comparative study of the adsorption and desorption of o-xylene onto bentonite clay and alumina, *Journal of Hazardous Materials*, **153** (2008) 852-859.

[20] C. Moreno-Castilla, M.A. Ferro-Garcia, J.P. Joly, I. Bautista-Toledo, F. Carrasco-Marin, and J. Rivera-Utrilla, Activated Carbon Surface Modifications by Nitric Acid, Hydrogen Peroxide, and Ammonium Peroxydisulfate Treatments, *Langmuir*, **11** (1995) 4386-4392.

[21] R.G. Bansal, J.B. Donnet, and F. Stoeckli, *Activated Carbon*, Marcel Dekker, New York and Basel, 1988.

[22] F. Stoeckli, *Porosity in carbon. Characterization and applications*. Eds. Patrick J. Arnold, London, 1995.

[23] E.P. Barrett, L.G. Joyner, and P.P. Halenda, The Determination of Pore Volume and Area Distributions in Porous Substances. I. Computations from Nitrogen Isotherms, *Journal of the American Chemical Society*, **73** (1951) 373-380.

[24] C. Lastoskie, K.E. Gubbins, and N. Quirke, Pore size distribution analysis of microporous carbons: a density functional theory approach, *The Journal of Physical Chemistry*, **97** (1993) 4786-4796.

[25] Y. Matsumura, Production of acidified active carbon by wet oxidation and its carbon structure, *Journal of Applied Chemistry and Biotechnology*, **25** (1975) 39-56.

[26] J.L. Figueiredo, M.F.R. Pereira, M.M.A. Freitas, and J.J.M. Órfão, Modification of the surface chemistry of activated carbons, *Carbon*, **37** (1999) 1379-1389.

[27] C. Moreno-Castilla, F. Carrasco-Marín, F.J. Maldonado-Hódar, and J. Rivera-Utrilla, Effects of non-oxidant and oxidant acid treatments on the surface properties of an activated carbon with very low ash content, *Carbon*, **36** (1998) 145-151.

[28] J.H. Zhou, Z.J. Sui, J. Zhu, P. Li, D. Chen, Y.C. Dai, and W.K. Yuan, Characterization of surface oxygen complexes on carbon nanofibers by TPD, XPS and FT-IR, *Carbon*, **45** (2007) 785-796.

[29] C. Moreno-Castilla, A.F. Pérez-Cadenas, F.J. Maldonado-Hódar, F. Carrasco-Marín, and J.L. Fierro, Influence of carbon-oxygen surface complexes on the surface acidity of tungsten oxide catalysts supported on activated carbons, *Carbon*, **41** (2003) 1157-1167.

[30] C.A. Leon, J.M. Solar, V. Calemma, and L.R. Radovic, Evidence for the protonation of basal plane sites on carbon, *Carbon*, **30** (1992) 797-811.

[31] G.M. Luckchis, Adsorption systems 1. Design by mass-transfer-zone concept, *Chemical Engineering*, **80** (1973) 111-116.

[32] W.J.J. Webber, *Physiochemical Processes for Water Quality Control*, Wiley-Interscience ed., New Cork, 1972.

[33] P.N. Cheremisinoff and F. Ellerbusch, *Carbon Adsorption Handbook*, Ann Arbor Science Pub. ed., Michigan, 1978.

[34] D. Cazorla-Amorós, J. Alcañiz-Monge, M.A. Casa-Lillo, and A. Linares-Solano, CO2 as an Adsorptive To Characterize Carbon Molecular Sieves and Activated Carbons, *Langmuir*, **14** (1998) 4589-4596.

[35] B. Marchon, J. Carrazza, H. Heinemann, and G.A. Somorjai, TPD and XPS studies of O2, CO2, and H2O adsorption on clean polycrystalline graphite, *Carbon*, **26** (1988) 507-514.

[36] A. Cartón, G.G. Benito, J.A. Rey, and M. de la Fuente, Selection of adsorbents to be used in an ethanol fermentation process. Adsorption isotherms and kinetics, *Bioresource Technology*, **66** (1998) 75-78.

[37] L. Gales, A. Mendes, and C. Costa, Hysteresis in the cyclic adsorption of acetone, ethanol and ethyl acetate on activated carbon, *Carbon*, **38** (2000) 1083-1088.

[38] B.B. Saha, I.I. El-Sharkawy, A. Chakraborty, S. Koyama, S.H. Yoon, and K. Choon Ng, Adsorption Rate of Ethanol on Activated Carbon Fiber, *Journal of Chemical Engineering Data*, **51** (2006) 1587-1592.

[39] I.I. El-Sharkawy, B.B. Saha ,S. Koyama, and K. Srinivasan, Isosteric heats of adsorption extracted from experiments of ethanol and HFC 134a on carbon based adsorbent, *International Journal of Heat and Mass Transfer*, **50** (2007) 902–907

[40] I.I. El-Sharkawy, B.B. Saha, S. Koyama, and K. Choon Ng, A study on the kinetics of ethanol-activated carbon fiber: Theory and experiments, *International Journal of Heat and Mass Transfer*, **49** (2006) 3104–3110.

[41] F. Carrasco-Marín, A. Mueden, A. Centeno, F. Stoeckli, and C. Moreno-Castilla, Water adsorption on activated carbons with different degrees of oxidation, *Journal of the Chemical Society, Faraday Transactions*, **93** (1997) 2211-2215.

Capítulo V

ABOUT THE CONTROL OF VOC´s EMISSIONS FROM BLENDED FUELS BY DEVELOPING SPECIFIC ADSORBENTS USING AGRICULTURAL RESIDUES

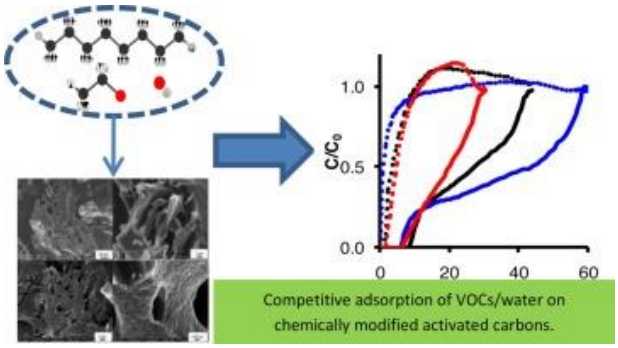

ABOUT THE CONTROL OF VOC´S EMISSIONS FROM BLENDED FUELS BY DEVELOPING SPECIFIC ADSORBENTS USING AGRICULTURAL RESIDUES

Article published in J. of Environmental Chem. Eng., 3 (2015) 2662-2669, doi: 10.1016/j.jece.2015.09.027


Journal of Environmental Chemical Engineering

About the control of VOC's emissions from blended fuels by developing specific adsorbents using agricultural residues

Highlights

- Specific adsorption sites for n-octane and ethanol are determined.
- *n*-octane is able to replace adsorbed ethanol from active sites.
- Water vapor hinders adsorption of compounds lowering the rate of the process.
- Carboxylic acid groups present the strongest interaction with water and ethanol.
- By mixing two adsorbents (with and without oxygen) simultaneous adsorption improved.

Abstract

Olive stones, which are an abundant residue from the olive oil industry, were thermally and chemically treated to obtain a series of cheap activated carbons with fitted surface chemistry and porosity. These biomaterials were used as specific filters for gaseous emissions treatments. Ethanol and n-octane were chosen as target VOCs. The performance of these filters in competitive VOCs adsorption processes and the influence of humidity were studied by analyzing the corresponding breakthrough curves. Relationships between VOCs chemical nature, adsorbent characteristics and experimental conditions were discussed. Carboxylic acid groups play a specific role on the adsorption of polar molecules, because they determine the interaction strength. The adsorption rate for n-octane was significantly reduced when water or ethanol were present, while adsorption capacity was almost equivalent. The influence of humidity is stronger on ethanol adsorption process, specifically when more oxidized samples were tested. A new filter was developed by mixing hydrophobic and hydrophilic adsorbents in order to improve the simultaneous adsorption of ethanol and n-octane. In this case, the constant rate of competitive adsorption processes is favoured for both VOCs, regarding columns with a single adsorbent, because they are adsorbed on independent sites.

Keywords: VOCs, air pollution, biofuels, filters, activated carbons, competitive adsorption.

Nomenclature

S_{BET}	B.E.T. surface area
W_0	micropore volume obtained by Dubinin-Radushkevich
L_0	micropore mean width by Stoeckli equation
V_{meso}	mesopore volume obtained by B.J.H.
C_0	inlet VOC concentration
C	outlet VOC concentration
$V_{0.02}$	breakthrough volume
$V_{0.90}$	saturation volume
$X_{0.02}$	amount adsorbed till breakthrough point
$X_{0.90}$	amount adsorbed till saturation point
X_R	amount retained at the end of competitive adsorption
H_{MTZ}	mass transfer zone height
R_{MTZ}	mass transfer zone rate of displacement
ϕ	fractional capacity
Du	degree of utility
ρ_B	bed density
W_e	equilibrium adsorption capacity
k_v	adsorption rate constant, from the Wheeler-Jonas model

5.1. INTRODUCTION

The production of blended gasoline in different formulations (E10 or E85, with 10 or 85% of ethanol respectively) is nowadays a sound alternative to typical fossil fuel, especially in developing countries which are rich in biomass resources. Although the use of this type of fuel becomes more and more common, several associated problems need to be considered: (i) ethanol from biomass contains a high proportion of water that has to be separated[1-4] (ii) ethanol-based fuels produce larger evaporative emissions than conventional fuels[5-7].

Thus, along the last years, special attention was paid to the air pollution caused by VOC emissions during refueling or when the engine is switched off. These emissions are enhanced by the presence of ethanol and other hydrophilic components in the fuel mixture, causing contamination and fuel loss[6,7]. The chemical degradation rate of these compounds in the atmosphere depends on the experimental conditions but it takes place mainly photocatalytically induced by OH and Cl radicals or other oxidants like NO_3 in the dark, likely contributing to the formation of ozone and other components of photochemical smog[8]. In such a basis, together with the improvement of tailpipes, devices such as canisters are now installed in cars to minimize evaporative emissions of these potentially dangerous gasses.

While tailpipes focus on the catalytic destruction of pollutants, canisters and filters are based on the performance of adsorbents which favours the recovery and reuse of evaporated fuel components, reducing in this way their emissions. Since ethanol and others hydrophilic components are emitted joint to other aromatic compounds in atmospheric conditions (humidity), physicochemical properties of adsorbents need to be fitted in order to achieve the best adsorptive behaviour depending on the gaseous mixture composition[9-12].

The separation of ethanol and water has been widely studied[13,14]. In wet conditions, water might well be absorbed and can compete for active sites with contaminants[15-17]. VOCs and water adsorption on carbon materials strongly depends on both, textural properties and surface chemistry[9-12]. Oxygen surface groups, called

primary centres, are able to interact with water molecules through the formation of hydrogen bonds[18].

In previous manuscripts, the preparation of carbon materials and their application as adsorbents of individual VOCs were presented[19,20]. The objective of this work is to evaluate the performance of some of these samples in more realistic working conditions. For that purpose, different filters were prepared and studied in the adsorption of VOCs mixtures in both dry and wet airflows. The obtained breakthrough curves were analyzed by different methods and results were correlated to the textural and chemical nature of adsorbents.

5.2. MATERIALS AND METHODS

5.2.1. Synthesis and characterization of adsorbents

Synthesis and characterization of adsorbents were detailed on previous works[19,20]. Briefly, olive stones were milled, carbonized at 400°C and then, impregnated with KOH and heated again up to 850 °C under nitrogen flux for chemical activation. After neutralizing the base excess and washing, the sample was dried at 110°C overnight and labelled as CA. Due to the severe experimental conditions of synthesis, this material is obtained as a fine powder with negligible inorganic matter content[20]. In order to increase CA hydrophilic character, oxygenated surface groups (OSG) were generated on the CA surface by oxidation with a saturated solution of ammonium peroxydisulphate ($(NH_4)_2S_2O_8$) in H_2SO_4 1M, reacting for 24 hours[21,22]. The excess of oxidizing agent and by-products were removed by washing with deionized water till sulphates absence and then the sample was dried and named CAOX. In order to fit the OSG nature, thermally labile carboxylic acid groups[23,24] were removed by heating a portion of CAOX sample up to 500 °C under inert atmosphere (nitrogen). This sample was denominated as CAOX500.

Samples morphology was studied by scanning electron microscopy (SEM) using a LEO (Carl Zeiss) GEMINI-1530 microscope[20]. Textural characterization was

carried out by analysing N_2 and CO_2 adsorption at −196 °C and 0 °C, respectively, using a Quantachrome Autosorb-1 equipment. BET, Dubinin–Radushkevich and Stoeckli equations were applied to determine the apparent surface area (S_{BET}), the micropore volume (W_0) and the mean micropore width (L_0). The BJH method was used to calculate the mesopore volume of the samples (V_{meso}). Surface chemistry was analyzed by quantifying oxygen content on the external surface (X-ray Photoemission Spectroscopy -XPS-) and bulk samples (Thermal Programmed Desorption -TPD-). Additional details can be found on published bibliography[19,20].

Water adsorption experiments under static conditions were also performed until saturation of the sample at room temperature. Water desorption from saturated samples was studied by Thermogravimetric Analysis (TG) and Differential Scanning Calorimetry (DSC) to determine water-adsorbent interactions with a METTLER-TOLEDO TGA/DSC1.

5.2.2. Dynamic adsorption experiments

Dynamic adsorption experiments were carried out by using columns of each adsorbent with a height of 6.7 cm, 4.2 cm and 4.1 cm for CA, CAOX and CAOX500, respectively. Additional experiments were also performed by mixing CA – CAOX (50-50 wt %), resulting in a column of 5.9 cm. The design of the adsorption system permits the fitting of the polluted air composition and to obtain breakthrough curves for either single component or mixtures, under dry or wet conditions. For this purpose, individual airflows which bubbled through liquid n-octane or ethanol (Aldrich, analytical reagent, purity >99.8%) at T = 0°C were diluted and mixed in the appropriate ratio to obtain a concentration in the feed of 480 ppm and 560 ppm for n-octane and ethanol respectively. When adsorption experiments were performed in wet airflows (3% of water in the final flow), the diluting air flux passed through water at room temperature. Gas chromatography with FID detection was used to quantify contaminants concentration at the column exit, but water could not be analyzed by this method. Each breakthrough curve was obtained three times for each adsorbent with a good reproducibility (differences between 5 and 7% were observed). Thus, the exposed results correspond to single experiments.

The analysis of breakthrough curves was performed by applying the mass transfer zone (MTZ) concept[25,26]. Different parameters were determined from the analysis of breakthrough curves: breakthrough ($V_{0.02}$) and saturation ($V_{0.90}$) points which are defined as the eluted volume (or time) till the VOC concentration at the column exit reached values of 2 and 90% of the initial VOC concentration, adsorbed amounts at these points $X_{0.02}$ and $X_{0.90}$, mass transfer zone height (H_{MTZ}) and the MTZ rate of displacement (R_{MTZ}).

Along the adsorbent bed there is a concentration gradient which is moving. The mass transfer zone (MTZ) is defined as the bed region where the adsorption process is taking place and, therefore, it is located between the saturated part of the bed and the clean one. Diffusion and adsorption happen at the same time and the mass transfer zone height (H_{MTZ}) is the parameter used to estimate the relative rate of both processes. So that, when adsorption is faster than diffusion, values of H_{MTZ} are small; however, when diffusion prevails, H_{MTZ} becomes larger. The calculation of this parameter was carried out by applying Eqs. (5.1) and (5.2) as described in bibliography[27]:

$$H_{MTZ} = h\left(\frac{V_{0.90} - V_{0.02}}{V_{0.02} + \phi(V_{0.90} - V_{0.02})}\right) \qquad \text{Equation 5.1}$$

$$\phi = \left(\frac{\int_{V_{0.02}}^{V_{0.90}} (C_0 - C)dV}{C_0(V_{0.90} - V_{0.02})}\right) \qquad \text{Equation 5.2}$$

Where $V_{0.02}$ and $V_{0.90}$were already defined, h is the height of the adsorption bed and ϕ is the fractional capacity which is related to the efficiency of the adsorption process within the MTZ and is calculated by the Eq. (5.2).

As adsorption occurs, part of the adsorbent is saturated and MTZ moves forward, so the MTZ displacement rate (R_{MTZ}) can be defined. This parameter is calculated by multiplying H_{MTZ} by flow rate and dividing by the difference between volumes at breakthrough and saturation points.

The degree of utility (Du(%)) was also obtained[28]. This parameter provides information about how much time over the total of the experiment the adsorptive bed is retaining all of the VOC molecules passing through the column. It is calculated as a ratio between the amount of VOC adsorbed at the breakthrough point ($X_{0.02}$) and the saturation point ($X_{0.90}$).

Additional information may be obtained by applying several mathematical models. One of the most employed is the model developed by Wheeler and Jonas (Eq. (5.3)) which is commonly used to obtain the adsorbed amount at equilibrium (W_e, $mg \cdot g^{-1}$) and the rate constant for the adsorption process (k_v, min^{-1})[29-32].

$$t = \frac{WW_e}{C_0 Q} - \frac{W_e \rho_B}{k_v C_0} \ln\left(\frac{C_0 - C}{C}\right)$$

Equation 5.3

Where C_0 and C are the inlet and outlet VOCs concentration at the time t, W the weight of sample, Q the volumetric flux, ρ_B the bed density, W_e and k_v were defined above. The rate constant k_v was employed to compare dynamic adsorption behaviour of the three activated carbons retaining each VOC under different experimental conditions.

5.3. RESULTS AND DISCUSSION

As commented, in a previous paper a series of activated carbons were developed[20] and applied to the adsorption of n-octane and ethanol[19] as representative components of biofuels. Results pointed out the strong influence of microporosity on n-octane adsorption capacity while ethanol adsorption is governed by surface chemistry[19]. In such a case, some of these samples were now selected to study the competitive adsorption process of both compounds as well as the influence of the presence of water vapour in the feed. For a better understanding, a brief summary of physicochemical properties of selected samples is included bellow.

5.3.1. Textural and chemical characterization

CA, CAOX and CAOX500 samples were obtained as described in the experimental section to fit their porosity and surface chemistry. The main physicochemical properties of these samples are summarized in Table 5.1.

The original activated carbon (CA) is a micro-mesoporous adsorbent, with high BET surface area (S_{BET}) and huge micropore and mesopore volumes. Since it was prepared at high temperature, its oxygen content is relatively low. Oxidation with ammonium peroxydisulphate produced an increase on total oxygen content, as determined by TPD (from 2.3% to 15.5%), but also a drastic reduction in porosity and surface area (from 2387 to 1661 $m^2\ g^{-1}$) for CAOX. After treatment at 500 °C, sample CAOX500 does not present carboxylic acid groups[20] as demonstrated by different techniques. However, these groups evolved only from the external surface, as denoted the O_{XPS} decrease, while the total oxygen content was not reduced significantly because carboxylic groups were transformed inside the pores in semiquinone species, which are stable at temperatures higher than 500 °C[19,20].

Table 5.1. Summary of the textural and chemical properties of adsorbents[20].

Sample	$X(H_2O)$ g_{H2O}/g_C	S_{BET} $m^2 \cdot g^{-1}$	W_0 (N_2) $cm^3 \cdot g^{-1}$	W_0 (CO_2) $cm^3 \cdot g^{-1}$	V_{meso} $cm^3 \cdot g^{-1}$	O_{TPD} %	O_{XPS} %
CA	2.12	2387	0.92	0.39	1.31	2.3	1.8
CAOX	1.00	1661	0.63	0.43	0.44	15.5	9.3
CAOX500	0.74	1696	0.68	0.48	0.50	14.0	5.6

In this case, we paid special attention to the hydrophilicity of the samples. Water adsorption on activated carbon strongly depends of both textural and surface chemistry[18]. The oxygen surface complexes, called primary centers, are able to interact with the water molecule forming hydrogen bonds. In general, water adsorption isotherms correspond to the type IV, and can be decomposed into two contributions. The first contribution, at low relative pressures, belongs to type I and the second is of

type V. The former has been associated with the adsorption by acidic centres and the micropore filling. The second one is related with the adsorption by weaker hydrophilic centres mainly of carbonyl type[33].

The amount of water adsorbed by each sample at saturation was quantified (Table 5.1). In general, this amount (if expressed as volume) corresponds to the filling of the micro and mesoporosity of samples. The largest water adsorption capacity was obtained for CA (2.12 g_{H2O}/g_C), due to its highly developed porosity. After oxidation, the water adsorption on CAOX (1.00 g_{H2O}/g_C) decreased according to the porosity decrease. However, when results for CAOX and CAOX500 (0.74 g_{H2O}/g_C) are compared, a new decrease in the amount of adsorbed water can be observed. In this case, because porosity is slightly enhanced after thermal treatments (Table 5.1), this decrease must be due to the elimination or transformation of carboxylic acid groups.

After saturation, water desorption was studied by TG/DSC experiments (Fig. 5.1). Results from TG (Fig. 5.1a) are in good agreement with those obtained by direct weighing of samples. Fresh samples were used as reference materials. In these cases, the weight loss started at lower temperatures as oxygen content of the samples becomes higher, mainly in the case of CAOX sample where the removal of oxygenated groups happened at around 200 ºC by desorption of less stable carboxylic acid groups. In spite of the smaller amount desorbed observed from oxidized samples, their TG profiles shifted to higher temperatures, which is also confirmed by DSC profiles (Fig. 5.1b) where the minimum of the curve appears at 110°C (CA) < 114°C (CAOX500) < 120°C(CAOX). This fact is indicative of a stronger interaction between water and oxygenated surface groups, mainly carboxylic acids.

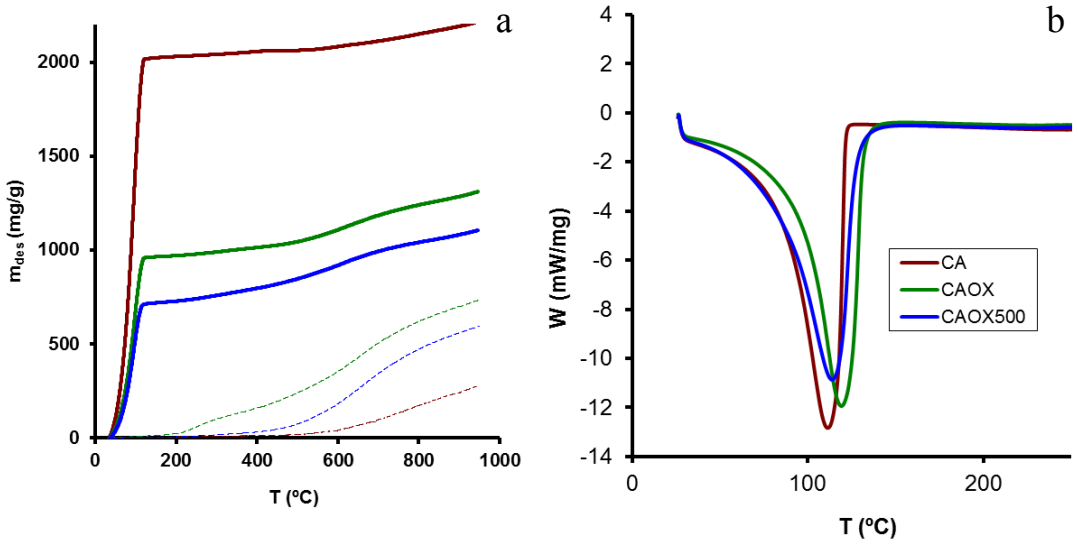

Figure 5.1. Desorption of water from saturated samples; dry samples shown as dashed lines (a) TG and (b) DSC profiles.

5.3.2. Performance of adsorbents in dynamic adsorption experiments

5.3.2.1. Influence of the humidity on the adsorption of individual VOCs

In Fig. 5.2 breakthrough curves for n-octane dynamic adsorption under dry and humid conditions are compared and the parameters obtained from them are summarized in Table 5.2. Changes on curve shapes, breakthrough and saturation points are observed at a glance and these changes differ as physicochemical properties of adsorbent do. Independently of the used adsorbent, earlier breakthrough points were always obtained for wet air experiments compared to dry air ones, showing the competition between water and VOCs for adsorption sites. Because water is also adsorbed, n-octane appeared faster at the exit of the column.

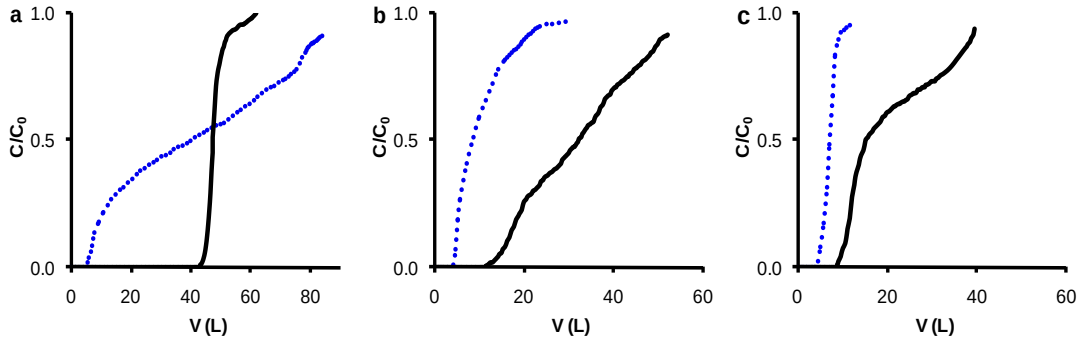

Figure 5.2. Comparisons of breakthrough curves obtained for the dynamic adsorption of n-octane under wet air (dashed) and dry air (continuous, from Ref. [19]) onto different activated carbons: a) CA, b) CAOX500, c) CAOX.

The difference between breakthrough points when water vapour is present becomes much larger in the case of CA than in the rest of samples, which is in agreement with the greater water adsorption previously discussed. Moreover, in spite of that initially n-octane concentration at the exit increases quickly under wet conditions, the breakthrough curve shows a remarkable slope decrease at C/C_0= 0.2 and this slope is maintained constant until C/C_0 = 0.8 when it increases again. This means that, after a first situation where water seems to be preferably adsorbed leading to a fast advance of n-octane along the column, CA surface reaches a stationary state where n-octane adsorption becomes slower than in dry conditions, but faster than at the beginning and it remains constant practically till the complete saturation of the column. This fact provokes a great difference between breakthrough and saturations points, also shown by the strong decrease on Du(%) values (Table 5.2). Nevertheless, adsorbed amounts at saturation ($X_{0.90}$) are quite similar for CA independently on the presence of humidity.

Because we previously pointed out that n-octane adsorption is related to the micropore volume[19], these results indicate that n-octane penetrated to a similar micropore volume either in dry or wet conditions, but obviously, more slowly in the case of wet ones. Taking into account physicochemical properties of this sample, it is very likely that a fast water adsorption is produced initially in the big volume of macro-mesopores present in this sample. Adsorbed water molecules hinder the accessibility of n-octane to microporosity, inducing a strong decrease on the breakthrough point (Fig. 5.2, Table 5.2). However, after covering adsorption sites of the external surface by

water, n-octane is progressively adsorbed into micropores, due to the stronger interaction between the CA hydrophobic surface (low oxygen content) and the non-polar molecule. This behaviour strongly influenced the Du(%) value, which largely decreased under wet conditions leading to the smallest Du value of the sample series, while H_{MTZ} became about ten times larger when water was present demonstrating a huge reduction on n-octane adsorption rate.

Table 5.2. Parameters obtained for the dynamic adsorption of n-octane under different conditions.

Sample	Air	$V_{0.02}$ L	$X_{0.02}$ mg g^{-1}	$V_{0.90}$ L	$X_{0.90}$ mg g^{-1}	H_{MTZ} cm	Du %
CA	dry*	43.9	206.3	52.0	223.8	0.34	93
	wet	5.8	27.0	82.9	200.2	3.65	16
CAOX500	dry*	12.9	61.9	50.9	153.7	1.37	44
	wet	4.5	21.0	20.1	46.7	1.93	54
CAOX	dry*	9.0	43.7	38.8	99.0	1.73	49
	wet	4.1	20.4	9.5	32.8	2.77	62

*From [19].

Textural and chemical transformations undergone during oxidation also influenced the shape and position of the breakthrough curves obtained for CAOX sample. Mesoporosity was significantly destroyed and some of the OSG generated were located at the micropore entrance increasing diffusional restrictions into the narrowest porosity (as denoted by a larger $W_0(CO_2)$ to $W_0(N_2)$ ratio for CAOX). Both facts produced the decrease of $X_{0.02}$ and the slope change observed for the curve obtained in dry conditions. The high oxygen content generated enhanced the hydrophilic character of carbon surface and, consequently, water adsorption became more favourable. Thus, in wet airflows, the amount of n-octane adsorbed at saturation decreased about three times regarding dry conditions, with adsorbed water blocking porosity. This sample presents, consequently, the worst adsorptive performance of the samples series, mainly in wet conditions. Du values present the contrary behaviour previously described for

CA sample. In this case, Du increases since the decrease of $X_{0.02}$valueswas not so significant as the one of $X_{0.90}$.

After the thermal treatment at 500°C some of the oxygenated surface groups blocking the micropore entrance were removed ($W_0(N_2)$ increased) decreasing also diffusional restrictions. Consequently, changes in the slope of the breakthrough curve practically disappeared. In wet conditions, n-octane adsorption was hindered by water in the feed as denoted by the greater slope of the breakthrough curve obtained under wet conditions. Nevertheless, the absence of carboxylic acid groups on the external surface (O_{XPS} decreased) provoked a smaller water adsorption regarding CAOX, and a certain slope change mainly at C/C_0>0.5. The greater hydrophilicity of CAOX regarding CAOX500, despite the similar oxygen content of both samples, resulted in a deeper reduction of the adsorption capacity and higher H_{MTZ} for the former adsorbent, showing the importance of OSG nature and their distribution along the porous texture.

In the case of ethanol adsorption (Fig. 5.3), ethanol and water compete for the same hydrophilic sites on carbon surface. Thus, in dry airflow, ethanol adsorption capacity ($X_{0.90}$) was strongly favoured by oxygenated groups present on the more oxidized sample CAOX (Table 5.3), but the influence of humidity was also stronger.

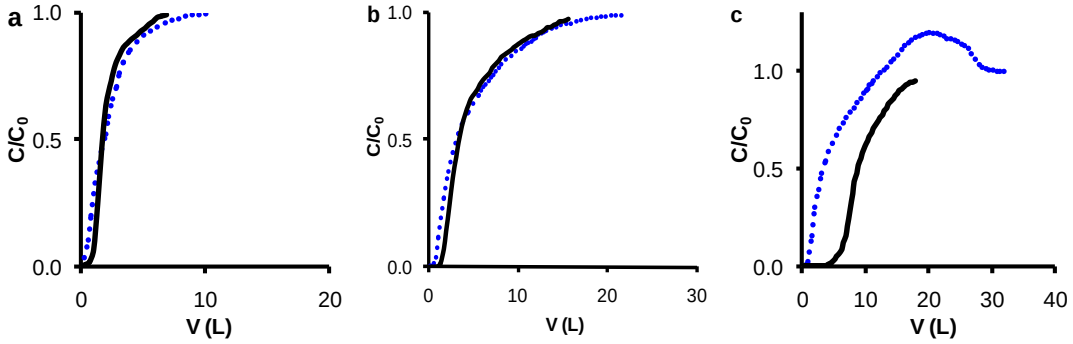

Figure 5.3. Comparisons of breakthrough curves obtained for the dynamic adsorption of ethanol under wet air (dashed) and dry air (continuous, from ref.[19]) onto different activated carbons: a) CA, b) CAOX500, c) CAOX.

The influence of adsorbent surface chemistry was also clearly proved by analysing the shape of breakthrough curves. In the case of CAOX sample, ethanol

relative concentration achieved values over 1 for the experiment carried out under wet conditions. This is a typical phenomenon when competitive adsorption is performed, since a more weakly adsorbed compound is replaced by a more strongly adsorbed one[34,35]. Thus, clearly, oxygenated surface groups on CAOX sample interacted more strongly with water than with ethanol, probably due to the larger dipole moment of the former (1.82 vs 1.69 D). This sample contains a great proportion of carboxylic acid groups. The specificity of these groups to water on ethanol/water competitive adsorption was remarked by results showed in Table 5.3. Carboxylic acids strongly favoured ethanol adsorption under dry conditions (Table 5.3), however, under wet conditions $X_{0.90}$ showed similar or even slightly higher values for CAOX500, because the strong interaction of water molecules with carboxylic groups decreased ethanol adsorption on CAOX. Moreover, ethanol was not replaced by water on CAOX500 (Fig. 5.3b). These results emphasize the need of controlling not only the hydrophilic character of the carbon surface, denoted mainly by the oxygen content, but also the nature of oxygenated surface groups present. Carboxylic acid groups have a deeper effect on the adsorption of polar VOCs molecules present in dry gaseous flows than other oxygenated surface groups; however, in wet conditions they may induce a negative effect on the adsorption of hydrophilic VOCs if their interaction with water was even stronger.

Table 5.3. Parameters obtained for the dynamic adsorption of ethanol under different conditions.

Sample	Air	$V_{0.02}$ L	$X_{0.02}$ mg g^{-1}	$V_{0.90}$ L	$X_{0.90}$ mg g^{-1}	H_{MTZ} cm	Du %
CA	dry*	1.2	5.0	4.1	10.7	2.80	67
	wet	0.2	1.4	4.8	11.0	4.88	13
CAOX500	dry*	1.5	8.0	11.1	25.5	2.53	41
	wet	0.7	3.9	11.9	24.8	2.99	20
CAOX	dry *	4.6	26.5	15.6	53.4	1.72	70
	wet	0.7	4.2	10.1	23.3	4.51	21

*From [19].

5.3.2.2. Competitive dynamic adsorption of ethanol and n-octane

Breakthrough curves for ethanol and n-octane competitive adsorption are shown in Fig. 5.4, and parameters calculated from them are summarized in Table 5.4. At a glance, it can be noted that: (i) n-octane achieved breakthrough point later than ethanol regardless of the employed adsorbent. The high n-octane adsorption capacity of CA sample is again due to the highly developed porosity of this sample (ii) n-octane was able to replace ethanol even in the case of oxidized samples CAOX and CAOX500, where the presence of oxygenated surface groups should provoke specific interactions with polar molecules (ethanol), as previously shown.

Water vapour and ethanol modified n-octane adsorption process in a similar way (smaller adsorption capacities and slower adsorption processes). Nevertheless, the adsorption capacity ($X_{0.90}$) of CA for n-octane in the presence of ethanol became even lower than under wet conditions (Table 5.2). When hydrophilic CAOX and CAOX500 adsorbents were used, n-octane adsorption capacity and breakthrough volumes were reduced, favouring the ethanol one. The highest ethanol adsorption capacityof CAOX led to the smallest n-octane adsorption one.

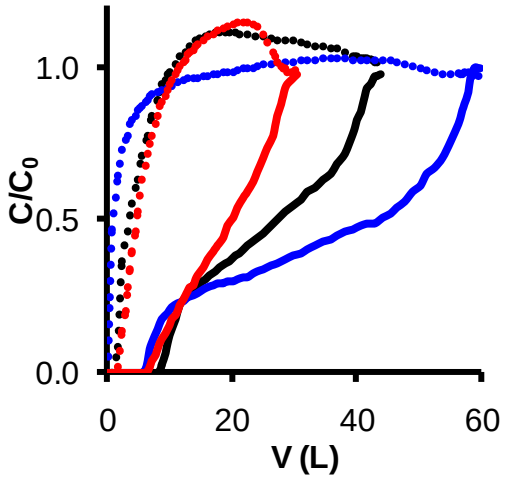

Figure 5.4. Competitive dynamic adsorption of ethanol (dashed curve) and n-octane onto CAOX (red), CAOX500 (black), CA (blue).

In order to evaluate the retained ethanol (X_R, $mg \cdot g^{-1}$), integration of ethanol curves was performed till the end of the experiment to discount the ethanol replaced by n-octane from weak adsorption sites. This parameter was higher for CAOX and decreased progressively for CAOX500 and CA. After removing carboxylic acid groups, n-octane adsorption capacity increased and X_R decreased, even though the total oxygen content was maintained. This phenomenon shows again the specificity of carboxylic groups for the adsorption of polar molecules.

Table 5.4. Parameters obtained for the competitive adsorption of ethanol and n-octane.

Sample	VOC	$V_{0.02}$ L	$X_{0.02}$ mg g^{-1}	$V_{0.90}$ L	$X_{0.90}$ mg g^{-1}	X_R mg g^{-1}
CA	ethanol	0.2	1.0	6.6	9.8	9.7
	n-octane	6.2	29.3	57.5	170.7	-
CAOX500	ethanol	1.0	6.0	8.2	21.2	12.2
	n-octane	8.4	42.3	41.3	123.4	-
CAOX	ethanol	1.6	8.9	9.0	27.2	18.8
	n-octane	6.8	32.8	28.1	90.0	-

It must be highlighted the ability of n-octane to replace the previously adsorbed ethanol on CAOX and CAOX500. This fact is not observed when CA was employed, as denoted by the shape of their ethanol breakthrough curves and the coincidence between $X_{0.90}$ and X_R parameters (Table 5.4), probably also conditioned by the low amount of ethanol adsorbed. According to previously reported results, adsorption sites of ethanol and n-octane are different, taking place mainly on OSG in the first case. Competitive ethanol/water adsorption also pointed out that the larger the dipole moment of the adsorbate, the stronger the interaction with these oxygenated groups, being part of the ethanol adsorbed molecules finally replaced by water ones with an energetically favourable adsorption. However, the dipole moment of n-octane is null and consequently the disruption of ethanol-OSG interactions should be due to additional effects.

The strong interaction of acid sites with ethanol molecules could lead to a chemical reaction between them. Two possibilities are given for such a process between alcohols and oxygenated surface groups: dehydration or dehydrogenation[21,36]. Dehydration is catalysed by acid groups while dehydrogenation needs the conjugated effect of acid and basic sites. Thus, taking into account the acid character of CAOX surface, dehydration seems to be the most plausible. Then, the produced water could displace a fraction of the adsorbed ethanol.

5.3.2.3. Fitting the columns content for simultaneous ethanol and n-octane adsorption

Looking for a better performance in the simultaneous adsorption of both components, a 50% CA - 50% CAOX mixture was prepared. Breakthrough curves for single component adsorption (n-octane, Fig. 5.5a and ethanol, Fig. 5.5b) and ethanol/octane competitive adsorption (Figure 5.5c) were obtained with this column. Adsorption parameters obtained from them are summarized in Table 5.5. Results showed an intermediate behaviour of this column regarding those obtained with CA and CAOX columns when adsorbing individual VOCs. A similar intermediate behaviour was also expected for competitive n-octane/ethanol adsorption processes, however, significant differences were observed regarding results previously exposed.

Thus, it is noteworthy that an increase in the breakthrough volume ($X_{0.02}$) for n-octane during competitive adsorption (Table 5.5) compared to CA sample (Table 5.4) is produced. This result is related to the presence of specific active sites for ethanol adsorption (CAOX component), thus avoiding or limiting the ethanol adsorption on CA which, as previously shown, hinders and retards the n-octane adsorption on CA. It should be noted also that the breakthrough point for n-octane is coincident with the saturation point for ethanol (at around 8.2 L). These results suggest that both activated carbons worked in the column separately, ethanol being adsorbed preferentially on carboxylic acid groups of CAOX which permitted a larger n-octane adsorption on CA. Thus, by fitting the ratio of hydrophobic/hidrophylic carbons on the column, it would be possible to obtain an improved adsorption column to be used for mixtures of pollutants with different polarity or concentrations.

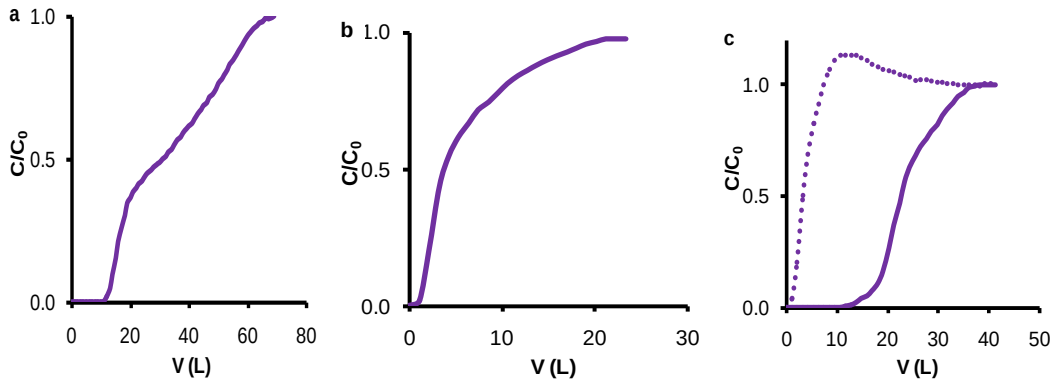

Figure 5.5. Breakthrough curves for CA-CAOX mixture. n-octane (a), ethanol (b) and competitive (c, ethanol · and n-octane -).

Table 5.5. Parameters obtained for single component and competitive dynamic adsorption of ethanol and n-octane onto CA-CAOX mixture.

Experiment	VOC	$V_{0.02}$ L	$X_{0.02}$ mg g^{-1}	$V_{0.90}$ L	$X_{0.90}$ mg g^{-1}
Single component	Ethanol	1.3	5.8	14.8	29.4
	n-octane	12.0	57.6	58.1	156.6
Competitive	Ethanol	1.0	5.6	6.2	16.6
	n-octane	13.6	65.0	32.3	110.9

5.3.3. Wheeler-Jonas analysis

Wheeler-Jonas equation[29-32] was used to determine the rate constant k_v of the dynamic adsorption processes using the three activated carbons under different experimental conditions. Results are compiled in Table 5.6.

Table 5.6. Values of k_v (min^{-1}) for the dynamic adsorption of ethanol or n-octane in different experimental conditions.

	n-octane			ethanol		
Sample	Dry air	Wet air	Competitive	Dry air	Wet air	Competitive
CA	5732	154	193	409	122	65
CAOX	222	136	710	714	245	651
CAOX500	746	380	487	151	155	420
CACAOX	292	-	1060	78	-	455

In dry airflow, the maximum k_v values were detected for the adsorption processes of n-octane on CA and ethanol on CAOX, in agreement with the textural and chemical influence previously described. In the case of n-octane adsorption onto CA, the process became much slower when water or ethanol were present, and the decrease in k_v was very large compared to results from other authors[30,32]. This could be due to the strong affinity of this highly porous and hydrophobic adsorbent for n-octane. The value of k_v became shorter after oxidation (CAOX), because both the porosity and the hydrophobicity decreased being partially recovered after removing carboxylic acid groups (CAOX500). The contrary tendency was observed for ethanol adsorption: the high value of k_v for ethanol adsorption onto CAOX under dry air denoted the specificity of carboxylic groups. Results for ethanol adsorption onto CAOX showed a strong reduction of adsorption rate when water vapour was present. It was observed in previous sections that water was able to replace ethanol from CAOX surface.

Results obtained in competitive experiments are of special interest. In these cases k_v values either for n-octane or ethanol adsorption was always higher than under wet airflow, which is related to the strong pore blockage that provoke the water adsorption, as previously commented. Similarly, when a column is prepared by mixing CA-CAOX, adsorption of n-octane occurred faster than in pure CA. By mixing both adsorbents, we compromised adsorption capacity and adsorption rate.

5.4. CONCLUSIONS

Influence of the presence of water in the dynamic adsorption of n-octane and ethanol onto several activated carbons was determined as well as competitive adsorption between both VOCs. All experimental results showed a strong relationship between the chemical surface functionality of the adsorbent and its behaviour in different conditions.

The presence of humidity influenced both ethanol and n-octane dynamic adsorption, reducing both rate of the process and adsorption capacity. Water adsorbed blocks the porosity of the sample depending on the OSG nature and distribution. Thus this effect was bigger on ethanol adsorption than in the case of octane, because both water and ethanol compete by the same adsorption sites, mainly when the adsorbents are functionalized with carboxylic acid groups (CAOX).These groups have a positive effect on the ethanol adsorption from dry airflow, but a negative effect in the presence of humidity due to the stronger interaction of water with carboxylic groups. In this case, ethanol previously adsorbed was replaced by water from the carbon surface.

When studying the competitive ethanol/n-octane adsorption, it was observed that ethanol hindered the access of n-octane to the internal porosity, as previously described for water. In the case of the least hydrophilic sample, CA, it implied a slight reduction in the n-octane adsorption capacity but a strong reduction in the adsorption rate of the process, as denoted also by the Wheeler-Jonas model. In the case of more hydrophilic samples CAOX and CAOX500, ethanol adsorption is favoured from the mixture. It is, however, observed that n-octane was also able to replace adsorbed ethanol from weak adsorption sites.

Finally, by mixing both extreme adsorbents, CA with a high surface area and a very low oxygen content, and CAOX, with a large oxygen (carboxylic acid groups) content but a shorter surface area, a larger rate for the simultaneous adsorption of both VOCs was achieved. This result might well be related to the presence of specific active sites for the adsorption of each molecule, ethanol being mainly adsorbed onto the

oxygenated groups present on CAOX and n-octane being mainly adsorbed onto CA surface.

5.5. REFERENCES

[1] A. Kyriakides, V. Dimas, E. Lymperopoulou, D. Karonis, and E. Lois, Evaluation of gasoline-ethanol-water ternary mixtures used as a fuel for an Otto engine, *Fuel*, **108** (2013) 208-215.

[2] M.B. Gramajo de Doz, C.M. Bonatti, and H.N. Sólimo, Water Tolerance and Ethanol Concentration in Ethanol-Gasoline Fuels at Three Temperatures, *Energy & Fuels*, **18** (2003) 334-337.

[3] C.A. Cardona and Ó.J. Sánchez, Fuel ethanol production: Process design trends and integration opportunities, *Bioresource Technology*, **98** (2007) 2415-2457.

[4] H.J. Huang, S. Ramaswamy, U.W. Tschirner, and B.V. Ramarao, A review of separation technologies in current and future biorefineries, *Separation and Purification Technology*, **62** (2008) 1-21.

[5] R.K. Niven, Ethanol in gasoline: environmental impacts and sustainability review article, *Renewable and Sustainable Energy Reviews*, **9** (2005) 535-555.

[6] M. Winther, F. Moller, and T.C. Jensen, Emission consequences of introducing bio ethanol as a fuel for gasoline cars, *Atmospheric Environment*, **55** (2012) 144-153.

[7] L.A. Graham, S.L. Belisle, and C.L. Baas, Emissions from light duty gasoline vehicles operating on low blend ethanol gasoline and E85, *Atmospheric Environment*, **42** (2008) 4498-4516.

[8] A. Moreno, S. Salgado, R. Taccone, P. Martín, and B. Cabañas, Atmospheric degradation of saturated alcohols: Room temperature rate coefficients for NO_3 radical reactions, *Atmospheric Environment*, **96** (2014) 229-235.

[9] K. Uddin, I.I. El-Sharkawy, T. Miyazaki, B.B. Saha, S. Koyama, H.S. Kil, J. Miyawaki, and S.H. Yoon, Adsorption characteristics of ethanol onto functional

activated carbons with controlled oxygen content, *Applied Thermal Engineering*, **72** (2014) 211-218.

[10] A. Martínez de Yuso, B. Rubio, and M.T. Izquierdo, Influence of activation atmosphere used in the chemical activation of almond shell on the characteristics and adsorption performance of activated carbons, *Fuel Processing Technology*, **119** (2014) 74-80.

[11] Y. Bai, Z.H. Huang, and F. Kang, Surface oxidation of activated electrospun carbon nanofibers and their adsorption performance for benzene, butanone and ethanol, *Colloids and Surfaces A: Physicochemical and Engineering Aspects*, **443** (2014) 66-71.

[12] A.J. Romero-Anaya, M.A. Lillo-Ródenas, and A. Linares-Solano, Factors governing the adsorption of ethanol on spherical activated carbons, *Carbon*, **83** (2015) 240-249.

[13] G. Liu, F. Xiangli, W. Wei, S. Liu, and W. Jin, Improved performance of PDMS/ceramic composite pervaporation membranes by ZSM-5 homogeneously dispersed in PDMS via a surface graft/coating approach, *Chemical Engineering Journal*, **174** (2011) 495-503.

[14] N. Wang, J. Liu, J. Li, J. Gao, S. Ji, and J.R. Li, Tuning properties of silicalite-1 for enhanced ethanol/water pervaporation separation in its PDMS hybrid membrane, *Microporous and Mesoporous Materials*, **201** (2015) 35-42.

[15] F. Carrasco-Marín, D. Fairén-Jiménez, and C. Moreno-Castilla, Carbon aerogels from gallic acid-resorcinol mixtures as adsorbents of benzene, toluene and xylenes from dry and wet air under dynamic conditions, *Carbon*, **47** (2009) 463-469.

[16] A.W. Heinen, J.A. Peters, and H.v. Bekkum, Competitive adsorption of water and toluene on modified activated carbon supports, *Applied Catalysis A: General*, **194-195** (2000) 193-202.

[17] A. Martínez de Yuso, M.T. Izquierdo, B. Rubio, and P.J.M. Carrott, Adsorption of toluene and toluene-water vapor mixture on almond shell based activated carbons, *Adsorption*, **19** (2013) 1137-1148.

[18] A.M. Slasli, M. Jorge, F. Stoeckli, and N.A. Seaton, Modelling of water adsorption by activated carbons: effects of microporous structure and oxygen content, *Carbon*, **42** (2004) 1947-1952.

[19] J.F. Vivo-Vilches, E. Bailón-García, A.F. Pérez-Cadenas, F. Carrasco-Marín, and F.J. Maldonado-Hódar, Tailoring activated carbons for the development of specific adsorbents of gasoline vapors, *Journal of Hazardous Materials*, **263, Part 2** (2013) 533-540.

[20] J.F. Vivo-Vilches, E. Bailón-García, A.F. Pérez-Cadenas, F. Carrasco-Marín, and F.J. Maldonado-Hódar, Tailoring the surface chemistry and porosity of activated carbons: Evidence of reorganization and mobility of oxygenated surface groups, *Carbon*, **68** (2014) 520-530.

[21] C. Moreno-Castilla, F. Carrasco-Marín, C. Parejo-Pérez, and M.V. López Ramón, Dehydration of methanol to dimethyl ether catalyzed by oxidized activated carbons with varying surface acidic character, *Carbon*, **39** (2001) 869-875.

[22] C. Moreno-Castilla, A.F. Pérez-Cadenas, F.J. Maldonado-Hódar, F. Carrasco-Marín, and J.L. Fierro, Influence of carbon-oxygen surface complexes on the surface acidity of tungsten oxide catalysts supported on activated carbons, *Carbon*, **41** (2003) 1157-1167.

[23] J.L. Figueiredo, M.F.R. Pereira, M.M.A. Freitas, and J.J.M. Órfao, Modification of the surface chemistry of activated carbons, *Carbon*, **37** (1999) 1379-1389.

[24] S. Morales-Torres, F.J. Maldonado-Hódar, A.F. Pérez-Cadenas, and F. Carrasco-Marín, Design of low-temperature Pt-carbon combustion catalysts for VOC's treatments, *Journal of Hazardous Materials*, **183** (2010) 814-822.

[25] G.M. Luckchis, Adsorption systems 1. Design by mass-transfer-zone concept, *Chemical Engineering*, **80** (1973) 111.

[26] W.J.J. Webber, *Physiochemical Processes for Water Quality Control*, Wiley-Interscience ed., New Cork, 1972.

[27] P.N. Cheremisinoff and F. Ellerbusch, *Carbon Adsorption Handbook*, Ann Arbor Science Pub. ed., Michigan, 1978.

[28] J.D. Méndez-Díaz, M.M. Abdel daiem, J. Rivera-Utrilla, M. Sánchez-Polo, and I. Bautista-Toledo, Adsorption/bioadsorption of phthalic acid, an organic micropollutant present in landfill leachates, on activated carbons, *Journal of Colloid and Interface Science*, **369** (2012) 358-365.

[29] G. Grévillot, S. Marsteau, and C. Vallières, A Comparison of the Wheeler-Jonas Model and the Linear Driving Force at Constant-Pattern Model for the Prediction of the Service Time of Activated Carbon Cartridges, *Journal of Occupational and Environmental Hygiene*, **8** (2011) 279-288.

[30] A. KhazraeiVizhemehr, F. Haghighat, and C.S. Lee, Gas-phase filters breakthrough models at low concentration - Effect of relative humidity, *Building and Environment*, **75** (2014) 1-10.

[31] J. Wu, O. Claesson, I. Fangmark, and L.G. Hammarstrom, A systematic investigation of the overall rate coefficient in the Wheeler-Jonas equation for adsorption on dry activated carbons, *Carbon*, 43 (2005) 481-490.

[32] G.O. Wood, A review of the effects of covapors on adsorption rate coefficients of organic vapors adsorbed onto activated carbon from flowing gases, *Carbon*, 40 (2002) 685-694.

[33] F. Kraehenbuehl, C. Quellet, B. Schmitter, and F. Stoeckli, The relationship between immersion calorimetry and the parameters of the water adsorption isotherm on active carbons, *Journal of the Chemical Society, Faraday Transactions*, 82 (1986) 3439-3445.

[34] M.A. Lillo-Ródenas, A.J. Fletcher, K.M. Thomas, D. Cazorla-Amorós, and A. Linares-Solano, Competitive adsorption of a benzene-toluene mixture on activated carbons at low concentration, *Carbon*, 44 (2006) 1455-1463.

[35] J.H. Yun, D.K. Choi, and S.H. Kim, Equilibria and dynamics for mixed vapors of BTX in an activated carbon bed, *AIChE Journal*, **45** (1999) 751-760.

[36] F.J. Maldonado-Hódar, A.F. Pérez-Cadenas, J.L.G. Fierro, and C. Moreno-Castilla, Influence of Carbon-Chlorine Surface Complexes on the Properties of Tungsten Oxide Supported on Activated Carbons. 2. Surface Acidity and

Skeletal Isomerization of 1-Butene, *The Journal of Physical Chemistry B*, **107** (2003) 5003-5007.

Capítulo VI

FITTING THE POROSITY OF CARBON XEROGEL BY CO_2 ACTIVATION TO IMPROVE THE TMP/n-OCTANE SEPARATION

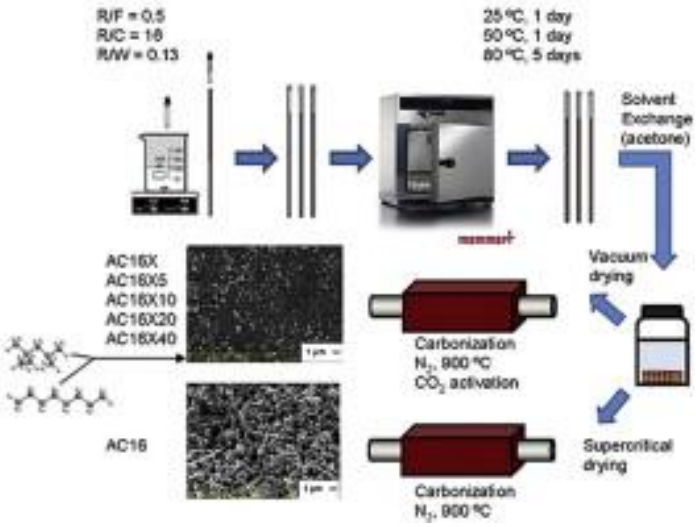

FITTING THE POROSITY OF CARBON XEROGEL BY CO_2 ACTIVATION TO IMPROVE THE TMP/n-OCTANE SEPARATION

Article published in Microporous and Mesoporous Mat., 209 (2015) 10-17, doi: 10.1016/ j.micromeso.2015.01.010

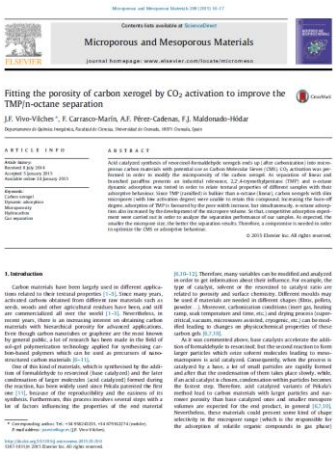
Microporous and Mesoporous Materials

Fitting the porosity of carbon xerogel by CO_2 activation to improve the TMP/n-octane separation

Highlights

- Acid catalyzed synthesis of RF gels ends up into microporous carbon materials.
- Adsorption capacity is related to wider micropore volume (W_0 (N_2)) for TMP.
- In the case of n-octane to both micropore volumes (W_0 (N_2) and W_0 (CO_2).
- Dynamic adsorption of n-octane is not influenced by the presence of TMP.

Abstract

Acid catalyzed synthesis of resorcinol-formaldehyde xerogels ends up (after carbonization) into microporous carbon materials with potential use as Carbon Molecular Sieves (CMS). CO_2 activation was performed in order to modify the microporosity of the carbon xerogel. As separation of linear and branched paraffins presents an industrial relevance, 2,2′,4-trymethylpentane (TMP) and n-octane dynamic adsorption was tested in order to relate textural properties of different samples with their adsorptive behaviour. Since TMP (ramified) is bulkier than n-octane (linear), carbon xerogels with slim micropores (with low activation degree) were unable to retain this compound. Increasing the burn-off degree, adsorption of TMP is favoured by the pore width increase, but simultaneously, n-octane adsorption also increased by the development of the micropore volume. So that, competitive adsorption experiment were carried out in order to analyze the separation performance of our samples. As expected, the smaller the micropore size, the better the separation results. Therefore, a compromise is needed in order to optimize the CMS or adsorptive behaviour.

Keywords: Carbon xerogel, dynamic adsorption, microporosity, hydrocarbon, gas separation.

6.1. INTRODUCTION

Carbon materials have been largely used in different applications related to their textural properties[1-5]. Since many years, activated carbons obtained from different raw materials such as seeds, woods and other agricultural residues have been, and still are commercialized all over the world[1-3]. Nevertheless, in recent years, there is an increasing interest on obtaining carbon materials with hierarchical porosity for advanced applications. Even though carbon nanotubes or graphene are the most known by general public, a lot of research has been made in the field of sol-gel polymerization technology applied for synthesising carbon-based polymers which can be used as precursors of nano-structured carbon materials[6-11].

One of this kind of materials, which is synthesised by the addition of formaldehyde to resorcinol (base catalyzed) and the later condensation of larger molecules (acid catalyzed) formed during the reaction, has been widely used since Pekala patented the first one[11], because of the reproducibility and the easiness of its synthesis. Furthermore, this process involves several steps with a lot of factors influencing properties of the end material[6,10-12]. Therefore, many variables can be modified and analyzed in order to get information about their influence. For example, the type of catalyst, solvent or the resorcinol to catalyst ratio are related to porosity and surface chemistry. Different moulds may be used if materials are needed in different shapes (films, pellets, powder...). Moreover, carbonization conditions (inert gas, heating ramp, soak temperature and time, etc.) and drying process (supercritical, vacuum, microwaves assisted, cryogenic, etc.) can be modified leading to changes on physicochemical properties of these carbon gels[6,7,10].

As it was commented above, base catalysts accelerate the addition of formaldehyde to resorcinol; but the second reaction to form larger particles which seize solvent molecules leading to meso-macropores is acid catalyzed. Consequently, when the process is catalyzed by a base, a lot of small particles are rapidly formed and after that the condensation of them takes place slowly, while, if an acid catalyst is chosen, condensation within particles becomes the fastest step. Therefore, acid catalyzed variants of Pekala's method lead to carbon materials with larger particles and narrower

porosity than base catalyzed ones and smaller mesopore volumes are expected for the end product, in general[6,7,10]. Nevertheless, these materials could present some kind of shape selectivity in the micropore range (which is the responsible for the adsorption of volatile organic compounds in gas phase) depending on the type of molecule which passes through the porous material.

Apart from the versatility due to possibilities offered by gelification, drying or carbonization steps, carbon gels can be activated by means of physical (usually water vapour or carbon dioxide) or chemical (alkaline hydroxides, corrosive salts, phosphoric acid, etc.) activation[7,10]. Carbon dioxide activation is known to generate changes on microporosity as CO_2 is able to react with active sites on carbon surface, oxidizing them and leading to oxygen complexes which are not stable at the activation temperature, decomposing in a second reaction[3,5,13]. As a result, new microporosity can be developed and micropores already present on less activated material might be broadened.

One of the most important aspects within fuel technology is the increasing of gasoline octane number[14-17]. This parameter is related to the performance of a fuel which is used in a compression engine. Even though octane rating is an arbitrary scale, i. e., an octane index is assigned to each compound which could be present in the mixture based on experimental results; in general, higher octane indexes are found for branched alkanes than for linear ones[16]. Therefore, separation of linear and branched paraffins is a research topic with an industrial relevance. In the case of different C8 alkanes, n-octane presents an octane index below 0, while 2,2',4-trimethylpentane (TMP) is one of the reference compounds in the octane rating being 100 its value (0 is assigned for n-heptane)[16].

In this work an acetic acid catalyzed resorcinol formaldehyde xerogel obtained in form of pellets was carbonized at high temperature under inert atmosphere (nitrogen). Resultant carbon xerogel was split in different portions which were activated with carbon dioxide till several burn-off degrees between 5 and 40 were achieved for each portion. That way, adsorbent series with increasing micropore width and volume were obtained. Beds of each adsorbent were prepared and exposed to

contaminated air fluxes with n-octane and/or TMP for obtaining breakthrough columns. Parameters derived from single component and competitive dynamic adsorption experiments can be related to material microporosity.

6.2. EXPERIMENTAL

6.2.1. Synthesis of RF carbon gels

Resorcinol – formaldehyde polymerization was carried out catalysed by acetic acid. The hydrogel was prepared by following a protocol similar to the one described in bibliography[7]. Same catalyst, solvent to resorcinol and resorcinol to catalyst ratios were chosen, but modifying gelification conditions (25 °C, 24 h; 50 °C, 24 h; 80 °C, 5 days). Cylindrical glass moulds with an inner diameter of 5 mm were used in order to obtain the material in pellets. Water was exchanged by acetone, even though supercritical drying was not performed, with the intention of reducing porosity collapse caused by water-polymer surface tension[10,12]. Xerogel was obtained by drying on a furniture working under vacuum conditions (65 mbar, 50 °C, 3 h). Aerogel was also synthesised for comparison purposes.

Carbonization was performed in a tubular oven working under N_2 atmosphere (300 cm^3 min^{-1}). A relatively small heating ramp was employed (2 °C min^{-1}) to avoid cracks. Materials were heated up till 900 °C keeping this temperature for 2 h. Samples were labelled as AC16 (aerogel) and AC16X (xerogel).

6.2.2. CO_2 activation of carbon xerogel

After carbonization, several portions of carbon xerogel were taken and activated with mixtures of carbon dioxide and nitrogen in different proportions at 870 °C till desired burn off percentages were achieved (5, 10, 20, 40). Carbon dioxide reacts with carbon walls by a gasification reaction, therefore an increase on micropore volume and/or width is expected as burn off degree becomes higher [3-5,7,13]. Samples were

named as AC16X5, AC16X10, AC16X20 and AC16X40. Finally, we ended up with five samples which mainly differ on their microporosity development.

6.2.3. Textural characterization

Sample microphotographs were taken with a Scanning electron microscope (Leo, Carl Zeiss, Geminy-153). Excitation energy of 20 kV was employed. Textural properties of samples were determined by adsorption isotherms of N_2 (−196 °C) and CO_2 (0 °C) using a Quadrasorb from Quantachrome after outgassing samples overnight at 110 °C under high vacuum (10^{-6} mbar). BET surface area, micropore volume (W_0) and micropore mean width (L_0) were calculated by applying BET[18], Dubinin-Radushkevich[19] and Stoeckli[20] equations respectively to the corresponding isotherms.

6.2.4. Dynamic adsorption experiments

Dynamic adsorption experiments were performed with an experimental set-up described in a previous work[21]. Gas chromatography with FID detection was also chosen to quantify VOC concentrations. As samples were obtained in shape of pellets, a greater weight (1.0 g) and a reactor with a larger inner diameter (0.8 cm) were employed.

Breakthrough curves for n-octane and 2,2',4-trimethylpentane (TMP) dynamic adsorption were obtained and analyzed by using an approach described by Cheremisinoff et al.[22] based on the mass transfer zone concept[23-25]. Description of result analysis and obtained parameters can be found in the paper mentioned above[21]. VOCs concentration was adjusted at 700 ppm by bubbling air through liquid contaminant and diluting it with another air flux.

With the purpose of evaluating the separation performance of different samples, competitive adsorption was also tested. In that case, TMP which is more weakly adsorbed raises relative concentrations higher than one, since n-octane molecules displace TMP ones from active sites[26,27]. The objective is to be able to separate both isomers since TMP is much bulkier than n-octane (Fig. 6.1).

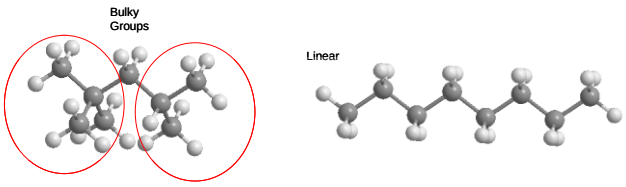

Figure 6.1. Molecular structure of TMP (left) and n-octane (right).

6.3. RESULTS AND DISCUSSION

6.3.1. Textural characterization. Isotherms and SEM

Previous works have demonstrated the influence of several parameters on the textural properties of carbon gels[6,10,12]. There are many factors within each step of the process that can be varied and related to different characteristics of the end material. In previous sections of this paper, we have enumerated some of them along the all synthesis and some possible post-treatments in order to modify the porosity.

One of these factors, the type of drying process, is crucial in the case of this kind of material, even more in the case of hydrogels (when water is chosen as solvent). Depending on the way hydrogel is dried, surface tension between solvent and gel may lead to a porosity collapse, because meso and macropores are formed during gelification process, when water is entrapped inside polymer particles[6,10,12]. Supercritical drying is known to be the most efficient technique to preserve porous texture, and aerogels presents wider meso-macropores and larger meso-macropore volumes in general than xerogels (dried by direct heat or vacuum) or cryogels (cryogenic drying). If supercritical carbon dioxide is chosen to remove water from the hydrogel, a previous solvent exchange (typically acetone) is needed since water is not soluble in supercritical CO_2. Previous works on our group have demonstrated that this step is also desirable for other drying processes[12]. Therefore, we decided to introduce it during the synthesis of carbon xerogel.

N_2 adsorption isotherms at -196 °C and CO_2 ones at 0 °C are shown in Fig. 6.2. Nitrogen isotherms (Fig. 6.2a) are typical for micro-mesoporous solids (a mixture of Type I and Type IV according to IUPAC), apart from the aerogel AC16 which is mainly microporous (Type I). The absence of mesopores on AC16 sample will be better understood after comparing SEM Microphotographs for both samples (Fig. 6.3).

AC16 surface (Fig. 6.3, top) is conformed by a net-like structure were carbon walls are interconnected forming large pores in form of canals, while in AC16X (Fig. 6.3, bottom) this macroporous network is not present. Drying process should be responsible for that since both materials were prepared with the same protocol but modifying this step. Probably a collapse of this macropore network happened, after drying under vacuum and carbonizing AC16X sample. This collapse produced the accumulation of spherical particles separated by mesopores that adsorbs nitrogen at high relative pressure values.

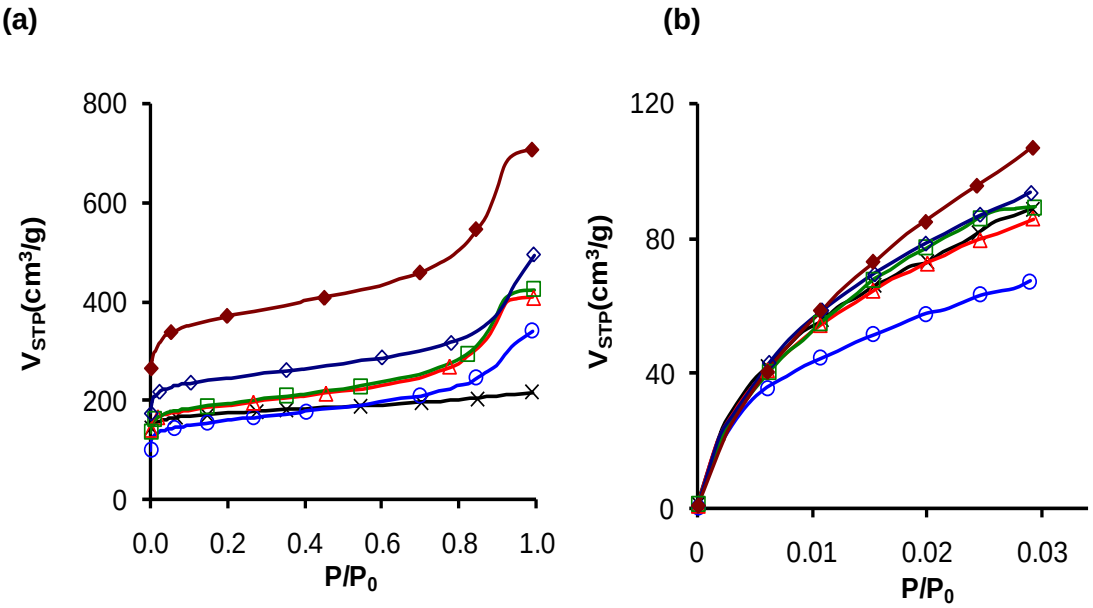

Figure 6.2. N_2 (a) and CO_2 (b) adsorption isotherms. AC16 (×), AC16X (○), AC16X5 (△), AC16X10 (□), AC16X20 (◊) and AC16X40 (◆).

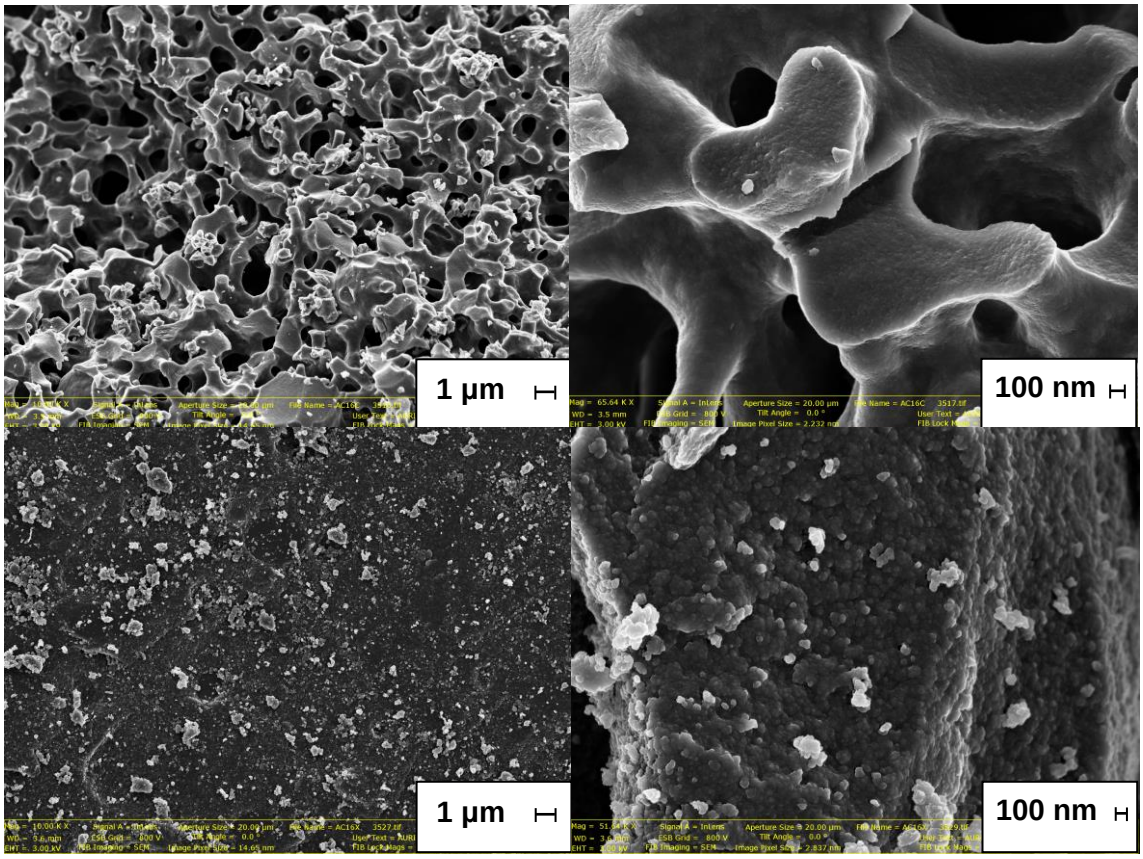

Figure 6.3. SEM microphotographs of AC16 (top) and AC16X (bottom).

Curiously when SEM microphotographs of Baumann et al.[7] and ours are compared, it looks like their aerogel particles are not so interconnected between them. The only difference between both aerogels is within the gelification process (3 days at 80 °C for Baumann et al.; 1 day 25 °C, 1 day 50 °C and 5 days 80 °C for AC16). It is very likely that the longer gelification time and the fact that 2 day at lower temperature were employed produced a greater cross-linkage and leaded to that structure on the ended material.

It is well known that carbon dioxide isotherms (Fig. 2b) are very useful when analyzing the slightest microporosity, as nitrogen at -196 °C can not penetrate into micropores with a very small width smaller[28,29]. Therefore, we ought to analyze both data all together in order to get more complete information about microporosity on our samples. Table 6.1 summarizes textural parameters derived from the analysis of N_2 and CO_2 isotherms as well as the actual burn-off degree for each material. We can see differences in porosity between carbon xerogel and aerogel. Micropore volumes

obtained from both N_2 and CO_2 are lower in the case of carbon xerogel. Larger mean micropore widths are also obtained.

Table 6.1. Textural properties of samples.

Sample	B.O. %	S_{BET} $m^2 \cdot g^{-1}$	W_0 (N_2) $cm^3 \cdot g^{-1}$	W_0 (CO_2) $cm^3 \cdot g^{-1}$	L_0 (N_2) nm	L_0 (CO_2) nm
AC16	-	657	0.26	0.29	0.68	0.60
AC16X	0.0	585	0.23	0.26	0.87	0.67
AC16X5	5.4	705	0.27	0.29	0.78	0.62
AC16X10	10.7	716	0.28	0.30	0.89	0.61
AC16X20	20.4	919	0.37	0.34	0.97	0.65
AC16X40	38.4	1381	0.49	0.37	1.18	0.68

As expected, gasification implies a micropore widening which is mainly responsible for the increase on S_{BET}. Furthermore, this porosity development is higher on W_0 (N_2) than on W_0 (CO_2). Fig. 6.4 shows how micropore volumes obtained with the two gases ($W_0(N_2)$ and $W_0(CO_2)$) are changing with burn-off degree of the samples: while W_0 (N_2) increases almost linearly, W_0 (CO_2) increases asymptotically. Variations in W_0 and L_0 for both gases explain how carbon dioxide activation is acting on our xerogel AC16X. On the one hand, for lowly activated samples (AC16X5 and AC16X10) carbon dioxide is mainly generating new microporosity, therefore L_0 obtained from both N_2 and CO_2 are even lower than for non activated sample and W_0 (CO_2) is still bigger than $W_0(N_2)$. On the other hand, highly activated samples (AC16X20 and AC16X40) present larger S_{BET}, W_0 (N_2) and L_0 (N_2), which means there is a pore widening on these samples. Changes on microporosity will be essential to explain dynamic adsorption results.

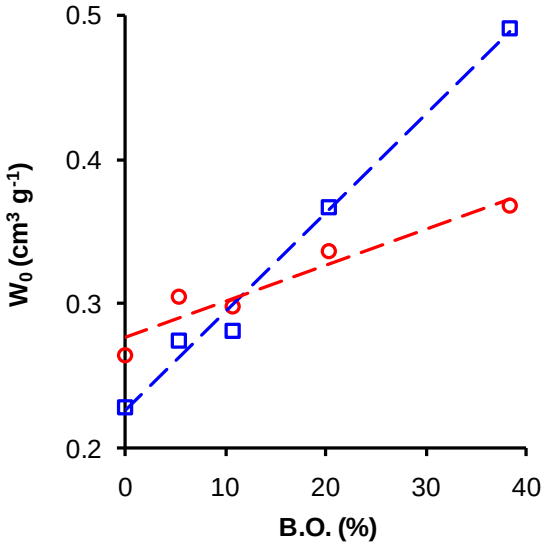

Figure 6.4. Variation of $W_0(N_2)$ (□) and $W_0(CO_2)$ (○) with the activation percentage.

6.3.2. Dynamic adsorption. TMP and n-octane single component

2,2',4-trimethylpentane (TMP) is a highly ramified C8 isomer. This kind of compounds increases gasoline octane number[14,15,17]. Its vapour pressure is relatively high; therefore, it would be present on a great proportion within gasoline evaporative emissions. For this reason, if we want an adsorbent to retain this kind of compound, a synthetic procedure which leads to a porous material with a large wide micropore volume ($W_0(N_2)$) has to be performed. Therefore, for canister-like applications, activated carbon materials with a great developed microporosity would be needed[21,30,31].

On the contrary, if our goal is to obtain a material for gas separation applications, broad microporosity has to be avoided. Since TMP is much bulkier than n-octane, the first one can not penetrate in micropores with a width smaller than 0.7 nm[14-17,32]. So that, n-octane would be retained when diffusing through adsorbent bed, as it can be adsorbed in the slightest micropores (ultramicropores, obtained from the analysis of CO_2 isotherms) whereas TMP will just diffuse through adsorbent meso and macroporosity.

Breakthrough columns for both TMP (Fig. 6.5a) and n-octane (Fig. 6.5b) dynamic adsorption show an increment on adsorption capacity and a delay on breakthrough point as microporosity is developed by carbon dioxide activation (Tables 6.2 and 6.3). As commented before, an increase on the micropore volume improves VOCs capture performance of the adsorbent. Nonetheless, since both adsorption capacities are increased (n-octane and TMP), highly activated AC16X20 and AC16X40 are more suitable to be utilized as total adsorbents than as materials for gas separation.

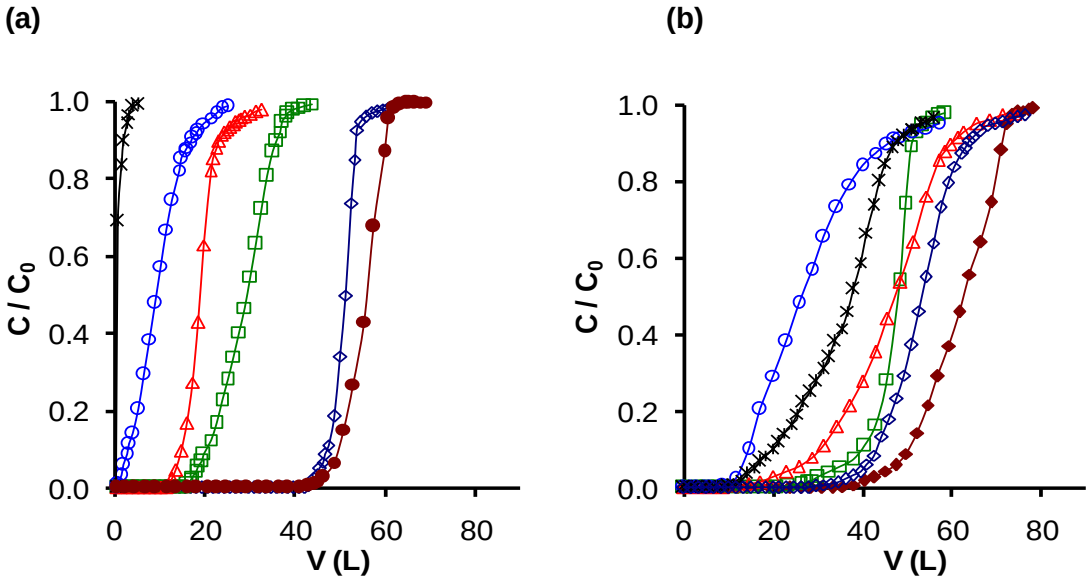

Figure 6.5. Breakthrough curves for dynamic adsorption of TMP (a) and n-octane (b). AC16 (×), AC16X (○), AC16X5 (△), AC16X10(□), AC16X20(◊) and AC16X40(◆).

Table 6.2. Parameters obtained from the analysis of TMP breakthrough curves.

Sample	Bed Height cm	$V_{0.02}$ L	$X_{0.02}$ mg g^{-1}	$V_{0.90}$ L	$X_{0.90}$ mg g^{-1}	H_{MTZ} cm	R_{MTZ} cm h^{-1}
AC16	4.4	0.0	0.0	1.9	0.3	-	-
AC16X	2.8	1.0	0.6	16.9	6.1	4.97	1.13
AC16X5	3.0	12.6	8.7	23.0	12.7	1.72	0.60
AC16X10	3.2	16.6	11.6	35.8	19.5	2.21	0.41
AC16X20	3.5	44.0	30.7	53.5	35.0	0.66	0.25
AC16X40	4.0	45.5	31.8	60.0	37.9	1.07	0.27

Table 6.3. Parameters obtained from the analysis of n-octane breakthrough curves.

Sample	$V_{0.02}$ L	$X_{0.02}$ mg g^{-1}	$V_{0.90}$ L	$X_{0.90}$ mg g^{-1}	H_{MTZ} cm	R_{MTZ} cm h^{-1}
AC16	26.8	18.2	48.0	26.2	2.45	0.42
AC16X	17.2	12.1	47.8	22.1	2.66	0.37
AC16X5	33.1	23.2	53.8	31.4	1.35	0.23
AC16X10	36.1	25.1	52.0	31.8	1.10	0.25
AC16X20	40.2	28.2	63.8	36.6	1.56	0.24
AC16X40	43.0	30.6	70.8	41.8	1.83	0.24

When aerogel and xerogel are compared, it is observed that the first one retain less TMP and more n-octane than the second one. In fact, breakthrough point for TMP in the case of aerogel is so early, that it is hard to obtain any reasonable parameter from its breakthrough curve. This behaviour is related to the narrower microporosity commented before for aerogel (which avoids the entry of TMP to it) and to the larger meso-macropore volume (which accelerates diffusion through pellets). In order to increase the adsorption capacity and to stablish relationships between microporosity and dynamic adsorption behaviour AC16X xerogel was activated.

Consequences of physical activation on textural properties were analyzed in the previous section. CO_2 activation generates new micropores for shortly activated samples and broadens micropores for highly activated ones. Therefore a larger increase on n-octane adsorption capacity than on TMP one was obtained for AC16X5 since this adsorbent present a larger volume of narrow micropores, while AC16X10 presents a similar increase on both adsorption capacities with respect to non activated AC16X (similar L_0 and larger W_0) and there is a huge increase on TMP adsorption capacity for AC16X20 and AC16X40 which have broader microporosity.

Once those results were analyzed, they were plotted versus textural properties, finding relationships between them. Different type of microporosity is governing the two adsorption processes. Breakthrough adsorption capacity ($X_{0.02}$) and saturation

adsorption capacities ($X_{0.90}$) obtained from TMP breakthrough curves can be related to wide micropore volume ($W_0(N_2)$) as it is shown in Fig. 6.6. In the case of n-octane dynamic adsorption, this process seems to be governed by both types of micropores ($W_0(N_2)$ and $W_0(CO_2)$), increasing the adsorption capacity as they increase (Fig. 6.7).

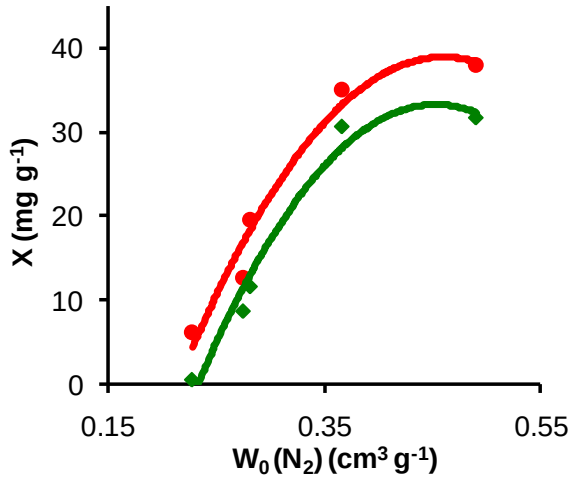

Figure 6.6. Variation of TMP adsorption capacity, $X_{0.02}$ (♦) and $X_{0.90}$ (•) with the wide micropore volume of the samples $W_0(N_2)$.

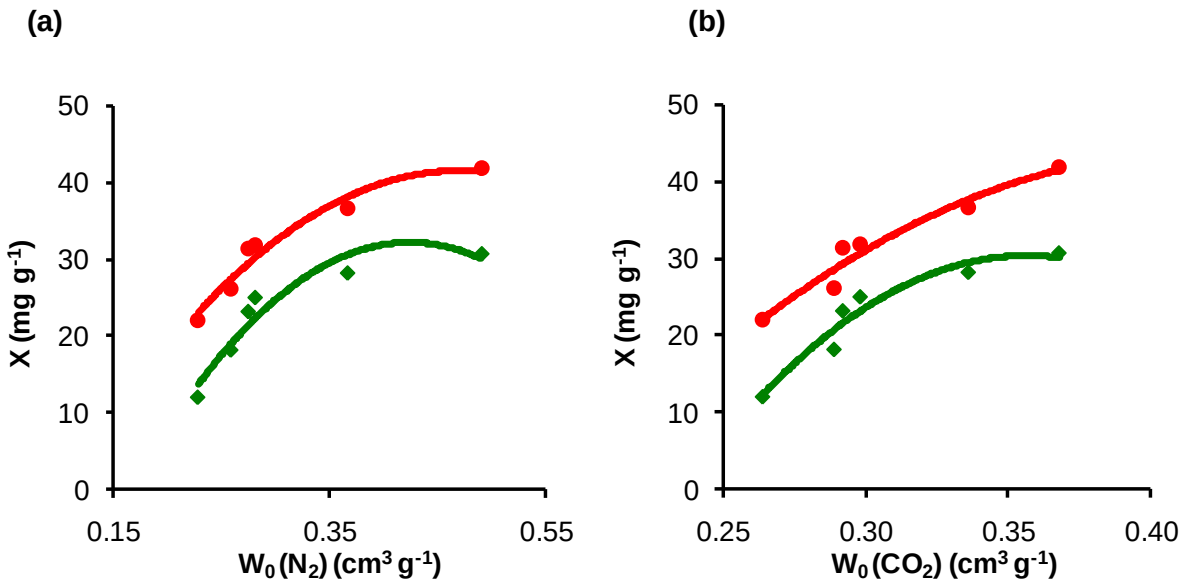

Figure 6.7. Variation of n-octane adsorption capacity, $X_{0.02}$ (♦) and $X_{0.90}$ (•) with the wide micropore volume of the samples $W_0(N_2)$ (a) and the narrow micropore volume $W_0(CO_2)$ (b).

To sum up, the microporosity of our materials needs to be fitted depending on the application. If we want a total adsorbent of hydrocarbons, we need porous solids with a well developed microporosity which will be capable of retaining bulky molecules. But, if the material will act as a gas separator, we need narrow micropores which can retain lighter molecules but not the bulkiest ones. In that case, combinations of activation and chemical vapour deposition (CVD) steps may be performed[33]. If so, micropore volume will increase but micropore widths at the entry will be tailored, avoiding the adsorption of ramified hydrocarbons.

6.3.3. TMP and n-octane competitive adsorption

After analyzing breakthrough curves for single component adsorption experiments, competitive adsorption was performed in order to evaluate the separation capability of different adsorbents. Since TMP is a ramified hydrocarbon, intermolecular forces are lower than in the case of n-octane. Therefore, TMP is more volatile than n-octane, which means saturation pressure at the same temperature is greater for the first one (at 25 °C, $P_0 \approx 52.0$ mmHg for TMP, $P_0 \approx 16.4$ mmHg for n-octane). Consequently, considering both VOCs and taking into account their hydrophobic nature (no possibilities of specific adsorbent-adsorbate interactions), TMP will be more weakly adsorbed than n-octane even in wide pores (in narrow ones it may not even penetrate).

Typically, when a competitive adsorption experiment takes place with two compounds like these, the weakly adsorbed one (TMP) is displaced from actives sites by the strongly adsorbed one (n-octane)[26,27]. As a consequence, TMP relative concentrations for this experiment achieve values above 1 because of this phenomenon (Fig. 6.8). So that, TMP adsorbed amount is going to decrease till a constant value, which will be the TMP adsorption capacity when adsorbent is saturated with TMP and n-octane. This value, measured in mg of contaminant per g of carbon as other adsorption capacities, will be named as X_R, which means adsorbed amount of TMP after it has been released (Table 6.4).

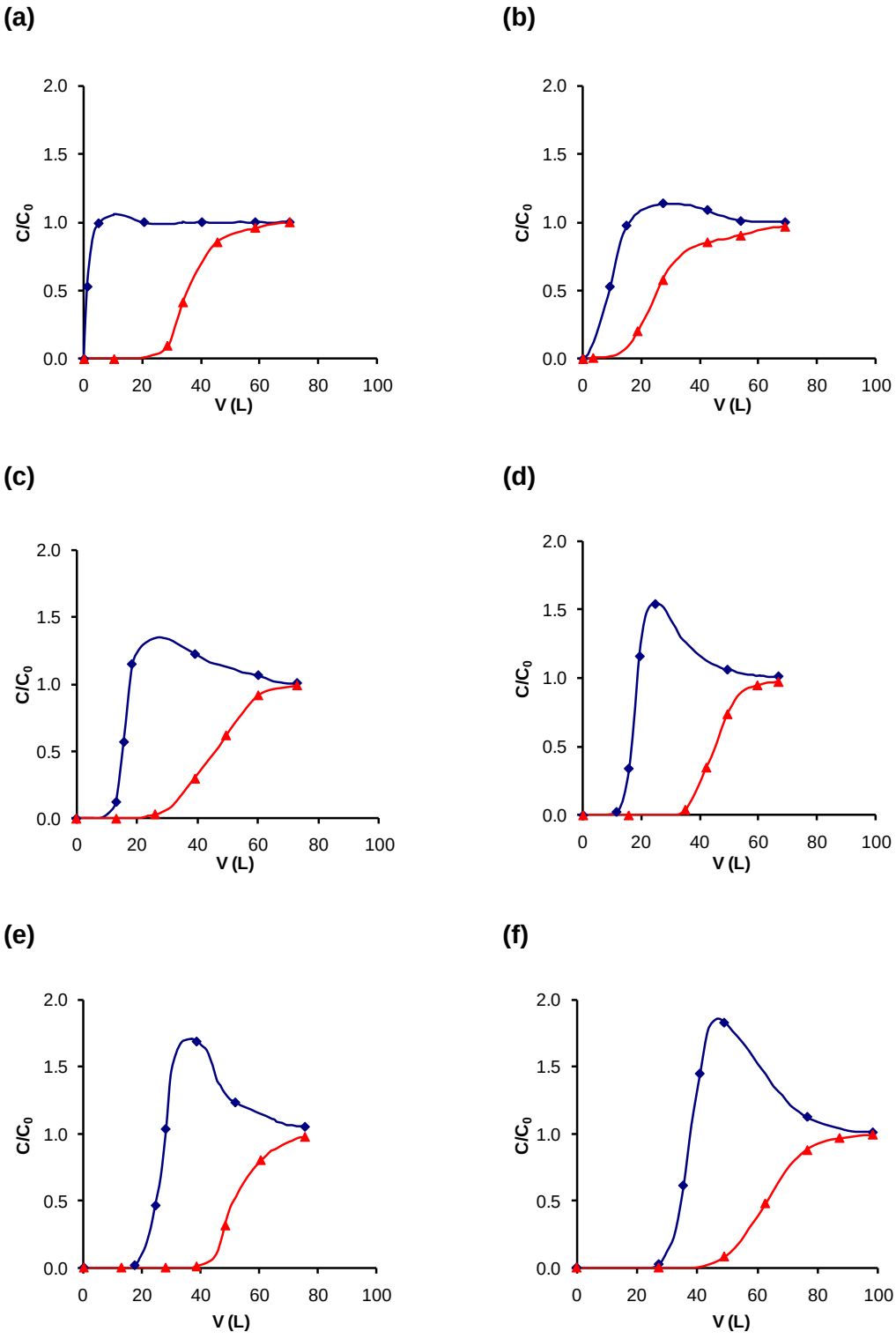

Figure 6.8. Breakthrough curves for competitive dynamic adsorption of TMP (♦) and n-octane (▲). (a) AC16, (b) AC16X, (c) AC16X5, (d) AC16X10, (e) AC16X20, (f) AC16X40.

Both single component and competitive n-octane dynamic adsorption seem to bring the same results, i.e., breakthrough curves present almost the same shape in all the samples no matter if TMP is or is not included in the contaminated air flux. This is better appreciated when adsorbed amount (X) of contaminant is plotted versus eluted volume for both single component and competitive adsorption (Fig. 6.9). It can be observed that n-octane adsorbed amount tendency is similar for both competitive and single component experiments in all the samples. Only for AC16X with the smallest micropore volume and n-octane adsorption capacity there is a small difference, because in this case the number of active sites for VOCs adsorption is much lower, then the influence of another adsorbable molecule (TMP) becomes higher.

Table 6.4. Parameters obtained from the analysis of competitive adsorption breakthrough curves.

Sample	VOC	$V_{0.02}$ L	$X_{0.02}$ mg g^{-1}	$V_{0.90}$ L	$X_{0.90}$ mg g^{-1}	X_R mg g^{-1}
AC16	TMP	0.2	0.0	2.7	0.5	0.0
	n-octane	23.3	16.1	48.8	25.0	
AC16X	TMP	1.7	0.9	13.5	5.5	3.0
	n-octane	10.2	7.1	52.8	20.4	
AC16X5	TMP	9.2	6.8	16.9	9.6	3.1
	n-octane	24.7	17.6	59.2	30.8	
AC16X10	TMP	11.6	8.0	18.1	10.7	4.3
	n-octane	34.3	23.8	54.5	31.0	
AC16X20	TMP	17.8	12.4	27.8	16.6	5.7
	n-octane	40.5	28.2	66.2	36.6	
AC16X40	TMP	26.8	18.4	37.6	22.9	8.5
	n-octane	43.7	30.5	77.8	43.2	

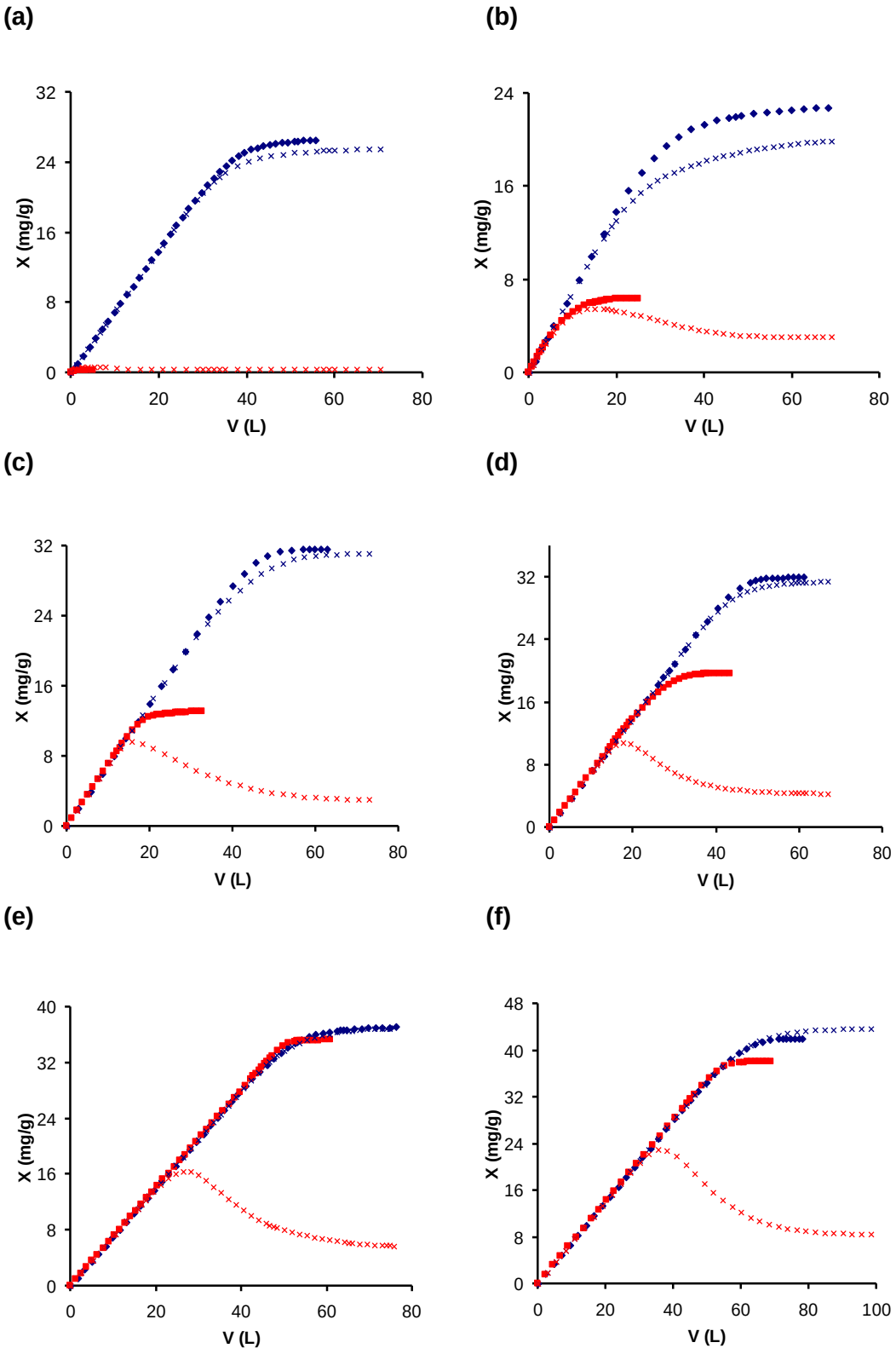

Figure 6.9. Variation of adsorbed amount (X) of TMP (red) and n-octane (blue) for single component (♦) and competitive (×) dynamic adsorption. (a) AC16, (b) AC16X, (c) AC16X5, (d) AC16X10, (e) AC16X20, (f) AC16X40.

There are two reasons that make n-octane adsorption not to be dependent on the presence of TMP in our experiments: the first one is that there are a lot of active sites within the narrow microporosity where TMP can not enter and n-octane can. The second is based on the same idea that the first paragraph of this section 3.3.; since our carbon gels present a hydrophobic nature, adsorbate-adsorbent interactions will be much greater for n-octane than for TMP, because methyl groups act as steric hindrance and intermolecular interactions are restricted. Based on those two premises, we can now easily explain what is happening in our competitive adsorption experiments. TMP is not even entering in the narrow microporosity and, in the case of wide one, n-octane is able to replace TMP so fast (due to its much larger affinity for the adsorbent) that we can not even see differences in results between both dynamic adsorption experiments.

Nevertheless, if a better separation performance is needed, wide microporosity (high burn-off degrees) should be avoided, because X_R values increase for further activated samples (Table 6.4). It is also important to consider that time with no one of the contaminant leaving the adsorption bed is being wasted (the earlier the breakthrough point for TMP, the better). Beds with late TMP breakthrough points (AC16X20, AC16X40) would not be useful as separator, but as total adsorbents. As it was previously pointed out, samples with a large narrow micropore volume (W_0 (CO_2)) and small micropore width (under 0.7 nm) are desirable at this purpose (samples AC16, AC16X5, AC16X10). Early n-octane breakthroughs (AC16X) are reducing the useful time of the separator and are not convenient.

6.4. CONCLUSIONS

Materials were prepared by acetic acid catalyzed polycondensation of resorcinol and formaldehyde. Both supercritical (aerogel) and vacuum (xerogel) drying were performed and, after carbonization, xerogel sample was split in several portions which were physically activated with CO_2. Finally, we ended up with six samples (AC16, AC16X, AC16X5, AC16X10, AC16X20 and AC16X40).

Samples were characterized by gas physical adsorption (N_2 and CO_2 isotherms) and Scanning Electron Microscopy (SEM) in order to analyze how both drying process

and activation were influencing the textural properties and the morphology of our material. Textural characterization data showed great differences between aerogel AC16 and xerogel AC16X. Micropore volume is larger for AC16, and changes on morphology can also be appreciated within the macroporosity range. SEM microphotographs of AC16 show a macropore network formed by interconnection of smaller spherical particles. However, in AC16X this structure is not present anymore, probably because it collapsed during the drying process.

Regarding to activation process and its consequences on textural properties, those are different depending on the activation percentage. For low activated samples (till 5-10%) new micropores are generated within the carbon material, therefore, there is an increase on micropore volume but the mean micropore width is equal or even smaller. When samples are further activated (above 20%) micropores are broadened, since most of the active sites for gasification reaction with carbon dioxide are inside already formed micropores. Because of that micropore volume keeps increasing, not due to new micropores, but mainly due to the micropore width enlargement.

After analyzing the influence of the drying and the physical activation processes on the textural properties of our samples, dynamic adsorption experiment with n-octane and/or TMP contaminated air fluxes were performed. For single gases experiment, relationships with both narrower and wider microporosity were obtained for n-octane adsorption capacities and only with broader microporosity for TMP ones. It is suitable to remember at this point that TMP is bulkier than n-octane and can not enter in the slightest micropores (below 0.7 nm), which is explaining these results.

When competitive adsorption results are examined and compared with those for n-octane dynamic adsorption on its own, the conclusion is clear: n-octane adsorption on our samples is not very influenced by the presence of TMP. Steric hindrance of TMP is leading to this behaviour in two different ways: avoiding the entering into the narrowest microporosity and attenuating adsorbate-adsorbent interactions with carbon surface active sites on wide micropores.

To sum up, by means of carbon dioxide activation, microporosity can be tailored depending on the application that we want for our carbon material (gas separation or VOCs filter). If we want to adsorb every hydrocarbons present on contaminated air (canister) it is needed a well developed microporosity to retain also the bulkiest compounds[21,30,31]. When our material will be utilised to separate branched from linear hydrocarbons, only narrow micropores are useful, so that large activation percentages should be avoided or other procedures to block micropore entries (as chemical vapour deposition) must be performed[33].

6.5. REFERENCES

[1] R.G. Bansal, J.B. Donnet, and F. Stoeckli, *Activated Carbon*, Marcel Dekker, New York and Basel, 1988.

[2] T.D. Burchel, *Carbon materials for advanced technologies*, Elsevier Science, Amsterdam, 1999.

[3] H. Marsh and F. Rodríguez-Reinoso, *Activated Carbon*, Elsevier, Oxford, 2006.

[4] C. Moreno-Castilla, F. Carrasco-Marín, M.V. López-Ramón, and M.A. Alvarez-Merino, Chemical and physical activation of olive-mill waste water to produce activated carbons, *Carbon*, **39** (2001) 1415-1420.

[5] F. Rodríguez-Reinoso and M. Molina-Sabio, Activated carbons from lignocellulosic materials by chemical and/or physical activation: an overview, *Carbon*, **30** (1992) 1111-1118.

[6] S.A. Al-Muhtaseb and J.A. Ritter, Preparation and Properties of Resorcinol–Formaldehyde Organic and Carbon Gels, *Advanced Materials*, **15** (2003) 101-114.

[7] T.F. Baumann, M.A. Worsley, T.Y.-J. Han, and J. Satcher, High surface area carbon aerogel monoliths with hierarchical porosity, *Journal of Non-Crystalline Solids*, **354** (2008) 3513-3515.

[8] M. Inagaki, Pores in carbon materials-importance of their control, *New Carbon Materials*, **24** (2009) 193-232.

[9] J. Lee, J. Kim, and T. Hyeon, Recent Progress in the Synthesis of Porous Carbon Materials, *Advanced Materials*, **18** (2006) 2073-2094.

[10] F.J. Maldonado-Hódar, Advances in the development of nanostructured catalysts based on carbon gels, *Catalysis Today*, **218–219** (2013) 43-50.

[11] R.W. Pekala, Low density, resorcinol-formaldehyde aerogels, US Patent, *US4997804 A*, 1991.

[12] E. Gallegos-Suárez, A.F. Pérez-Cadenas, F.J. Maldonado-Hódar, and F. Carrasco-Marín, On the micro- and mesoporosity of carbon aerogels and xerogels. The role of the drying conditions during the synthesis processes, *Chemical Engineering Journal*, **181–182** (2012) 851-855.

[13] S. Román, J.F. González, C.M. González-García, and F. Zamora, Control of pore development during CO2 and steam activation of olive stones, *Fuel Processing Technology*, **89** (2008) 715-720.

[14] J.F. Denayer, W. Souverijns, P.A. Jacobs, J.A. Martens, and G.V. Baron, High-Temperature Low-Pressure Adsorption of Branched C5−C8 Alkanes on Zeolite Beta, ZSM-5, ZSM-22, Zeolite Y, and Mordenite, *Journal of Physical Chemistry B*, **102** (1998) 4588-4597.

[15] L.I. Devriese, J.A. Martens, J.W. Thybaut, G.B. Marin, G.V. Baron, and J.F.M. Denayer, A new methodology to probe Shape Selectivity in Porous Adsorbents, *Microporous and Mesoporous Materials*, **116** (2008) 607-613.

[16] G.C. Laredo, J. Castillo, and J.O. Marroquin, Gas-phase diffusion of linear and multi-branched alkanes on a carbon molecular sieve by the ZLC method, *Separation and Purification Technology*, **103** (2013) 36-42.

[17] J.A.C. Silva and A.E. Rodrigues, Separation of n/iso-paraffins mixtures by pressure swing adsorption, *Separation and Purification Technology*, **13** (1998) 195-208.

[18] S. Brunauer, P.H. Emmett, and E. Teller, Adsorption of gases in multimolecular layers, *Journal of the American Chemical Society*, **60** (1938) 309-319.

[19] M.M. Dubinin, Inhomogeneous microporous structures of carbonaceous adsorbents, *Carbon*, **19** (1981) 321-324.

[20] F. Stoeckli, *Porosity in carbon. Characterization and applications*. Eds. Patrick J. Arnold, London, 1995.

[21] J.F. Vivo-Vilches, E. Bailón-García, A.F. Pérez-Cadenas, F. Carrasco-Marín, and F.J. Maldonado-Hódar, Tailoring activated carbons for the development of specific adsorbents of gasoline vapors, *Journal of Hazardous Materials*, **263, Part 2** (2013) 533-540.

[22] P.N. Cheremisinoff and F. Ellerbusch, *Carbon Adsorption Handbook*, Ann Arbor Science Pub. ed., Michigan, 1978.

[23] G.M. Luckchis, Adsorption systems 1. Design by mass-transfer-zone concept, *Chemical Engineering*, **80** (1973) 111.

[24] A.J. Michaels, *Industrial Chemistry, Vol. 44*, Washington D.C., 1952.

[25] W.J.J. Webber, *Physiochemical Processes for Water Quality Control*, Wiley-Interscience ed., New Cork, 1972.

[26] G.O. Wood, A review of the effects of covapors on adsorption rate coefficients of organic vapors adsorbed onto activated carbon from flowing gases, *Carbon*, **40** (2002) 685-694.

[27] L. Yanxu, C. Jiangyao, and S. Yinghuang, Adsorption of multicomponent volatile organic compounds on semi-coke, *Carbon*, **46** (2008) 858-863.

[28] D. Cazorla-Amorós, J. Alcañiz-Monge, M.A. Casa-Lillo, and A. Linares-Solano, CO2 as an Adsorptive To Characterize Carbon Molecular Sieves and Activated Carbons, *Langmuir*, **14** (1998) 4589-4596.

[29] D. Lozano-Castelló, D. Cazorla-Amorós, and A. Linares-Solano, Usefulness of CO_2 adsorption at 273 K for the characterization of porous carbons, *Carbon*, 42 (2004) 1233-1242.

[30] U. Mohr, Activated carbon canisters for automobiles, *Filtration & Separation*, **34** (1997) 1016-1018.

[31] K. Sato and N. Kobayashi, Adsorption and Desorption Simulation of Carbon Canister Using n-Butane as Model Compound of Gasoline, *Journal of the Japan Petroleum Institute*, **54** (2011) 136-145.

[32] S. Lagorsse, F.D. Magalhaes, and A. Mendes, Carbon molecular sieve membranes: Sorption, kinetic and structural characterization, *Journal of Membrane Science*, **241** (2004) 275-287.

[33] D. Lozano-Castello, J. Alcaniz-Monge, D. Cazorla-Amorós, A. Linares-Solano, W. Zhu, F. Kapteijn, and J.A. Moulijn, Adsorption properties of carbon molecular sieves prepared from an activated carbon by pitch pyrolisis, *Carbon*, **43** (2005) 1643-1651.

Capítulo VII

BIOGAS UPGRADING BY SELECTIVE ADSORPTION ONTO CO_2 ACTIVATED CARBON FROM WOOD PELLETS

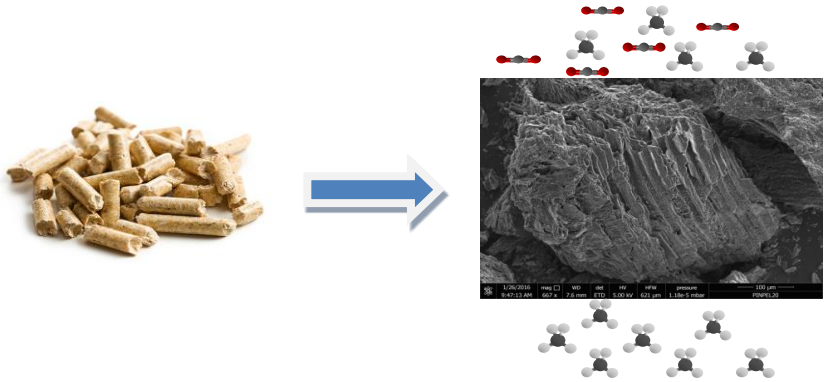

BIOGAS UPGRADING BY SELECTIVE ADSORPTION ONTO CO_2 ACTIVATED CARBON FROM WOOD PELLETS

Article sent to Journal of Environmental Chemical Engineering

Highlights

- Activated carbon from commercial pine wood pellets was prepared.
- Physical activation increased micropore volume and the accessibility to macropores.
- Changes in porosity lead to a very selective CO_2 adsorbent for biogas upgrading.
- The material is an excellent candidate for CO_2/CH_4 separation in dynamic conditions.

Abstract

An activated carbon from commercial pine wood pellets was obtained by means of physical activation with carbon dioxide. Carbonized sample was also prepared in order to compare both samples. Carbonization lead to a material with very low micropore volume, which was increased when physical activation was performed ($W_0(N_2)$ from 0.00 to 0.22 $cm^3 \cdot g^{-1}$ and $W_0(CO_2)$ from 0.21 to 0.31 $cm^3 \cdot g^{-1}$). After characterizing their porous texture, samples were tested as CO_2 selective adsorbent in a mixture of CH_4 and CO_2; at first high pressure isotherms of both compounds were obtained at different temperatures to calculate the adsorbed amount of each compound at given pressure and temperature (for PINPEL20: CO_2, q_{sat} = 6.66 $mol \cdot kg^{-1}$ and ΔH_{ads}= 28.4 $kJ \cdot mol^{-1}$; CH_4, q_{sat} = 3.36 $mol \cdot kg^{-1}$ and ΔH_{ads}= 19.0 $kJ \cdot mol^{-1}$). Variations on isosteric heat of adsorption with uptake were also analysed (it was increased with uptake in the case of CO_2 and the opposite tendency was found for CH_4). Selectivity resulted larger for the activated sample (2.9 versus 1.9 at 1 bar and 30 °C), so this one was chosen to perform dynamic adsorption experiments. Breakthrough curves demonstrated the outstanding performance of sample as CO_2 selective adsorbent in both single component experiments (Breakthrough time 995 s for CH_4 and 1545 s for CO_2) and competitive adsorption (950 s for CH_4 and 1373 s for CO_2). Activated sample showed an excellent behaviour as CO_2 selective adsorbent for biogas upgrading.

Keywords: Activated carbon; biogas upgrading; carbon dioxide; selective adsorption.

7.1. INTRODUCTION

There is an increasing interest on finding alternatives to fossil fuels, especially in countries which are energetically dependent on others. Nowadays, it is more and more frequent to find processes in which biomass is used to obtain biofuels such as bioethanol or biodiesel, and also biogas (produced by anaerobic digestion of organic waste). Biogas and natural gas in general (methane) is a cleaner energy source than other heavier hydrocarbons, since it produces the highest amount of energy regarding the quantity of CO_2 generated during its combustion[1-5]. Nevertheless, in the case of biogas, the main drawback is its high content on carbon dioxide (it might be as high as 40% or more) which significantly reduces its heating capacity. Therefore, for biogas to be used, a previous separation step in order to reduce the CO_2 content is needed[6-12].

There are several methodologies for biogas upgrading such as amine absorption[13,14], membrane separation[15], cryogenic distillation or adsorption-based technologies[6-9,12,16,17]. Nowadays, the most used is the CO_2 absorption by liquid amines; however, the interaction between amines and CO_2 is very strong, so a high energy supply is needed in order to regenerate the absorptive system[7]. Adsorption-based technologies present as main advantage the lower energetic demand for regeneration, and also they are easier to scale-down than the others[3,7-12,16,17]. Regeneration can be performed by several methods as changing pressure (Pressure Swing Adsorption, PSA), temperature (Temperature Swing Adsorption, TSA; Electric Swing Adsorption, ESA) or applying vacuum (vacuum pressure swing adsorption, VPSA).

Regarding the adsorbent, typically zeolites[10,12,17,18] or activated carbons[1,6,9,11,12,16-25] are used, but there are also several works where metal-organic frameworks (MOFs) serve at this purpose[7,8,17,21,26]. Each of them present advantages and drawbacks, but activated carbons are the ones with lower price, since they can be obtained from agricultural waste materials. Activated carbons from very different origins have been tested, sometimes functionalized with different heteroatoms[1,19,20,24,27]. When choosing the activation method, it needs to be considered that a preferential adsorption for CO_2 regarding CH_4 is required. In this sense, physical activation with

CO_2 is preferable to steam or chemical activation, since these methods produce a larger micropore widening[9].

As it was previously mentioned, activated carbons can be obtained from a wide variety of natural sources, being common choices agricultural wastes. From them, wood-based materials are frequently used as raw materials[9,25,28-30]. In Spain, but also in other countries, wood pellets obtained from hot extrusion of pine wood residues in the shape of chips from logging or pruning waste are replacing almond shells or olive stones on house-heating systems. This cheap raw material is a good candidate to obtain activated carbon, since it is already pelletized, and it can be activated without destroying its structure. In some published research works people make their own pellets from wood sawdust and ashes with binders[30], but the use of already commercialized materials with no binder will lower the cost of final material.

In our work, an activated carbon obtained by physical activation of pine wood pellets used in domestic heating applications was selected to be tested on the selective adsorption of CO_2 from a CH_4/CO_2 mixture. After characterizing its porous texture, equilibrium isotherms of target molecules were obtained at different temperatures in order to calculate maximum adsorbed amounts and specific heats of adsorption. Finally, adsorptive beds were packed into a column in order to perform breakthrough experiments for single component and binary mixtures of CH_4 and CO_2.

7.2. MATERIALS AND METHODS

7.2.1. Synthesis of samples

Pine wood pellets supplied by Los Reyes del Pellet C.B. were used as raw material. These pellets are prepared by hot extrusion of pine chips with pressure and temperature. The humidity must be controlled, since there is no binder as lignin will serve this purpose, and proper water proportion is required. These pellets were used to obtain two samples: one by carbonization under N_2 atmosphere and another by carbonization/activation with CO_2. The pellets were weighed and thermal treatments were applied with a heating ramp of 10°C min^{-1} up to 900°C. Carbonization was

performed on N_2 (300 cm^3min^{-1}) and once at 900°C the samples were either kept at this temperature for two hours (PINPEL); or the inlet gas was switched to CO_2 and the temperature maintained for five hours in the case of physically activated sample (PINPEL20). Final yield of the carbonization/activation process was 25% in the case of PINPEL and 20% in the case of PINPEL20, so the burn off degree of sample PINPEL20 resulted on 20% (regarding the one carbonized under nitrogen, activated sample weighed 20% less).

7.2.2. Textural characterization of samples

N_2 adsorption-desorption isotherms at -196 °C and CO_2 adsorption at 0 °C were obtained in a QUADRASORB SI (Quantachrome Inc.) and analysed in order to determine textural properties of material. Specific surface area (S_{BET}) from BET equation applied to N_2 isotherm and micropore volumes (W_0) calculated from Dubinin-Raduskevich model for the two gases were obtained, as well as micropore mean width (L_0) from Stoeckli equation. BJH model was applied to desorption branch of N_2 isotherms in order to obtain the Pore Size Distribution (PSD) in the mesopore range. QSDFT was also applied in order to obtain PSD for microporosity. Scanning electron microscopy was also used to take microphotographs of sample surface. The instrument used was a Leo, Carl Zeiss, Geminy-153.

Mercury Intrusion Porosimetry was performed at Pedro Nunes Institute, Coimbra using an AUTOPORE IV 9500 (Micromeritics). This technique was applied to obtain PSD for wider mesopores and macropores and to calculate bulk densities of samples, in order to estimate the amount adsorbed of different gases per volume unit (which could be more important than the mass based amount in some cases).

7.2.3. Equilibrium isotherms of CH_4 and CO_2 at high pressures

The CH_4 and the CO_2 adsorption isotherms at 30, 50 and 70°C were obtained in a pressure range from 0 to 10 bar by using a magnetic suspension balance (Rubotherm, Germany). This instrument presents as its main advantage, comparing to conventional gravimetric apparatus, the fact that the measuring module is physically separated from

the sample container and the rest of the instrument so more drastic measurement conditions can be used. This system is also more accurate than conventional equipments and density measurements can be assessed since it contains a reference volume (sinker) inside.

Before measuring the adsorption isotherms, samples were activated under vacuum (P<0.01bar) at 150°C for 24 hours and Helium pycnometry was performed in order to calculate skeletal density and sample volume, so correction of buoyancy effect could be made. Then gases were introduced at different pressures and variations on weight were followed till equilibrium was achieved. The amount adsorbed at several pressures were obtained in order to calculate and analyse the adsorption/desorption isotherms. Isotherms were fitted to Langmuir or Toth model (Equation 7.1 and 7.2), using the same fitting for the three isotherms at different temperatures. After that, individual fittings were applied to 30 and 50°C isotherms and isosteric pressures were obtained from 70°C isotherm experimental data and from the individual fittings at 50°C and 30°C. Isosteric heats of adsorption where then calculated by applying Equation 7.3:

$$q = q_{sat}\frac{bP}{(1+(bP)^n)^{1/n}} \qquad \text{Equation 7.1}$$

$$b = b_0 e^{\frac{-\Delta H_{ads}}{RT}} \qquad \text{Equation 7.2}$$

$$(\Delta H_{ads})_q = -R\left(\frac{\partial(lnP)}{\partial(1/T)}\right)_q \qquad \text{Equation 7.3}$$

Where q, adsorbed amount, and, q_{sat}, saturation capacity (mol kg^{-1}); b, Langmuir/Toth constant (bar^{-1}); n, the heterogeneity parameter (n=1 for the Langmuir model); P and T, pressure and temperature (bar, K); and ΔH_{ads}, heat of adsorption (kJ mol^{-1}).

7.2.4. Breakthrough experiments

A bed with 113.5g of PINPEL20 was packed into a column of 90.1 cm (Fig. 7.1). Glass wool was placed at both ends of the column, so final height of the bed was

88.1 cm. Once packed, column was pressurized at 2 bar with He and activation was performed by heating the system up to 150 °C (2 °C min^{-1}, 24 hours) under a continuous flow of He. After cooling, the bed was weighed again, resulting in 111.4 g of dry PINPEL20 (around 2% of mass loss). A Gas Chromatograph Master GC (DANI) with FID and TCD detection and a capillary column (HPPLOT U) was used to quantify CH_4 and CO_2 at the exit (T injector, 180 °C; T oven, 50 °C; T TCD, 180 °C). Three mass flow controllers (MFC) were used to set the amount of each gas that would enter inside the column and a mass flow meter (MFM) was placed at the exit. Three thermocouples were placed at different heights of the system to record the temperature histories of both adsorption and desorption processes (one of the sensors was placed touching the wall of the stainless steel column to measure changes on its temperature).

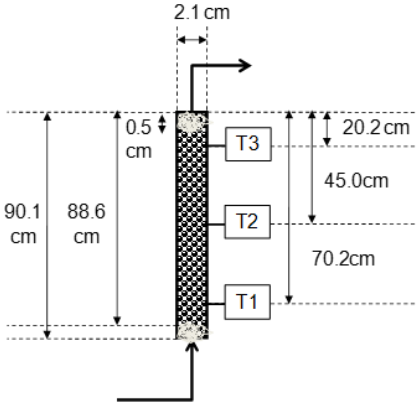

Figure 7.1. Length of column for PINPEL20 and other important distances.

Conditions for breakthrough experiments were P = 1.5 bar; T = 30 °C; Q = 0.3 L min^{-1} (STP); x = 0.6 for CO_2 and 0.4 for CH_4. When single component adsorption was tested, gases were diluted with He to get the total flux. In the case of desorption, He passed through the column in the same conditions (P, T and Q).

7.3. RESULTS AND DISCUSSION

7.3.1. Textural Characterization

N_2 isotherm (Fig. 7.2a) corresponds to a micro-mesoporous material in the case of PINPEL20. Almost no N_2 adsorption was observed for the sample PINPEL. CO_2

isotherms (Fig. 7.2b) were also obtained in order to get narrow micropore volume. PSD was determined by QSDFT, BJH and Mercury Intrusion Porosimetry in order to cover the range of porosity between wider micropores (> 0.7 nm) and macropores (Fig. 7.2c). When PINPEL and PINPEL20 are compared, two remarkable things are observed: the first consists on a huge increment on micropore volume, which is common for carbon materials activated with CO_2; but also, there is an increment on the mesopore volume obtained by BJH and macropore one obtained by Mercury Intrusion Porosimetry. Since these pores are similar in size to those present on PINPEL sample, it could be concluded that CO_2 is reacting also within the inter-particle voids (wood pellets are formed by extrusion of small particles which link one to another by means of humidity, heat and pressure due to the lignin and wood resins) improving the accessibility to the porosity of the sample. In terms of bulk density, the increase of porosity for sample PINPEL20 results in a remarkable reduction of this parameter compared to the one of PINPEL (Table 7.1). Micropore widening is also denoted by the increment on $W_0(N_2)$ and $L_0(CO_2)$.

Table 7.1. Textural properties obtained from N_2 and CO_2 isotherms and Hg porosimetry.

Sample	S_{BET}	$W_0(N_2)$	$W_0(CO_2)$	$L_0(CO_2)$	V_{BJH}	ρ_{Hg}
	$m^2 \cdot g^{-1}$	$cm^3 \cdot g^{-1}$	$cm^3 \cdot g^{-1}$	Nm	$cm^3 \cdot g^{-1}$	$g \cdot cm^{-3}$
PINPEL	0	0.00	0.21	0.61	0.03	0.83
PINPEL20	561	0.22	0.31	0.84	0.10	0.52

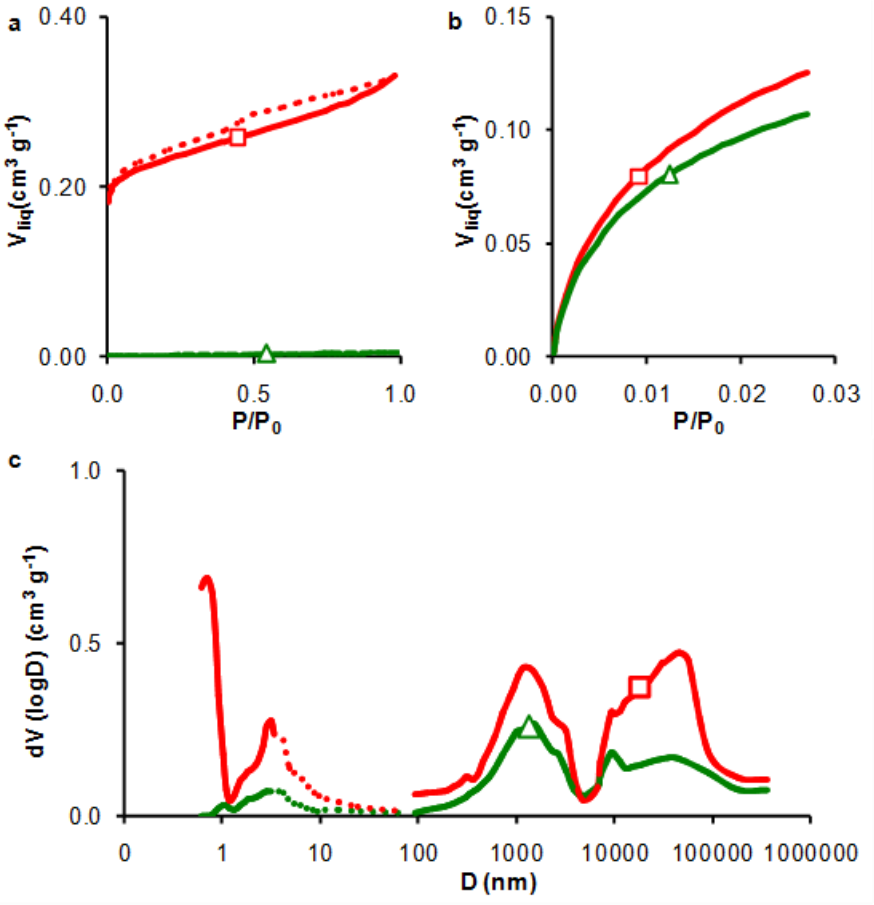

Figure 7.2. a) Adsorption (continuous) and desorption (dashed) N_2 isotherms at -196°C. b) Adsorption CO_2 isotherms at 0°C. c) PSD obtained from different techniques QSDFT (continuous); BJH (dots); Hg porosimetry (symbol). PINPEL20 (□), PINPEL (△).

SEM microphotographs of carbon surface were obtained in order to analyse the morphology of carbonized wood pellets and the consequences of CO_2 activation on it (Fig. 7.3). They reveal that CO_2 activation affected not only the microporosity of the sample, but also the external surface, since carbon dioxide reacted with wood walls. This is in good agreement with the fact that mesopore and macropore volume increased after activation, as it was previously pointed out.

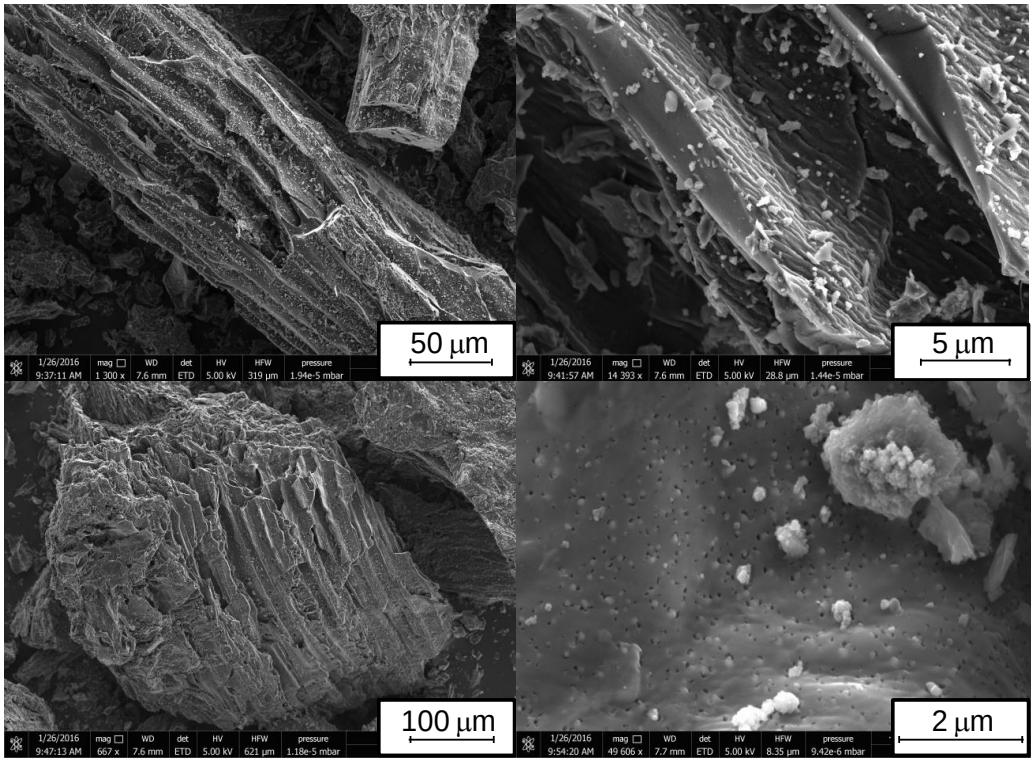

Figure 7.3. SEM microphotographs of samples PINPEL (top) and PINPEL20 (bottom).

7.3.2. CO_2 and CH_4 isotherms at different temperatures

Once porous texture of samples was characterized, they were introduced in a gravimetric equipment in order to obtain adsorption-desorption isotherms for the target gases, CO_2 and CH_4 (Fig. 7.4). Variation of the isosteric heat of adsorption with adsorbed amount was calculated by analyzing the isotherms at different temperatures. Desorption was also performed to observe if isotherms presented hysteresis loops. As commented, experimental data were fitted to Langmuir or Toth model depending on the suitability of each one. From them, different parameters were obtained by minimizing the fitting error regarding experimental points (Table 7.2).

PINPEL was only used in order to compare its behaviour with the one of PINPEL20, and, due to its poorer selectivity and its lower CO_2 adsorption capacity this sample was not tested in CO_2/CH_4 separation under dynamic conditions. By using Langmuir/Toth fittings (for CO_2 and CH_4) variation of ideal selectivity with total

pressure for a 50%/50% mixture of both gases was obtained (Fig. 7.5), showing that PINPEL20 presented the largest selectivity in the all range of pressure tested.

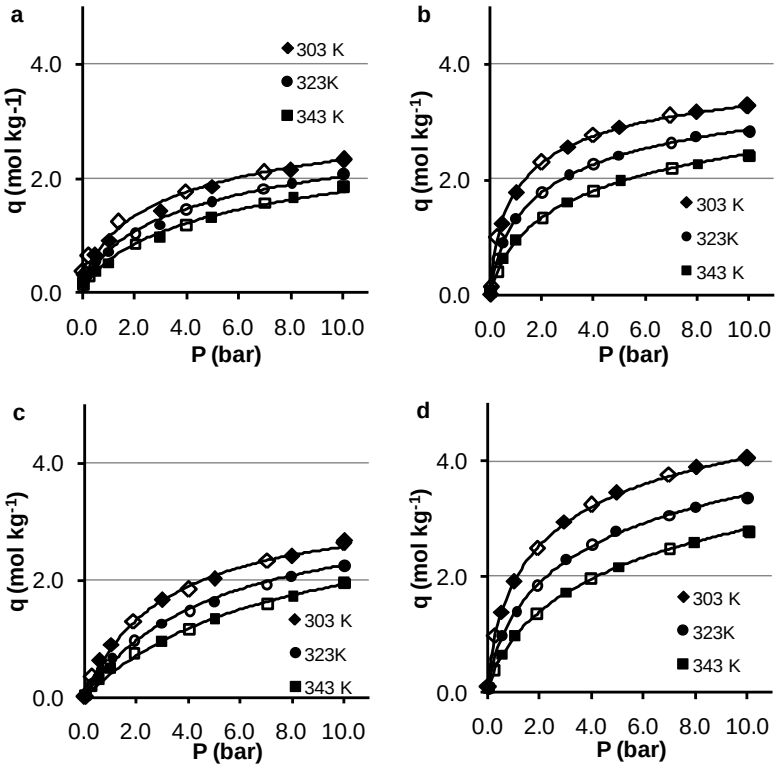

Figure 7.4. Adsorption (close) and desorption (open) isotherms of CH_4 (a, c) and CO_2 (b, d). PINPEL (top), PINPEL20 (bottom).

Table 7.2. Parameters obtained from CO_2 and CH_4 isotherms by applying Langmuir or Toth model.

Sample	Compound	Model	q_{sat} mol kg^{-1}	b_0 bar^{-1}	$\|\Delta H_{ads}\|$ kJ mol^{-1}	n
PINPEL	CH_4	Toth	4.05	$3.12 \cdot 10^{-4}$	19.9	0.52
	CO_2	Toth	4.49	$1.60 \cdot 10^{-5}$	30.0	0.53
PINPEL20	CH_4	Langmuir	3.36	$1.72 \cdot 10^{-4}$	19.0	-
	CO_2	Toth	6.66	$1.79 \cdot 10^{-5}$	28.4	0.49

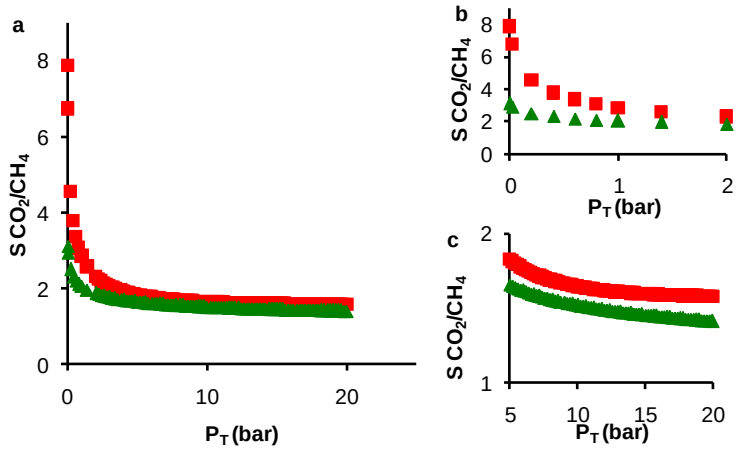

Figure 7.5. Variation of CO_2/CH_4 ideal selectivity for a 50%/50% mixture with total pressure for PINPEL20 (■) and PINPEL (▲). a) All the range of P; b) Low pressures; c) High pressures.

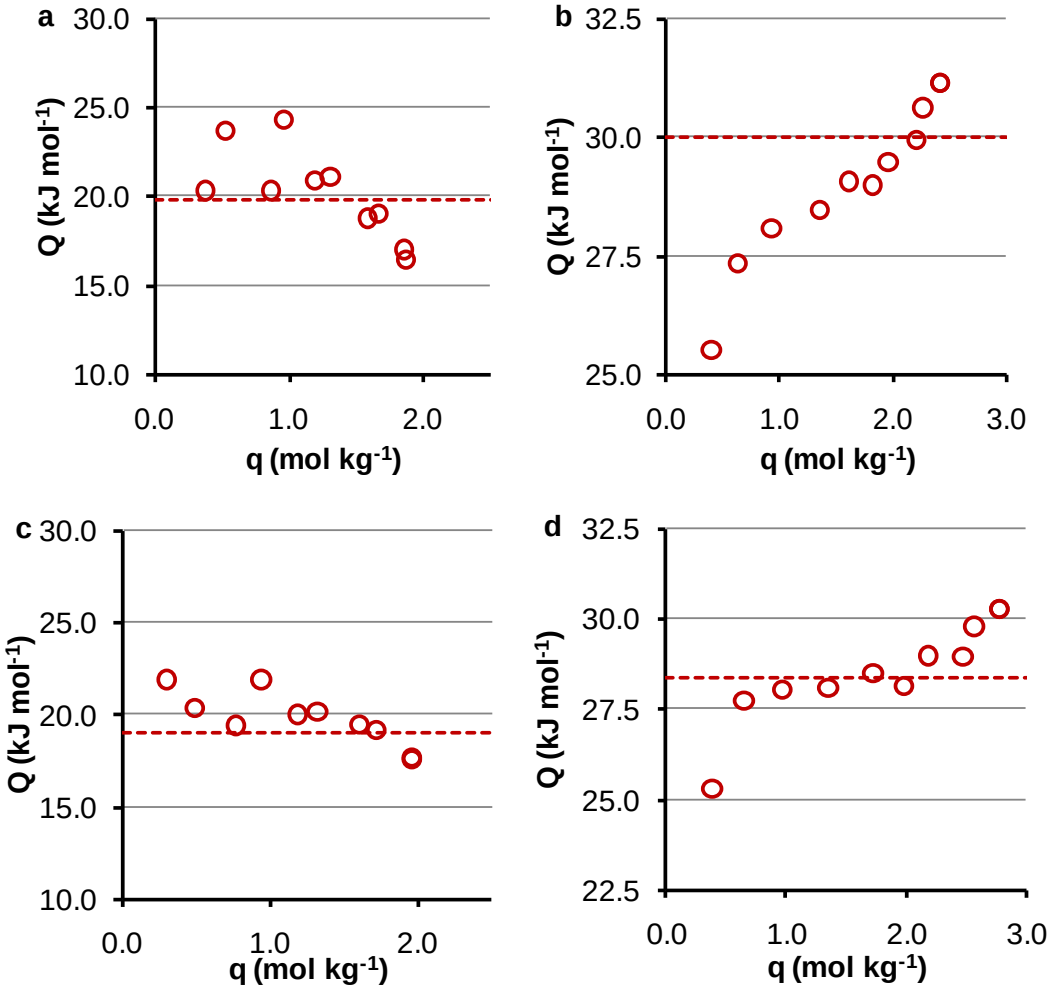

Figure 7.6. Variation of isosteric heat of adsorption (Q) with adsorbed amount (q) for CH_4 (a, c) and CO_2 (b, d). PINPEL (top), PINPEL20 (bottom).

From the analysis of the isotherms, variation of isosteric heat of adsorption with adsorbed amount can be also studied. In this case, similar conclusions were obtained for the two samples: the isosteric heat of adsorption decreased with uptake in the case of CH_4 and increased when CO_2 was used as adsorbate (Fig. 7.6). Heat of adsorption calculated from Langmuir or Toth fitting are included on the plots as a reference.

7.3.3. Breakthrough experiments

Breakthrough experiments were performed only with the activated sample PINPEL20 since it was the one with the highest CO_2/CH_4 selectivity. Instrument and conditions were described on the previous section. After measuring the concentration of each gas and the volumetric flow rate (STP) at the exit at different times, these values were converted to molar fluxes in order to represent its variation with time. To represent breakthrough curves by using molar fluxes presents as main advantage that its integration to obtain adsorbed amounts is direct. When breakthrough curves of CO_2 and CH_4 were compared (Fig. 7.7 and 7.8), it was observed an earlier breakthrough time for the methane (995s versus 1545s) even though concentration of carbon dioxide on the stream was larger than the one of methane (60% for CO_2 and 40% for CH_4). The adsorbent was totally regenerated after the experiment by switching inlet gas to pure He. Regarding temperature profiles, it is observed that temperature increased more when CO_2 was adsorbed. This is related to the difference between heat of adsorptions for both compounds (Table 7.2).

When binary adsorption breakthrough curves (Fig. 7.9a) were analyzed and compared with single component experiments, several differences were observed. For instance, the breakthrough point for methane remained more or less the same (Table 7.3) while the adsorbed amount became smaller. The opposite tendency was observed for CO_2, where the adsorption front is more dispersed, so breakthrough time was shortened, but after displacing the methane, adsorbed amount at the end resulted very similar to the one for single component experiment. In fact, this dispersion was clearly observed in temperature profiles (Fig. 7.9b and 7.9c), and was due to the displacment of methane by the carbon dioxide front. When the adsorption front reached the thermocouple located at the middle of the column, the adsorption peaks for CH_4 and

CO_2 were already distinguishable, and the second one (corresponding to CO_2 adsorption) became wider than the peak observed for single component adsorption.

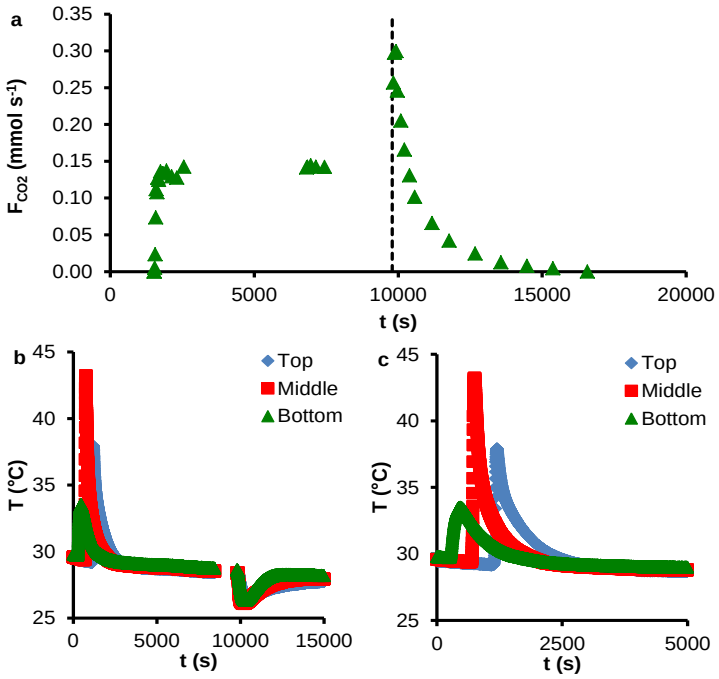

Figure 7.7. a) Breakthrough curve for dynamic adsorption of CO_2 (60%) onto PINPEL20. b) Temperature profiles for the three sections of the column. c) Temperature profiles detailed for adsorption.

Table 7.3. Parameters obtained from the analysis of PINPEL20 breakthrough curves.

Experiment	Inl. Conc. %	q_{ads} mol kg^{-1}	t_b s	q_{ads} (V) mol dm^{-3}
Single CO_2	60% CO_2 (in He)	2.14	1545	1.11
Single CH_4	40% CH_4 (in He)	0.99	995	0.52
Binary	40% CH_4	0.43	1373	0.22
	60% CO_2	2.14	950	1.11

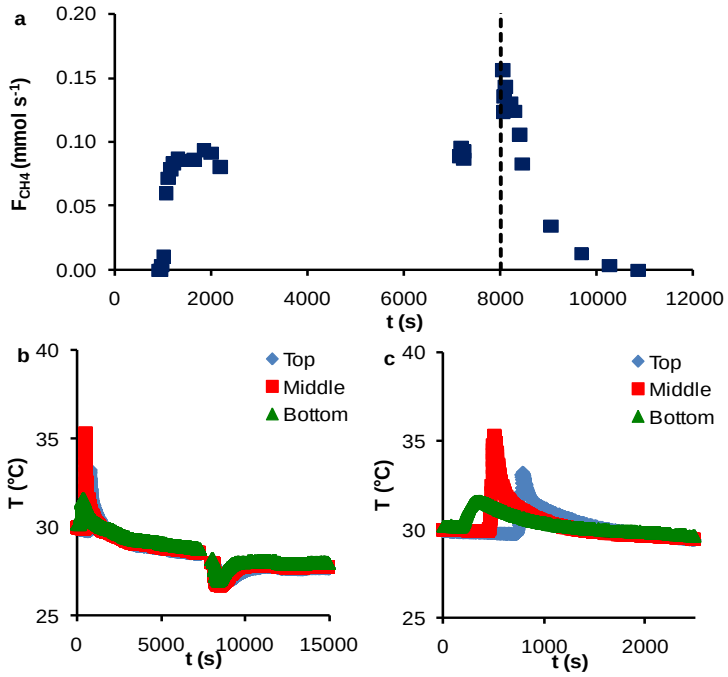

Figure 7.8. a) Breakthrough curve for dynamic adsorption of CH_4 (40%) onto PINPEL20. b) Temperature profiles for the three sections of the column. c) Temperature profiles detailed for adsorption.

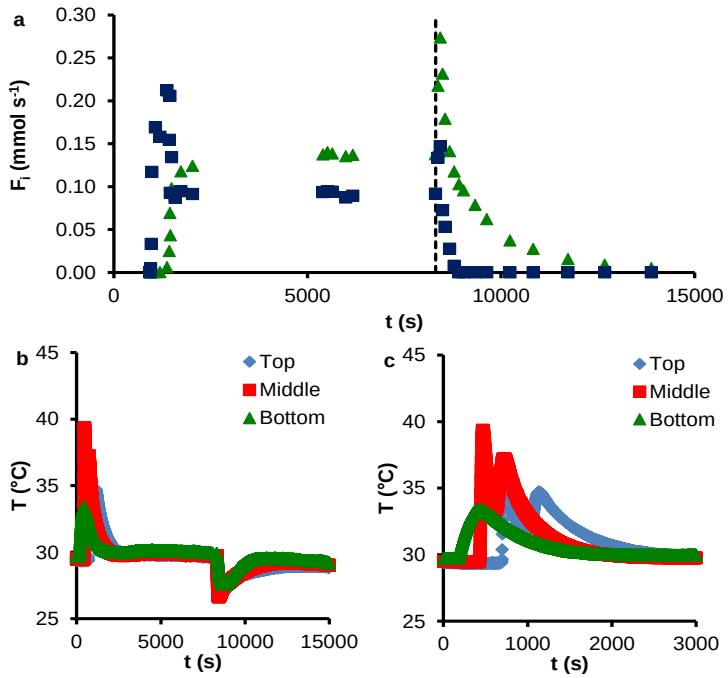

Figure 7.9. a) Breakthrough curve for dynamic adsorption of a gas mixture (60% CO_2 (▲)and 40% CH_4 (■)) onto PINPEL20. b) Temperature profiles for the three sections of the column. c) Temperature profiles detailed for adsorption.

7.4. CONCLUSIONS

An activated carbon with excellent CO_2 to CH_4 selectivity was prepared from commercial wood pellets used on domestic heating applications by physical activation with carbon dioxide at high temperature. The treatment generated a considerable volume of micropores which mean width was around 0.84 nm. These micropores are responsible for the difference between CO_2 adsorbed amount for PINPEL20 sample and the one for PINPEL. This increment on CO_2 adsorbed amount was much larger than on CH_4 one, so there was a great increment on CO_2/CH_4 selectivity in the all range of pressures.

Equilibrium adsorption results are in good agreement with breakthrough ones, since breakthrough time and adsorbed amount for CO_2 are larger than for CH_4. Furthermore, when both compounds were introduced inside the reactor, the breakthrough for CH_4 occurred much earlier than for CO_2 and there was a part of the experiment where only methane was detected at the exit of the column, moreover, for several seconds with concentrations of 100%. Therefore, under these conditions, PINPEL20 was able to separate CH_4 and CO_2, obtaining pure CH_4 from a 60% CO_2 and 40% CH_4 mixture.

To sum up, PINPEL20 is a sample obtained from a cheap commercial product constituted by biomass waste (wood pellets), activated with CO_2 at high temperature, which is a simple and relatively fast process, and with excellent properties as CO_2/CH_4 selective adsorbent. Therefore, it would be a really good candidate to be applied on biogas upgrading by adsorption-based technologies.

7.5. REFERENCES

[1] W. Djeridi, N. Ben Mansour, A. Ouederni, P.L. Llewellyn, and L. El Mir, Influence of the raw material and nickel oxide on the CH4 capture capacity behaviors of microporous carbon, *International Journal of Hydrogen Energy*, **40** (2015) 13690-13701.

[2] J. Alcañiz-Monge, D. Lozano-Castelló, D. Cazorla-Amorós, and A. Linares-Solano, Fundamentals of methane adsorption in microporous carbons, *Microporous and Mesoporous Materials*, **124** (2009) 110-116.

[3] M. Gu, B. Zhang, Z. Qi, Z. Liu, S. Duan, X. Du, and X. Xian, Effects of pore structure of granular activated carbons on CH4 enrichment from CH4/N2 by vacuum pressure swing adsorption, *Separation and Purification Technology*, **146** (2015) 213-218.

[4] S. Biloé, V. Goetz, and A. Guillot, Optimal design of an activated carbon for an adsorbed natural gas storage system, *Carbon*, **40** (2002) 1295-1308.

[5] J. Alcañiz-Monge, M.A. Casa-Lillo, D. Cazorla-Amorós, and A. Linares-Solano, Methane storage in activated carbon fibres, *Carbon*, **35** (1997) 291-297.

[6] Y.J. Wu, Y. Yang, X.M. Kong, P. Li, J.G. Yu, A.M. Ribeiro, and A.E. Rodrigues, Adsorption of Pure and Binary CO2, CH4, and N2 Gas Components on Activated Carbon Beads, *Journal of Chemical Engineering Data*, **60** (2015) 2684-2693.

[7] P. Serra-Crespo, R. Berger, W. Yang, J. Gascon, and F. Kapteijn, Separation of CO2/CH4 mixtures over NH2-MIL-53−An experimental and modelling study, *Chemical Engineering Science*, **124** (2015) 96-108.

[8] A.F.P. Ferreira, A.M. Ribeiro, S. Kulaç, and A.E. Rodrigues, Methane purification by adsorptive processes on MIL-53(Al), *Chemical Engineering Science*, **124** (2015) 79-95.

[9] N. Álvarez-Gutiérrez, M.V. Gil, F. Rubiera, and C. Pevida, Adsorption performance indicators for the CO2/CH4 separation: Application to biomass-based activated carbons, *Fuel Processing Technology*, **142** (2016) 361-369.

[10] J.A.C. Silva, A.F. Cunha, K. Schumann, and A.E. Rodrigues, Binary adsorption of CO2/CH4 in binderless beads of 13X zeolite, *Microporous and Mesoporous Materials*, **187** (2014) 100-107.

[11] Y.J. Kim, Y.S. Nam, and Y.T. Kang, Study on a numerical model and PSA (pressure swing adsorption) process experiment for CH4/CO2 separation from biogas, *Energy*, **91** (2015) 732-741.

[12] M.C. Campo, A.M. Ribeiro, A.F.P. Ferreira, J.C. Santos, C. Lutz, J.M. Loureiro, and A.E. Rodrigues, Carbon dioxide removal for methane upgrade by a VSA process using an improved 13X zeolite, *Fuel Processing Technology*, **143** (2016) 185-194.

[13] J. Kim, D.A. Pham, and Y.I. Lim, Gas–liquid multiphase computational fluid dynamics (CFD) of amine absorption column with structured-packing for CO2 capture, *Computers & Chemical Engineering*, **88** (2016) 39-49.

[14] Y. Liu, H. Li, G. Wei, H. Zhang, X. Li, and Y. Jia, Mass transfer performance of CO2 absorption by alkanolamine aqueous solution for biogas purification, *Separation and Purification Technology*, **133** (2014) 476-483.

[15] Z. Bacsik, O. Cheung, P. Vasiliev, and N. Hedin, Selective separation of CO2 and CH4 for biogas upgrading on zeolite NaKA and SAPO-56, *Applied Energy*, **162** (2016) 613-621.

[16] B.M. Jeong, E.S. Ahn, J.H. Yun, C.H. Lee, and D.K. Choi, Ternary adsorption equilibrium of H2/CH4/C2H4 onto activated carbon, *Separation and Purification Technology*, **55** (2007) 335-342.

[17] J. McEwen, J.D. Hayman, and A. Ozgur Yazaydin, A comparative study of CO2, CH4 and N2 adsorption in ZIF-8, Zeolite-13X and BPL activated carbon, *Chemical Physics*, **412** (2013) 72-76.

[18] M. Kacem, M. Pellerano, and A. Delebarre, Pressure swing adsorption for CO2/N2 and CO2/CH4 separation: Comparison between activated carbons and zeolites performances, *Fuel Processing Technology*, **138** (2015) 271-283.

[19] H.R. Yu, S. Cho, B.C. Bai, K.B. Yi, and Y.S. Lee, Effects of fluorination on carbon molecular sieves for CH4/CO2 gas separation behavior, *International Journal of Greenhouse Gas Control*, **10** (2012) 278-284.

[20] S. Furmaniak, P. Kowalczyk, A.P. Terzyk, P.A. Gauden, and P.J.F. Harris, Synergetic effect of carbon nanopore size and surface oxidation on CO2 capture from CO2/CH4 mixtures, *Journal of Colloid and Interface Science*, **397** (2013) 144-153.

[21] Z.H. Rada, H.R. Abid, J. Shang, Y. He, P. Webley, S. Liu, H. Sun, and S. Wang, Effects of amino functionality on uptake of CO2, CH4 and selectivity of CO2/CH4 on titanium based MOFs, *Fuel*, **160** (2015) 318-327.

[22] M.V. Gil, N. Álvarez-Gutiérrez, M. Martínez, F. Rubiera, C. Pevida, and A. Morán, Carbon adsorbents for CO2 capture from bio-hydrogen and biogas streams: Breakthrough adsorption study, *Chemical Engineering Journal*, **269** (2015) 148-158.

[23] C.A. Grande, R. Blom, A. Möller, and J. Möllmer, High-pressure separation of CH4/CO2 using activated carbon, *Chemical Engineering Science*, **89** (2013) 10-20.

[24] T. Dasgupta, S.N. Punnathanam, and K.G. Ayappa, Effect of functional groups on separating carbon dioxide from CO2/N2 gas mixtures using edge functionalized graphene nanoribbons, *Chemical Engineering Science*, **121** (2015) 279-291.

[25] D.J. Seo, Z. Gou, H. Fujita, T. Fujii, and A. Sakoda, Simple fabrication of molecular sieving carbon for biogas upgrading via a temperature controlled carbonization of Phyllostachys pubescens, *Renewable Energy*, **86** (2016) 693-702.

[26] X. Wu, M. Niknam Shahrak, B. Yuan, and S. Deng, Synthesis and characterization of zeolitic imidazolate framework ZIF-7 for CO2 and CH4 separation, *Microporous and Mesoporous Materials*, **190** (2014) 189-196.

[27] A. Heidari, H. Younesi, A. Rashidi, and A.A. Ghoreyshi, Evaluation of CO2 adsorption with eucalyptus wood based activated carbon modified by ammonia solution through heat treatment, *Chemical Engineering Journal*, **254** (2014) 503-513.

[28] A.R. Mohamed, M. Mohammadi, and G.N. Darzi, Preparation of carbon molecular sieve from lignocellulosic biomass: A review, *Renewable and Sustainable Energy Reviews*, **14** (2010) 1591-1599.

[29] A. Amaya, N. Medero, N. Tancredi, H. Silva, and C. Deiana, Activated carbon briquettes from biomass materials, *Bioresource Technology*, **98** (2007) 1635-1641.

[30] M.G. Plaza, I. Durán, F. Rubiera, and C. Pevida, CO2 adsorbent pellets produced from pine sawdust: Effect of coal tar pitch addition, *Applied Energy*, **144** (2015) 182-192.

[31] M.J. Regufe, J. Tamajon, A.M. Ribeiro, A. Ferreira, U.H. Lee, Y.K. Hwang, J.S. Chang, C. Serre, J.M. Loureiro, and A.E. Rodrigues, Syngas Purification by Porous Amino-Functionalized Titanium Terephthalate MIL-125, *Energy Fuels*, **29** (2015) 4654-4664.

Capítulo VIII

RESORCINOL-FORMALDEHYDE CARBON XEROGEL AS SELECTIVE ADSORBENT OF CARBON DIOXIDE PRESENT ON BIOGAS

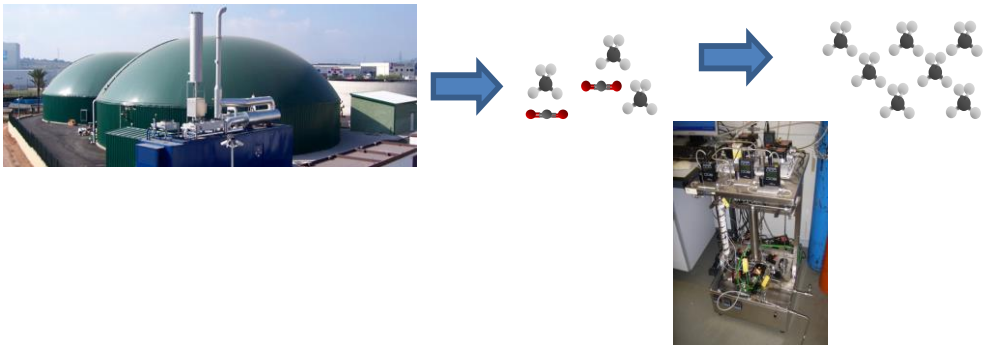

RESORCINOL-FORMALDEHYDE CARBON XEROGEL AS SELECTIVE ADSORBENT OF CARBON DIOXIDE PRESENT ON BIOGAS

Article to be sent to Separation and Purification Technology

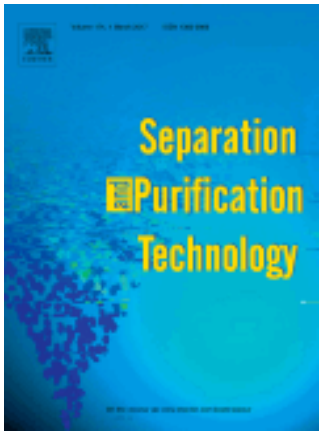

Highlights

- Resorcinol-Formaldehyde carbon xerogel was obtained employing Cs_2CO_3 as catalyst.
- An adsorbent with developed microporosity and macroporosity was synthesized.
- This material showed a large CO_2 to CH_4 selectivity in equilibrium adsorption.
- Carbon xerogel could be an excellent CO_2 selective adsorbent from CO_2/CH_4 mixtures.

Abstract

A carbon xerogel obtained by carbonization of a Resorcinol-Formaldehyde polymer which was synthesized using Cs_2CO_3 as catalyst was employed as CO_2 selective adsorbent for biogas upgrading. The material presented a large narrow micropore volume ($W_0(CO_2)$ = 0.34 $cm^3 \cdot g^{-1}$) and macropore one; as expected for a carbon xerogel, these macropores were very regular in size. The CO_2 preferential adsorption onto this material was tested by analysing equilibrium isotherms of both gases (CO_2 and CH_4) and breakthrough curves at different inlet concentrations. Equilibrium studies showed a large CO_2 uptake (q_{sat} = 6.57 $mol \cdot kg^{-1}$ and ΔH_{ads}= 28.4 $kJ \cdot mol^{-1}$) regarding CH_4 one (q_{sat} = 3.83 $mol \cdot kg^{-1}$ and ΔH_{ads}= 19.6 $kJ \cdot mol^{-1}$) which results in a high CO_2 to CH_4 selectivity, specially at low pressures. Dynamic adsorption of both gases at different concentrations demonstrated the excellent performance of our xerogel in biogas upgrading by selective adsorption of CO_2.

Keywords: Carbon xerogel; biogas upgrading; carbon dioxide; selective adsorption.

8.1. INTRODUCTION

Biogas is obtained by anaerobic digestion of diverse materials such as manure, crops and food industry wastes. Depending on the source, its composition may vary, but it contains mainly carbon dioxide (more than 30%) and methane (about 60%)[1-4]. The rest of contaminants which conformed the rest of the mixture are air and really hazardous compounds such as siloxanes or hydrogen sulphide at low concentrations[4,5]. These are removed before biogas can be utilized in electric power plants or other applications where it is not necessary to remove CO_2. Nevertheless, biogas needs to be transformed into biomethane (CO_2 separation) for applications which imply the transport of liquefied CH_4 (LBG), since methane needs to be compressed[6-10]. Furthermore, the main application of biomethane it is to be used as fuel, so high heat capacity, which is lower for CO_2 than for CH_4, is required.

In order to perform the separation of CO_2, process known as biogas upgrading, several technologies have been studied. Cryogenic distillation[7] or membrane separation[9] are some of the alternatives to liquid amine absorption[8,10,11], the one utilized nowadays in the industry. The main problem with the chemical absorption is the amount of energy required to regenerate the amines[6,10,12]. To solve this problem, adsorption-based technologies are presented as a sound alternative for CO_2/CH_4 separation, and there is an increasing interest on finding suitable materials for the selective adsorption of carbon dioxide from biogas stream[6,10,12-20]. Several materials have been tested at this purpose: Metal-organic frameworks (MOFs)[16,21], functionalized silica[17,20], zeolites[13,15] and carbon based materials[12,14,18,19,22-25]. From these last, activated carbons from agricultural wastes could be a proper choice due to their low prize, which makes them very competitive[12,18,19]; however, their main drawback is that the control of pore size through activation methods is hard, and often, their textural properties strongly depends on the raw material.

Over the last years, a great effort has been made in finding synthetic routes which yield nanostructured carbon materials from polymeric precursors[22,26-30]. Carbon precursors obtained by sol-gel polymerization of different monomers (such as aromatic compounds or sugars) have been widely studied[29-32]. From them, resorcinol-

formaldehyde gels are commonly found in literature for different applications since Pekala patented the first one in the early 90s[26,27]. The versatility of this process where people can vary the catalyst, dilution ratio, solvent, temperature, drying method and other variables, joint to its reproducibility are the two main factors which make it so attractive for researchers[29,31-35].

In our work, a resorcinol-formaldehyde carbon xerogel was utilized as CO_2 selective adsorbent for biogas upgrading. The material was synthesized, characterized by diverse techniques, and then tested in the adsorption of both gases (carbon dioxide and methane) under equilibrium and dynamic conditions. Results were analyzed in order to optimize the textural properties of samples which will be used in future work.

8.2. MATERIALS AND METHODS

8.2.1. Synthesis of XCs300

A carbon xerogel was obtained by carbonization of a polymer made by resorcinol and formaldehyde (Fig. 8.1). The recipe used to obtain this xerogel was very similar to one already published by our group[34]. Briefly, resorcinol and formaldehyde in a 1:2 molar proportion were dissolved in water (R/W=0.07) joint to the polymerization catalyst which was Cs_2CO_3 (R/C=300). Once reactants and catalyst were totally dissolved, solution was transferred to cylindrical glass moulds with 6 mm of inner diameter, and moulds were sealed. Then, a temperature program was selected to perform the gelification and curing of the RF hydrogel (1 day, 25 °C; 1 day, 50 °C and 5 days, 80 °C). The polymeric precursor was then removed from glass moulds, cut into pellets of 2-3 cm and dried in a furnace at 110°C till constant weight to obtain the organic Xerogel (in the case of Morales-Torres et al. water was exchanged by acetone before drying). This xerogel was put into a tubular oven and carbonized at 900 °C (1.5 $°C \cdot min^{-1}$) on nitrogen. The sample was labelled as XCs300.

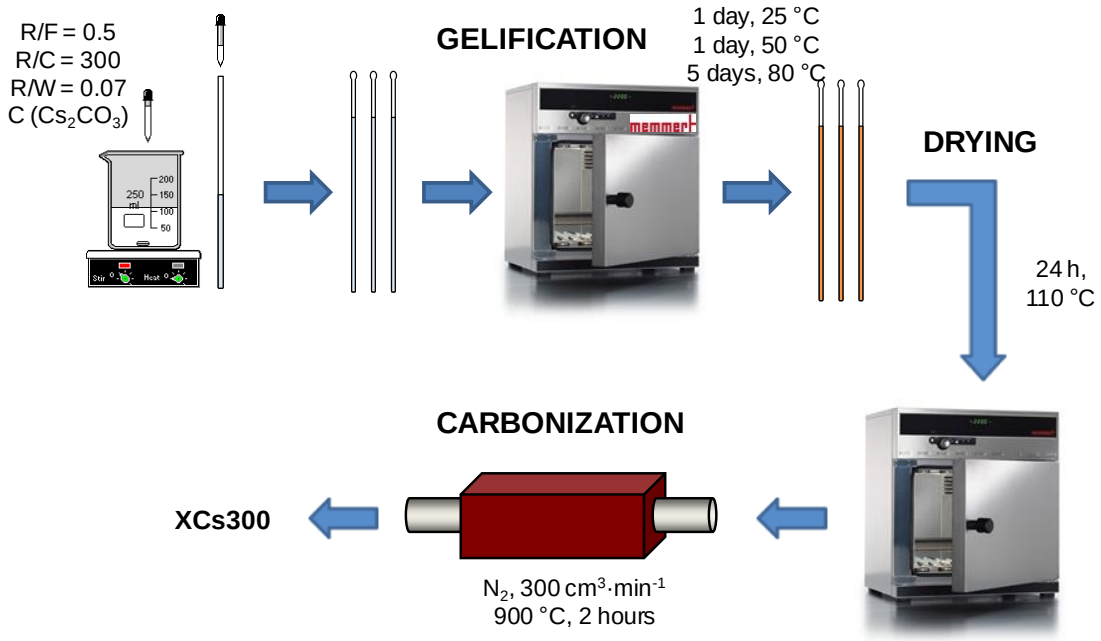

Figure 8.1. Synthesis of XCs300.

8.2.2. Textural characterization

N_2 adsorption-desorption isotherms at -196°C and CO_2 adsorption ones at 0°C were obtained in a QUADRASORB SI (Quantachrome Ins.). Brunauer-Emmett-Teller (BET) equation[36] was applied to N_2 isotherm to obtain specific surface area (S_{BET}) and Dubinin-Raduskevich model[37] was applied to the two isotherms to calculate micropore volumes (W_0), as well as micropore mean width (L_0) from Stoeckli equation[38]. Barrett-Joyner-Halenda (BJH) model[39] was applied to desorption branch of N_2 isotherms in order to obtain the Pore Size Distribution (PSD) in the mesopore range and QSDFT was employed to procure PSD for microporosity. Scanning electron microscopy was also used to take microphotographs of sample surface. The instrument used was a Leo, Carl Zeiss, Geminy-153.

Mercury Intrusion Porosimetry was performed with an AUTOPORE IV 9500 (Micromeritics) at Instituto Pedro Nunes, Coimbra, in order to analyse PSD for wider mesopores and macropores and to calculate bulk densities of samples.

8.2.3. Equilibrium isotherms of CH_4 and CO_2 at high pressures

Isotherms of target compounds were obtained at different temperatures (30 °C, 50 °C and 70 °C). The pressure was varied from 0 to 10 bars and differences in weight were registered with a magnetic suspension balance (Rubotherm, Germany).

Firstly, samples were activated under vacuum at 150°C for 24 hours and after cooling, Helium pycnometry was performed to obtain skeletal density and sample volume, so buoyancy correction could be performed. After that, different pressures of methane or carbon dioxide were introduced into the equipment, measuring the weight changes on the sample and waiting till equilibrium was reached. From these data, gas uptakes at different pressures were obtained ($kg \cdot mol^{-1}$) and equilibrium isotherms were analysed by fitting experimental points to Langmuir/Toth model (Equations 8.1 and 8.2) and the same equation was used for the three isotherms of each gas. Finally, in order to obtain the variation of isosteric heat of adsorption with loading (Equation 8.3) individual regression curves were adjusted to experimental points at 30°C and 50°C. These plots and experimental points at 70°C were used to calculate the characteristic curve for each adsorbent-adsorbate system from isosteric pressures.

$$q = q_{sat}\frac{bP}{(1+(bP)^n)^{1/n}} \qquad \text{Equation 8.1}$$

$$b = b_0 e^{\frac{-\Delta H_{ads}}{RT}} \qquad \text{Equation 8.2}$$

$$(\Delta H_{ads})_q = -R\left(\frac{\partial(lnP)}{\partial(1/T)}\right)_q \qquad \text{Equation 8.3}$$

Where q, adsorbed amount, and, q_{sat}, saturation capacity ($mol\ kg^{-1}$); b, Langmuir/Toth constant (bar^{-1}); n, the heterogeneity parameter (n=1 for the Langmuir model); P and T, pressure and temperature (bar, K); and ΔH_{ads}, heat of adsorption ($kJ\ mol^{-1}$).

8.2.4. Breakthrough experiments

Adsorptive bed was packed with 10.2 g of XCs300, resulting on a column of 9.1 cm in height, with an inner diameter of 2.3 cm (Fig. 8.2). The activation was performed on He (100 $cm^3 \cdot min^{-1}$) at 150 °C for 24 hours. Detection at the exit was made by using an infrared gas analyser GasDataLMSxiTypeG4.18 (GasDataLtd,UK).

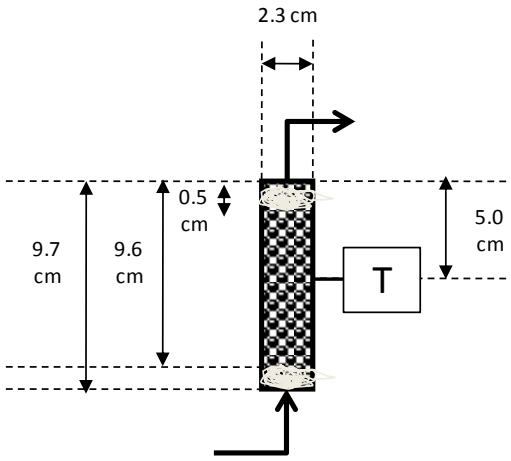

Figure 8.2. Length of column for XCs300 and other important distances.

Several breakthrough tests were performed at 30°C and 2.5 bar, varying inlet concentration. Three mass flow controllers (MFC) were used to set the amount of each gas that would enter inside the column and a mass flow meter (MFM) was placed at the exit. Temperature variation was registered by means of a thermocouple located at the middle part of the column. Once saturated, XCs300 was isothermally regenerated by switching inlet gas to Helium.

8.3. RESULTS AND DISCUSSION

8.3.1. Textural Characterization

XCs300 is a micro-mesoporous xerogel with a type I-IV nitrogen isotherm (Fig. 8.3a) where a great amount of gas was adsorbed at low pressures but the adsorption continued at higher pressures. A large hysteresis loop which covers different

pressures indicates the presence of mesopores of diverse width as denoted by the PSD curve (Fig. 8.3c). A large portion of micropores are narrow, therefore, $W_0(CO_2)$, micropore volume calculated from CO_2 isotherm (Fig. 8.3b), resulted larger than $W_0(N_2)$, calculated from N_2 one (Table 8.1). Regarding Mercury Intrusion Porosimetry, the corresponding PSD showed a maximum at 100 nm with macropores very regular in size (±20nm) and rising 4.0 $cm^3 \cdot g^{-1}$ which is a considerable volume. This homogeneity in the pore size within the meso-macropore range is usual for carbon gels[29,31,32], since these pores are generated during the sol-gel polymerization (although a shrinkage is produced when gels are dried and carbonized, so the width of these pores is reduced, but homogeneity is maintained). The large volume of macropores present on XCs300 is responsible for its low bulk density (Table 8.1).

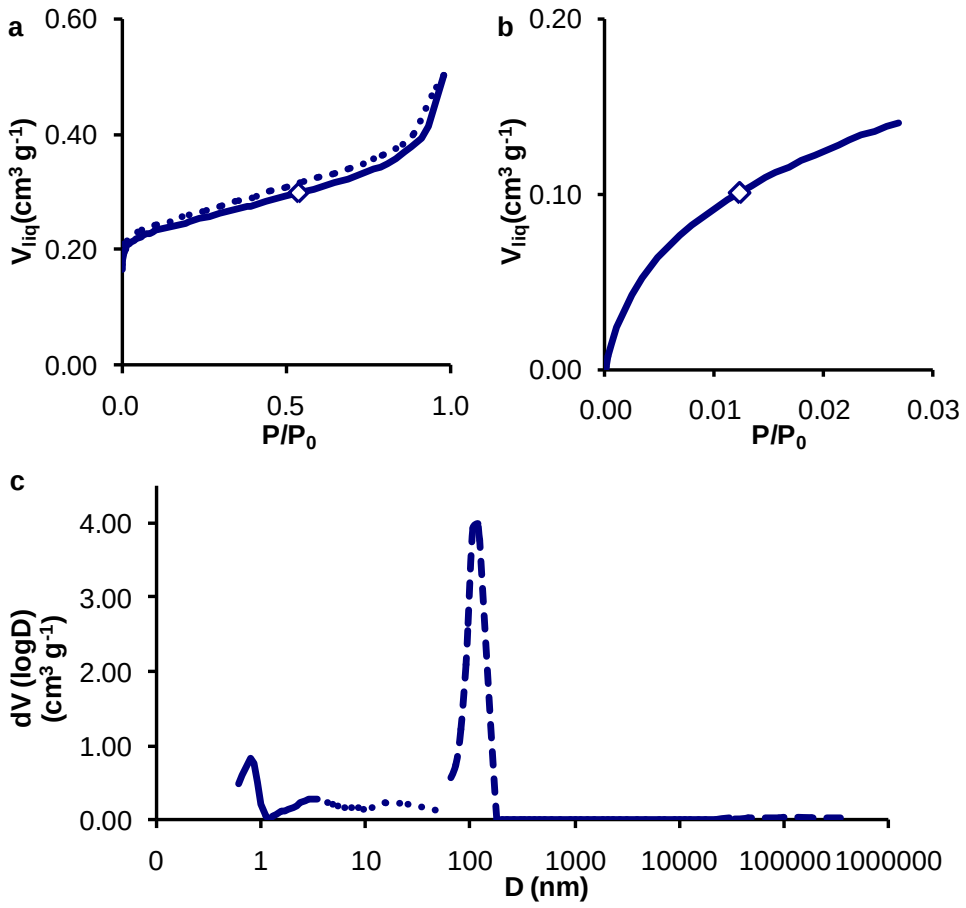

Figure 8.3. a) Adsorption (continuous) and desorption (dashed) N_2 isotherms at -196°C. b) Adsorption CO_2 isotherms at 0°C. c) PSD obtained from different techniques QSDFT (continuous); BJH (dots); Hg porosimetry (dashed). XCs300.

Table 8.1. Textural properties of sample XCs300.

Sample	S_{BET} $m^2 \cdot g^{-1}$	$W_0(N_2)$ $cm^3 \cdot g^{-1}$	$W_0(CO_2)$ $cm^3 \cdot g^{-1}$	$L_0(CO_2)$ nm	V_{BJH} $cm^3 \cdot g^{-1}$	ρ_{Hg} $g \cdot cm^{-3}$
XCs300	591	0.23	0.34	0.73	0.27	0.58

SEM microphotographs showed the typical structure for Resorcinol-Formaldehyde carbon gels. Xerogels are conformed by spherical particles which are more or less condensed depending on the synthesis conditions, the drying and the carbonization process. In the case of XCs300, it is constituted by particles of approximately 50 nm, very regular in size, but forming some agglomerates. The void space between each group of condensate particles was about 100 nm which is consistent with PSD obtained by Mercury Intrusion Porosimetry.

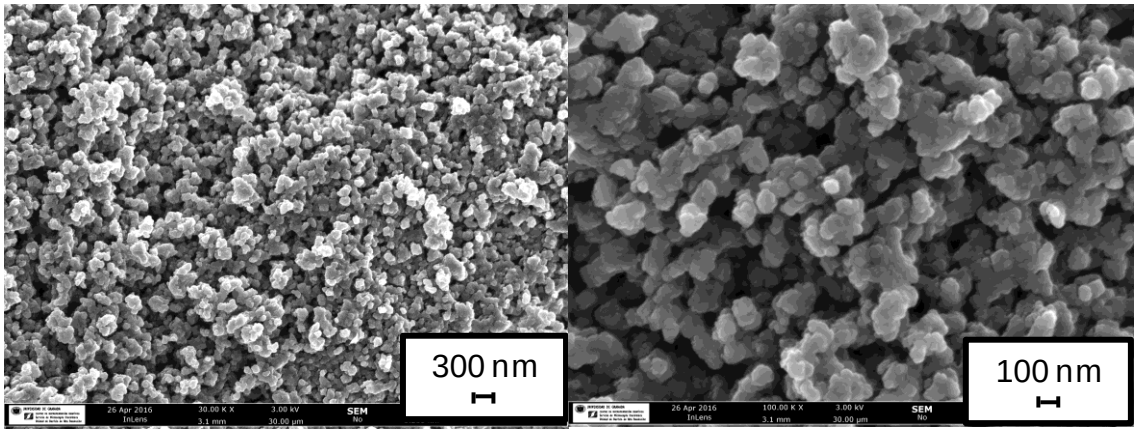

Figure 8.4. SEM microphotographs of XCs300.

8.3.2. Equilibrium CO_2 and CH_4 isotherms at different temperatures

Once porous texture of sample was characterized, it was introduced in a gravimetric equipment in order to obtain adsorption-desorption isotherms for the target gases, CO_2 and CH_4 (Fig. 8.4). As commented in previous section, experimental data

were fitted to Langmuir/Toth model and different parameters were obtained (Table 8.2).

Adsorption isotherms illustrated the preferential CO_2 adsorption regarding CH_4 onto XCs300. At low pressures, CO_2 uptake was several times larger than CH_4's one, and in the range from atmospheric pressure up to 10 bar, the CO_2 adsorbed amount resulted higher than twice the CH_4 one. This is better observed when ideal selectivity for a 50%/50% mixture of both gases is plotted versus total pressure (Fig. 8.5).

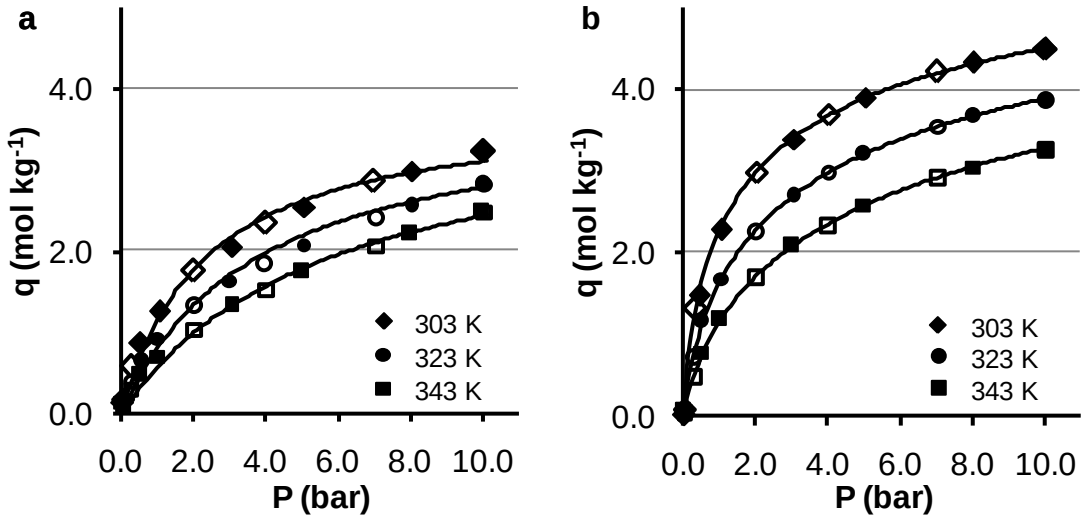

Figure 8.4. Adsorption (close) and desorption (open) isotherms of CH_4 (a) and CO_2 (b).

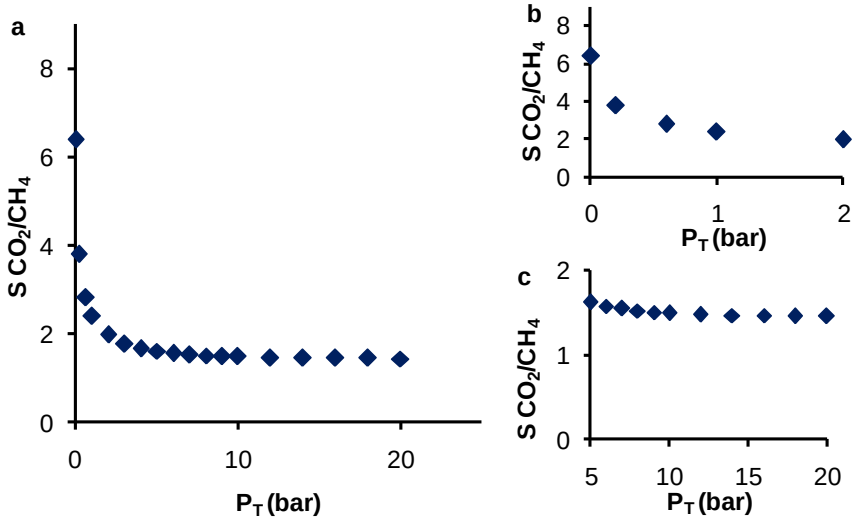

Figure 8.5. Variation of CO_2/CH_4 selectivity with total pressure for XCs300. a) All the range of P; b) Low pressures; c) High pressures.

Table 8.2. Parameters obtained from CO_2 and CH_4 isotherms with Langmuir/Toth model.

Compound	Model	q_{sat} $mol \cdot kg^{-1}$	b_0 bar^{-1}	ΔH_{ads} $kJ \cdot mol^{-1}$	n
CH_4	Langmuir	3.83	$1.81 \cdot 10^{-4}$	19.6	-
CO_2	Toth	6.57	$2.17 \cdot 10^{-5}$	28.4	0.53

Isosteric heat of adsorption was obtained at each loading in order to obtain the characteristic curve for each adsorbate-adsorbent system (Fig. 8.6). The heat of adsorption increased with loading in the case of CO_2 while the opposite tendency was observed for CH_4 adsorption, therefore, the affinity of XCs300 was stronger for CO_2.

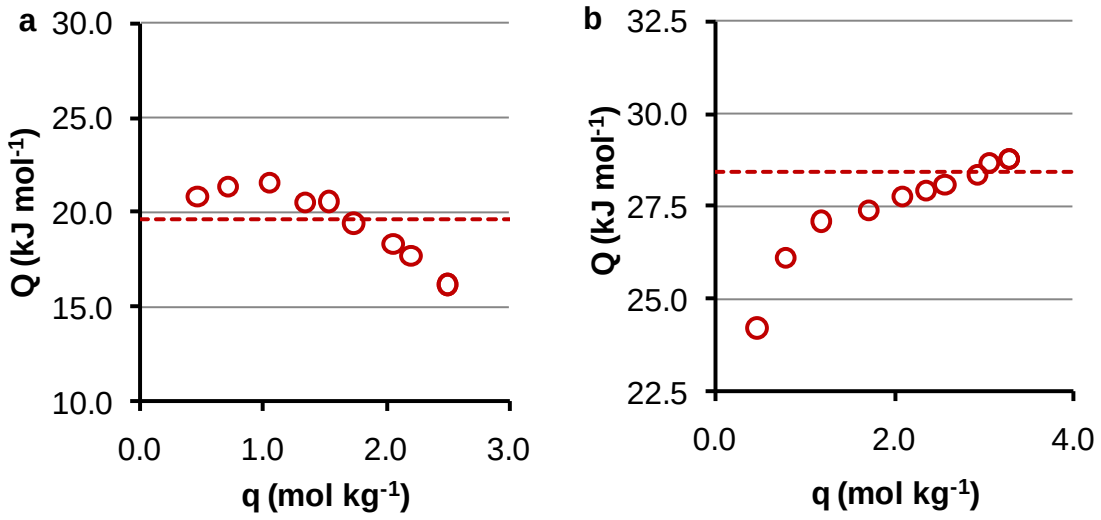

Figure 8.6. Variation of isosteric heat of adsorption (Q) with loading (q) for CH_4 (a) and CO_2 (b).

8.3.3. Dynamic adsorption experiments

Single component breakthrough tests were carried out at different concentrations for each of the gases. Experiments were conducted at 2.5 bar,

temperature was kept at 30°C and temperature variations due to the adsorption and the desorption processes were registered.

Breakthrough curves at 2.5 bar were obtained at several inlet gas concentration to evaluate the adsorptive behaviour of XCs300. Differences in breakthrough times were observed for CH_4 (Fig. 8.7) and CO_2 (Fig. 8.8), specially at larger concentrations, since partial pressure was higher, and the isotherm started to curve (if adsorption capacity increased linearly with gas pressure, breakthrough curves should not change significantly, but this is not the case).

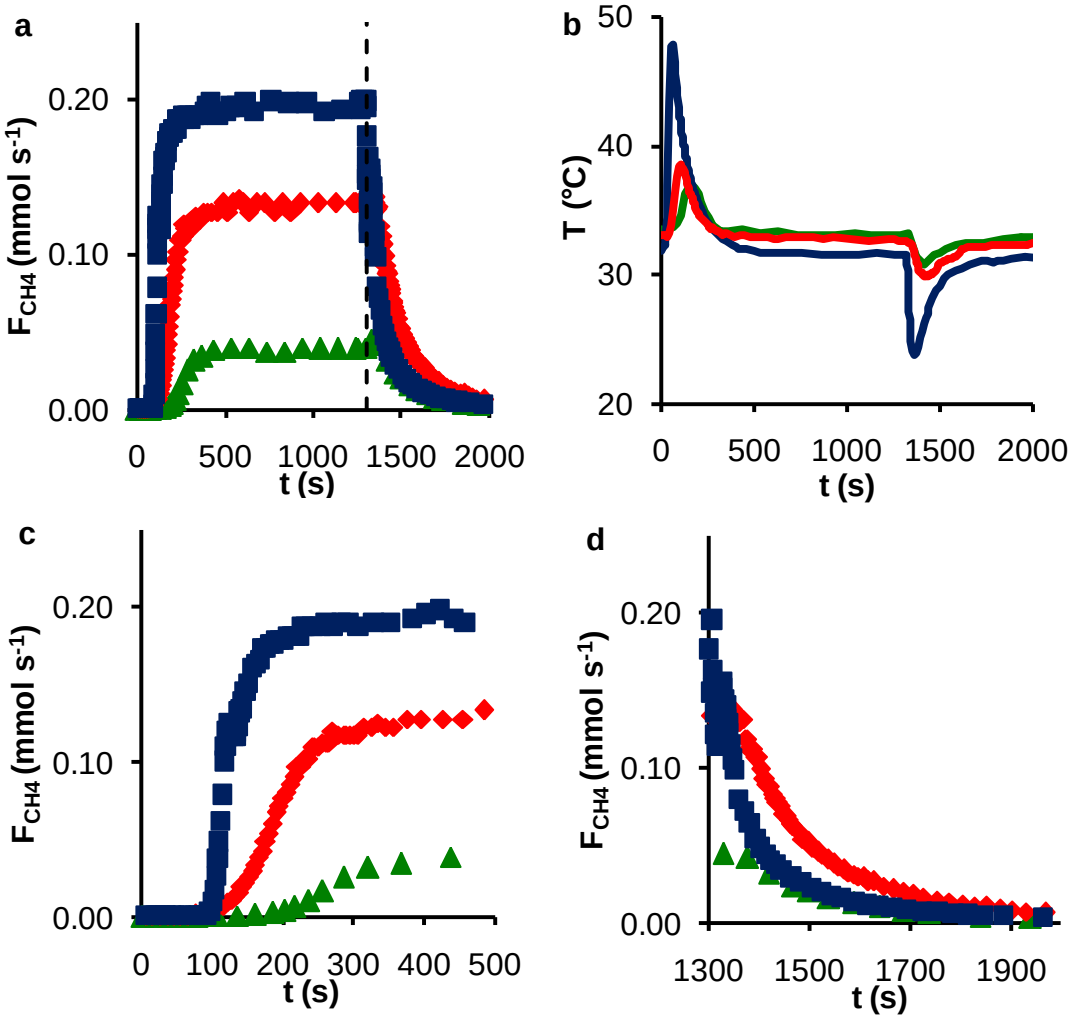

Figure 8.7. Breakthrough curves for CH_4 adsorption onto XCs300. a) Entire experiments, b) Temperature profiles, c) Adsorption branch, d) Desorption branch (after dashed line on a). 100%(■), 63%(◆) and 22%(▲) CH_4 diluted with He.

When breakthrough curves for pure components (100%) are compared, it becomes clear that CH_4 breakthrough time was shorter than CO_2 ones. This difference increased as gas partial pressures decreased, which was not surprising since CO_2 to CH_4 selectivity was larger at low pressures (Fig. 8.5). Regeneration was completed no matter what the conditions were.

Regarding differences between curves at increasing concentration, these are larger in the case of CO_2, where the delay on breakthrough time as concentration decreased were larger. This was also in good agreement with the isotherms (Fig. 8.4), since the adsorption of CO_2 was very large at low pressures and then increased slowly.

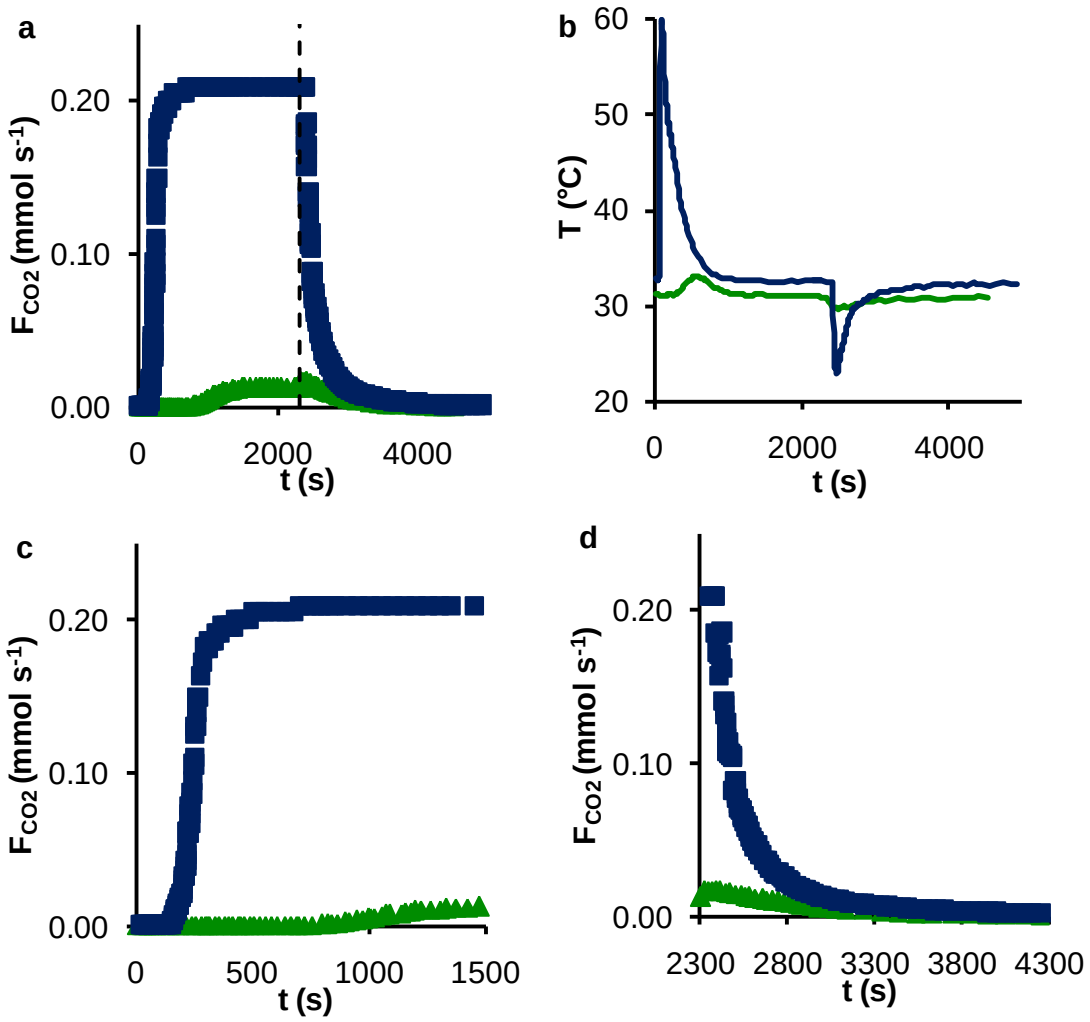

Figure 8.8. Breakthrough curves for CO_2 adsorption onto XCs300. a) Entire experiments, b) Temperature profiles, c) Adsorption branch, d) Desorption branch. 100%(■), 40%(◆) and 8%(▲) CO_2 diluted with He.

Regarding temperature profiles, as expected, the temperature increase was larger as the adsorbed amount was, and also greater for the CO_2 since the specific heat of adsorption was larger and the adsorbed amount also. Single component breakthrough tests, joint to equilibrium isotherms, demonstrated the preferential adsorption of CO_2 regarding CH_4. Nevertheless, binary adsorption experiments should be performed in order to evaluate the behaviour of XCs300 when both gases are present.

Table 8.3. Parameters obtained from single component breakthrough curves at 2.5 bar.

Compound	Inl. Conc.	q_{ads}	t_b
	%	mol kg^{-1}	s
CH_4	22	0.20	136
CH_4	63	2.56	106
CH_4	100	2.60	98
CO_2	8	0.98	756
CO_2	100	6.08	146

8.4. CONCLUSIONS

A carbon xerogel was prepared by carbonization of a resorcinol-formaldehyde gel polymerized using Cs_2CO_3 as catalyst. This material was prepared by a similar procedure to one already published by our group, since porous texture of this sample could be proper for the desired application, which was biogas upgrading.

The micro-mesoporous solid obtained, named XCs300, was characterized and tested as selective adsorbent of CO_2 in CO_2/CH_4 mixtures. This material presented a large volume of micropores, which would be responsible for adsorption, but also mesopore and macropore, these last very regular in size, which would favour the

regeneration of the adsorbent. XCs300 showed high CO_2 to CH_4 selectivity in equilibrium conditions, adsorbing more than twice carbon dioxide regarding methane.

Dynamic adsorption experiments confirmed the excellent behaviour of this sample on biogas upgrading, since breakthrough times for CO_2 were always larger than CH_4 ones even at high concentrations, where the differences between uptakes for the two gases were shorter. Results reflected that XCs300 would be a good candidate to be used as CO_2 selective adsorbent.

8.5. REFERENCES

[1] A. Wu, D. Lovett, M. McEwan, F. Cecelja, and T. Chen, A spreadsheet calculator for estimating biogas production and economic measures for UK-based farm-fed anaerobic digesters, *Bioresource Technology*, **220** (2016) 479-489.

[2] J. Pessuto, B.S. Scopel, D. Perondi, M. Godinho, and A. Dettmer, Enhancement of biogas and methane production by anaerobic digestion of swine manure with addition of microorganisms isolated from sewage sludge, *Process Safety and Environmental Protection*, **104, Part A** (2016) 233-239.

[3] N. Pérez-Rodríguez, D. García-Bernet, and J.M. Domínguez, Effects of enzymatic hydrolysis and ultrasounds pretreatments on corn cob and vine trimming shoots for biogas production, *Bioresource Technology*, **221** (2016) 130-138.

[4] L. Corno, R. Pilu, F. Tambone, B. Scaglia, and F. Adani, New energy crop giant cane (Arundo donax L.) can substitute traditional energy crops increasing biogas yield and reducing costs, *Bioresource Technology*, **191** (2015) 197-204.

[5] N. de Arespacochaga, C. Valderrama, J. Raich-Montiu, M. Crest, S. Mehta, and J.L. Cortina, Understanding the effects of the origin, occurrence, monitoring, control, fate and removal of siloxanes on the energetic valorization of sewage biogas – A review, *Renewable and Sustainable Energy Reviews*, **52** (2015) 366-381.

[6] B. Wu, X. Zhang, Y. Xu, D. Bao, and S. Zhang, Assessment of the energy consumption of the biogas upgrading process with pressure swing adsorption using novel adsorbents, *Journal of Cleaner Production*, **101** (2015) 251-261.

[7] M.J. Tuinier and M. van Sint Annaland, Biogas Purification Using Cryogenic Packed-Bed Technology, *Industrial & Engineering Chemistry Research*, **51** (2012) 5552-5558.

[8] G. Leonzio, Upgrading of biogas to bio-methane with chemical absorption process: simulation and environmental impact, *Journal of Cleaner Production*, **131** (2016) 364-375.

[9] A. Molino, M. Migliori, Y. Ding, B. Bikson, G. Giordano, and G. Braccio, Biogas upgrading via membrane process: Modelling of pilot plant scale and the end uses for the grid injection, *Fuel*, **107** (2013) 585-592.

[10] Q. Sun, H. Li, J. Yan, L. Liu, Z. Yu, and X. Yu, Selection of appropriate biogas upgrading technology-a review of biogas cleaning, upgrading and utilisation, *Renewable and Sustainable Energy Reviews*, **51** (2015) 521-532.

[11] H. Nie, H. Jiang, D. Chong, Q. Wu, C. Xu, and H. Zhou, Comparison of Water Scrubbing and Propylene Carbonate Absorption for Biogas Upgrading Process, *Energy Fuels*, **27** (2013) 3239-3245.

[12] N. Álvarez-Gutiérrez, S. García, M.V. Gil, F. Rubiera, and C. Pevida, Towards Bio-upgrading of Biogas: Biomass Waste-based Adsorbents, *Energy Procedia*, **63** (2014) 6527-6533.

[13] T. Montanari, E. Finocchio, E. Salvatore, G. Garuti, A. Giordano, C. Pistarino, and G. Busca, CO2 separation and landfill biogas upgrading: A comparison of 4A and 13X zeolite adsorbents, *Energy*, **36** (2011) 314-319.

[14] M.V. Gil, N. Álvarez-Gutiérrez, M. Martínez, F. Rubiera, C. Pevida, and A. Morán, Carbon adsorbents for CO2 capture from bio-hydrogen and biogas streams: Breakthrough adsorption study, *Chemical Engineering Journal*, **269** (2015) 148-158.

[15] M.C. Campo, A.M. Ribeiro, A.F.P. Ferreira, J.C. Santos, C. Lutz, J.M. Loureiro, and A.E. Rodrigues, Carbon dioxide removal for methane upgrade by

a VSA process using an improved 13X zeolite, *Fuel Processing Technology*, **143** (2016) 185-194.

[16] X. Wu, B. Yuan, Z. Bao, and S. Deng, Adsorption of carbon dioxide, methane and nitrogen on an ultramicroporous copper metal-organic framework, *Journal of Colloid and Interface Science*, **430** (2014) 78-84.

[17] Y. Belmabkhout and A. Sayari, Adsorption of CO2 from dry gases on MCM-41 silica at ambient temperature and high pressure. 2: Adsorption of CO2/N2, CO2/CH4 and CO2/H2 binary mixtures, *Chemical Engineering Science*, **64** (2009) 3729-3735.

[18] N. Álvarez-Gutiérrez, M.V. Gil, F. Rubiera, and C. Pevida, Adsorption performance indicators for the CO2/CH4 separation: Application to biomass-based activated carbons, *Fuel Processing Technology*, **142** (2016) 361-369.

[19] D.J. Seo, Z. Gou, H. Fujita, T. Fujii, and A. Sakoda, Simple fabrication of molecular sieving carbon for biogas upgrading via a temperature controlled carbonization of Phyllostachys pubescens, *Renewable Energy*, **86** (2016) 693-702.

[20] Q. Xue and Y. Liu, Mixed-amine Modified SBA-15 as Novel Adsorbent of CO2 Separation for Biogas Upgrading, *Separation Science and Technology*, **46** (2011) 679-686.

[21] A.F.P. Ferreira, A.M. Ribeiro, S. Kulaç, and A.E. Rodrigues, Methane purification by adsorptive processes on MIL-53(Al), *Chemical Engineering Science*, **124** (2015) 79-95.

[22] X.q. Zhang, W.c. Li, and A.h. Lu, Designed porous carbon materials for efficient CO2 adsorption and separation, *New Carbon Materials*, **30** (2015) 481-501.

[23] S. Fatemi, M. Vesali-Naseh, M. Cyrus, and J. Hashemi, Improving CO2/CH4 adsorptive selectivity of carbon nanotubes by functionalization with nitrogen-containing groups, *Chemical Engineering Research and Design*, **89** (2011) 1669-1675.

[24] J. Wang, R. Krishna, J. Yang, K.P.R. Dandamudi, and S. Deng, Nitrogen-doped porous carbons for highly selective CO2 capture from flue gases and natural gas upgrading, *Materials Today Communications*, **4** (2015) 156-165.

[25] M. Nandi, K. Okada, A. Dutta, A. Bhaumik, J. Maruyama, D. Derks, and H. Uyama, Unprecedented CO2 uptake over highly porous N-doped activated carbon monoliths prepared by physical activation, *Chemical Communications*, **48** (2012) 10283-10285.

[26] R.W. Pekala, Low density, resorcinol-formaldehyde aerogels, US Patent, *US4997804 A*, 1991.

[27] R.W. Pekala, Organic aerogels from the polycondensation of resorcinol with formaldehyde, *Journal of Materials Science*, **24** (1989) 3221-3227.

[28] J. Yu, M. Guo, F. Muhammad, A. Wang, G. Yu, H. Ma, and G. Zhu, Simple fabrication of an ordered nitrogen-doped mesoporous carbon with resorcinol–melamine–formaldehyde resin, *Microporous and Mesoporous Materials*, **190** (2014) 117-127.

[29] N. Rey-Raap, J. Angel Menéndez, and A. Arenillas, RF xerogels with tailored porosity over the entire nanoscale, *Microporous and Mesoporous Materials*, **195** (2014) 266-275.

[30] J. Pampel, C. Denton, and T.P. Fellinger, Glucose derived ionothermal carbons with tailor-made porosity, *Carbon*, **107** (2016) 288-296.

[31] S.A. Al-Muhtaseb and J.A. Ritter, Preparation and Properties of Resorcinol–Formaldehyde Organic and Carbon Gels, *Adv. Mater.*, **15** (2003) 101-114.

[32] F.J. Maldonado-Hódar, Advances in the development of nanostructured catalysts based on carbon gels, *Catalysis Today*, **218–219** (2013) 43-50.

[33] E. Gallegos-Suárez, A.F. Pérez-Cadenas, F.J. Maldonado-Hódar, and F. Carrasco-Marín, On the micro- and mesoporosity of carbon aerogels and xerogels. The role of the drying conditions during the synthesis processes, *Chemical Engineering Journal*, **181-182** (2012) 851-855.

[34] S. Morales-Torres, F.J. Maldonado-Hódar, A.F. Pérez-Cadenas, and F. Carrasco-Marín, Structural characterization of carbon xerogels: From film to monolith, *Microporous and Mesoporous Materials*, **153** (2012) 24-29.

[35] J.F. Vivo-Vilches, F. Carrasco-Marín, A.F. Pérez-Cadenas, and F.J. Maldonado-Hódar, Fitting the porosity of carbon xerogel by CO2 activation to improve the TMP/n-octane separation, *Microporous and Mesoporous Materials*, **209** (2015) 10-17.

[36] S. Brunauer, P.H. Emmett, and E. Teller, Adsorption of Gases in Multimolecular Layers, *Journal of the American Chemical Society*, **60** (1938) 309-319.

[37] M.M. Dubinin, Inhomogeneous microporous structures of carbonaceous adsorbents, *Carbon*, **19** (1981) 321-324.

[38] F. Stoeckli, *Porosity in carbon. Characterization and applications*. Eds. Patrick J. Arnold, London, 1995.

[39] E.P. Barrett, L.G. Joyner, and P.P. Halenda, The Determination of Pore Volume and Area Distributions in Porous Substances. I. Computations from Nitrogen Isotherms, *Journal of the American Chemical Society*, **73** (1951) 373-380.